Dolomitization and diagenesis of the lower Muschelkalk, Northeast Spain

Henton, Jonathan Mark

Dolomitization and Diagenesis of the Lower Muschelkalk, Northeast Spain

Jonathan Mark Henton

A thesis submitted to the University of Durham for the degree of Doctor of Philosophy

Department of Geological Sciences September, 1990

Declaration

The content of this thesis is the original work of the author and has not previously been submitted for a degree at this or any other university. Other people's work is acknowledged by reference.

Jonathan Mark Henton
Department of Geological Sciences,
University of Durham.

Copyright

Dolomitization and Diagenesis of the Lower Muschelkalk, Northeast Spain

Jonathan Mark Henton

The Lower Muschelkalk crops out in the Catalan Coastal Ranges (the Catalan Basin) and eastern Iberian Ranges (the Valencia-Cuenca Basin) and occurs extensively in the subsurface of the Ebro Basin. The Lower Muschelkalk forms a carbonate platform that was deposited on red Buntsandstein siliciclastics and locally-developed evaporitic and calcareous shales. The Middle Muschelkalk rests with a sharp contact on the underlying Lower Muschelkalk and in contrast to it, exhibits marked regional thickness and facies variations. The Triassic of northeast Spain generally subsided during the Mesozoic and was uplifted during the early Paleogene. Tertiary subsidence was important in the Ebro Basin and the Neogene basins of the Catalan Coastal Ranges.

The Lower Muschelkalk has a maximum thickness of about 100m in the Catalan Basin and southeastern Valencia-Cuenca Basin, but thins towards the northwest before pinching out completely. The lower part of the Lower Muschelkalk consists of peritidal carbonates (El Brull Unit) passing upwards into bioclastic lagoonal sediments (Olesa Unit) and lagoonal to oolitic sand-belt deposits (Vilella Baixa Unit) interpreted as broadly transgressive sediments deposited on a homoclinal ramp which form a Transgressive Systems Tract (TST). The TST is overlain by locally-developed shallow subtidal to intertidal deposits and by intertidal to supratidal dolomicrites (Lower Member and Upper Member of the Colldejou Unit). This aggradational to retrogradational package constitute a Highstand Systems Tract (HST). The Olesa Unit and Vilella Baixa Unit pinch out towards the northwest of the Valencia-Cuenca Basin and the Ebro Basin and the succession becomes dominated by peritidal sediments. Lateral facies changes in the Olesa Unit and Vilella Baixa Unit indicate a downramp transition from northeast to southwest of the Catalan Basin.

Paleokarstic surfaces are locally important in the Vilella Baixa Unit and the Lower Member of the Colldejou Unit and the underlying sediments appear to have been subjected to meteoric stabilization with early aragonite dissolution and replacement. These horizons have locally resisted later dolomitization. Subsurface paleokarsts are locally important in the Catalan Basin and may be related to Paleogene uplift and intraformational dissolution.

Sulphates and evidence of former sulphates are common in the Lower Muschelkalk. Most sulphates were syndepositional but others were related to shallow-burial fabric-replacive dolomitization. Sulphate dissolution occurred in two phases; during burial diagenesis related to hydrothermal fluids; and in association with uplift into meteoric phreatic and vadose environments when dolomites suffered calcitization.

Three types of dolomite are recognised in the Lower Muschelkalk: peritidal dolomite occurring in the Upper Member of the Colldejou Unit and in the peritidal facies of the El Brull Unit; fabric-replacive dolomite occurring in the TST; and baroque dolomite as a late cement and locally mosaic-forming phase. Trace element and isotope geochemistry indicates consistently greater depletion in strontium and ^{18}O in the fabric-replacive dolomite than in the peritidal dolomite and differing trends in iron and manganese. These features are consistent with downwards-migrating fluids acting on contrasting precursors. The fabric-replacive dolomite and peritidal dolomite are considered to have formed as a result of Middle Muschelkalk evaporite-related brines migrating downwards through relatively homogeneous, unstable aragonite-rich peritidal sediments of the Colldejou Unit into more heterogeneous, partially stabilised calcitic limestones of the TST. Sequence stratigraphy allows easy comparison with other similar brine-reflux models of dolomitization.

The baroque dolomite is geochemically distinct with depleted $\delta^{18}O$ values and high iron and manganese contents indicating precipitation at elevated temperatures from reducing fluids associated with local hydrothermal mineralization.

Calcitization has locally affected the Lower Muschelkalk dolomites producing a wide variety of fabrics. Geochemistry and petrography indicate that dedolomitic calcite formed as a result of uplift-related dissolution of sulphates by near-surface, soil-influenced meteoric-derived groundwaters.

Acknowledgements

I would like to thank my three supervisors: Dr. Maurice Tucker (University of Durham) for advice and guidance during the course of the research and the preparation of this thesis; Dr. Francesc Calvet (University of Barcelona) for invaluable assistance and discussion during fieldwork and research in Spain; and Dr. Baruch Spiro (British Geological Survey, Keyworth) for considerable help with aspects of the geochemical analysis and interpretation.

Financial assistance was provided by the Natural Environmental Research Council and is gratefully acknowledged.

Technical facilities were made available at the University of Durham, Dept. of Geological Sciences (XRD, AAS, CL) and Dept. of Engineering (SEM); Royal Holloway and Bedford New College (ICPAES); University of Barcelona (SEM); and at the British Geological Survey Isotope Geology Section, London now moved to Keyworth (Stable Isotopes).

Technical assistance was provided by Ron Hardy, Paul Laverick, and Dave Stevenson (University of Durham); Pete Oakley (University of Newcastle); Pete Greenwood (BGS); and Alison Warren (RHBNC).

Thanks are also due to Ron Lambert and particularly George Randall for the preparation of numerous CL polished, orientated thin sections; to Gerry Dresser and Alan Carr for photography; Karen Atkinson for help with draughting; Carole Blair, Jeanette Finn and Lynne Gilchrist for secretarial work and for 'turning a blind eye' to this and that; and to Dave Asbery for 'fixing' just about everything, including my car stereo.

I would like to thank Rob Gawthorpe, Alick Leslie, Gerald Roberts, Dave Hunt and Steve Moss for the occasional helpful discussion about sedimentological research and for the even more helpful discussions about everything else. I would also like to acknowledge all the other students, postgrad.s and members of staff who have helped to make my stay at Durham a very pleasurable one. Paula Radice deserves a special mention for remaining cheerful despite living with three geologists.

I would also like to thank my parents, to whom I dedicate this thesis, for their support over the years.

CONTENTS

CHAPTER 1: INTRODUCTION TO THE DOLOMITIZATION AND DIAGENESIS OF THE LOWER MUSCHELKALK, NORTHEAST SPAIN

1.1 DISCUSSION OF THE THESIS OBJECTIVES

The Lower Muschelkalk of northeast Spain is the lower of two carbonate horizons which together with the clastic and evaporitic Middle Muschelkalk form the mid-Triassic strata of much of northeast Spain. The Lower Muschelkalk exhibits quite similar regional depositional features but these have been subjected to varying degrees and styles of diagenesis and dolomitization.

A principal aim of this thesis has been to investigate the dolomitization of the Lower Muschelkalk. Dolomites and dolomitization have been an important field of research for many years and several models have been proposed (see Section 5.1). Dolomites are of considerable economic importance as hydrocarbon reservoirs. Schmoker *et al.* (1985) showed statistically that in the U.S.A. dolomite reservoirs, although fewer, are generally larger than limestone reservoirs and contain about 60% of the oil originally in place in carbonate reservoirs. The statistics also tend to indicate that dolomitization tends to improve reservoir properties relative to those otherwise expected. Carbonates are hosts to a large number of economic minerals, in particular 'Mississippi Valley Type' Pb-Zn ores, which generally occur in dolomitized host rocks (Scoffin, 1987). Small-scale commercially exploited hydrothermal mineralization is locally associated with the Lower Muschelkalk carbonates of northeast Spain (see Section 4.7).

The Lower Muschelkalk of northeast Spain was particularly suitable for the study of dolomitization owing to the quality of the exposure and because the basic lithostratigraphy, particularly in the Catalan Coastal Ranges, had already been established. In order to understand the dolomitization, it has been important to examine the depositional and early diagenetic history of the strata because this has in part controlled the style of dolomitization. Three distinct dolomite facies are present in the Lower Muschelkalk. Stratigraphically-controlled fine-grained dolomicrites with well-preserved peritidal sedimentary structures overlie a petrographically variable stratigraphy-discordant fabric-replacive dolomite which is clearly after near-normal marine limestones. Baroque dolomite is the third dolomite facies and is only locally important as a late cement phase and in places as a replacive mosaic.

The relationships between the peritidal dolomite and underlying fabric-replacive dolomite are well-exposed in the Catalan Coastal Ranges and analogous lithologies occur in the Iberian Ranges. The orientation of the Iberian Ranges is perpendicular to the Catalan Coastal Ranges and provide an important insight into lateral facies

changes in the Lower Muschelkalk as the carbonate deposits become thinner towards the edge of the basin.

Geochemical analyses of the dolomites were carried out in order to ascertain any geochemical distinction between the two dolomite types. It is clearly important to be able to discriminate between stratigraphically-controlled laterally-extensive dolomites from stratigraphy-discordant replacive dolomites. Geochemical analyses were also performed in order to investigate the paleohydrology of the basin.

1.2 OUTLINE OF THE THESIS

Chapter 2 introduces the Triassic of western and central Europe, and that of northeast Spain in particular. The regional tectonic and structural setting, paleoclimate and main outcrop areas are described. The principal lithostratigraphic units of the Mediterranean Triassic facies, which forms much of the Triassic of northeast Spain, are briefly introduced and the chronostratigraphy of the main outcrop areas compared. Post-depositional burial and uplift patterns are also estimated on the basis of sediment accumulation thicknesses and unconformities in different areas.

Chapter 3 describes the principal depositional sedimentary features of the Lower Muschelkalk. The Catalan Coastal Ranges are the main study-area and in this region the Lower Muschelkalk is divided into four units which are then compared with outcrops from the Iberian Ranges and with reported data on the Triassic of the Balearic Islands and the subsurface of the Ebro Basin. The deposition of the Lower Muschelkalk is interpreted in terms of a homoclinal carbonate ramp. A sequence stratigraphic framework for the Triassic of northeast Spain is introduced and described for the Lower Muschelkalk.

Chapter 4 describes the detailed sedimentology, petrography and some aspects of the diagenesis of the Lower Muschelkalk of the Catalan Coastal Ranges and Iberian Ranges. The topics covered in the chapter include the bioclastic content of the Lower Muschelkalk, oolites and pisolites, siliciclastics, tepees, paleokarsts, hydrothermal mineralization, pseudomorphs after evaporites and silicification.

Chapter 5 describes the petrography and field relations of the three principal dolomite facies that occur in the Lower Muschelkalk of the Catalan Coastal Ranges and Iberian Ranges.

Chapter 6 describes the geochemical characteristics of the Lower Muschelkalk and interprets the data in order to constrain the diagenetic environments and processes. Dolomites, limestones and various minor components from the Catalan Basin and Valencia-Cuenca Basin were analysed for trace elements, oxygen and carbon stable

isotopes. Dolomites were also examined for crystal stoichiometry and ordering by X-ray diffraction.

Chapter 7 reviews the principal outcrop, petrographic and geochemical features of the dolomites of the Lower Muschelkalk of the Catalan Coastal Ranges and Iberian Ranges and proposes a coherent model. The dolomitization processes are discussed in terms of the sequence stratigraphic framework of the Lower Muschelkalk.

Chapter 8 describes the outcrop and petrographic features of the calcitized dolomites of the Lower Muschelkalk. Trace element and stable isotopic data are used in order to constrain the dedolomitization process.

Chapter 9 lists the principal conclusions of the study.

CHAPTER 2: THE TRIASSIC OF NORTHEAST SPAIN

2.1 INTRODUCTION

The Triassic of western and central Europe is governed by regional extension that resulted in the subsidence of a complex network of grabens and troughs forming an integral part of the rift/rift-wrench systems which developed into the major break-up axes of Pangea (Ziegler, 1982; Vegas and Banda, 1982).

Pangea formed during the Upper Paleozoic Variscan-Alleghanian orogeny as a result of the collision between Gondwana, Laurentian and Baltic cratons as well as intervening microcontinents (Rast, 1988). During the late Permian northeast Spain lay on the northwestern margin of Tethys and much of the area was positive and being eroded (Ziegler, 1982). During the Triassic western and central Europe underwent progressive marine transgression emanating from Tethys as the Triassic rift systems began to develop and the North Atlantic began to open (Fig. 2.1; Manspeizer, 1988) and rift basins began to develop on the Iberian Peninsula (Sopena *et al.*, 1988). The Triassic sedimentation on the northern and western shelves of Tethys was controlled by an interplay between sea level change, clastic influx and subsidence which gave rise to the development of the so-called Germanic Facies Province, characterised by a three-fold division into Buntsandstein clastics, Muschelkalk carbonates and evaporites and Keuper evaporites and clastics (Ziegler, 1982). The Germanic Facies of the Triassic contrasts with the Alpine Triassic which was developed on the southern margin and deeper parts of Tethys and includes the large carbonate build-ups which are now exposed in the Dolomites and southern Alps.

The principal phase of post-Triassic tectonics in the northeast Iberian Peninsula was during the Paleogene Alpine Compression (Guimera, 1984) and resulted in a series of mountain ranges (*e.g.* Catalan Coastal Ranges, Iberian Ranges) separated by intermontane basins filled by Tertiary deposits (*e.g.* Ebro Basin). The exposures of the Triassic are limited to the ranges areas between the Tertiary basins (Fig. 2.2).

The Mediterranean Triassic is the most easterly of three Triassic facies belts which show progressively less marine influence towards the west (Gandin *et al.*, 1982; Sopena *et al.*, 1983). The Mediterranean Triassic crops out in the Catalan Coastal Ranges and the eastern Iberian Ranges and has also been recognised in the subsurface in extensive areas of the Ebro Basin (Gandin *et al.*, 1982; Jurado, 1988). The most westerly of the Triassic facies belts is the Hesperic Triassic, cropping out in the Central Mountain Ranges, and the intermediate is the Iberian Triassic of the Iberian Ranges (Fig. 2.3). Towards the northeast the Mediterranean Triassic passes into the

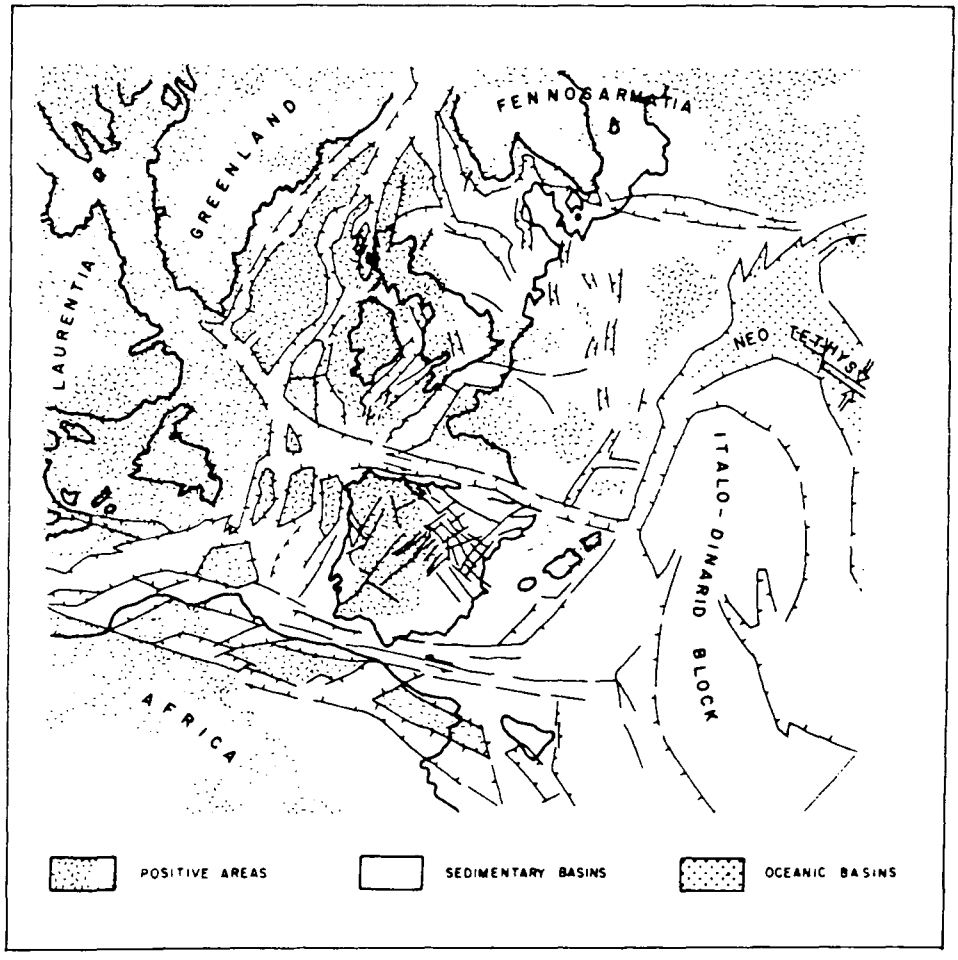

Fig. 2.1. Plate arrangement during the Early Triassic and main fault systems in the Central and North Atlantic area (from Sopena *et al.*, 1988).

Pyrenean Triassic which shows affinities with the Iberian Triassic (Virgili *et al.*, 1977).

2.2 STRUCTURAL SETTING OF NORTHEAST SPAIN

Three mountain chains are present in northeast Spain: the Pyrenees, the Iberian Ranges and the Catalan Coastal Ranges (Fig 2.4). The Ebro Basin, Tertiary in age, formed as the foreland basin to these three Alpine structural units (Anadon *et al.*, 1985).

The Catalan Coastal Ranges and Iberian Ranges are composed of Paleozoic Hercynian basement unconformably overlain by Triassic (and locally ?Upper Permian) to Cretaceous sediments. The dominant structures of the Catalan Coastal Ranges (Anadon *et al.*, 1979; Guimera, 1984) are near-vertical basement-involved northeast-southwest longitudinal faults which are slightly oblique to the overall direction of the ranges (Fig. 2.4). Transverse, northwest-southeast basement faults with somewhat smaller displacements also occur in the Catalan Coastal Ranges. The principal structures of the Iberian Ranges are northwest-south-east basement faults and these are connected to the Catalan Coastal Ranges by the Linking Zone where the major basement faults are east-west (Guimera, 1984).

In the Catalan Coastal Ranges the basement-involved faults probably developed during the Late Paleozoic as strike-slip faults (Anadon *et al.*, 1985). Thickness and facies variations in the Mesozoic cover suggest that the faults were periodically active as normal faults during the Triassic (Marzo, 1980; Marzo & Calvet, 1985; Calvet *et al.*, 1990). During the Alpine orogeny the faults were again reactivated as strike-slip faults with a local transpressive component. Later, some of these moved as normal faults during a Neogene extensional phase (Anadon *et al.*, 1985). The northwest-southeast trending faults of the Catalan Coastal Ranges have a predominant strike-slip movement and in some cases displace the longitudinal faults (Guimera, 1984).

2.3 TRIASSIC CLIMATE AND PALEOLATITUDE OF NORTHEAST SPAIN

During the Triassic the global climate was more equable than present owing to the absence of ice-caps (Hallam, 1985). During the early Triassic northeast Spain was at a paleolatitude of about 10°N in a dry continental climate. By the late Triassic to early Jurassic Spain had migrated to 20-25°N into a seasonally wet climate (Tucker & Benton, 1983; Hallam, 1985).

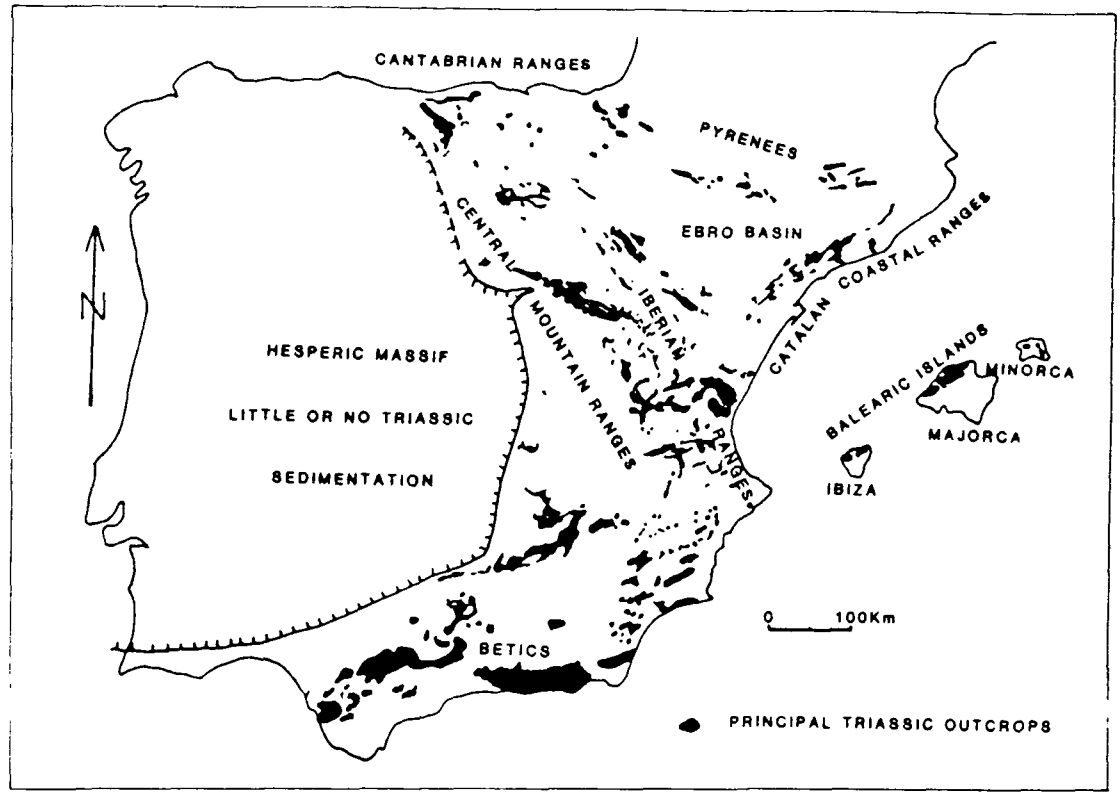

Fig. 2.2. Principal areas of Triassic exposure. Compiled from Freeman (1972) and Sopena *et al.*, (1983).

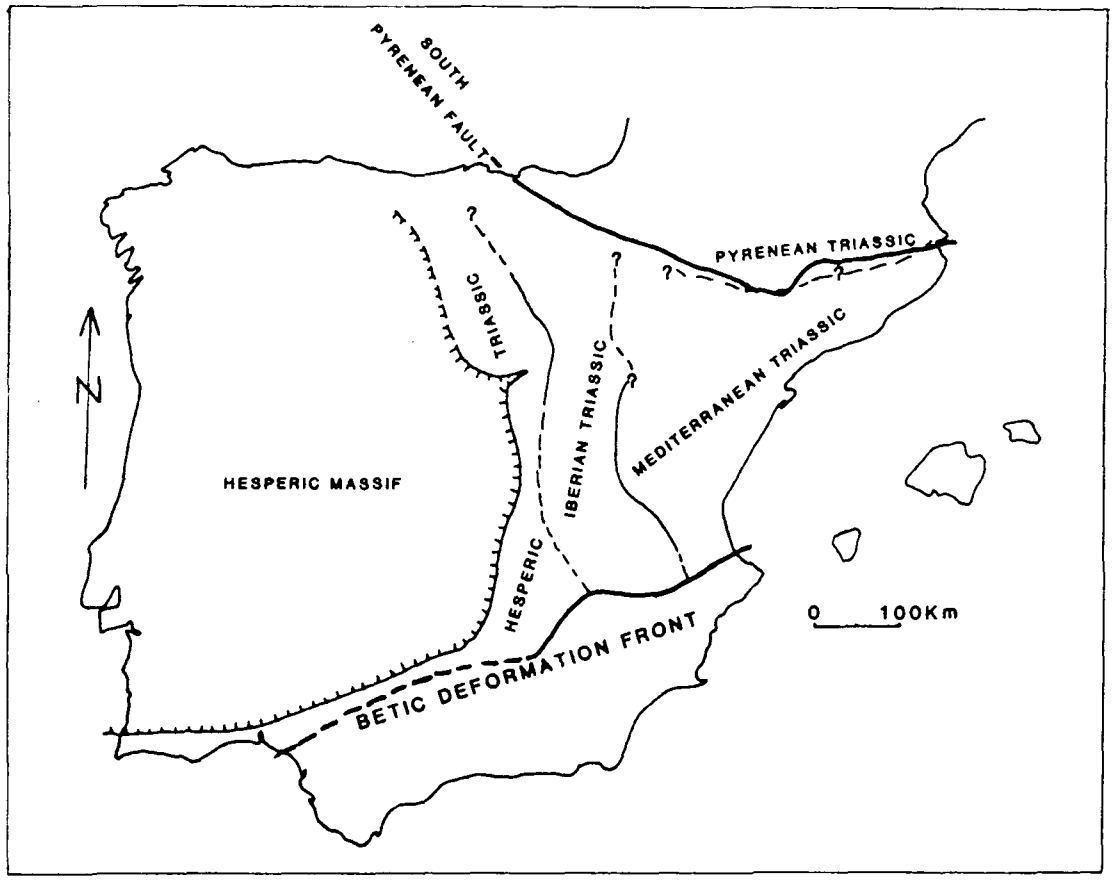

Fig. 2.3. The Triassic facies belts of Spain.

2.4 MEDITERRANEAN TRIASSIC OF NORTHEAST SPAIN

2.4.1 Introduction

The Mediterranean Triassic (Fig. 2.3) is exposed in the Catalan Coastal Ranges and the eastern Iberian Ranges (the Valencia-Cuenca Basin) and subcrops in extensive areas of the Ebro Basin where it has been penetrated by boreholes (Gandin *et al.*, 1982; Jurado, 1988).

The Mediterranean Triassic broadly consists of a Germanic-style succession of alternate 'transgressive' carbonates and/or evaporites and 'regressive' siliciclastics and/or evaporites (Sopena *et al.*, 1983; Calvet *et al.*, 1990). The Mediterranean Triassic involves three transgressive cycles above the Buntsandstein: the Lower Muschelkalk, the Upper Muschelkalk, and the Imon Formation. Between these carbonate units are wedged evaporites and clastics of the Middle Muschelkalk and the Keuper. The chronostratigraphy of these lithostratigraphic units is discussed in Section 2.5. The Iberian Triassic only involves the deposits of the last two transgressions and towards the Meseta Highlands of central Spain in the Hesperic Triassic, only the last transgressive episode (Imon Formation) is present (Fig. 2.5; Virgili *et al.*, 1977; Garrido-Megias & Villena, 1977; Gandin *et al.*, 1982; Sopena *et al.*, 1983). Therefore, on a broad scale the transgressive carbonate facies of northeast Spain display an onlapping, retrogressive or back-stepping arrangement (Marzo & Calvet, 1985; Calvet *et al.*, 1990). The extents of the Lower and Upper Muschelkalk transgressions are shown in the paleogeographical maps of Fig. 2.6.

The Mediterranean Triassic has been most extensively studied in the Catalan Coastal Ranges where local variations in facies and thickness are thought to have resulted from active faulting in the Triassic, and domains have been recognised. The domains for the Muschelkalk of the Catalan Basin are shown in Fig. 2.7. The concept was first applied to the Buntsandstein (Marzo, 1980), later to the Muschelkalk (Marzo & Calvet, 1985; Calvet *et al.*, 1990) and to the Keuper (Salvany & Orti Cabo, 1987). The domains are most marked during the clastic-evaporite portions of the succession and the Upper Muschelkalk.

The Mediterranean Triassic has been considered by several workers in terms of depositional sequences. The framework adopted in this thesis is that of Calvet *et al.* (1990) and is discussed in more detail in Section 3.7.

The Mediterranean Triassic can be divided into six lithostratigraphic units (Virgili, 1958; Calvet *et al.*, 1990): Buntsandstein; Lower Muschelkalk; Middle Muschelkalk; Upper Muschelkalk; Keuper; and Imon Formation.

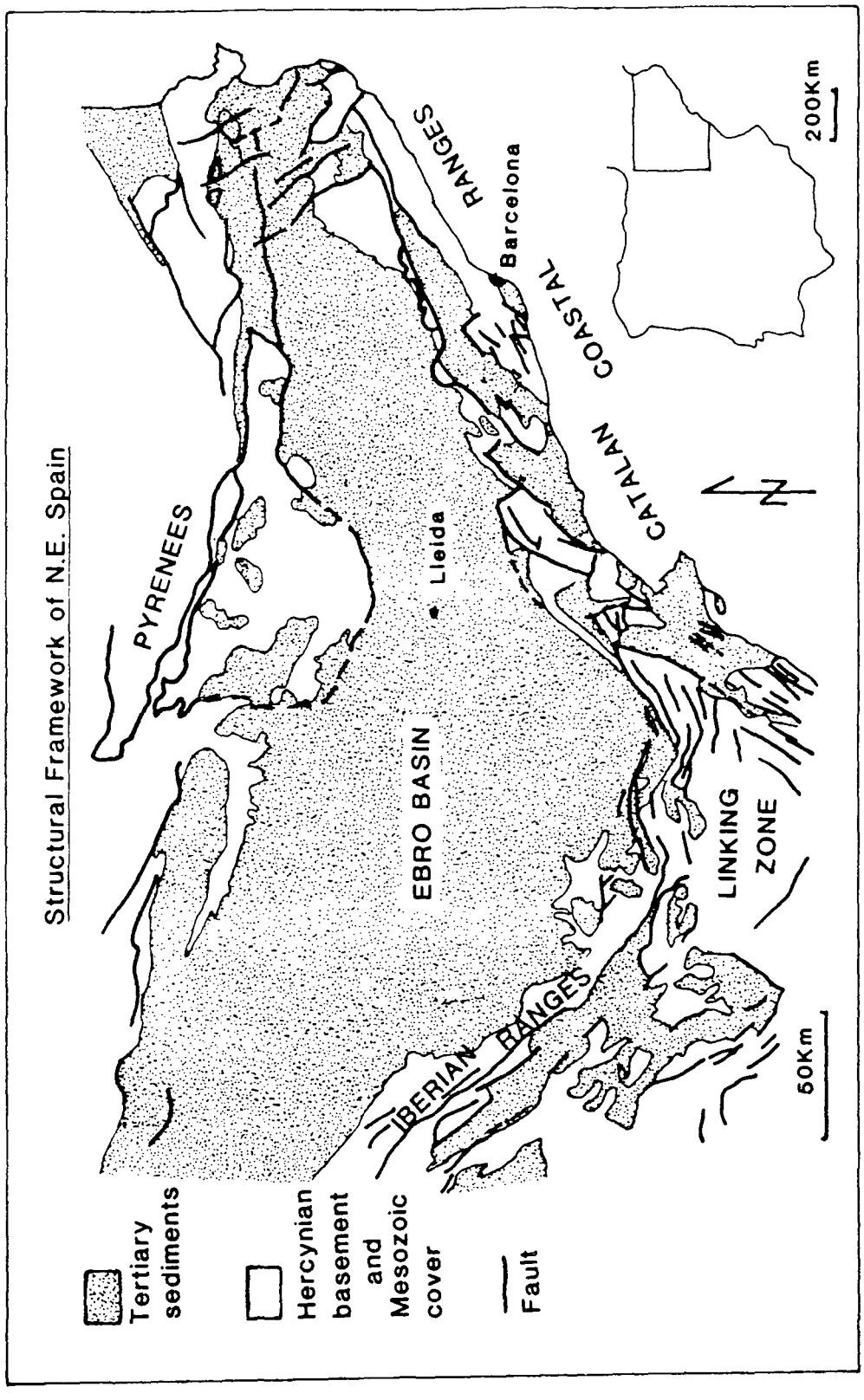

Fig. 2.4. Structural framework of northeast Spain (adapted from Anadon *et al.*, 1985).

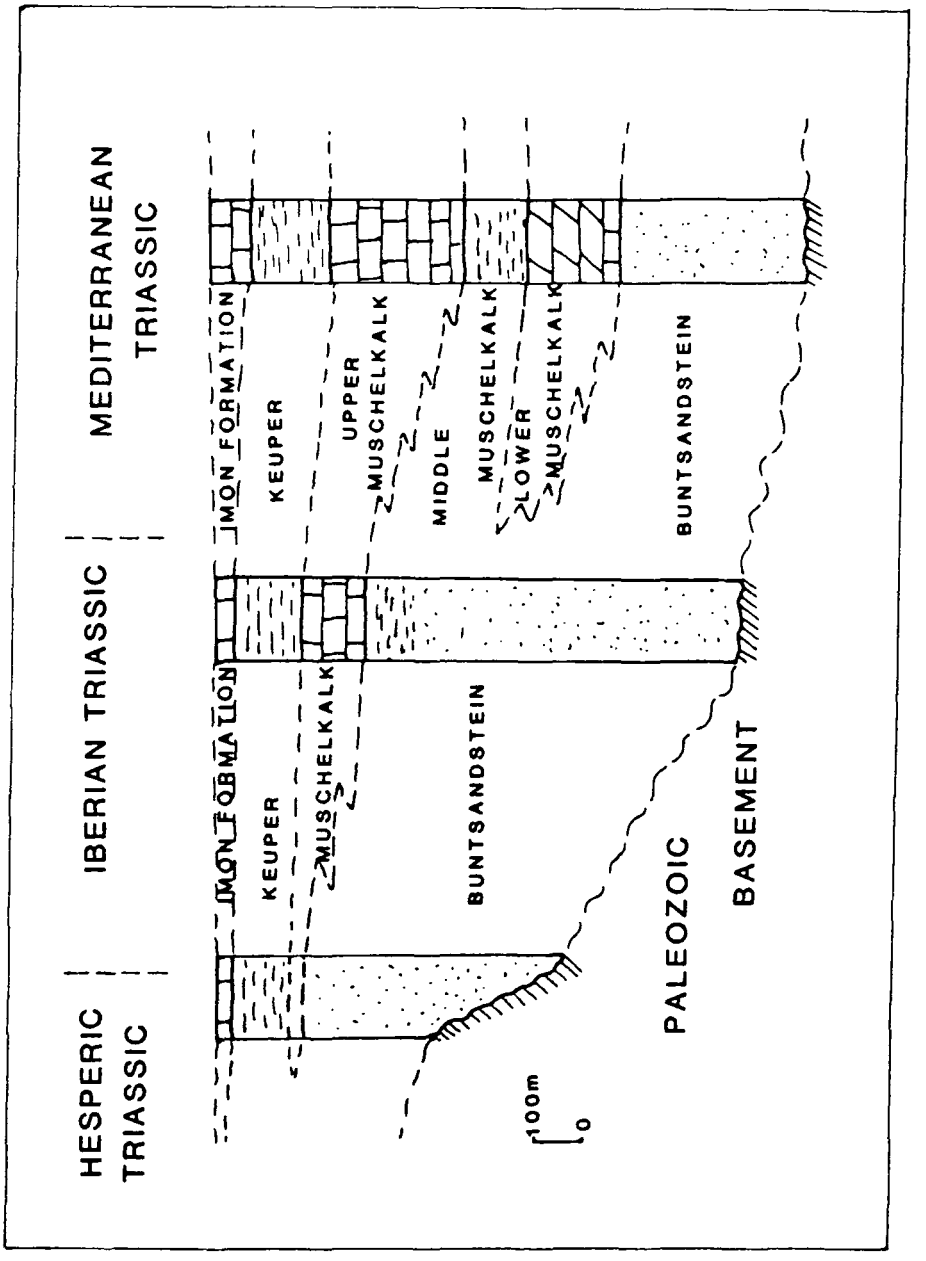

Fig. 2.5. Approximate lithostratigraphy of the Triassic of northeast Spain (after Virgili *et al.*, 1977).

2.4.2 Buntsandstein

The Buntsandstein consists of conglomerates, sandstones and mudstones and exhibits considerable thickness variations (Fig. 2.8) from more than 600m in parts of the Ebro Basin to less than 100m (Sopena *et al.*, 1983). The Buntsandstein rests with an angular unconformity on Paleozoic Hercynian basement. A lutite-carbonate-evaporite complex, equivalent to the Röt Facies of Germany and the southern North Sea, is locally developed at the top of the Buntsandstein (Orti Cabo, 1982).

2.4.3 Lower Muschelkalk

The Lower Muschelkalk consists of limestones and dolomites and has a thickness of up to 100m in the Catalan Coastal Ranges. The Lower Muschelkalk thins towards the west and north-west and is absent in the Iberian Triassic, and may also be missing in the Pyrenean Triassic (Virgili *et al.*, 1977).

The Lower Muschelkalk is the subject of this thesis and is discussed at length in the following chapters. A brief introduction to the Lower Muschelkalk of the Catalan Basin is given here and a summary log is shown in Fig. 2.9.

The Lower Muschelkalk rests upon Buntsandstein conglomerates and sandstones and consists of peritidal carbonates and oolite grainstone complexes deposited on a homoclinal ramp. The boundary with the uppermost part of the Buntsandstein is transitional. There is a sharp boundary at the top of the Lower Muschelkalk with the overlying evaporites and clastics of the Middle Muschelkalk.

The Lower Muschelkalk of the Catalan Basin can be considered in terms of two sedimentary packages (Calvet *et al.*, 1990; Section 3.7). The lower package is generally 50-60m thick and consists of peritidal laminated dolomicrites and limestones (the El Brull Unit) overlain by massive carbonate mud deposits with a normal marine fauna which pass upwards into grainstone-capped, shallowing-upward cycles (the Olesa Unit and Vilella Baixa Unit) and is interpreted as a Transgressive Systems Tract (TST). The TST has undergone extensive dolomitization which is generally fabric-destructive but locally preserves fine-scale sedimentary structures. A dolomitization front separates limestones below from dolomites above and is discordant to bedding on an outcrop and regional scale. The extent of the dolomitization is very variable. In some areas almost all the systems tract has been dolomitized but elsewhere only the top few metres have been affected.

The upper sedimentary package of the Lower Muschelkalk of the Catalan Basin is 30-40m thick and is separated from the dolomitized grainstones of the TST by a regional disconformity that has locally undergone minor karstification. However, in some

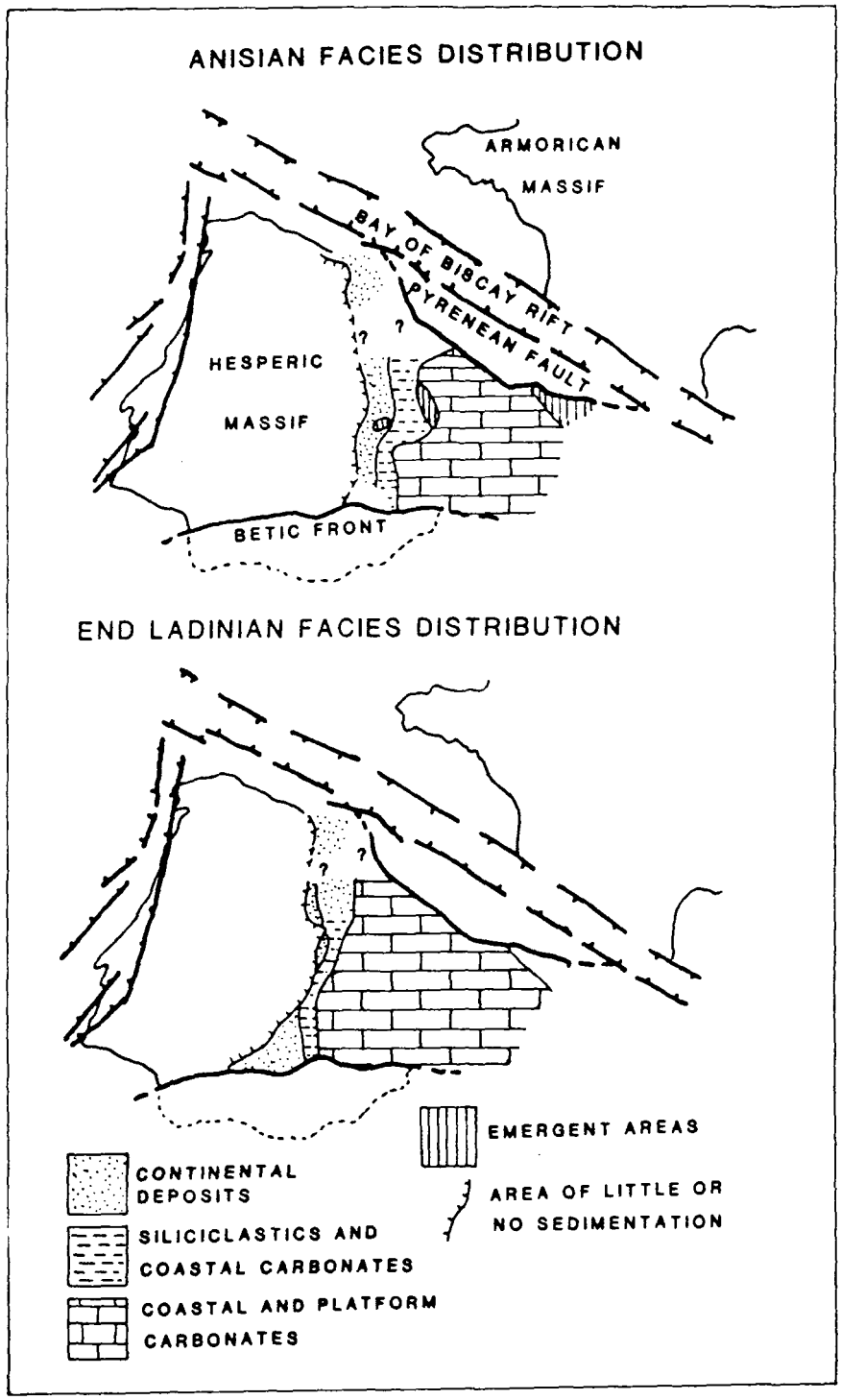

Fig. 2.6. Facies distribution during the Anisian and end-Ladinian showing the extent of the Lower Muschelkalk and Upper Muschelkalk (after Sopena *et al.*, 1983).

areas the boundary is not sharp but more gradual over several metres. This sedimentary package consists of fine-grained laminated peritidal deposits with a sparse restricted fauna (the Colldejou Unit) and is broadly aggradational to retrogradational and is interpreted as a Highstand Systems Tract (HST). The dolomitization is pervasive and has preserved the fine-grained nature of the sediments. The HST is capped by a desiccated planar stromatolite with tepees, collapse breccias and vadose calcite cements and a laminated crust is locally present and has been interpreted as a caliche crust (Esteban *et al.*, 1977). This upper boundary is a regional unconformity which marks the boundary between the Lower Muschelkalk carbonates and sabkha-style evaporites and clastics of the Middle Muschelkalk and is interpreted to be a sequence boundary.

The Lower Muschelkalk in the southeast of the eastern Iberian Ranges (or Valencia-Cuenca Basin) is similar to that of the Catalan Basin. However, towards the northwest of the Valencia-Cuenca Basin the Lower Muschelkalk thins and becomes more marginal and peritidal-dominated.

2.4.4 Middle Muschelkalk

The Middle Muschelkalk consists of red and grey mudstones with intercalated sulphate evaporites, and rare volcanics and sandstones (Esteban *et al.*, 1977; Cabaneros & Masriera, 1977; Orti Cabo, 1982; Calvet *et al.*, 1990). The Middle Muschelkalk exhibits considerable variation in thickness from less than 50m in parts of the Catalan Coastal Ranges to more than 300m in parts of the subsurface of the Ebro Basin (Jurado, 1988). The Middle Muschelkalk contains anhydrite and halite in the subsurface and at outcrop in the Catalan Coastal Ranges there are nodular evaporites (gypsum-anhydrite) as well as laminated evaporite beds (see Section 3.2.4.2). Much of the Middle Muschelkalk is considered to have been deposited in a sabkha environment with some evaporite deposition from more permanent evaporitic lakes.

2.4.5 Upper Muschelkalk

The Upper Muschelkalk consists of limestones, dolomites and shales and varies in thickness in the Catalan Coastal Ranges from 100-140m (Marzo & Calvet, 1985; Calvet *et al.*, 1990). There is a rapid transition from the Middle Muschelkalk fluvial clastics and evaporites into the Upper Muschelkalk carbonates. The facies in the Upper Muschelkalk show quite marked lateral variations and can be ascribed to different domains (Calvet & Tucker, 1988; Calvet *et al.*, 1990).

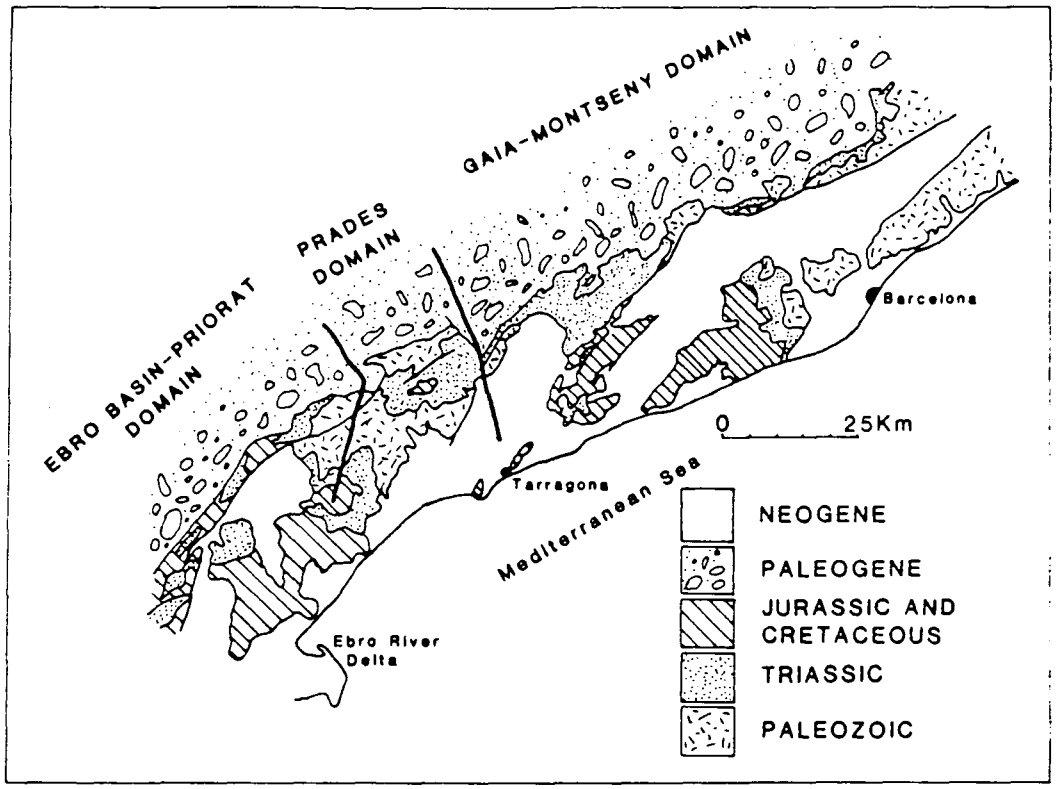

Fig. 2.7. Triassic domains for the Muschelkalk of the Catalan Basin (adapted from Calvet *et al.*, 1990)

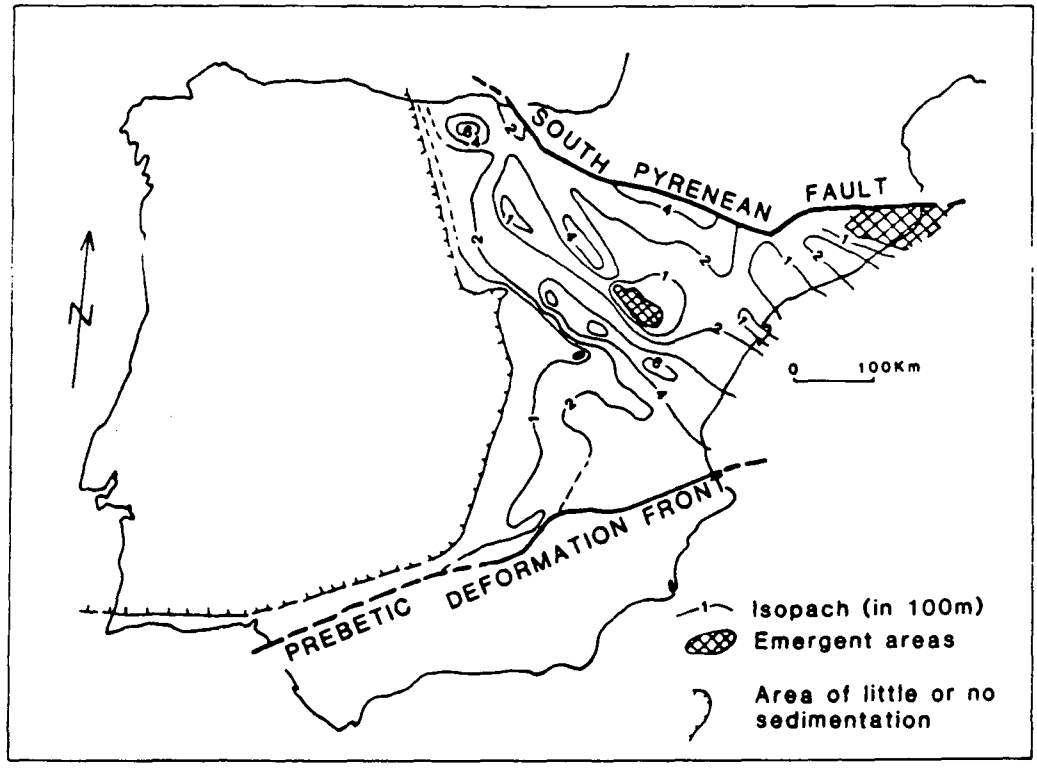

Fig. 2.8. Isopach map for the Buntsandstein lithofacies (from Sopena *et al.*, 1983)

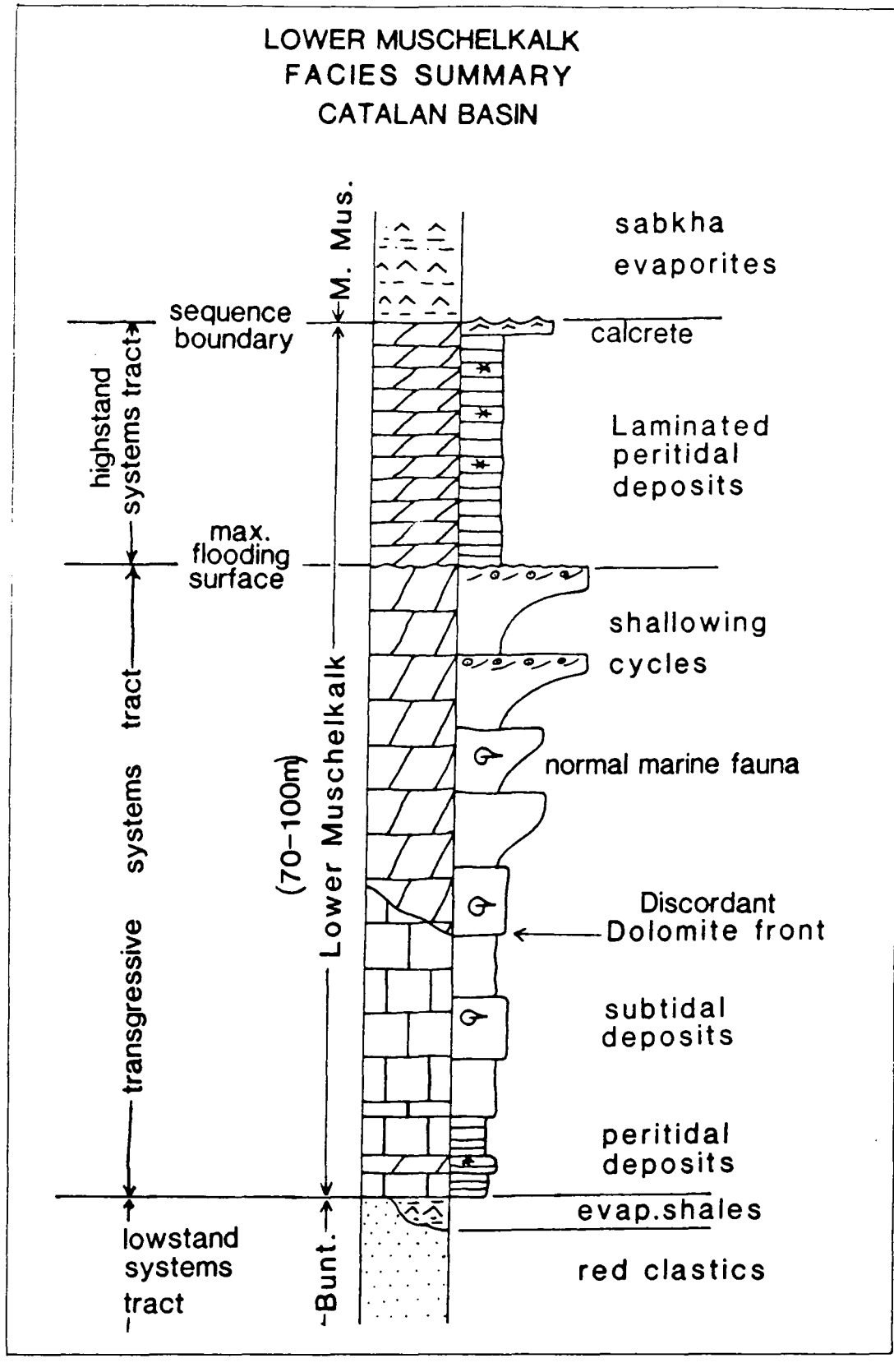

Fig. 2.9. Generalised graphic log for the Lower Muschelkalk of the Catalan Basin showing major sequence stratigraphic divisions (see Section 3.7).

2.4.6 Keuper

There is a gradual transition from the Upper Muschelkalk carbonates into the Keuper evaporites. The Keuper consists of evaporites, marls, carbonates, minor sandstones and locally volcaniclastic sediments and lavas (Gandin *et al.*, 1982; Calvet *et al.*, 1990). The Keuper exhibits large thickness variations of 50-150m in the Catalan Coastal Ranges and up to 280m in the eastern Iberian Ranges (the Valencia-Cuenca Basin) where the sequence is particularly well developed (Orti Cabo, 1982).

2.4.7 Imon Formation

The Imon Formation mainly consists of dolomites and varies in thickness from 40-70m in the Catalan Coastal Ranges (Calvet *et al.*, 1990).

2.5 CHRONOSTRATIGRAPHY OF THE TRIASSIC OF NORTHEAST SPAIN

The chronostratigraphy of the Triassic of northeast Spain is not well established owing to the general sparsity of fossils for much of the succession. Palynomorphs have been used to establish a chronostratigraphy for the Mediterranean Triassic of the Catalan Basin (Sole de Porta *et al.*, 1987). Chronostratigraphies for different regions of the Triassic are discussed by Virgili *et al.* (1977) and Sopena *et al.* (1983) and are summarised in Fig. 2.10. The onset of Buntsandstein deposition is clearly diachronous and ranges from latest Permian to Ladinian in age. The age of the lowermost Muschelkalk sedimentatation also becomes younger towards the west.

2.6 POST-DEPOSITIONAL BURIAL AND UPLIFT OF THE TRIASSIC

Six sediment accumulation curves to the base of the Lower Muschelkalk are shown in Fig 2.11. The curves are constrained by borehole data for the two Ebro Basin areas, and by generalised lithological columns for the other four areas (Marzo & Calvet, 1985; Jurado, 1988). The curves use undecompacted sedimentary thicknesses.

The Triassic of northeast Spain generally subsided during the Mesozoic and was uplifted during the early Paleogene. The Ebro Basin and the northern Catalan Coastal Ranges were uplifted and eroded and succeeding Paleogene sediments were deposited on the Triassic with an angular unconformity. During the Neogene the southwestern Ebro Basin continued to subside but in the northeast there was uplift and some erosion of the Paleogene sediments. In the northern Catalan Coastal Ranges there has been local uplift and exposure of the Triassic during the Neogene. The burial history of the Triassic of the Iberian Ranges is similar to the southern Catalan Coastal Ranges with subsidence during the Mesozoic and deposition of Jurassic and Cretaceous sediments, followed by uplift and erosion during the Tertiary.

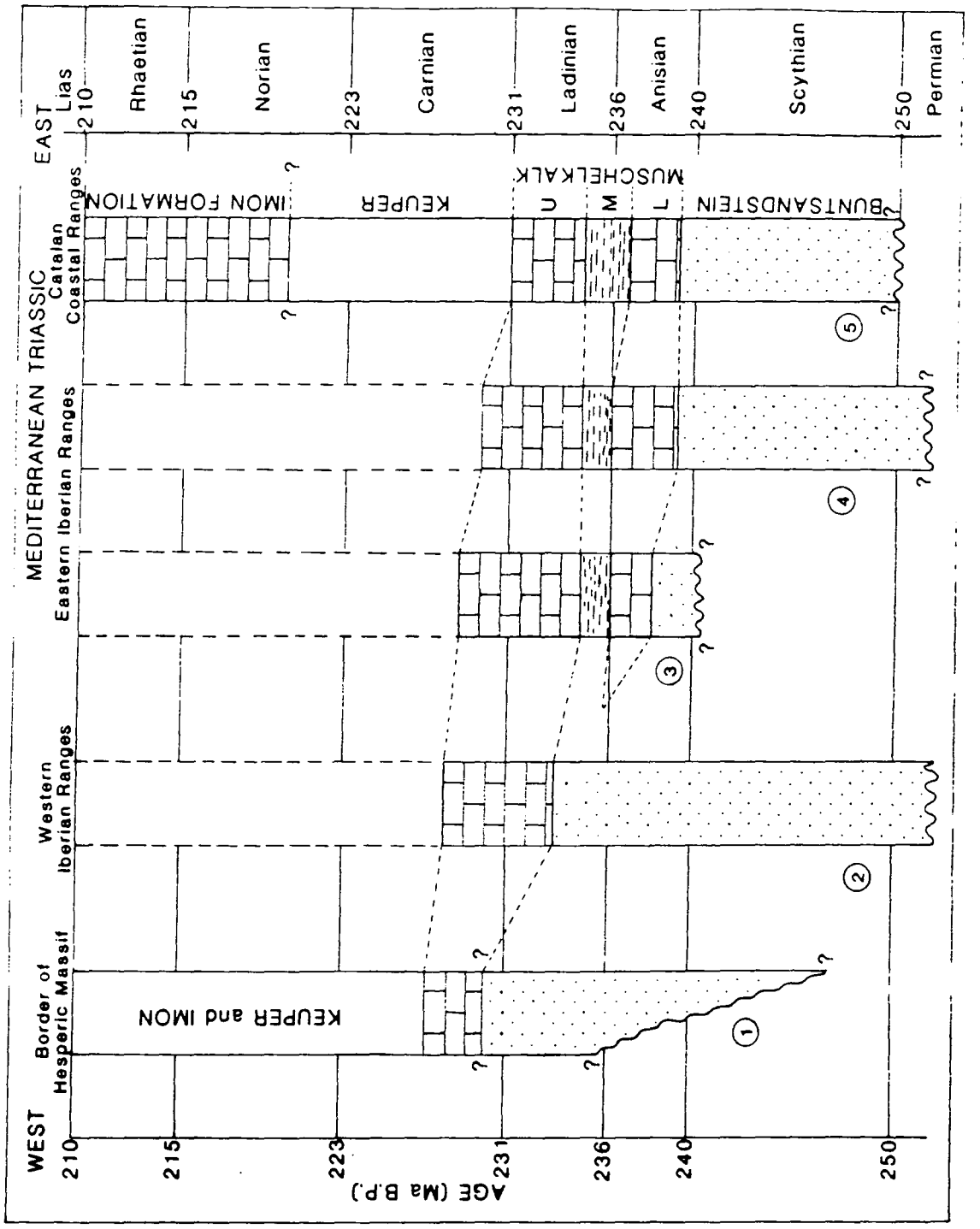

Fig. 2.10. Approximate chronostratigraphy for the Triassic of NE Spain. Compiled from Virgili *et al.*, (1977): ① ; Sopena *et al.*, (1983): ② , ③ , ④ ; Sole de Porta *et al.* (1987): ⑤ .

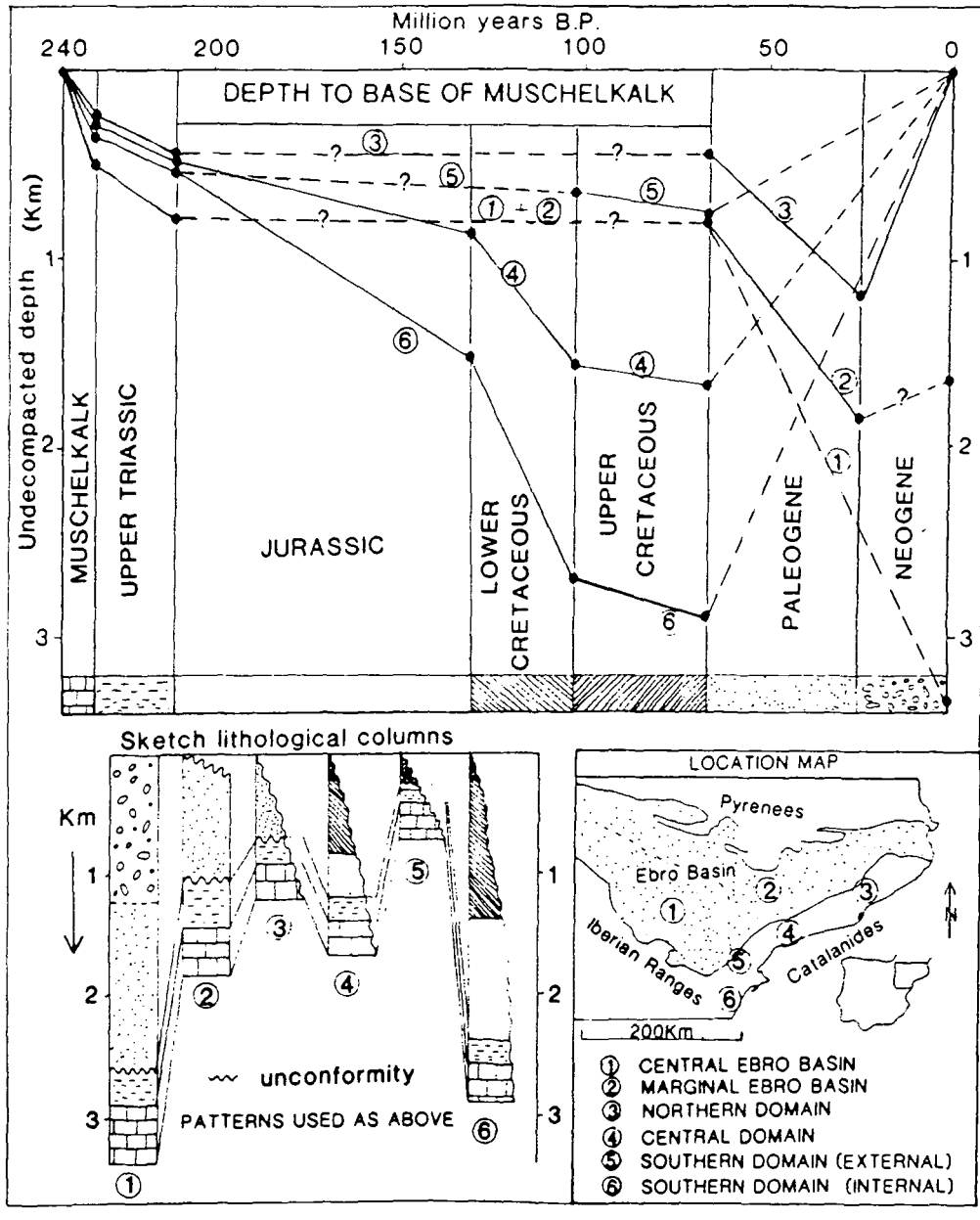

Fig. 2.11. Approximate time-depth curves to the base of the Muschelkalk together with sketch lithological columns for different areas of the Triassic of northeast Spain.

CHAPTER 3: LOWER MUSCHELKALK SEDIMENTOLOGY

3.1 INTRODUCTION

The Lower Muschelkalk of northeast Spain crops out in the Catalan Coastal Ranges and the eastern Iberian Ranges and has been penetrated by borehole in extensive areas of the Ebro Basin (Fig. 2.2; Jurado, 1988). Lateral age-equivalents to the Lower Muschelkalk also occur on the Balearic Islands (Freeman, 1972; Llompart *et al.*, 1987).

The Catalan Coastal Ranges are the principal study-area of this investigation but exposures have also been examined in the Iberian Ranges and compared with the reported nature of the Lower Muschelkalk from the Ebro Basin and the Balearic Islands. This chapter will concentrate on the macroscopic sedimentary features of the Lower Muschelkalk and the interpreted depositional environment. Petrography, diagenesis and particular aspects of the sedimentology such as oolites, tepees, karsts *etc.* will be considered in greater detail in Chapter 4.

3.2 CATALAN COASTAL RANGES

The Lower Muschelkalk of the Catalan Coastal Ranges was deposited in the so-called Catalan Basin and has been described by several workers (*e.g.* Virgili, 1958; Ramon, 1985; Ramon & Calvet, 1987). A generalised Triassic lithostratigraphy for the area is shown in Fig. 3.1. The Lower Muschelkalk is well exposed in the coastal hills and commonly forms prominent scarps. The recent study by Calvet & Ramon (1987) and subsequently by Calvet *et al.* (1990) subdivided the Lower Muschelkalk into four informal units, which from base to top are:

i) El Brull Unit: laminated limestones and dolomites.
ii) Olesa Unit: bioclastic limestones and dolomites.
iii) Vilella Baixa Unit: bioturbated limestones and dolomites.
iv) Colldejou Unit: laminated dolomicrites.

Much of the Triassic succession of the Catalan Basin exhibits regional thickness and stratigraphic variations which have been used to determine paleogeographical domains (Section 2.4.1). However, during the deposition of the Lower Muschelkalk the domains are not well defined and, in contrast to the Upper Muschelkalk (Calvet & Tucker, 1988), the general sequence and overall thickness is similar throughout the Catalan Coastal Ranges. However, some regional facies variations do occur, particularly in the Olesa Unit and Vilella Baixa Unit and these are discussed below.

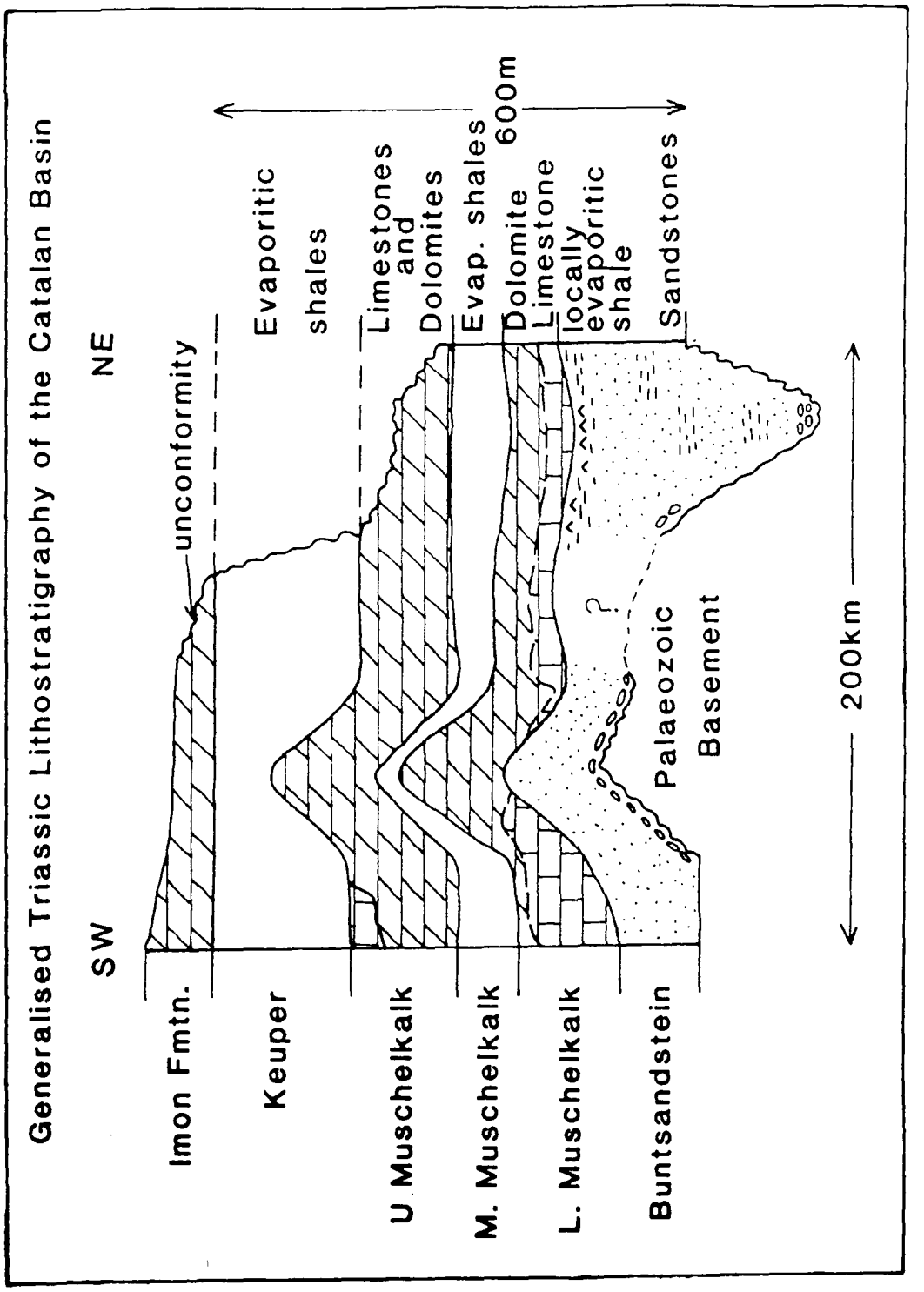

Fig. 3.1. Generalised Triassic lithostratigraphy of the Catalan Basin.

The localities mentioned in the text are shown in Fig. 3.2 and their exact locations are given in Appendix 1.

On a large scale the Lower Muschelkalk carbonates have been interpreted in terms of the carbonate ramp model (Ahr, 1973; Read, 1985; Tucker & Wright, 1990) and the various facies were deposited in the shallow ramp environment (see Section 3.6 for further discussion).

3.2.1 El Brull Unit

The El Brull Unit is the lowermost unit of the Lower Muschelkalk and is developed throughout the Catalan Coastal Ranges. Localities where the El Brull Unit has been examined are shown in Fig. 3.3 with some information regarding regional differences. Graphic logs of the El Brull Unit are shown in Fig.s 3.4 and 3.5.

The El Brull Unit varies in thickness from 5-14m and generally has a transitional contact with the underlying lutite-evaporite-carbonate complex of the uppermost Buntsandstein (Orti Cabo, 1982). The El Brull Unit commonly exhibits dedolomitization textures which obscure the sedimentary features (see Chapter 8). The principal characteristic of the El Brull Unit is the presence of peritidal sedimentary structures such as microbial lamination and stromatolites, tepees, fenestrae, pseudomorphs after evaporites, collapse breccias, sparse fauna and laminated dolomicrites (see Wright, 1984).

3.2.1.1 Lutite-evaporite-carbonate complex and lower El Brull Unit

The upper part of the lutite-evaporite-carbonate complex consists of finely-laminated shales which are banded into laterally persistent red and green layers on a decimetre scale (Fig. 3.6). Yellow, marly layers are also present and these contain fine sand to silt-grade subangular quartz grains, local detrital muscovite, patchy inclusion-rich ochre dolomite and ferroan calcite pseudomorphs after anhydrite. The lutite-evaporite-carbonate complex is interpreted to have been deposited on a supratidal evaporitic coastal mud-flat with salinas and areas of more permanent water with deposition of laminated evaporites (Marzo & Calvet, 1985).

The transitional contact with the overlying El Brull Unit is through two to three shale-carbonate cycles (Fig. 3.7). The shale layers are more calcareous in the upper cycles than in the lower and contain pseudomorphs after evaporites. The carbonate layers are 0.5-1.4m thick and consist of yellow-red-purple silty dolomite. The carbonate layers are locally brecciated with angular clasts of laminated dolomicrite containing stellate pseudomorphs after evaporites. These are interpreted as collapse breccias. Laminar to domal stromatolites, up to 10cm high, occur in some of the

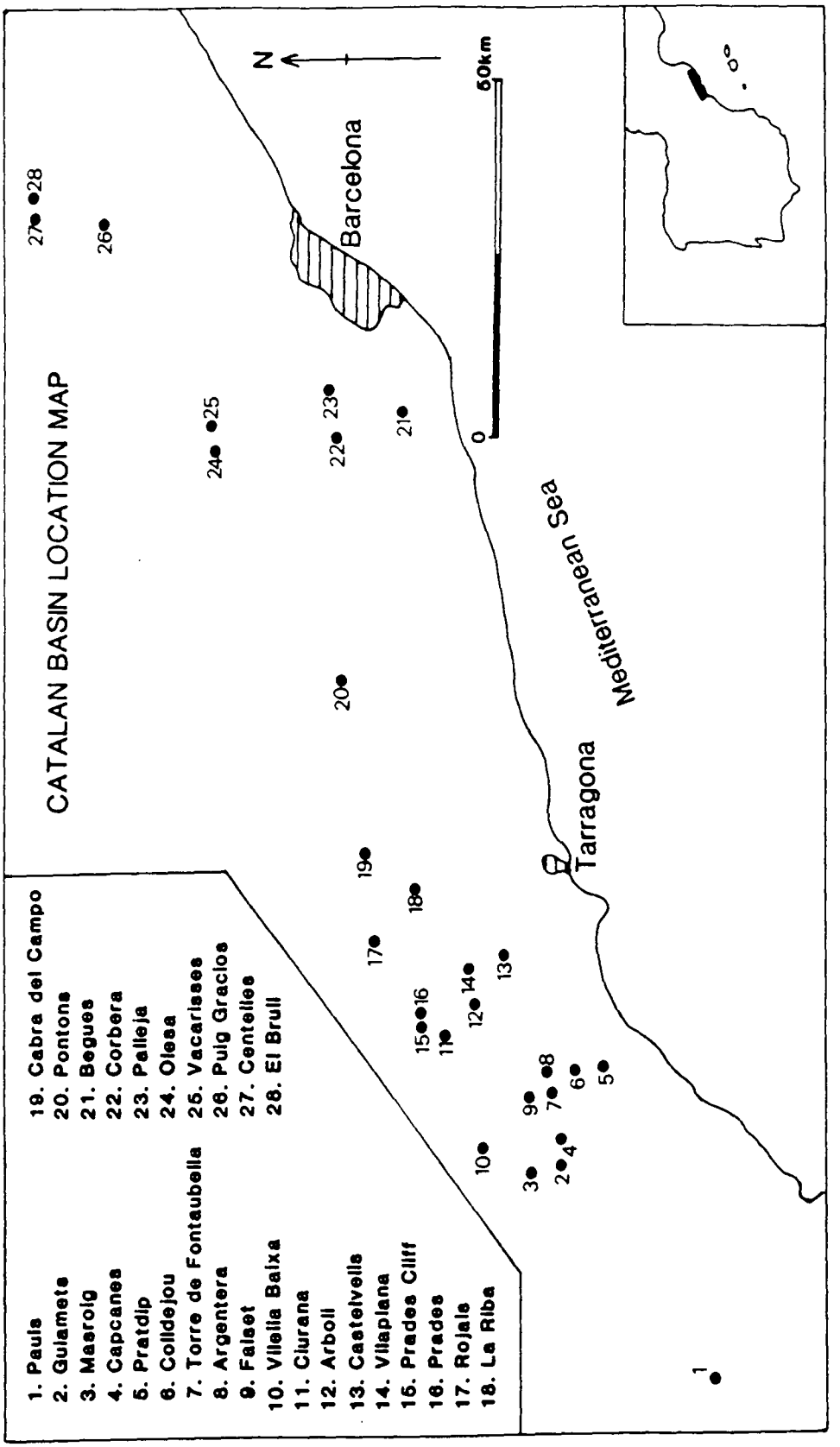

Fig. 3.2. Catalan Coastal Ranges locations map.

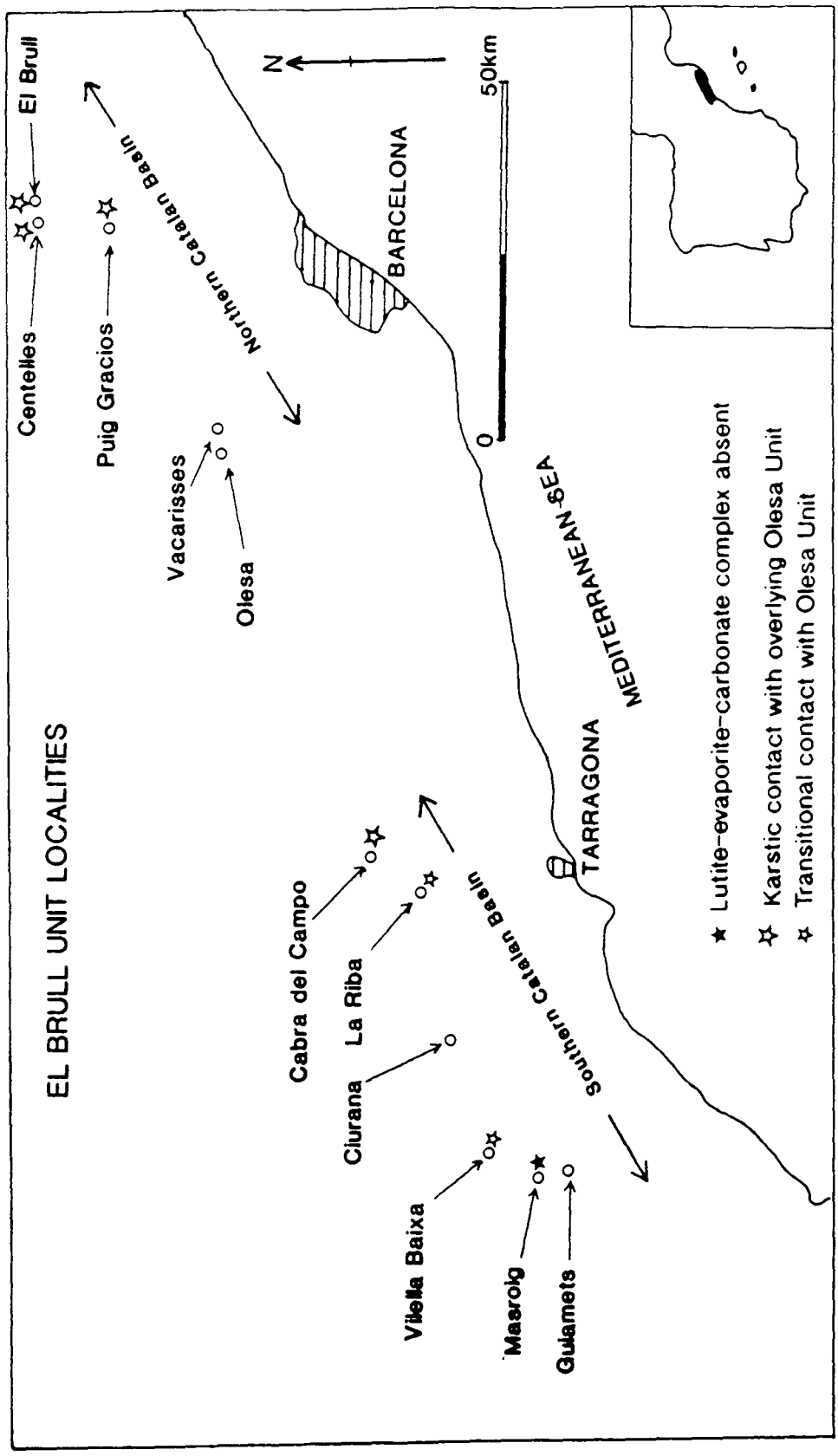

Fig. 3.3 El Brull Unit localities of the Catalan Coastal Ranges.

carbonate layers. The tops of the carbonate layers are sharp and at one locality (Ciurana; Fig.s 3.7 and 3.8) are laminated with small (10-20cm high) tepees and pseudoanticlines (see Section 4.5). The laminae of the shale layer of the next cycle fill the troughs between the tepees of the underlying carbonate horizon.

The shale-carbonate cycles are interpreted to have been deposited in a supratidal mud-flat to coastal salina environment with evaporite and carbonate deposition and local stromatolites and peritidal tepees.

In some areas (*e.g.* Masroig, Fig. 3.5) the lutite-evaporite-carbonate complex is not present and the El Brull Unit rests on red cross-bedded sandstones of the Buntsandstein and the shale-carbonate cycles are not present. The uppermost 10cm of sandstone has contorted bedding and is sharply overlain with a planar contact by laminated, fenestral quartzose dolomite with calcite pseudomorphs after gypsum suggesting that the sandstone was uncemented at the time of the onset of carbonate deposition.

3.2.1.2 Upper El Brull Unit in the northern Catalan Coastal Ranges

In the northern part of the Catalan Coastal Ranges (Fig. 3.4) the upper part of the El Brull Unit is up to 8m thick and consists of bioturbated grey mudstones and wackestones with peloids, echinoderm, gastropod and foraminiferal fragments which pass up into laminated ostracod-bearing wackestones with minor bioturbation. In this region the top of the El Brull Unit is marked by a laminated peloidal limestone which is locally dolomitic with silt-grade quartz, calcite pseudomorphs after evaporites and ?stromatolitic lamination. The intraformational karst that marks the upper contact of the El Brull Unit in the northern area is developed on this horizon (see Section 4.6). Below the karstic surface the dolomites are commonly calcitized (see Chapter 8). The limestone to dolomite sequence is interpreted to be produced by a shallowing-upward cycle from muddy, shallow-subtidal to supratidal deposits.

3.2.1.3 Upper El Brull Unit in the southern Catalan Coastal Ranges

In the southern part of the Catalan Coastal Ranges (Fig. 3.5) the upper part of the El Brull Unit consists of one to two dolomite-limestone cycles. The dolomite layers are up to 2m thick and consist of laminated dolomicrite with pseudomorphs after evaporites and pass up into bioturbated peloidal lime wackestones with echinoderm, ostracod and molluscan fragments. A thin graded oolitic layer, 0.2m thick, with a sharp erosive base is present in the bioclastic wackestones at Vilella Baixa. The uppermost limestone layers represent the transitional contact with the bioclastic limestones of the overlying Olesa Unit. The dolomite-limestone alternations are

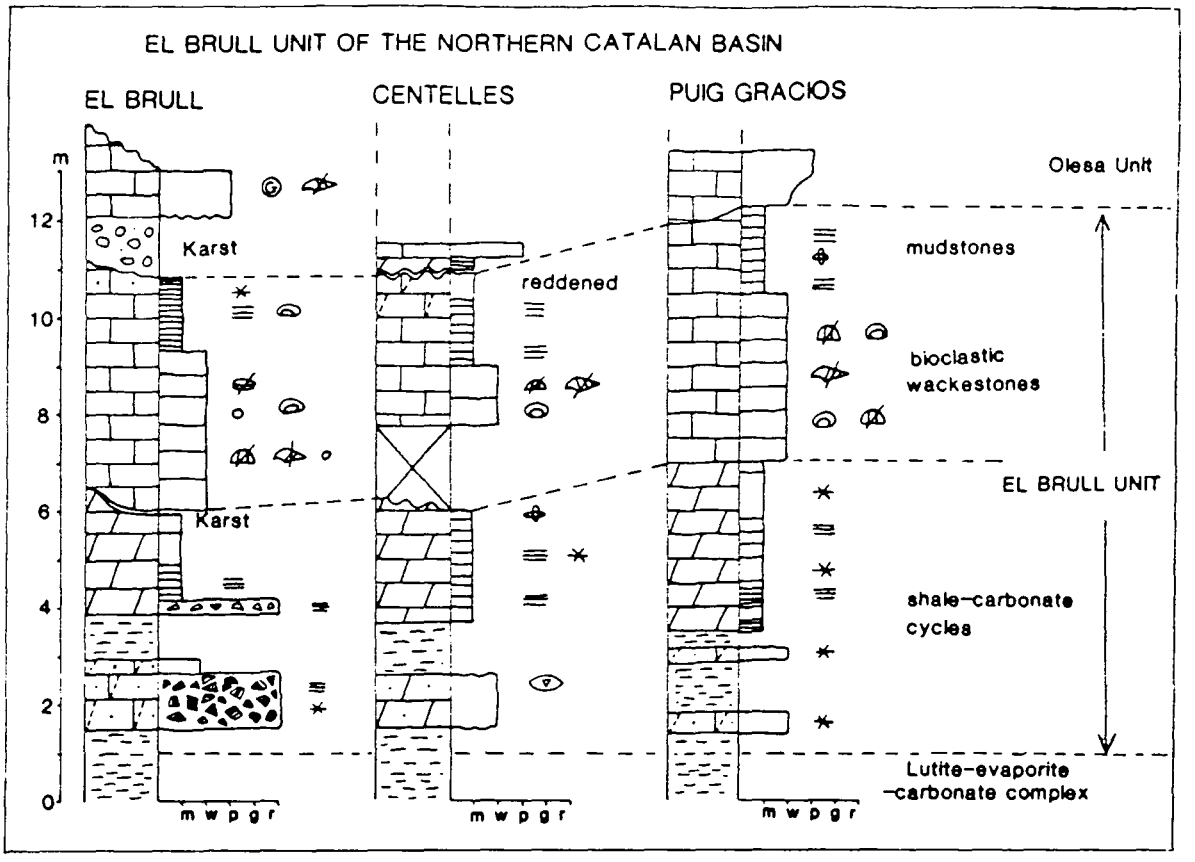

Fig. 3.4. Graphic logs of the El Brull Unit from the northern Catalan Coastal Ranges (for explanation of the symbols see Appendix 1).

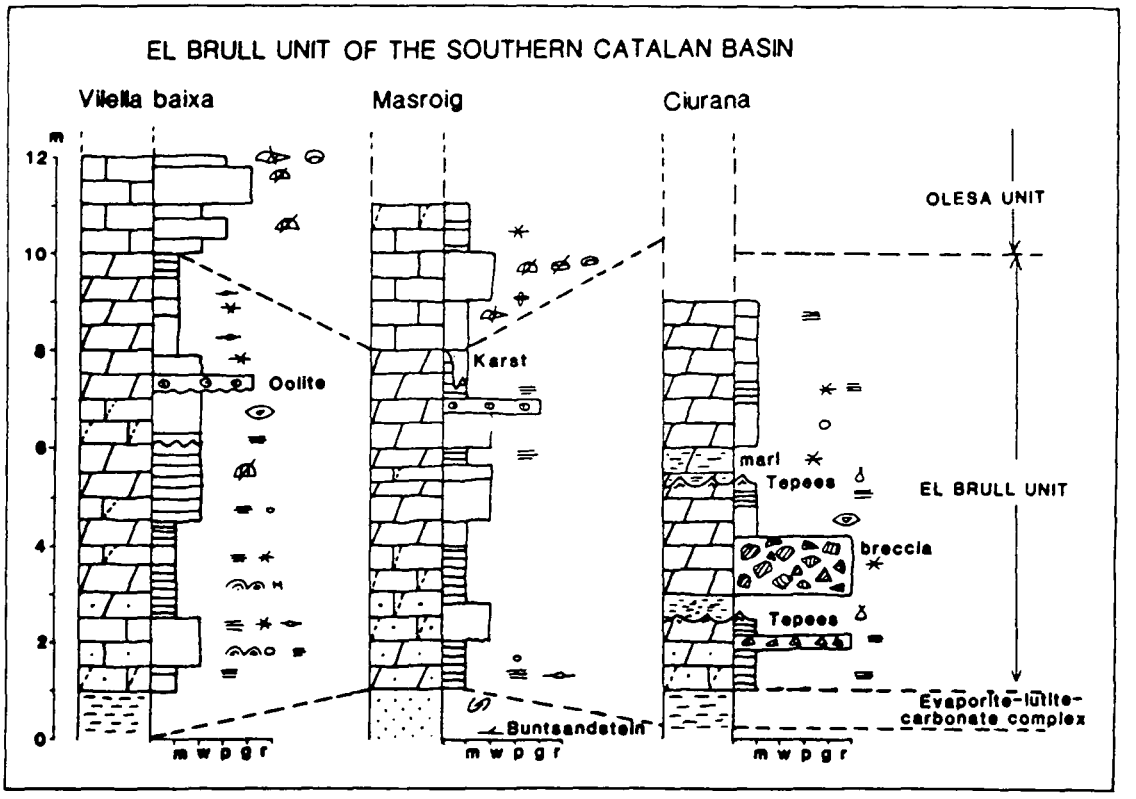

Fig. 3.5. Graphic logs of the El Brull Unit from the southern Catalan Coastal Ranges (for explanation of the symbols see Appendix 1).

Fig. 3.6. Laminated green and red shales of the evaporite-lutite-carbonate complex below the basal carbonate layer of the El Brull Unit. Centelles locality.

Fig. 3.7. Shale-carbonate cycles cycles at the base of the El Brull Unit. Ciurana locality.

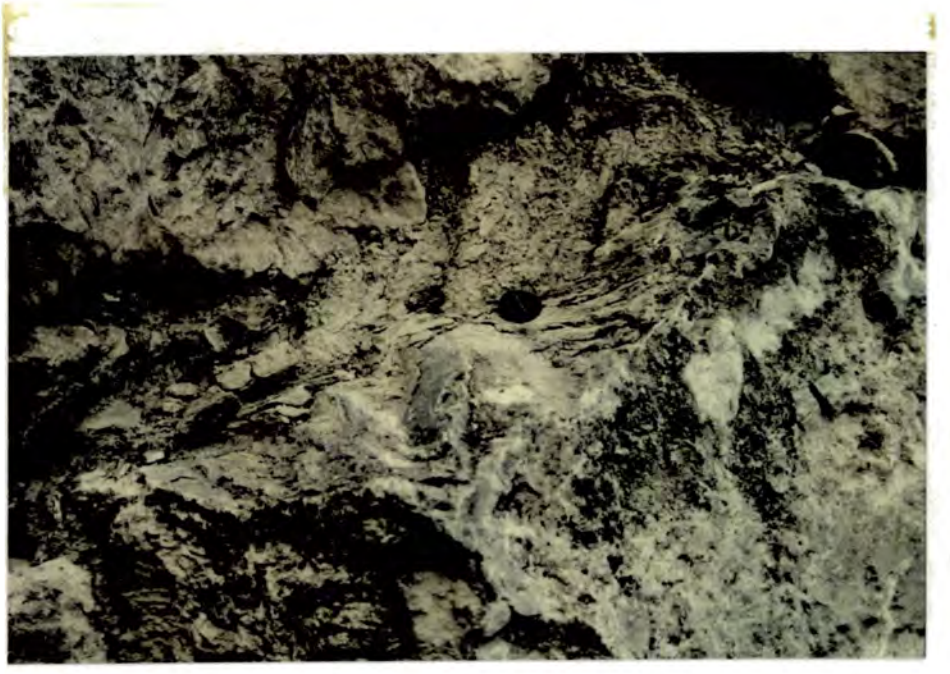

Fig. 3.8. Pseudoanticlines at the top of a shale-carbonate cycle covered and filled by the shale layer of the next cycle. Ciurana locality.

interpreted to be transgressive deepening-up cycles produced by the transition from peritidal dolomicrites into well-circulated lagoonal deposits with near-normal marine salinity. The thin oolitic layer may have been deposited as a spillover lobe from the oolitic shoals which lay further offshore. Similar but thicker spillover lobes have been described from the present-day Bahamas (Hine, 1977; and see Section 4.3 for discussion of oolites).

3.2.2 Olesa Unit

The Olesa Unit is 4-12m thick and consists of grey bioclastic limestones. Olesa Unit localities are shown in Fig. 3.9. In the northern part of the Catalan Coastal Ranges the Olesa Unit is well-developed and has a sharp base whereas towards the south the unit thins and has a transitional lower contact. Throughout the Catalan Coastal Ranges the top of the Olesa Unit is marked by a lithofacies change from the bioclastic limestones into laminated to bioturbated lime mudstones of the basal part of the Vilella Baixa Unit. In the central and southern part of the Catalan Coastal Ranges the Olesa Unit is commonly obscured by obliterative dolomitization and the exposure is generally poorer.

3.2.2.1 Olesa Unit in the northern Catalan Coastal Ranges

The Olesa Unit shows considerable uniformity over much of the northern part of the Catalan Coastal Ranges and some individual beds can be traced laterally for over 30km (Fig. 3.10). The base of the Olesa Unit is marked by an intraformational karst (see Section 4.6) overlain by a laminated, peloidal ostracod-bearing mudstone which passes upwards into more massive bioturbated wackestones and packstones with a diverse fauna of small gastropods, ostracods and bivalve and echinoderm debris. The wackestones and packstones are interpreted as well-oxygenated, near-normal salinity lagoonal deposits.

The top 1.5m of the Olesa Unit is marked by three cycles of wackestone overlain by a similar thickness of bioclastic packstone (Fig. 3.11). Each cycle is about 0.5m thick and the three packstone layers can be traced laterally for over 30km. The wackestone layers are finely laminated with a sparse fauna of ostracods, bivalve and echinoderm debris. Rare ceratite fossils (*Paraceratites sp.*) have been recovered from one of the wackestone layers at Olesa de Montserrat (Schmidt, 1932; Sole de Porta *et al.* 1987). The lamination is generally parallel and with clay seams and lenses. However, gentle, low-angle small-scale hummocky cross-stratification is locally present in the packstones (Fig. 3.12). The packstone layers have sharp bases and tops and are generally massive with no clear internal grading or structure. Locally the basal few centimetres of the beds are cross-laminated and the tops contain bed-parallel, oval-cross-section burrows

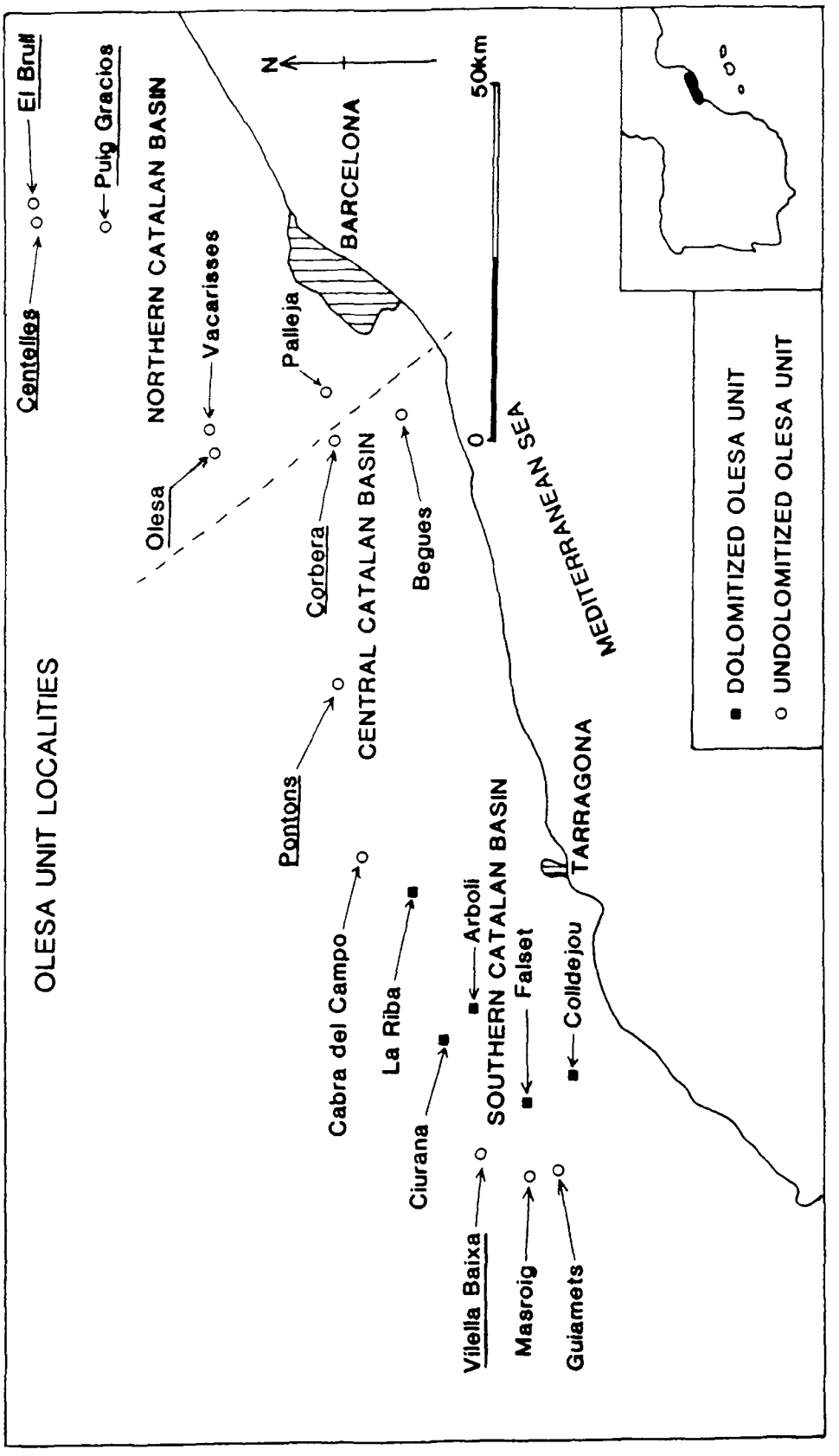

Fig. 3.9. Olesa Unit localities of the Catalan Coastal Ranges and regional variations.

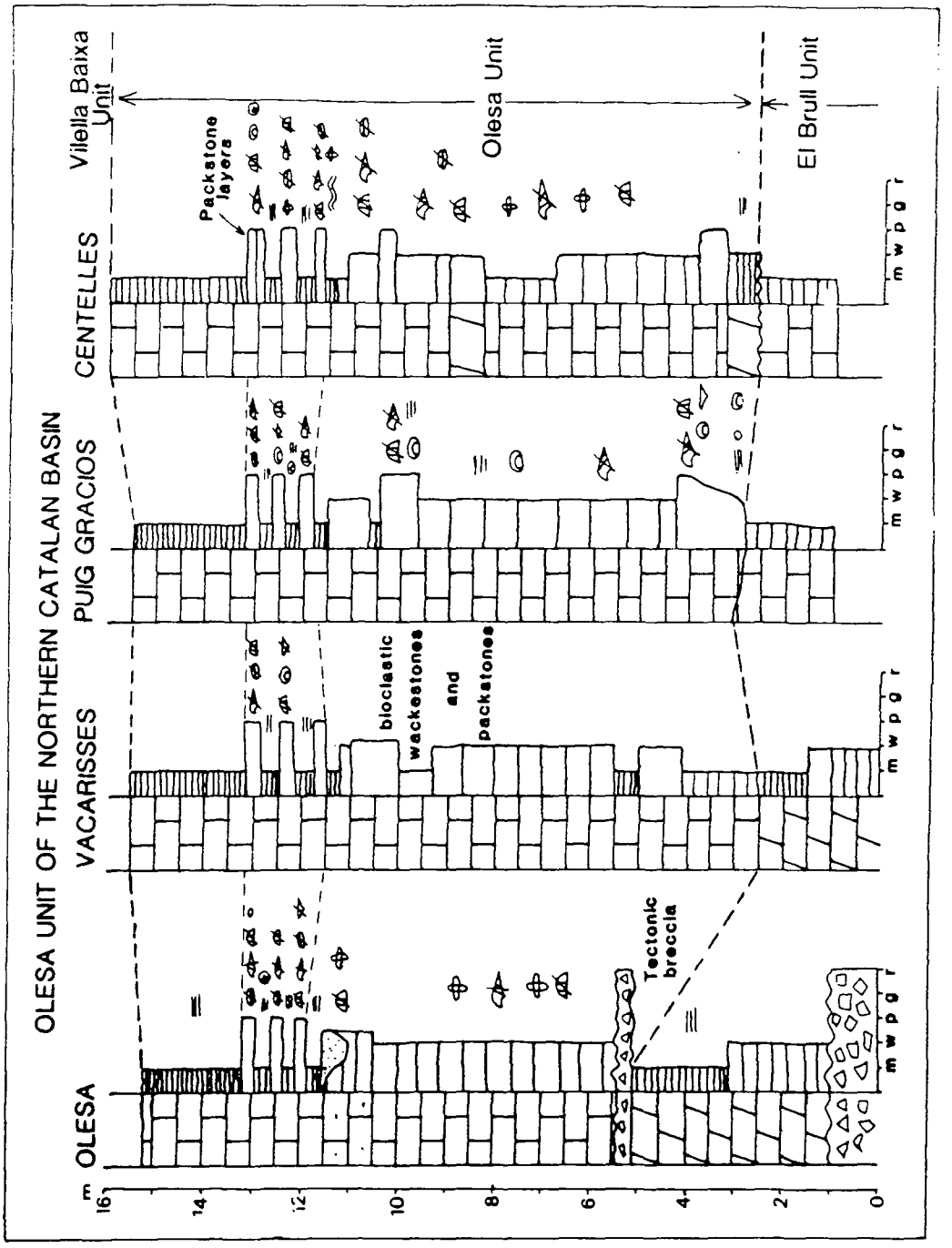

Fig. 3.10. Graphic logs of the Olesa Unit from the northern Catalan Coastal Ranges (for explanation of the symbols see Appendix 1).

(?*Planolites*). The packstone beds have an abundant and varied fauna of echinoderm debris, brachiopod and bivalve fragments, ostracods, foraminifera and small (less than 5mm) gastropods (Fig. 3.13). The uppermost packstone layer is overlain by laminated mudstones which are taken to mark the base of the Vilella Baixa Unit.

The packstone layers are interpreted as tempestites (Aigner, 1985). The wackestone layers represent background sedimentation below wave-base in a low-energy lagoonal setting. The rare pelagic ceratite fossils were presumably living in the upper, more oxygenated part of the lagoonal water column. The lack of bioturbation suggests hypersalinity and/or poorly oxygenated bottom waters reducing the benthos. The storm events resulted in minor hummocky cross-stratification and redeposition of bioclastic debris and lime-mud derived from the more open marine parts of the ramp. The lime-mud fraction would have remained in suspension and may have been transported shorewards in a similar way to the storm beds produced by cyclones on the Great Barrier Reef Shelf, Australia (Gagan *et al.*, 1988). The storm beds are well-preserved as a result of only minor bioturbation suggesting that the hypersaline/low oxygen bottom conditions must have rapidly reestablished after each storm event. The thickness and coarse bioclastic nature of the packstone layers suggests that these storm deposits were 'proximal' to their source area (Aigner, 1985).

3.2.2.2 Olesa Unit of the Central and Southern Catalan Coastal Ranges

Fabric-destructive dolomitization has affected much of the Olesa Unit in the Central and Southern Catalan Coastal Ranges and the original lithofacies cannot be determined (Fig. 3.14; Chapter 5). At localities where the Olesa Unit is undolomitized there are fossiliferous bioturbated wackestones to packstones and locally grainstones which commonly have a transitional lower contact with the El Brull Unit and a sharp upper contact with the laminated mudstones of the overlying Vilella Baixa Unit.

At Corbera, the three wackestone-packstone cycles described above in (i) are absent and the Olesa Unit consists of bioturbated wackestones and packstones with a rich and diverse marine fauna including small (up to 0.5mm) gastropods, ostracods, and echinoderm and thin-shelled bivalve fragments (Fig. 3.14). The packstones occur in discrete layers up to 1.3m thick and may represent coalesced storm layers.

At Pontons, the Olesa Unit includes three small-scale (up to 1.5m thick) coarsening-upwards cycles which grade from mudstones and wackestones into bioclastic packstones (Fig. 3.14). The top of one cycle consists of a 0.2m thick oobiopelsparite with well-sorted grains (less than 0.4mm across) of gastropod and echinoderm debris with isopachous fringing cement. These cycles are interpreted to be the products of migration of small ooid and bioclastic shoals in agitated well-oxygenated waters in

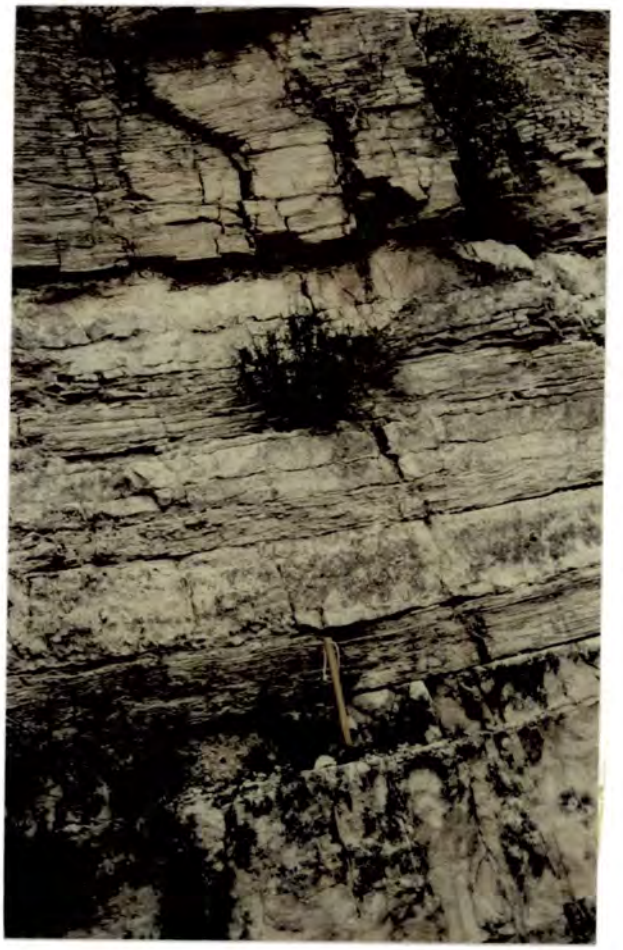

Fig. 3.11. Three regionally extensive packstone layers interbedded with laminated wackestones. Olesa Unit. Centelles locality.

Fig. 3.12. Small-scale hummocky cross-stratification in one of the regionally extensive packstone layers. Olesa Unit. Centelles locality.

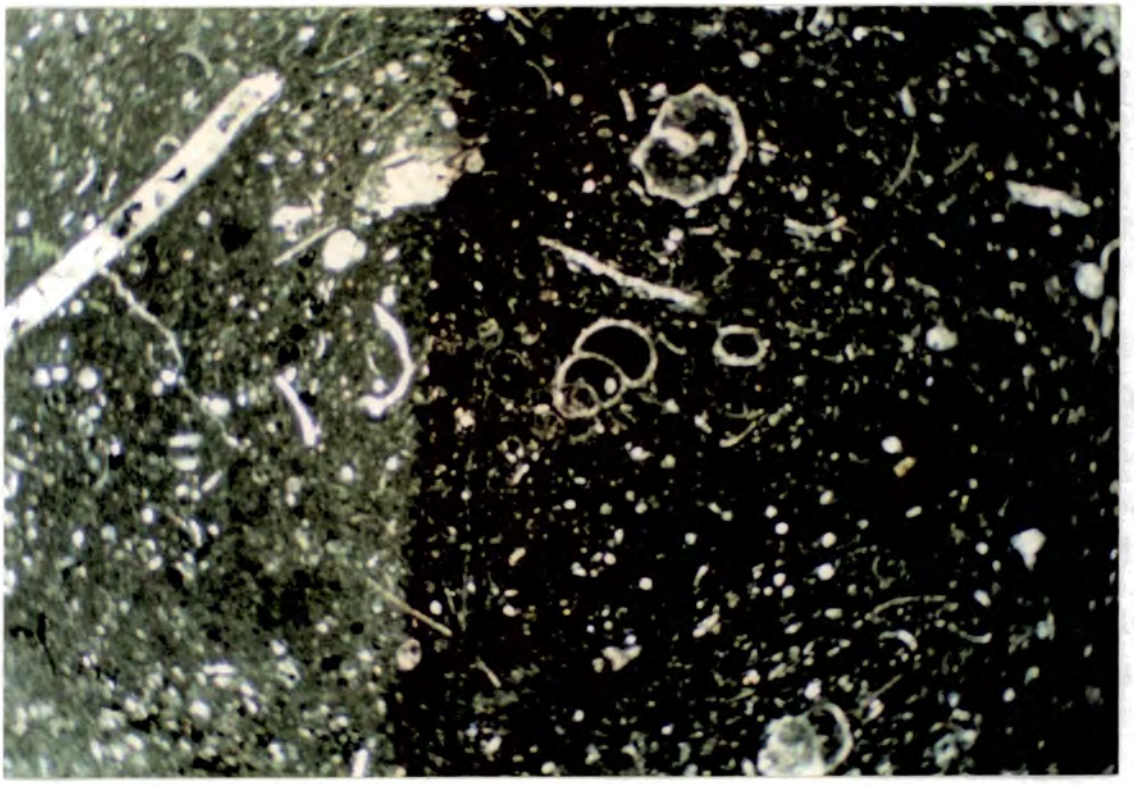

Fig. 3.13 Photomicrograph of regionally extensive bioclastic packstone layer with abundant molluscan debris. [Half stained thin section. XPL. PG24. Width of view = 14mm]

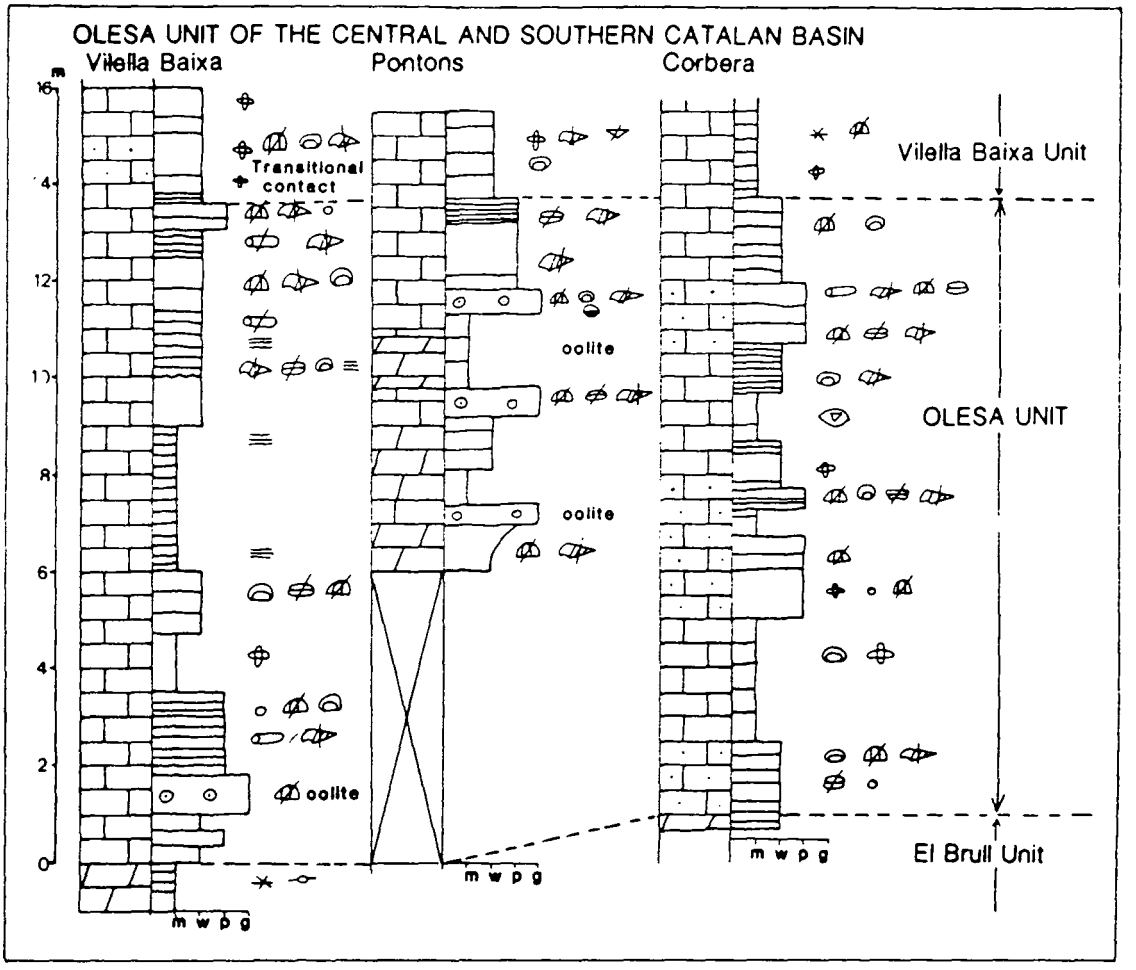

Fig. 3.14. Graphic logs of the Olesa Unit from the central and southern Catalan Coastal Ranges (for explanation of the symbols see Appendix 1).

relatively open conditions associated with early marine cementation and mark the position of the onset of sand-belt deposition on the carbonate ramp (for discussion of the oolites see Section 4.3; and sand-belt review see Handford, 1988).

At Vilella Baixa, the Olesa Unit has a transitional lower contact with the underlying El Brull Unit, and consists of about 10-12m of laminated bioclastic wackestones to packstones which are locally bioturbated and more massive. The distinction between the Olesa Unit and the cycles present in the lower part of the overlying Vilella Baixa Unit is not as marked at this locality as further to the northeast in the Catalan Coastal Ranges.

Thus, in the central and southern Catalan Coastal Ranges the Olesa Unit represents more open marine conditions with richer and more diverse fauna, greater bioturbation, and local development of oobioclastic shoals than in the northern Catalan Coastal Ranges where there were more lagoonal conditions and periods of low benthic population and little bioturbation.

3.2.3 Vilella Baixa Unit

The Vilella Baixa Unit exhibits considerable lateral variations in the Catalan Coastal Ranges (Fig. 3.15). The Vilella Baixa Unit varies in thickness from 30-40m, increasing towards the southwest, and generally consists of coarsening-upwards cycles from thin laminated or bioturbated mudstones to thicker bioclastic packstones and grainstones. The cycles are much better developed towards the southwest where dasycladacean algal packstones and oolitic grainstones are common. Dolomitization has commonly obliterated the depositional facies of at least the upper part of the Vilella Baixa Unit. The upper boundary of the Vilella Baixa Unit is generally a sharp contact between dolomitized grainstones and laminated dolomicrites of the overlying Colldejou Unit (see Section 3.24). However, locally the boundary is not sharp and the transition is gradual. The Vilella Baixa Unit will be described from a number of different areas (Fig. 3.15).

3.2.3.1 Area 1 (Northern Catalan Coastal Ranges)

The Vilella Baixa Unit shows considerable lateral facies continuity in this area and is 30-35m thick consisting of two coarsening-upwards cycles (Fig. 3.16).

The lower cycle is 8-15m thick, rests sharply upon the uppermost packstone layer of the Olesa Unit and consists of laminated mudstones which pass upwards through a number of thin (0.5-1.0m) bioturbated mudstone/wackestone horizons into bioturbated and locally rippled peloidal wackestones with echinoderm, gastropod and

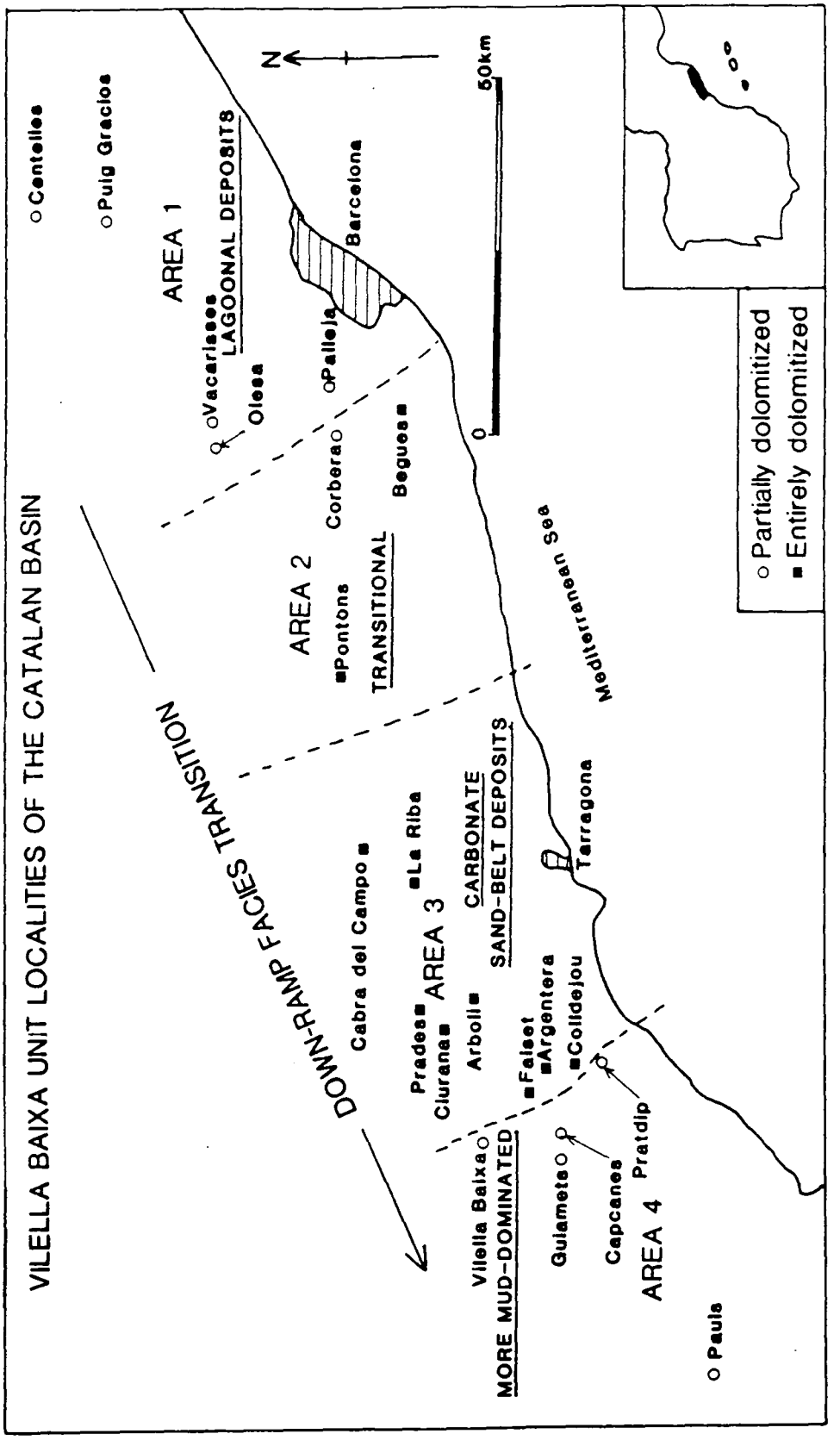

Fig. 3.15. Vilella Baixa Unit localities of the Catalan Coastal Ranges and regional variations.

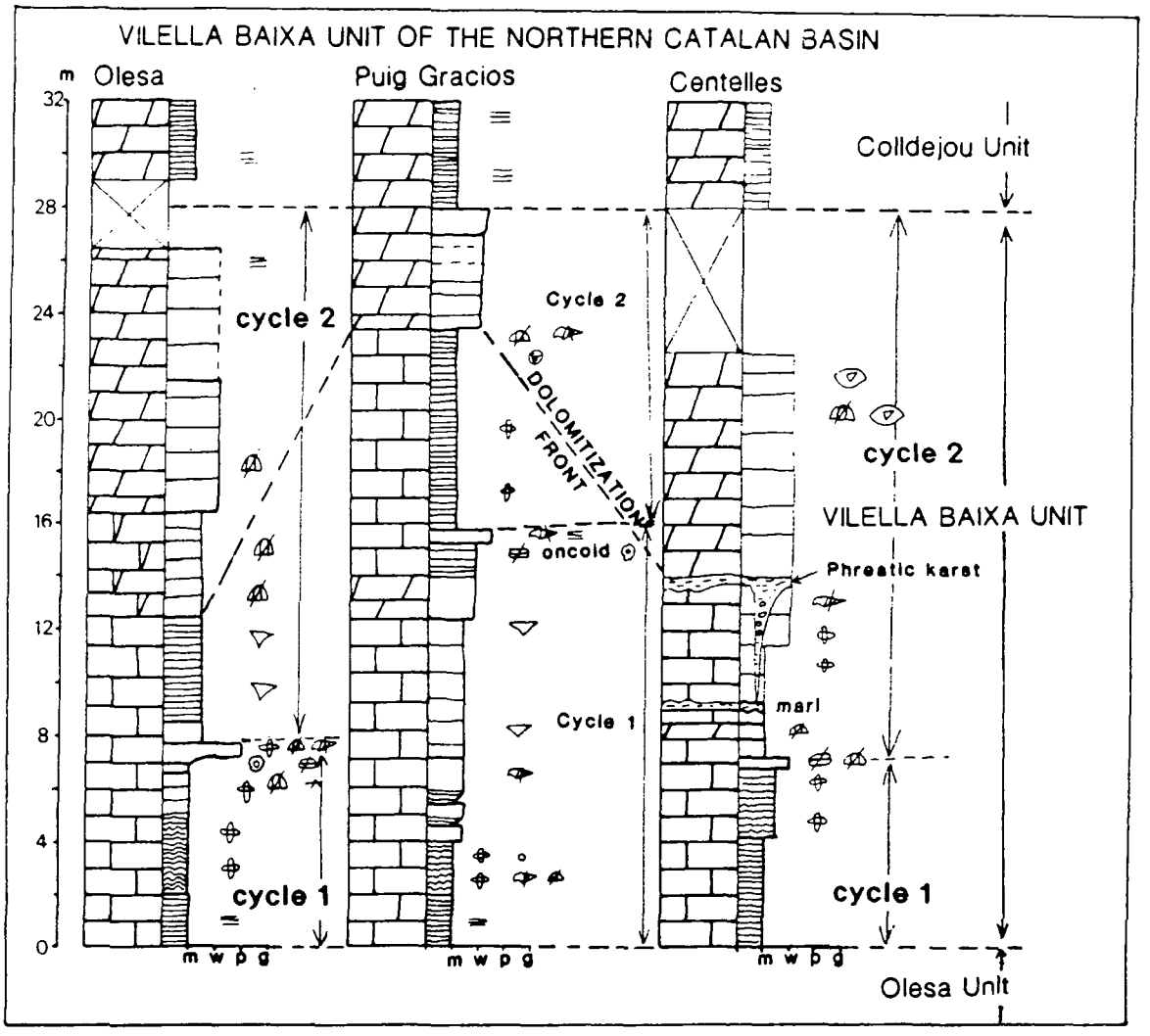

Fig. 3.16. Graphic logs of the Vilella Baixa Unit from the northern Catalan Coastal Ranges (for explanation of the symbols see Appendix 1).

bivalve debris. The top of the cycle is marked by a massive sharp-based oncoidal and bioclastic packstone (Fig. 3.16).

The upper cycle is similar to the lower but contains whole unabraded brachiopod fossils (*Mentzelia mentzeli*; Section 4.2.10) in the bioturbated mudstones and wackestones and the top of the cycle is generally obscured by fabric-destructive dolomitization. The brachiopod fossils are considered to be preserved in life position and the paleoenvironment as low-energy and restricted (Calzada & Gaetani, 1977).

These two cycles are interpreted as the products of shallowing-upwards from unbioturbated lagoonal mudstones to less restricted wackestones and packstones deposited above wave-base. The mudstone-wackestone alternations may be produced by migration of mud-banks similar to those described in Florida (*e.g.* Bosence *et al.*, 1985). In contrast to the rest of the Catalan Coastal Ranges oolites are absent, suggesting that in this area oolite shoals were not developed and that the deposition was essentially lagoonal.

3.2.3.2 Area 2 (Corbera-Pontons)

The Vilella Baixa Unit is 35m thick at Corbera and consists of four cycles (Fig. 3.17). The lower three cycles are 5-10m thick and are similar to the lagoonal, shallowing-up cycles described for Area 1. The uppermost cycle, however, is more complex and consists of laminated to bioturbated mudstones passing upwards into more massive bioturbated wackestones capped by 1.5m of massive oolitic and bioclastic grainstone which marks the top of the Vilella Baixa Unit. Two thin (0.2m and 0.3m) laterally persistent, cross-laminated oolitic grainstone horizons with sharp bases and tops also occur towards the top of the cycle. This mud-shoal cycle is interpreted as representing the transition from lagoonal to oolitic sand-belt deposits. The two thin oolite layers may represent tidal deltas or thin spillover lobes directed back into the lagoon from the seaward oolitic shoals.

The Vilella Baixa Unit at Pontons (Fig. 3.17) is similar to that of Corbera and also consists of shallowing-up cycles.

3.2.3.3 Area 3 (Central Catalan Coastal Ranges)

The Vilella Baixa Unit in this area is more varied than to the north-west (Areas 1 and 2).The Vilella Baixa Unit at La Riba (Fig. 3.18), although only partially exposed, contains a mud-shoal cycle capped by an oolitic grainstone similar to that described in Corbera. The oolites in this region are locally pisolitic and are interpreted as ooid shoals which have become emergent and been subjected to meteoric diagenesis and *in situ* pisolite growth (see Section 4.3.1). A thick (4m) dasycladacean algal packstone is

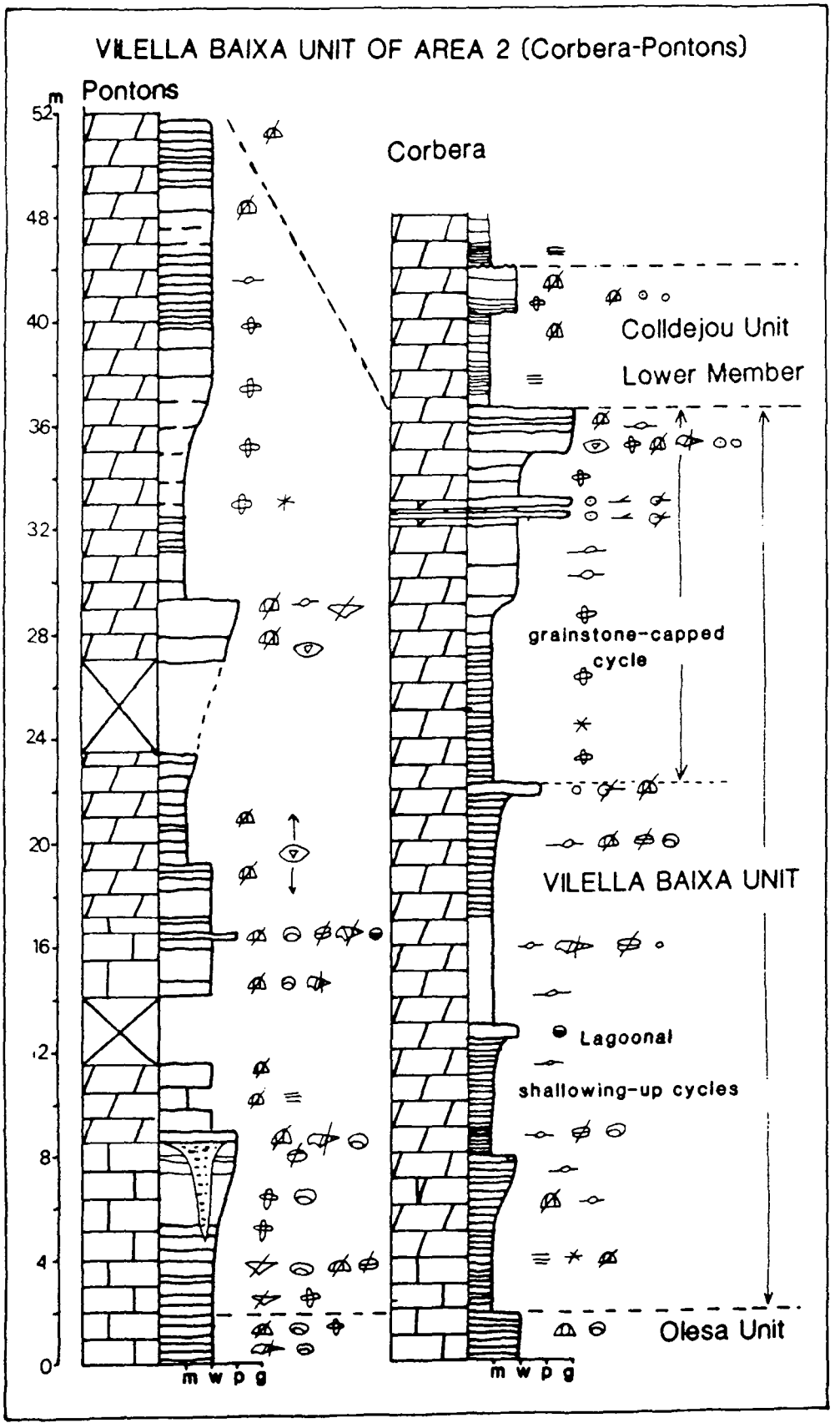

Fig. 3.17. Graphic logs of the Vilella Baixa Unit from Area 2 (Corbera-Pontons). For explanation of the symbols see Appendix 1.

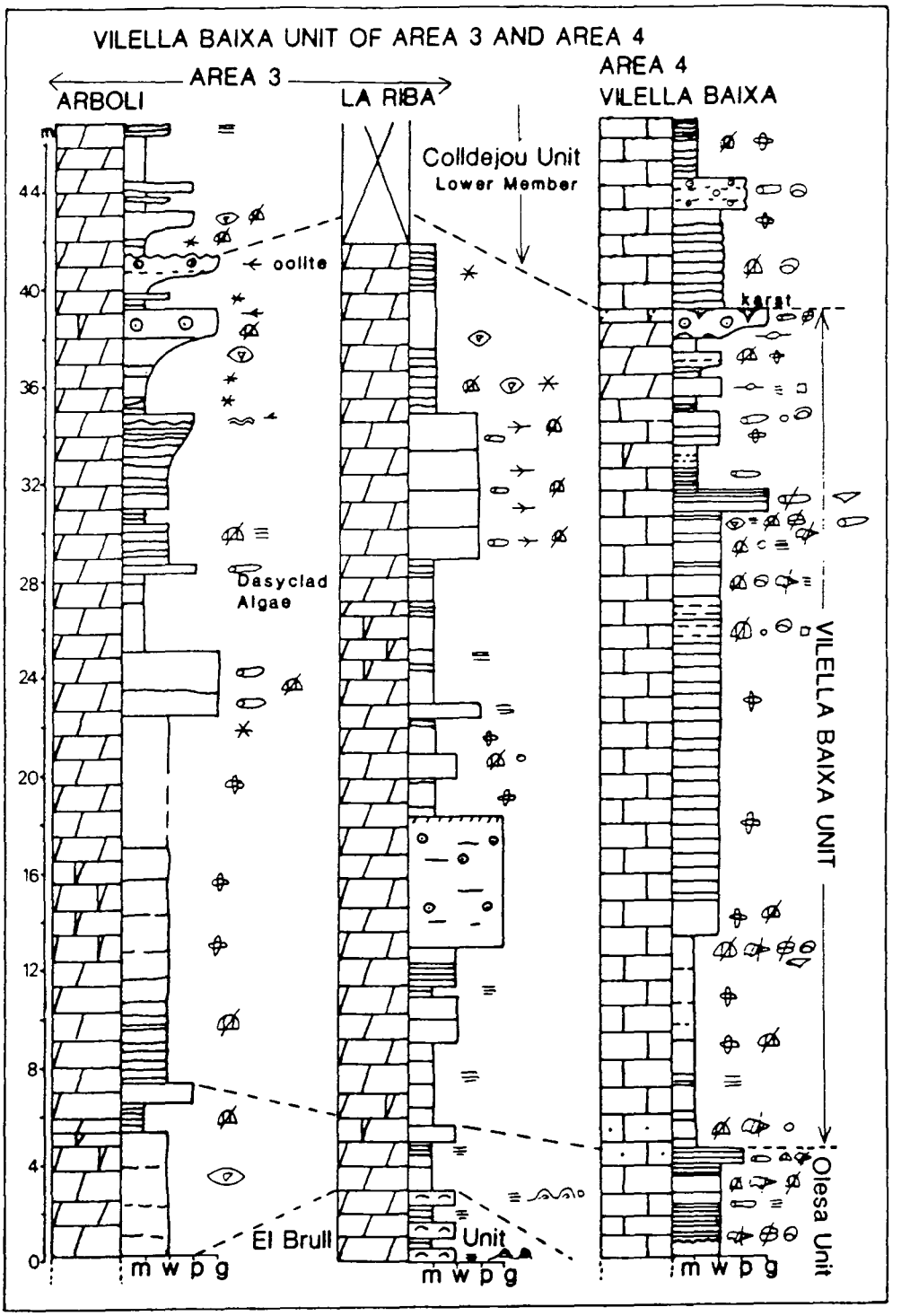

Fig. 3.18. Graphic logs of the Vilella Baixa Unit from Area 3 (Central Catalan Coastal Ranges) and Area 4 (Southern Catalan Coastal Ranges). For explanation of the symbols see Appendix 1.

Fig. 3.19. Mud-shoal cycle from the Vilella Baixa Unit at Arboli. Mudstones and wackestones with a normal marine fauna pass upwards into a cross-laminated, sharp-topped and locally karstified oolite.

also present which displays herring-bone cross-lamination and contains oncolites and intraclasts. Similar algal packstones are known to accumulate in modern tidal channels, *e.g.* in the Bahamas, and they may also occur in association with oolite shoals (Bathurst, 1975).

The Vilella Baixa Unit is well exposed at Arboli (Fig. 3.18) and contains a number of coarsening and thickening-upwards cycles. Dasycladacean algal packstones are common and three mud-shoal cycles (each 3-4m thick) are well-developed. The tops of the cycles are marked by 0.5-1.0m thick cross-laminated oolites with bipolar paleocurrent directions, interpreted to be the deposits of tidal oolite shoals (Fig. 3.19). The tops of the oolites are sharp and locally microkarstic (see Section 4.6.1.1).

In the Central Catalan Coastal Ranges the top of the Vilella Baixa Unit is a sharp contact between the dolomitized oolitic sands at the top of one of the mud-shoal cycles and overlying laminated dolomicrites of the Colldejou Unit.

3.2.3.4 Area 4 (Southern Catalan Coastal Ranges)

The Vilella Baixa Unit is generally not well exposed in this area; however, at the eponymous locality the exposure is excellent and the unit is 40m thick and more mud-dominated than in Area 3 (Fig. 3.18). The lower 25m consist of laminated to poorly and well-bioturbated peloidal wackestones with a sparse fauna of ostracods, and bivalve and echinoderm debris. This sequence is capped by a dasycladacean bioclastic packstone. The upper part of the unit consists of small-scale (2-4m) mud-shoal cycles with oolites and algal packstones. The upper contact of the Vilella Baixa Unit in this area is transitional and not sharp.

The Vilella Baixa Unit in this area is interpreted as lagoonal deposits which pass upwards into the tidal channel and oolitic shoal sediments similar to those described for Area 3.

3.2.4 Colldejou Unit

The Colldejou Unit is 20-40m thick and can be considered in two parts: a transitional lower member, only locally developed, and an upper laminated dolomicrite member (Fig. 3.20).

3.2.4.1 Transitional lower Member

The transitional lower member of the Colldejou Unit has a maximum thickness of about 19m and is only developed in certain areas (Fig. 3.20). The lower member is distinguished from the underlying Vilella Baixa Unit on the basis of a decrease in

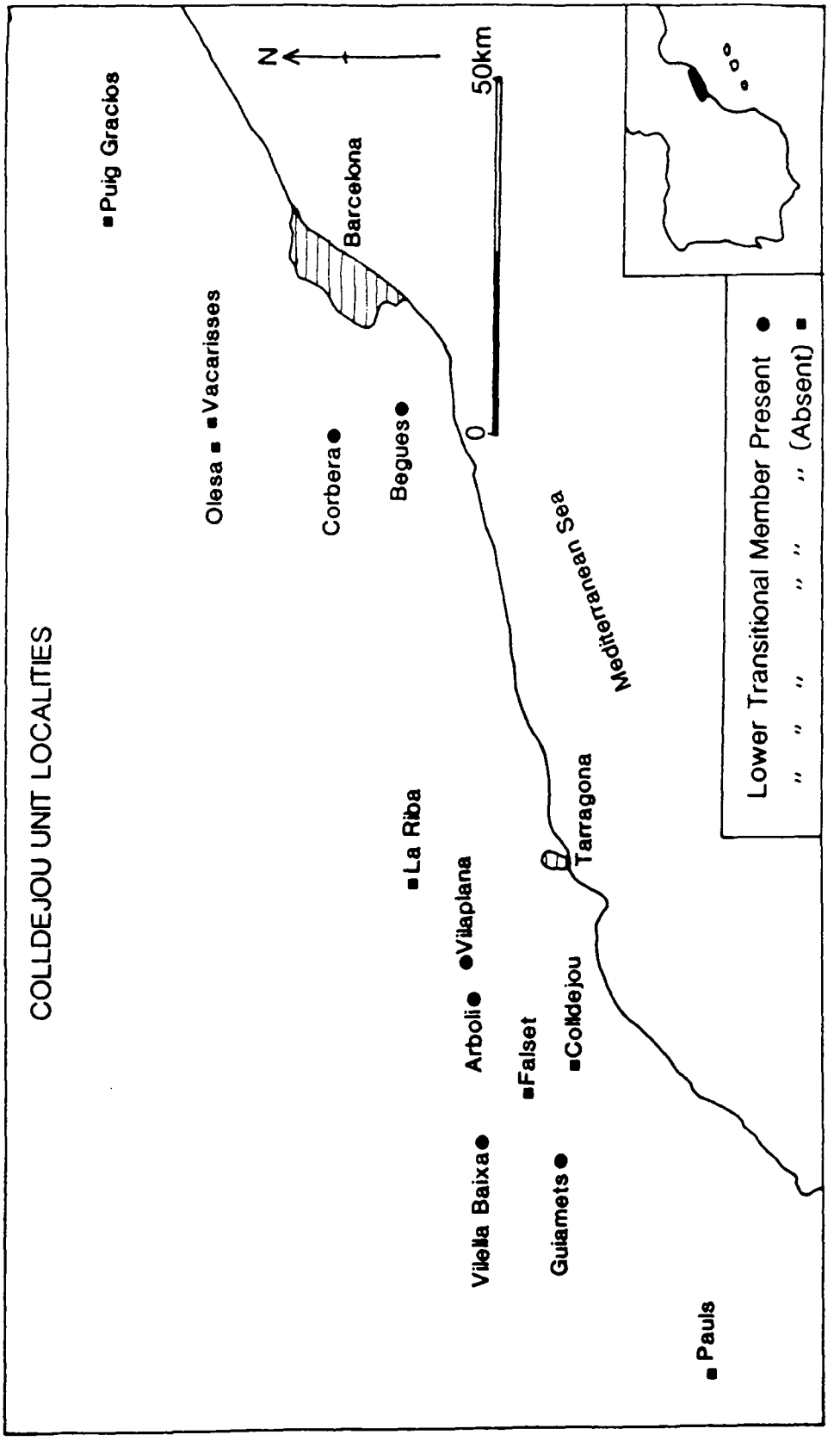

Fig. 3.20. Colldejou Unit localities of the Catalan Coastal Ranges.

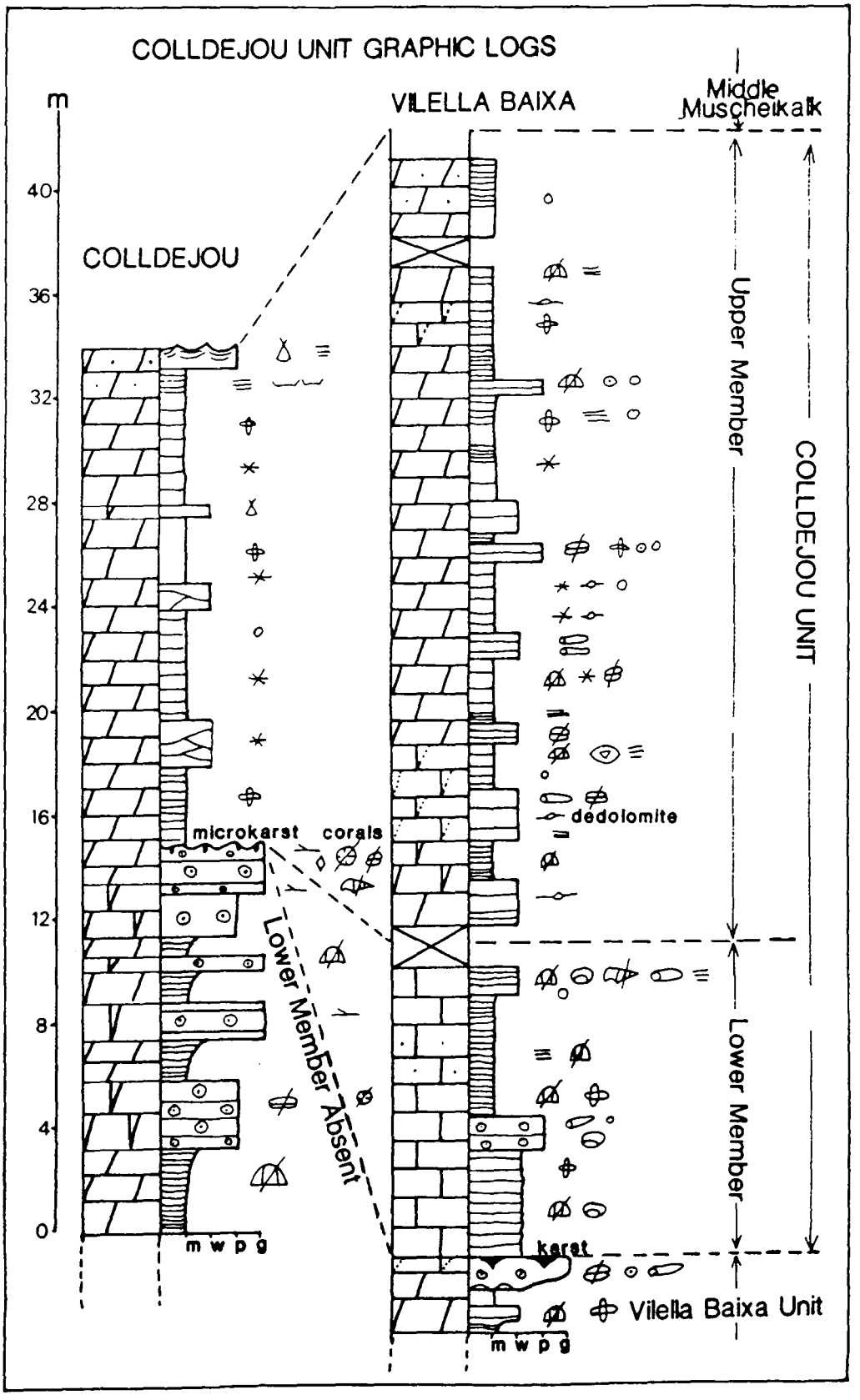

Fig. 3.21. Graphic logs of the Colldejou Unit from Vilella Baixa locality (Lower Member of the Colldejou Unit present) and Colldejou locality (Lower Member absent). For explanation of the symbols see Appendix 1.

faunal diversity and abundance, and the laminated, fine-grained nature of the sediments which suggests a lower energy environment. The abundance of fauna tends to decrease upwards through the transitional member.

At Vilella Baixa the transitional lower member is 16m thick and is only partially dolomitized. The principal facies are i) bioturbated and locally laminated peloidal mudstones/wackestones with a sparse fauna of ostracods and echinoderm debris, and ii) dasycladacean algal wackestones and packstones with minor ostracod, gastropod and echinoderm debris (Fig. 3.20). Thin sharp-topped oolitic and bioclastic horizons, up to 0.5m thick are present at some of the localities (*e.g.* Arboli).

Several exposures of the lower transitional member contain lenticular beds, up to 1.0m thick which pinch out laterally. The morphology of the lenticular layers is interpreted to be the result of subaerial exposure and karstic processes and represents original topography at the time of deposition of the overlying dolomicrites (see Section 4.6.1.2).

The depositional environment of the lower member of the Colldejou Unit is interpreted to be shallow subtidal to lower intertidal with local emergence and erosion.

3.2.4.2 Upper laminated dolomicrite member (Fig.s 3.21, 3.22, 3.23)

The upper member of the Colldejou Unit varies in thickness from 10-20m and consists almost exclusively of grey-white laminated dolomicrites with abundant stellate pseudomorphs after evaporites (Section 4.8). Bioturbated horizons and layers of peloidal grainstone are common. Where the lower member is not present the laminated dolomicrites rest directly upon dolomitized oolites of the Vilella Baixa in a widely developed disconformity which is interpreted to be locally microkarstified (Fig. 3.24; Section 4.6.1.1). Much of the lamination is fine-scale and probably microbial with laminoid fenestrae. At one locality a small, 10cm high domal stromatolite is preserved projecting above a laminated horizon. At other localities larger laterally-linked hemispheroidal stromatolites are present (Fig. 3.25). Towards the top of the upper member pseudomorphs after evaporites become more common and polygonal desiccation cracks occur.

The top of the upper member is generally marked by tepees and pseudoanticlines up to 0.5m in amplitude (for discussion of tepees see Section 4.5). Dedolomitization has commonly occurred (Chapter 8). A laminated crust developed at the top of the upper member in the northern Catalan Coastal Ranges has been interpreted as a caliche crust by Esteban *et al.* (1977) and there is a sharp contact with the overlying Middle

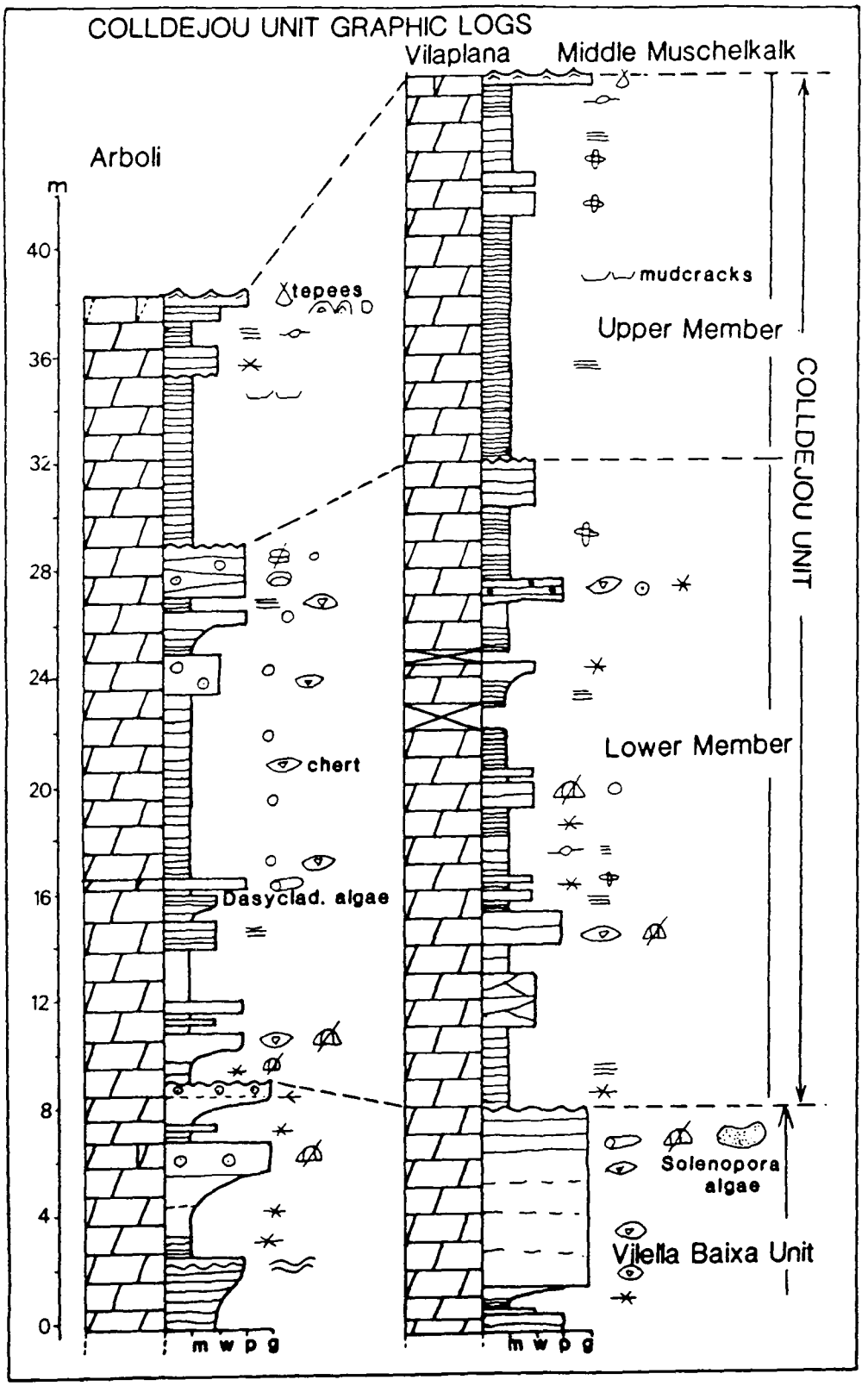

Fig. 3.22. Graphic logs of the Colldejou Unit. For explanation of the symbols see Appendix 1.

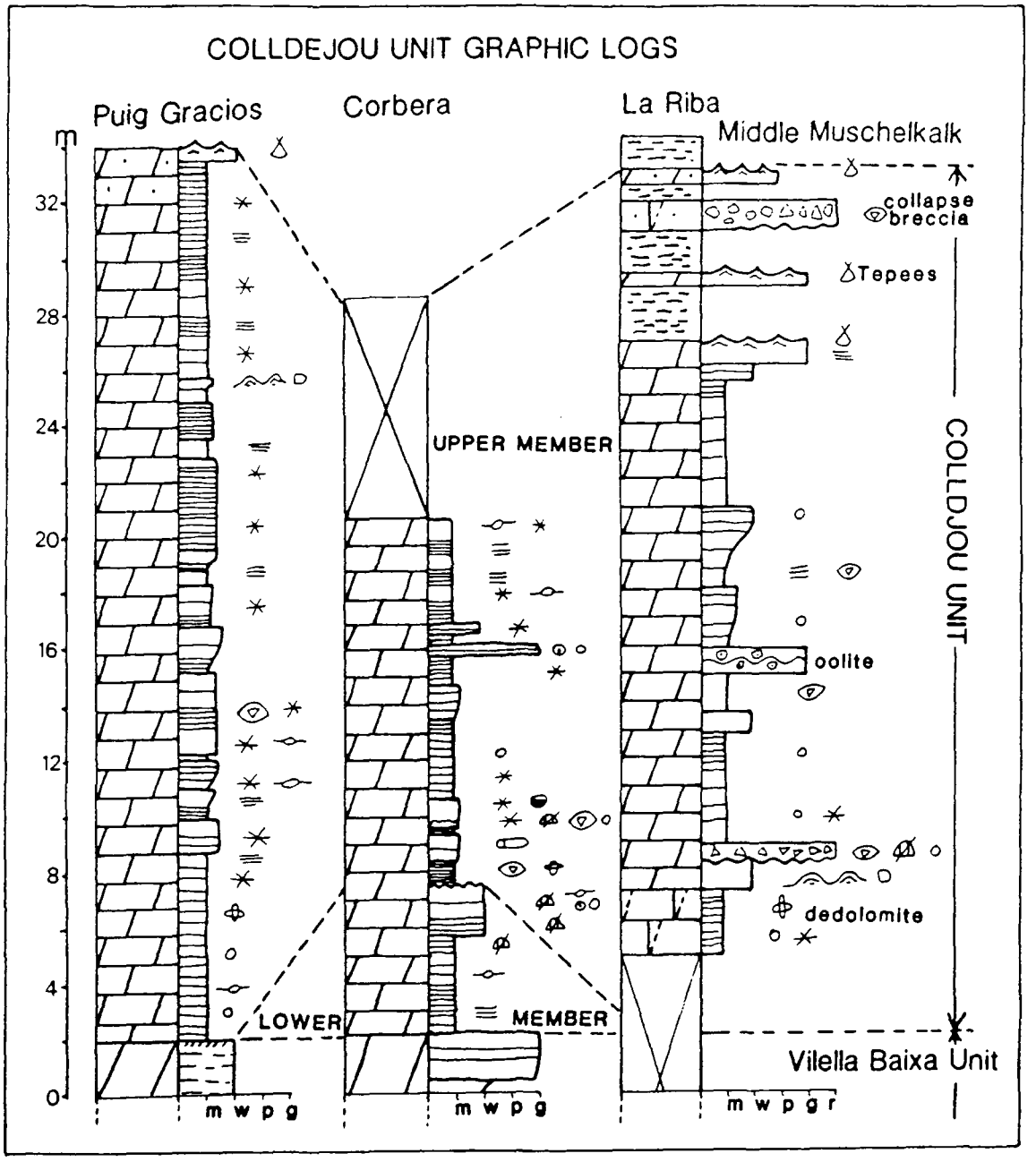

Fig. 3.23. Graphic logs of the Colldejou Unit. For explanation of the symbols see Appendix 1.

Fig. 3.24. Contact between laminated dolomicrites of the Upper Member of the Colldejou Unit and dolomitized oolite of theVilella Baixa Unit. The contact is sharp and is locally microkarstified. Colldejou locality.

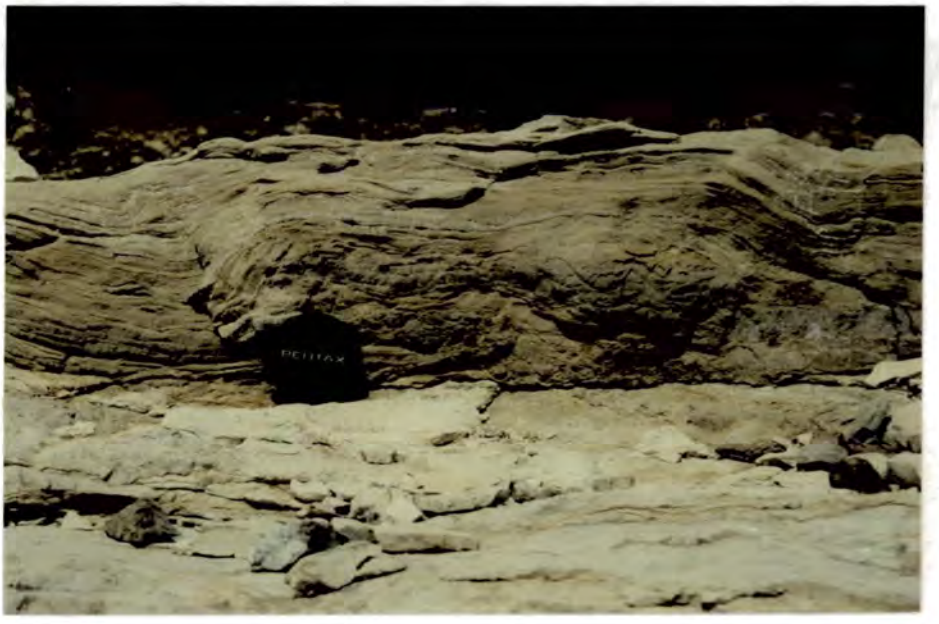

Fig. 3.25. Stromatolitic lamination near the top of the Colldejou Unit. Arboli locality.

Muschelkalk evaporitic shales. In some areas (*e.g.* at La Riba, Fig. 3.23) the contact is more transitional through a number of red marly shale horizons (*ca.* 1.0m thick) interlayered with carbonate beds containing tepees and collapse breccias. The basal part of the Middle Muschelkalk includes nodular chicken-wire gypsum as well as laminated evaporite horizons (Fig.s 3.26, 3.27).

The depositional environment of the upper member of the Colldejou Unit is interpreted as intertidal to supratidal with carbonate deposition, passing into sabkha evaporite and shales.

3.2.5 Synthesis of Catalan Basin Lower Muschelkalk sedimentology

The lower three units of the Lower Muschelkalk represent a broadly transgressive sequence from evaporative mud-flat and peritidal deposits (uppermost Buntsandstein and El Brull Unit) to well-oxygenated, normal salinity lagoonal/marine environment (Olesa Unit) and into the sand-belt/oolitic shoal and lagoonal deposits of the Vilella Baixa Unit. The regional thickness and facies variations indicate that there is no shelf-edge break of slope preserved in the Catalan Basin and the overall depositional environment can be interpreted in terms of the carbonate ramp model (Section 3.6; Ahr, 1973; Tucker & Wright, 1990). The lateral variations in the Olesa Unit and the Vilella Baixa Unit consistently indicate more open marine conditions in the central and southern Catalan Coastal Ranges than in the northern. During the deposition of the Vilella Baixa Unit oolite shoals developed in the central and southern Catalan Coastal Ranges but not in the northern where there were more protected lagoonal conditions. The lateral facies change from more proximal to outer lagoonal/sand-belt deposition can be compared with the facies of the Upper Muschelkalk. The Upper Muschelkalk has been interpreted as a relatively deep-water carbonate ramp with a lateral facies change from shallow-water proximal deposits in the northeast to distal outer ramp in the southwest of the Catalan Coastal Ranges (Calvet & Tucker, 1988). Thus, in the Upper Muschelkalk the general orientation of the carbonate ramp was similar to the Lower Muschelkalk. However, during the Lower Muschelkalk the lateral facies change is not as marked as during the Upper Muschelkalk indicating that paleoslopes from northeast to southwest were more gentle during the Lower Muschelkalk deposition.

A similarity between the Upper Muschelkalk and the Lower Muschelkalk is the unimportance of storm deposits in comparison to other ramp models (*e.g.* Markello & Read, 1981; Aigner 1984, 1985). During the deposition of the Olesa Unit the carbonate ramp was relatively open and some storm deposits have been recognised. Storm deposits have generally not been identified in the Vilella Baixa Unit possibly reflecting the more protected lagoonal environment that resulted from the

Fig. 3.26. Contact between the Upper Member of the Colldejou Unit and the Middle Muschelkalk sabkha-facies shales and evaporites. Arboli locality.

Fig. 3.27. Nodular chicken-wire texture gypsum fom the Middle Muschelkalk. Colldejou locality.

development of the oolitic and bioclastic shoals, preserved in the central and southern Catalan Coastal Ranges. However, in a similar way to the Upper Muschelkalk, the general dearth of storm deposits in the Lower Muschelkalk may reflect the orientation of the Catalan carbonate ramp relative to the prevailing winds and storms (Calvet & Tucker, 1988).

The Colldejou Unit marks the onset of a broadly regressive sequence from intertidal and supratidal carbonates to the evaporitic shales and red-beds of the Middle Muschelkalk. The initial stages of regression involved minor karstification in some areas resulting in a sharp contact between outer shallow ramp oolitic shoal deposits of the Vilella Baixa Unit and the regressive Colldejou Unit dolomicrites. In some areas subsidence allowed the deposition of the transitional lower member of the Colldejou Unit.

3.3 EASTERN IBERIAN RANGES

The Lower Muschelkalk of the eastern Iberian Ranges was deposited in the so-called Valencia-Cuenca Basin (Calvet *et al.*, 1990). Previous workers have not considered the Lower Muschelkalk sedimentology in detail and few sedimentary logs have been produced (Freeman, 1972; Lopez Gomez, 1987; Perez Arlucea, 1987). In this study the Lower Muschelkalk was examined at a number of localities along an approximate transect northwest from Valencia (Fig 3.28; Appendix 1).

3.3.1 Introduction

The Lower Muschelkalk of the Valencia-Cuenca Basin varies in thickness from about 80m near Valencia to about 20m near Cuenca in the northwest before pinching out completely (see Section 2.4.1). Towards the southeast the Lower Muschelkalk is similar to that of the Catalan Basin but towards the northwest the deposits become more marginal with less marine influence, a greater degree of tidal-flat/peritidal sedimentation and more marked siliciclastic input.

3.3.2 Serra

At Serra the Lower Muschelkalk is incompletely exposed and subsequent diagenesis, particularly dedolomitization, has obscured depositional textures. The Lower Muschelkalk rests upon Buntsandstein evaporitic shales equivalent to the lutite-evaporite-carbonate complex of the Catalan Basin. The lowermost horizon of the Lower Muschelkalk is a dolomicrite with domal stromatolites and microbial lamination interpreted as a peritidal deposit equivalent to part of the El Brull Unit (see Section 3.2.1).

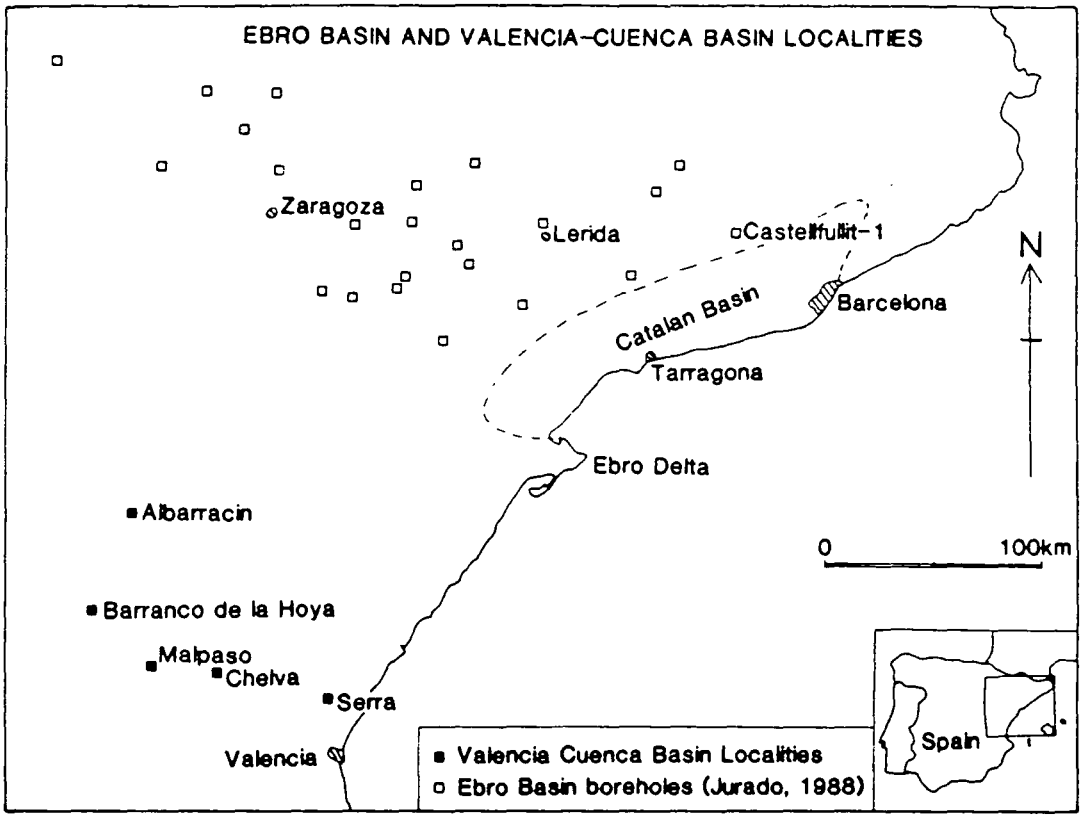

Fig. 3.28. Localities from the eastern Iberian Ranges (Valencia-Cuenca Basin) and borehole locations from the Ebro Basin.

The intermediate part of the section has suffered extensive fabric-destructive dedolomitization and is equivalent to the Olesa Unit and Vilella Baixa Unit. Parallel-laminated dolomicrites are interbedded with cross-laminated oolites. The oolites are up to 0.6m thick, contain dolomicrite intraclasts and have erosive bases and sharp, rippled tops which are locally burrowed (Fig. 3.30). One oolite layer pinches out laterally. The laminated mudstones overlying the uppermost oolite layer are locally bioturbated and contain a diverse fauna of bivalves, brachiopods and echinoderm fragments. The oolitic layers are interpreted as relatively thin spillover lobes directed into the lagoonal environment adjacent to the marine sand-belt (Handford, 1988). Similar but thicker modern spill-over lobes with sharp terminations have been observed in the Bahamas (Hine, 1977).

The uppermost Lower Muschelkalk at Serra consists of unfossiliferous parallel-laminated dolomicrite with abundant stellate pseudomorphs after evaporites. It is interpreted as an intertidal-supratidal deposit equivalent to the upper member of the Colldejou Unit.

3.3.3 Chelva

At Chelva the Lower Muschelkalk is only 38m thick and rests directly upon Buntsandstein arenites (Fig. 3.29). The lower half of the sequence contains several sandstone layers, up to 1.0m thick, interbedded with laminated and locally bioturbated dolomites with a sparse fauna of echinoderm fragments. The sandstone layers have erosive bases and sharp tops and appear massive (Fig. 3.31). Sandstone petrography is discussed in Section 4.4.1.

The interbedding of siliciclastics and carbonates has been described by Dolan (1989) on a variety of scales and attributed to eustatic and tectonic controls. However, in the case of the Lower Muschelkalk the small-scale interlayering and proximity of oolites, sandstones and mixed ooid-quartz grainstones suggests that the facies were probably juxtaposed and deposition was synchronous (*cf.* Handford, 1988). The sandstones are interpreted as deposits of tidal inlet channels that crossed lagoonal and tidal-flat environments and passed into the oolite sand-belt. Thicker sandstone packages that occur at other localities may represent channel axes as opposed to margins or may just be thicker as a result of being more proximal and closer to the clastic source.

The upper half of the Lower Muschelkalk at Chelva consists of well-laminated, unfossiliferous but locally bioturbated dolomicrites containing pseudomorphs after evaporites. A collapse breccia and two thin (0.2m) oolite layers are present towards the top of the section. This upper part of the Lower Muschelkalk is interpreted as

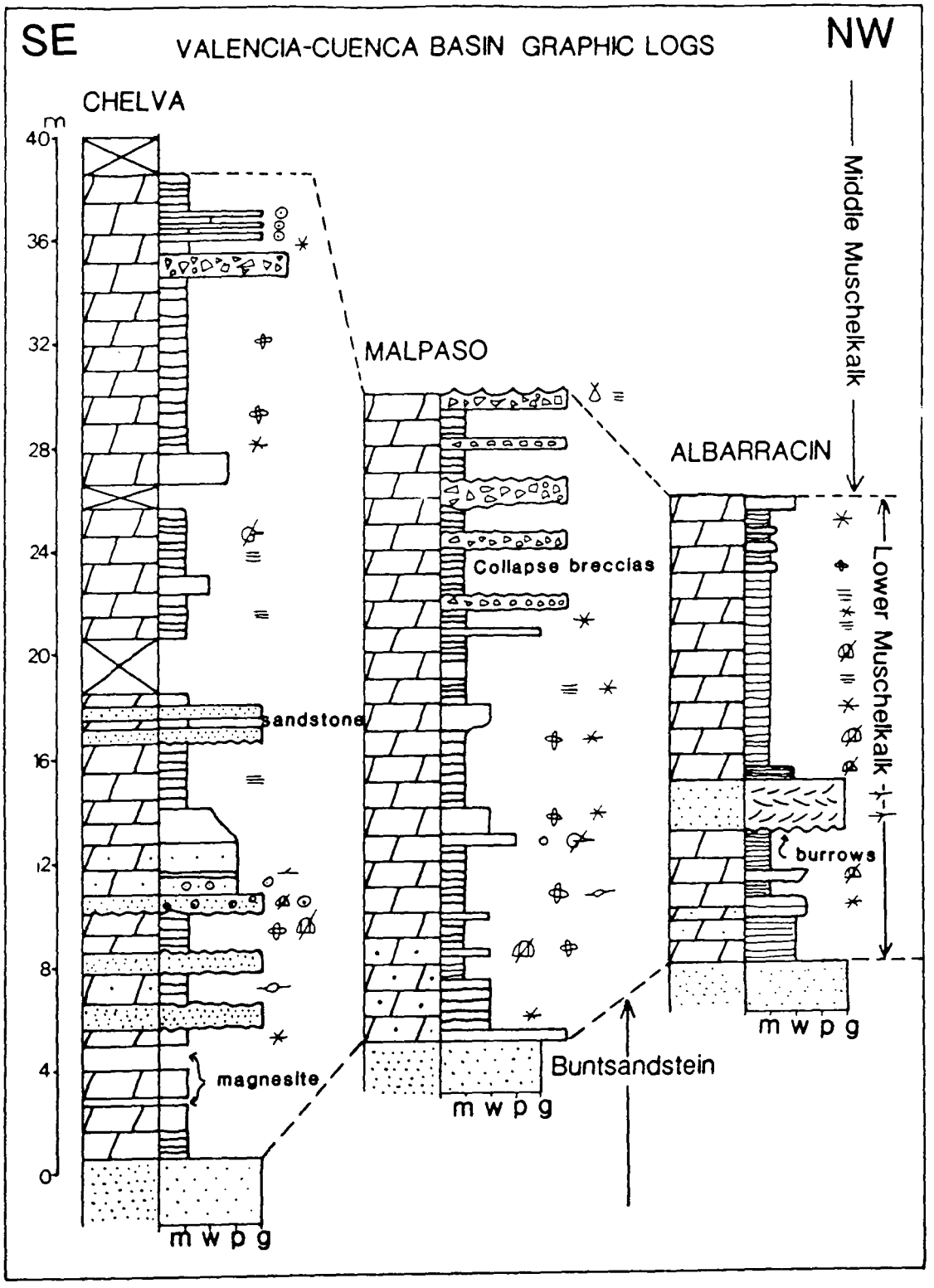

Fig. 3.29. Graphic logs of the Lower Muschelkalk from the Valencia-Cuenca Basin. For explanation of the symbols see Appendix 1.

equivalent to the upper member of the Colldejou Unit. The two oolite layers are somewhat enigmatic and may represent distal washover fans.

At Chelva the lagoonal/sand-belt deposits of the Lower Muschelkalk (the Olesa Unit and the Vilella Baixa Unit) are considerably reduced in thickness and contain abundant siliciclastics which are evidence for a nearby clastic shoreline. The upper part of the Lower Muschelkalk, equivalent to the Colldejou Unit is relatively unaltered in thickness.

3.3.4 Malpaso (Fig. 3.29)

At Malpaso the Lower Muschelkalk is only 25m thick and rests directly upon Buntsandstein sandstones. Fossiliferous horizons are rare and most of the section consists of laminated dolomicrites with pseudomorphs after evaporites. Several collapse breccias are present towards the top of the sequence which is marked by tepees.

There is no equivalent to the Olesa Unit and Vilella Baixa Unit at this locality and the entire sequence is interpreted as intertidal to supratidal deposits.

3.3.5 Barranco de la Hoya and Albarracin

The Lower Muschelkalk is similar at these two localities and is about 18m thick consisting mostly of unfossiliferous, laminated silty dolomites. Sandstone layers occur in the lower half of the sequence at both localities (Fig 3.29). At Albarracin one 2m thick trough cross-bedded sandstone layer is well-exposed and has a sharp erosive base with some *Rhizocorallium* burrows. As mentioned in Section 3.3.3 these thicker sandstone layers may represent channel axes of tidal inlets proximal to the shoreline where they are cutting across tidal-flat carbonates.

The upper half of the sequence at Albarracin and Barranco de la Hoya consists of peritidal dolomicrites equivalent to the upper member of the Colldejou Unit.

3.3.6 Synthesis of Iberian Ranges Lower Muschelkalk sedimentology

The lateral facies change in the Lower Muschelkalk from southeast to northwest in the Valencia-Cuenca Basin shows the transition from the Catalan Basin-style Lower Muschelkalk to the thinner, peritidal-dominated marginal succession. The upper part of the sequence, equivalent to the Colldejou Unit, becomes more significant towards the northest. In other words, the thinning of the Lower Muschelkalk is at the expense of the lagoonal/sand-belt deposits equivalent to the Olesa Unit and the Vilella Baixa Unit, and the overlying peritidal deposits are relatively unaltered in thickness.

Fig. 3.30. Cross-laminated oolite layer with sharp base and rippled top interbedded with dolomicrites. Small rounded dolomicrite intraclasts are present near the top of the oolite. Serra locality.

Fig. 3.31. Sandstone layer from the lower part of the Lower Muschelkalk at Chelva in the Valencia-Cuenca Basin.

Siliciclastics are an important part of the Lower Muschelkalk in the more marginal parts of the Valencia-Cuenca Basin, reflecting a greater proximity to the locally clastic shoreline.

3.4 LOWER MUSCHELKALK OF THE EBRO BASIN SUBSURFACE

The Lower Muschelkalk has been penetrated by borehole at a large number of localities in the Ebro Basin (Section 2.2; Fig. 3.28). Jurado (1988) produced graphic logs for the Triassic of the subsurface of the Ebro Basin on the basis of core and wire-line log data.

The Lower Muschelkalk adjacent to the Catalan Coastal Ranges has a similar thickness to the Catalan Basin sequence and can be subdivided into the same units (*e.g.* Castellfullit, Fig. 3.32). Jurado (1988) described similar facies from core as those described at outcrop. However, it is to be noted that in the subsurface discrete layers and stellate roses of anhydrite are present corresponding to the collapse breccias and calcite pseudomorphs observed at the surface. Sulphate dissolution and replacement has been related to dedolomitization (see Section 8.4.1).

Towards the northwest of the Ebro Basin the Lower Muschelkalk generally decreases in thickness and Jurado (1988) noted an increase in clastic and evaporitic layers suggesting a more proximal and peritidal-related depositional environment. This is similar to the lateral facies change observed at outcrop in the Valencia-Cuenca Basin. However, the clastic layers are generally fine-grained and Jurado (1988) recognised relatively few sandstones.

3.5 LOWER MUSCHELKALK OF THE BALEARIC ISLANDS

The Muschelkalk of the Balearic Islands has not been extensively studied. Freeman (1972) reported that the Muschelkalk facies of the Balearic Islands is very uniform and the only difference between Mallorca and Menorca is the greater degree of dolomitization on Mallorca.

The Muschelkalk of Menorca is about 110m thick and rests upon Buntsandstein siliciclastics and consists of three mainly calcareous units (Llompart *et al.*, 1987). The chronostratigraphy is imprecise, but the lower of the three units is probably at least in part equivalent to the Lower Muschelkalk of the Catalan Basin.

The most notable features of the Menorcan Muschelkalk are the relative thinness with respect to age-equivalents on the mainland and the absence of any sliciclastic equivalent to the Middle Muschelkalk.

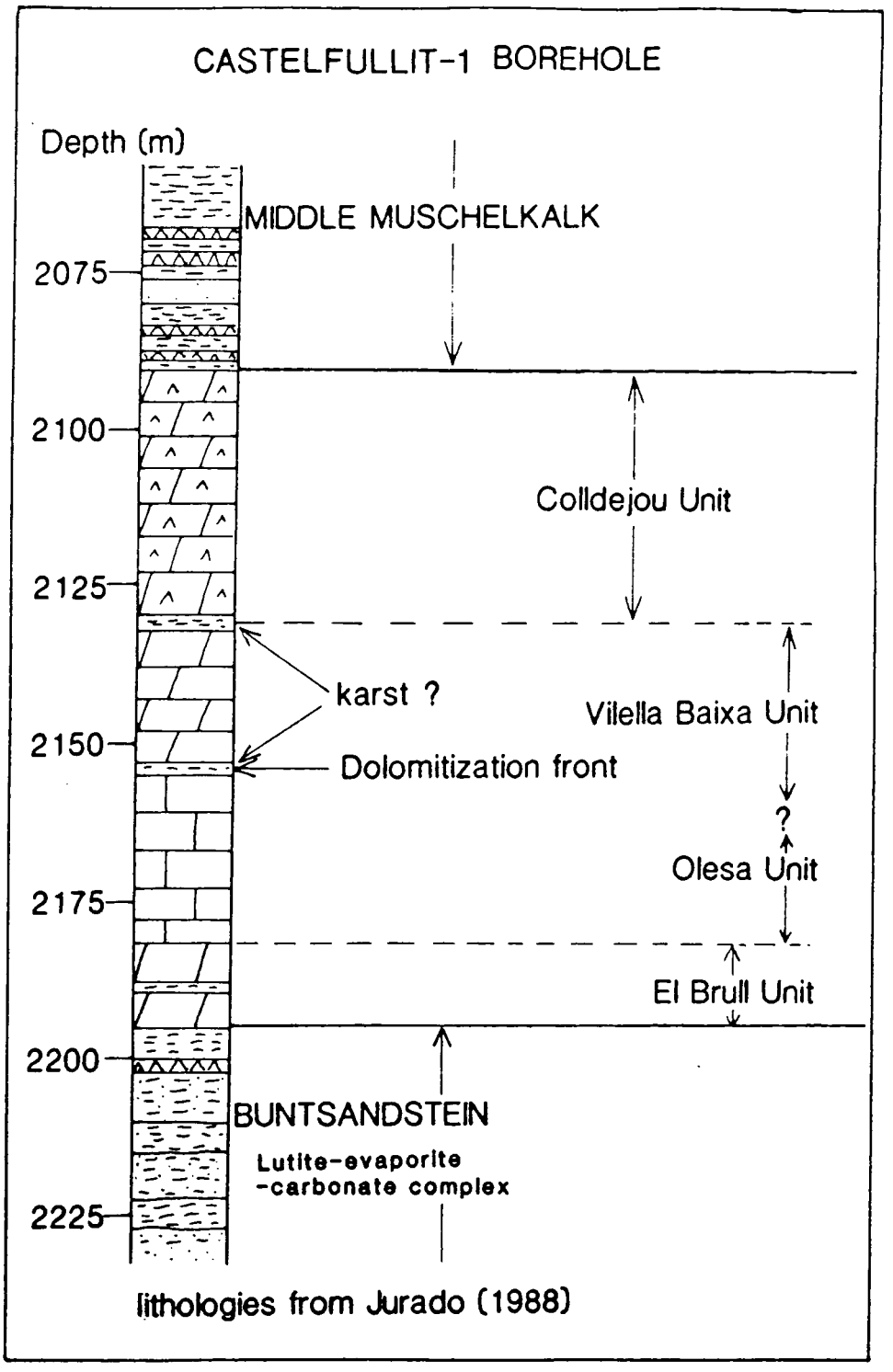

Fig. 3.32. The Lower Muschelkalk from the Castelfullit borehole in the northeast of the Ebro Basin. Lithologies are from Jurado (1988) and are interpreted in terms of the Lower Muschelkalk of the Catalan Basin.

3.6 SYNTHESIS OF LOWER MUSCHELKALK SEDIMENTOLOGY

The Lower Muschelkalk from the subsurface of the Ebro Basin and at outcrop in the Catalan Basin and Valencia-Cuenca Basin have no marked regions of rapid thickness change associated with facies change from shallow to deeper-water carbonates. This suggests that there is no shelf-edge break preserved within the study-area. The Lower Muschelkalk isopach map (Fig. 3.33) indicates a general thinning towards the northwest with local areas, such as around Lerida, remaining relatively high with condensed sequences. The thin nature of the Balearic Islands carbonate sequence, age-equivalent to the Lower Muschelkalk, suggests that this area may also have been a basement high.

The absence of a shelf-edge break suggests that the Lower Muschelkalk can be considered in terms of a homoclinal ramp model (Read, 1985). Gradual lateral thickness and facies changes in the Olesa Unit and Vilella Baixa Unit of the Catalan Basin suggest a down-ramp transition from a lagoonal environment in the northeast to shoal-water sand-belt deposits in the southwest and as such may be similar to the 'ramp with barrier ooid pellet shoal complex' of Read (1985), a modern example of which is the Holocene Trucial Coast, Persian Gulf (Purser & Evans, 1973; Tucker & Wright, 1990). However, no patch reefs have been identified in the sand-belt/tidal channel facies and, if present, any larger seaward reefs, like those of the Trucial Coast, would not be exposed, but would lie further to the south or offshore, away from the paleoshoreline. The presence of the oolite shoals towards the southeast of the Catalan Basin may be in part related to the presence of the Lerida High to the north (Fig. 3.33).

The lower three units of the Catalan Basin represent a general transgression from terrestrial and mud-flat deposits (Buntsandstein and lutite-evaporite-carbonate complex) through peritidal sediments (El Brull Unit) to lagoonal and sand-belt deposits (Olesa Unit and Vilella Baixa Unit).

The Lower Muschelkalk of the Valencia-Cuenca Basin provides an opportunity to examine at outcrop the facies transitions from relatively distal deposits in the southeast, equivalent to the Catalan Basin, to the thinner, more marginal terrestrial-influenced sediments in the northeast equivalent to those of the northwestern Ebro Basin. Towards the northwest of the Valencia-Cuenca Basin sandstones become more important in the Lower Muschelkalk. The oolite sand-belt of the ramp was cut by clastic and mixed clastic-ooid tidal channels. A similar model has been proposed by Handford (1988) for the Mississippian Reservoir, Damme Field, southwestern Kansas. Relatively few coarse clastic intervals have been recognised by Jurado (1988) in the marginal parts of the Lower Muschelkalk of the subsurface of the Ebro Basin.

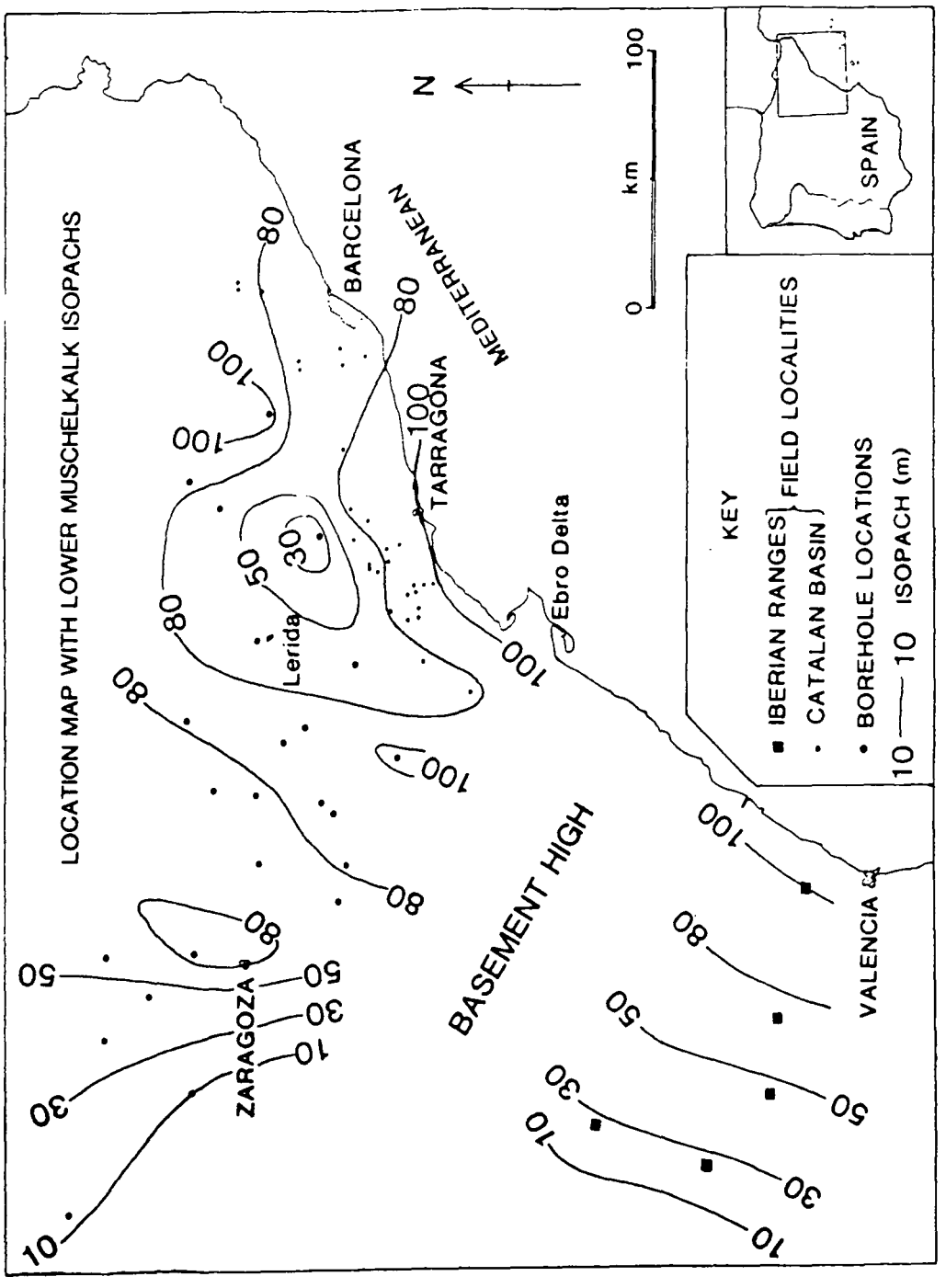

Fig. 3.33. Isopach map of the Lower Muschelkalk of northeast Spain. Compiled from measurements of outcrop in the Catalan Coastal Ranges and the estern Iberian Ranges and using borehole information from the subsurface of the Ebro Basin (Jurado, 1988).

However, shale layers are abundant in the Ebro Basin and these may reflect a relatively distal clastic source.

The Colldejou Unit of the Catalan Basin represents a relatively uniform 'blanket' of peritidal deposits that can also be recognised in the upper part of the Lower Muschelkalk of the Valencia-Cuenca Basin. The Colldejou Unit typically has a sharp disconformable base and the transitional lower member is only locally developed. The Colldejou Unit shows a broadly regressive nature becoming more supratidal towards the top.

The upper part of the Lower Muschelkalk of the Valencia-Cuenca Basin, equivalent to the Colldejou Unit, does not thin to the northwest as rapidly as the underlying transgressive deposits and thus becomes more important towards the northwest.

3.7 LOWER MUSCHELKALK SEQUENCE STRATIGRAPHY

This section discusses the use of sequence stratigraphy and describes the framework for the Lower Muschelkalk which has been adopted in this study. For definitions of terms used in this chapter see Van Wagoner *et al.* (1988). This section is not intended to be an exhaustive review of sequence stratigraphy but merely to highlight some of the more interesting aspects of the subject.

3.7.1 Introduction to sequence stratigraphy

Sequence stratigraphy and depositional sequences were initially conceived as a result of the increased use of high-quality seismic surveying and processing techniques which enabled interpretation of seismic sections in terms of sedimentary packages or 'seismic sequences'. The seismic sequences were bounded by unconformities or disconformities and were described in terms of their internal arrangement of reflectors and seismic character (see Vail *et al.*, and other papers in Payton, 1977). Subsequent work has concentrated on the sedimentary facies that may be deposited during changes of relative sea-level and there has been considerable debate about the use of sequence boundaries to define global (eustatic) changes of sea-level as opposed to tectonic-induced changes of relative sea-level (*e.g.* Hubbard, 1988; Calvet *et al.*, 1990). Depositional sequences have been subdivided into depositional systems tracts and parasequences (Van Wagoner *et al.*, 1988) which result from changes in relative sea-level and are therefore dependent upon eustasy, tectonics and sediment accumulation (Kendall & Lerche, 1988). The sequence stratigraphic approach has moved away from studies of seismic sections and the framework has been found increasingly useful when considering sedimentary packages at outcrop (*e.g.* papers in Wilgus *et al.*, 1988).

3.7.2 Sequence stratigraphy of carbonate systems

The majority of sequence stratigraphic studies have been on clastic systems and the depositional system tracts framework and models are relatively well established (Posamentier & Vail, 1988; Posamentier *et al.*, 1988). Carbonate sequence stratigraphy and systems tracts models for a rimmed shelf have been proposed by Sarg (1988). The effect of sea-level changes on a carbonate ramp is discussed by Dolan (1989) and a simple model for ramp systems tracts has been put forward by Calvet *et al.* (1990). Other sequence stratigraphic studies of carbonate systems are given in Crevello *et al.* (1989).

Carbonate systems do not behave in the same way as clastic systems during fluctuations of relative sea-level. The controls on carbonate deposition are outlined by Sarg (1988). Carbonate sediments tend to accumulate *in situ* and are much more abundantly produced in shallow, warm, clear marine conditions. In siliciclastic systems the deep basinal deposition increases during lowstands, as a result of sediment bypassing of subaerially exposed shelves, and decreases during highstands (Posamentier *et al.*, 1988). Conversely, for a carbonate platform system the greatest degree of resedimentation into the basin may occur as a result of the increased carbonate productivity during a highstand whereas during a lowstand the carbonate productivity is low and erosion is mainly chemical (karstic) rather than mechanical (Dolan, 1989).

Climate is another important control on carbonate sedimentation and sequence development (Sarg, 1988). In an arid or semi-arid climate. such as that of the Lower Muschelkalk of northeast Spain, evaporites are common deposits in lagoons and supratidal flats. Climate also influences the degree of karstic weathering and diagenesis during subaerial exposure.

The type of carbonate platform (rimmed shelf, ramp, epeiric platform, isolated platform and drowned platform; Tucker & Wright, 1990) will clearly alter the development of depositional sequences. Carbonate ramps, especially homoclinal ramps such as that proposed for the Lower Muschelkalk of northeast Spain, will respond to relative sea-level change in a different way to a rimmed shelf. The distinction between Type 1 and Type 2 sequence boundaries is made on whether relative sea-level drops below the shelf-edge (or depositional-shoreline break) and therefore has no significance for a homoclinal ramp. Relative sea-level changes on a homoclinal ramp may merely result in the shoreward or oceanward movement of the facies belts (Sarg, 1988). However, this may be dependent upon the rate of relative sea-level change.

3.7.3 Depositional systems tracts and the Lower Muschelkalk

Depositional sequences in the Triassic of the Iberian Peninsula have been defined by several authors (*e.g.* Garrido-Megias & Villena, 1977; Orti Cabo, 1987; Esteban & Robles in Anadon *et al.* , 1987; Marzo & Calvet, 1985). The most recent attempt by Calvet *et al.* (1990) used the depositional sytems tracts philosophy of Haq *et al.* (1987), Vail *et al.* (1987) and Bally (1987) and is adopted in this study. It should be noted that the outcrop pattern of the Lower Muschelkalk of the Catalan Basin is not ideally suited to the division into depositional sequences. Only shallow-ramp depositional facies are exposed in the Lower Muschelkalk and the laterally equivalent basinal facies presumably lie to the southeast in the subsurface. Nevertheless consideration of the sedimentary packages in terms of depositional sequences is useful and worthwhile.

Following the scheme of Calvet *et al.* (1990) the mid-Triassic strata of the Catalan Basin can be subdivided into two depositional sequences (Fig. 3.34). Depositional Sequence 1 is of principal interest in this study and consists of the uppermost Buntsandstein (the lutite-evaporite-carbonate complex) and the Lower Muschelkalk. Depositional sequence 2 consists of the Middle Muschelkalk and Upper Muschelkalk.

The lutite-evaporite-carbonate complex is variable in thickness and is only locally developed, and is considered to be the Lowstand Systems Tract (LST-1). The El Brull Unit (peritidal), Olesa Unit (lagoonal) and Vilella Baixa Unit (carbonate sand-belt) are the Transgressive Systems Tract (TST-1). The Colldejou Unit (intertidal to supratidal) is a Highstand Systems Tract (HST-1). The major transgressive surface (Ts-1) is the base of the El Brull Unit and the maximum flooding surface (Mfs-1) is the widely developed disconformity at the base of the Colldejou Unit. The top of the Colldejou Unit is the sequence boundary between the HST-1 of Depositional Sequence 1 and the Middle Muschelkalk which represents the Lowstand Systems Tract (LST-2) of Depositional Sequence 2.

The systems tracts recognised in the Catalan Basin can also be identified in the Valencia-Cuenca Basin. The Lower Muschelkalk sections of the southeastern Valencia-Cuenca Basin are similar to the Catalan Basin deposits, *e.g.* at Serra, the Lower Muschelkalk rests upon a lutite-evaporite-carbonate complex equivalent to LST-1, and consists of lagoonal to shoal deposits (TST-1) overlain by laminated peritidal sediments (HST-1). It is interesting to note that although imprecise, the chronostratigraphy of the Triassic (Fig. 2.10) suggests that the deposition of TST-1 began earlier in the Catalan Basin than in the eastern Iberian Ranges in accord with the transgressive nature of the base of TST-1. The TST-1 in the Valencia-Cuenca Basin thins more rapidly to the northwest than the HST-1 until most of the section

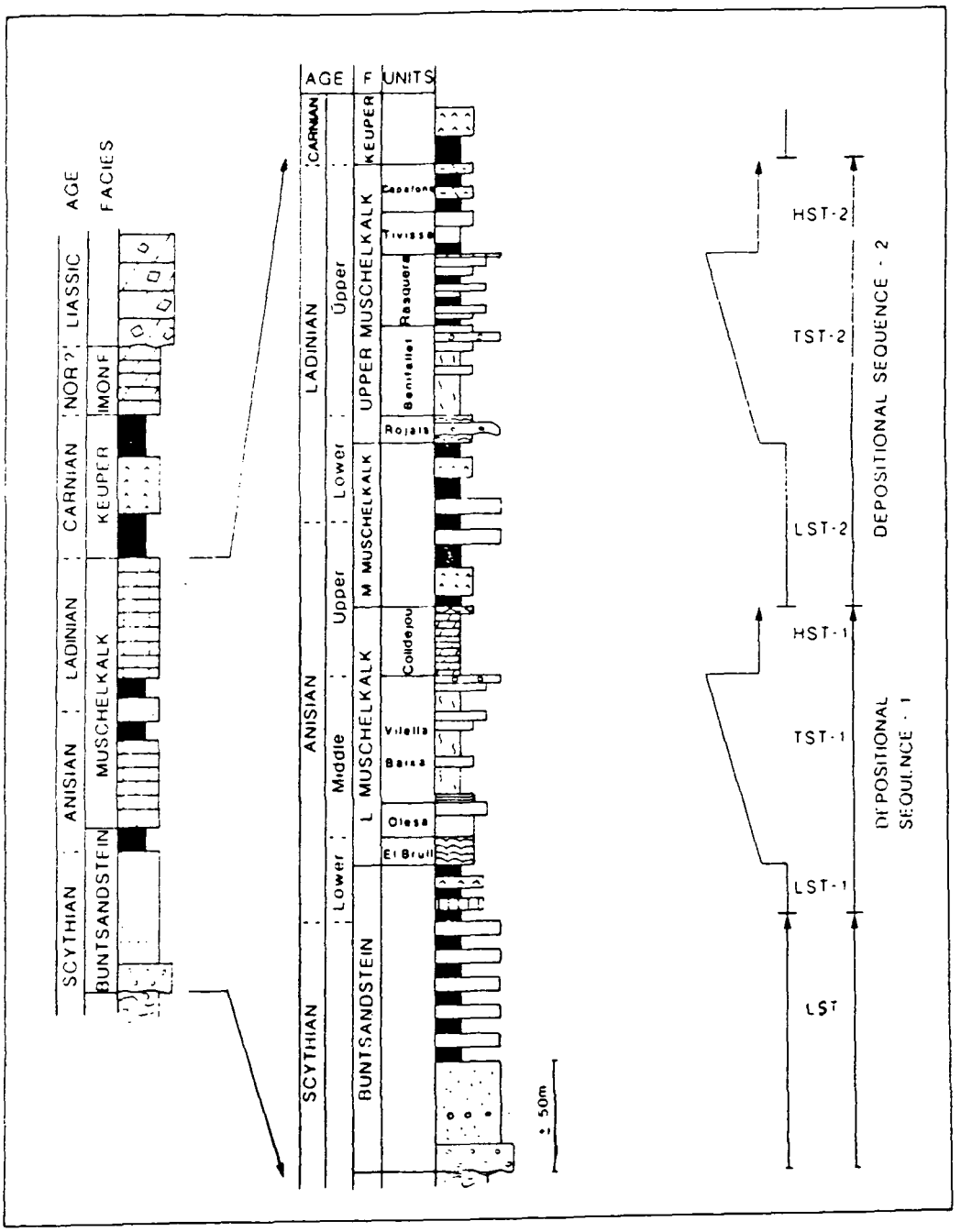

Fig. 3.34. Statigraphical, chronostratigraphical and depositional sequences of the Lower and Middle Triassic of the Catalan Basin (from Calvet *et al.*, 1990).

consists of shallow lagoonal or peritidal deposits. The relative constancy of thickr of HST-1 as the depositional sequence thins towards the northwest reflects broadly aggradational-to-regressive nature of the systems tract.

The overlying Middle Muschelkalk (or LST-2) consists of regressive sabkha evaporites and clastics which were deposited over the top of the subhorizontal surface of the HST-1 as the facies belts migrated oceanward during the relative sea-level fall and lowstand.

CHAPTER 4: PETROGRAPHY AND DIAGENESIS OF THE LOWER MUSCHELKALK

4.1 INTRODUCTION

This chapter describes the detailed sedimentology, petrography and some aspects of the diagenesis of the Lower Muschelkalk. The chapter is divided into several subsections and references are made to chapter three in order to explicate the stratigraphic significance of each subject. Dolomitization is discussed separately in the following chapters.

4.2 BIOCLASTS

The following types of skeletal grains have been identified. Wilson (1975), Bathurst (1975), Scholle (1978) and Flugel (1982) were used as the principal references.

4.2.1 Dasycladacean algae

Dasycladacean algae are common in the upper part of the Vilella Baixa Unit in the southwestern Catalan Coastal Range (see Section 3.2.3), and generally occur in dolomitized algal packstones and grainstones (Fig. 8.10). Well-preserved specimens display chambered thallus walls and resemble the *Physoporella-Oligoporella* genus that has been used to recognise the Anisian of the Alpine Triassic facies (Ott, 1972, in Flugel, 1982). Dedolomitization commonly destroys the skeletal structure (see Section 8.3.3). Dasycladacean algal grainstones indicate concentration of tests in tidal bars and shallow lagoonal channels (Wilson, 1975).

4.2.2 Solenoporacean Algae

Only one example of a solenoporacean alga has been found. The specimen occurred as a fragment in the upper 2m of the Vilella Baixa Unit at Vilaplana in the southern Catalan Coastal Ranges (Fig. 3.22). Solenoporacean algae indicate normal marine waters (Wilson, 1975).

4.2.3 Calcispheres

Calcite spar calcispheres, 0.1-0.15mm in diameter occur in mudstones and wackestones of the Olesa Unit and lower Vilella Baixa Unit. Some of these calcispheres have a single wall structure and probably represent calcified reproductive parts of dasycladacean algae (Section 4.2.1; Adams *et al.*, 1984). Other calcispheres may be calcite casts of radiolaria or unilocular foraminifera.

4.2.4 Foraminifera

Foraminifera have been recognised in the Vilella Baixa Unit and Olesa Unit. Most of the foraminifera are multilocular, similar to small gastropods, and are typical of Triassic shallow-water carbonates (Flugel, 1982). One uniserial example has been identified.

4.2.5 Ostracods

Thin and thick-valved ostracods are widespread in the Lower Muschelkalk, but do not occur in the upper Colldejou Unit. Ostracods are euryhaline and are often the only fauna in the restricted intertidal facies of the Colldejou Unit (Fig. 4.1).

4.2.6 Bivalves

Two groups of bivalves have been recognised and occur in the Vilella Baixa Unit and Olesa Unit.

4.2.6.1 Thin-shelled bivalves with prismatic shell structure (Fig. 4.2)

These bivalves occur as single valves up to 1.5cm long in mudstones and wackestones. The good preservation indicates original calcite skeletal mineralogy and quiet-water conditions. They appear similar to the Triassic *Halobia sp.* which are thought to have existed on soft, muddy substrates (Scholle, 1978) and like *Daonella sp.* , which occurs in the Upper Muschelkalk of the Catalan Basin (Calvet & Tucker, 1989).

4.2.6.2 Thick-shelled bivalves, replaced by calcite spar

The thick-shelled bivalves occur mainly in bioclastic packstones and grainstones. The smaller examples (1-3mm) are generally articulated, but the larger specimens are usually preserved as fragmented single valves. The shell structure is lost and replaced by calcite spar cement. The fragments are commonly enclosed by a micrite envelope indicating fragmentation in relatively high energy conditions and subsequent micritization.

4.2.7 Gastropods

Gastropods are common in the Olesa Unit bioclastic packstones (see Section 3..2.2.1 and Fig. 3.13) and also occur in the Vilella Baixa Unit. Two groups of gastropods were recognized:

i) Smooth-shelled with circular to elliptical-section thin-walled whorls

ii) Thick-walled prismatic-section whorls

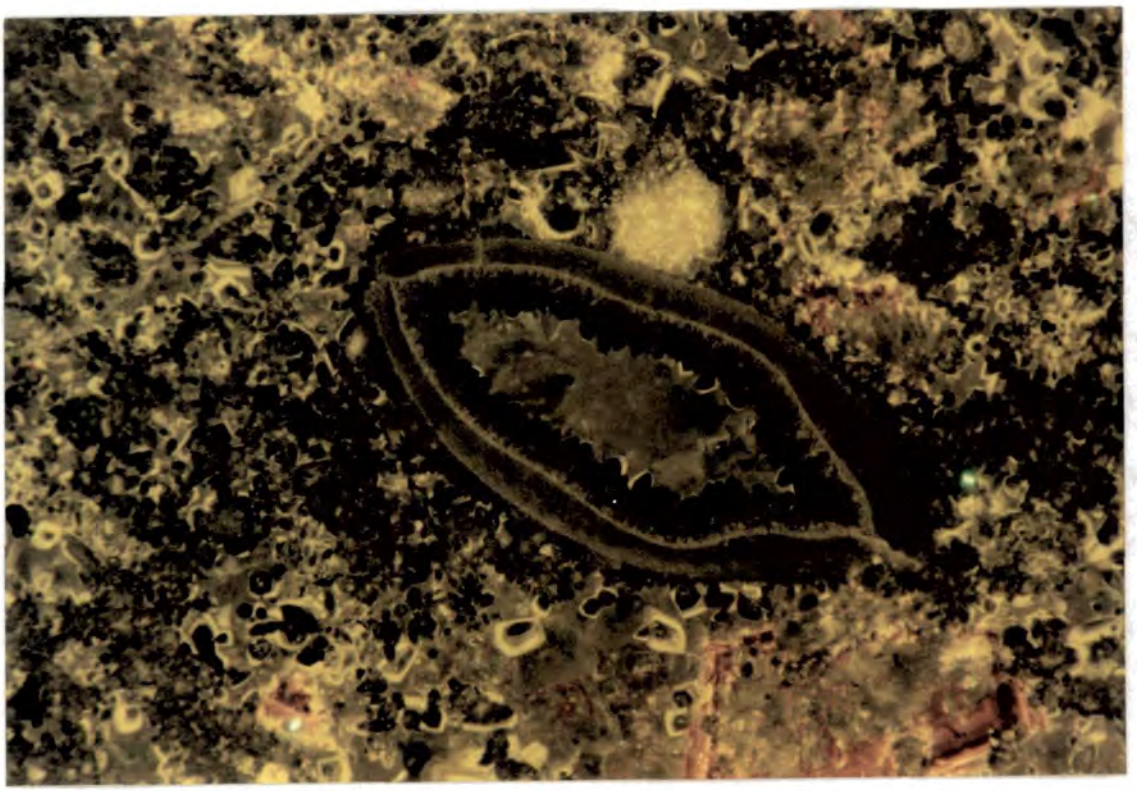

Fig. 4.1. CL photomicrograph of ostracod shell in recrystallised micritic limestone. Generally dull-luminescent with non-luminescent phreatic cement lining ostracod valves. Red-luminescent baroque dolomite cement also present. [CL. CB31. Width of view = 0.7mm]

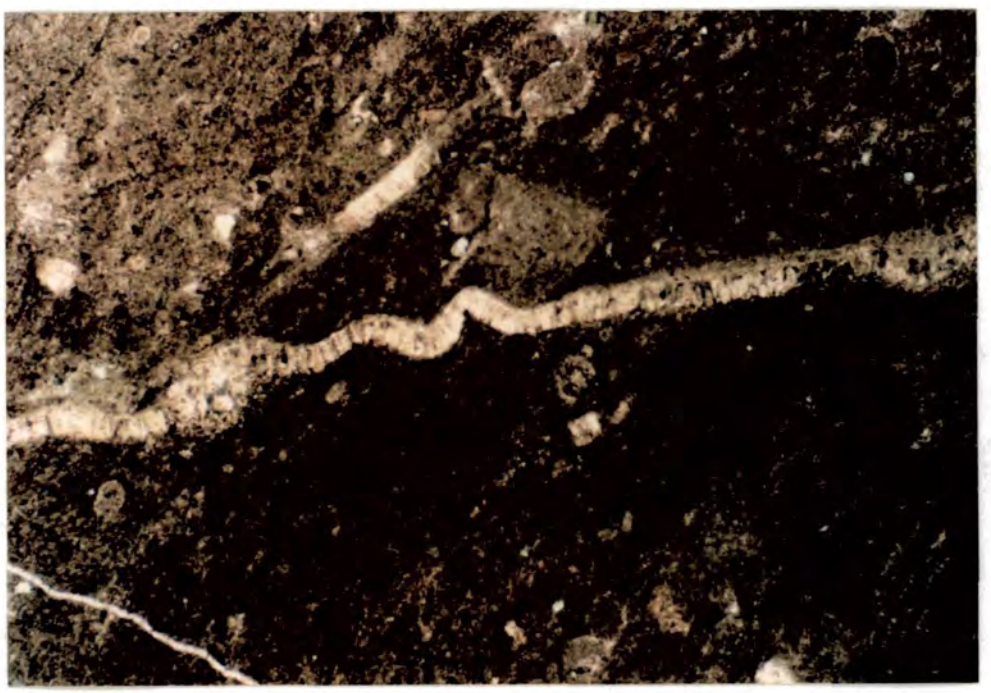

Fig. 4.2. Thin-shelled bivalve with well-preserved prismatic shell structure. [XPL. PT10. Width of view = 3mm]

In both cases the original shell material was probably aragonite and has been replaced by calcite spar.

4.2.8 Echinoderm fragments

Echinoderm fragments are commonly preserved and occur in mudstones to grainstones of the Vilella Baixa Unit and Olesa Unit. Echinoderm fragments are not common in the peritidal facies of the El Brull Unit and Colldejou Unit. The fragments are generally abraded and rounded but some can be recognized as crinoid elements and echinoid spines. When preserved in biosparites the fragments commonly have a syntaxial calcite spar cement. The echinoderm fragments have a speckly red luminescence under cathodoluminescence whereas the calcite overgrowths are non-luminescent. The speckles may represent microdolomitic inclusions (Blake *et al.*, 1982).

4.2.9 Corals

Corals are not common fossils in the Lower Muschelkalk and have only been recognized at one locality (Colldejou, Fig. 3.21). The corals occur as 1-2cm sized fragments in an oopelbiomicrite packstone and have been replaced by calcite spar (Fig. 4.4). The irregular margins of some of the fragments may represent borings. These corals are examples of early hermatypic scleractinian corals and required warm, shallow well-lighted waters (Clarkson, 1979). However, no patch-reefs have been identified in the Lower Muschelkalk and these examples may have been solitary.

4.2.10 Brachiopods

Brachiopods occur as whole unabraded fossils (principally *Mentzelia mentzeli*) in the micritic bioturbated wackestones of the lower part of the Vilella Baixa Unit (Section 3.2.3). Fragments of brachiopods also occur in bioclastic packstones and grainstones in the Vilella Baixa Unit. The whole brachiopods are considered to be in life-position and the paleoenvironment as low-energy and restricted (Calzada & Gaetani, 1977). The foliated shell structure is commonly well-preserved in original non-luminescent calcite. However, the margins of some of the fragments, although still showing good skeletal detail, is dull red-luminescent indicating some alteration (Popp *et al.*,1986). These brachiopods have been used for stable isotope analysis (Section 6.2.4).

4.3 OOLITIC AND PISOLITIC GRAINSTONES AND PACKSTONES

Oolites and pisolites have been recognised in the Lower Muschelkalk of the central and southern Catalan Coastal Range, and also in the eastern Iberian Ranges (see Chapter 3). The oolites mainly occur in the upper part of the Vilella Baixa Unit at the

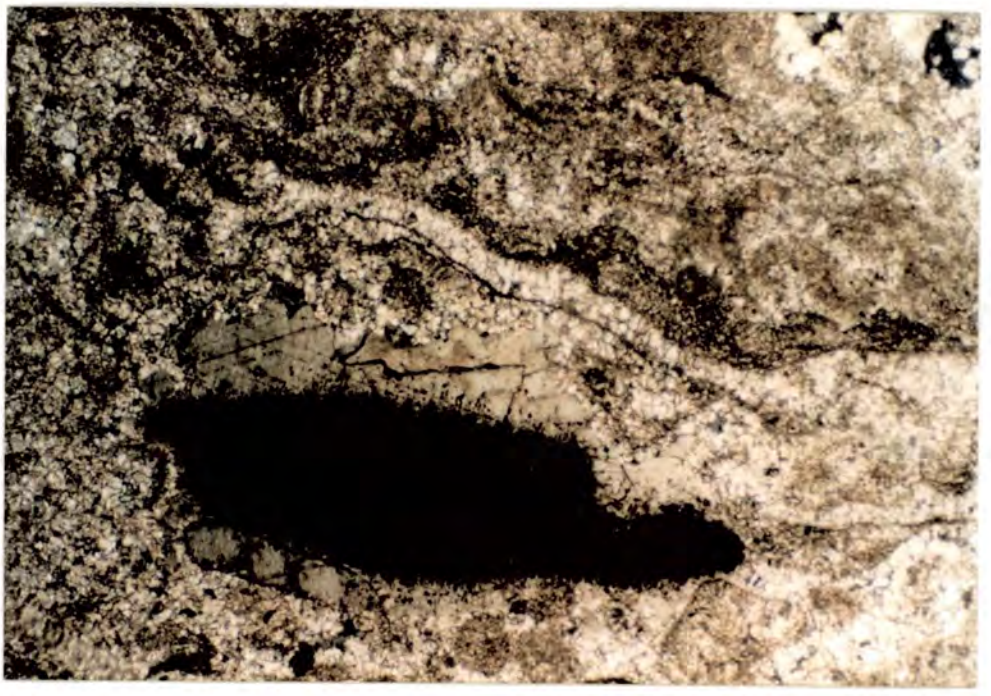

Fig. 4.3. Rounded speckled echinoderm fragment with well-developed syntaxial calcite cement in lime wackestone. [XPL. G10. Width of View = 3mm]

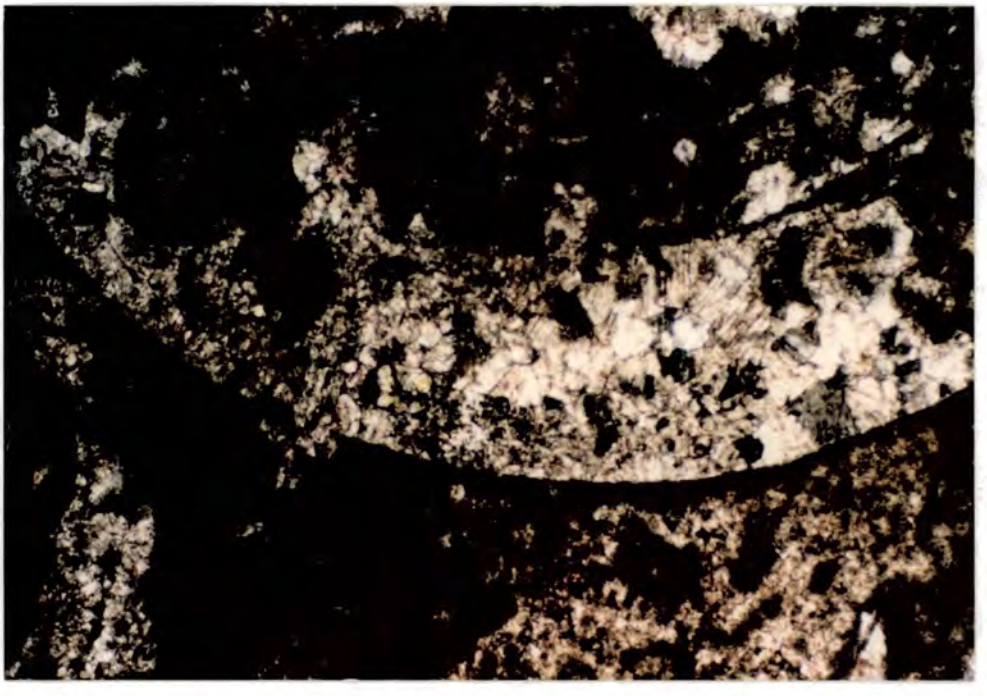

Fig. 4.4. Fragment of coral. Original aragonitic skeleton replaced by coarse calcite spar. [Stained thin section. XPL. C17. Width of View = 3mm]

top of coarsening-up cycles (Fig. 3.19). The tops of these cycles are locally karstified (Section 4.6.1.1) and the underlying oolites exhibit evidence of early meteoric diagenesis including development of pisolitic fabrics, dissolution and formation of oomolds, and compaction structures. Thin oolite layers also occur in the El Brull Unit and Colldejou Unit (see Section 3.2). Many of the oolites have been dolomitized with a variable degree of fabric preservation (Section 5.5.1.2).

The oolitic packstones generally consist of ooids and scarce bioclastic debris with a micritic matrix, locally neomorphosed to microspar. These oomicrites were probably deposited in an off-shoal position in low-energy conditions with little winnowing of the carbonate mud.

The oolitic grainstones are well-sorted and commonly cross-bedded. These oosparites are interpreted as high-energy ooid-shoal deposits where carbonate mud would be winnowed out to leave a porous and permeable ooid sand. Some of the oosparites have a layering on a mm scale of fine and coarse ooids. Such layering may arise from avalanche cross-bedding on an ooid shoal (Scoffin, 1987).

The pisolites generally occur below karstic horizons and are interpreted as ooid shoals which have undergone emergence and meteoric diagenesis promoting the formation of irregular laminae.

4.3.1 Ooid and pisoid petrography

For a review of ooid and pisoid microstructure, mineralogy and occurrence see Tucker & Wright (1990) and references therein.

4.3.1.1 Ooid Petrography (Fig.s 4.5, 4.6)

The ooids vary in size from 0.3-0.5mm in diameter and are generally better-sorted in the grainstones than in the packstones. The nuclei of the ooids are usually indistinct. However, some are elongate and composed of microspar and probably represent fine molluscan shell-debris. Fragments of broken ooids are also reworked as nuclei in some cases.

The cortices of the ooids, when well-preserved, have a fine-scale concentric lamination implying that the ooids were free to rotate during their growth. There is no clear radial component to the fabric. The ooid microstructure is interpreted to have been originally aragonitic and subsequently altered to calcite and dolomite. This observation is in agreement with studies of temporal variation of ooid mineralogy which generally suggest that aragonite was the principal marine carbonate precipitate during the mid-Triassic (see Sandberg, 1983; Wilkinson *et al.*, 1984).

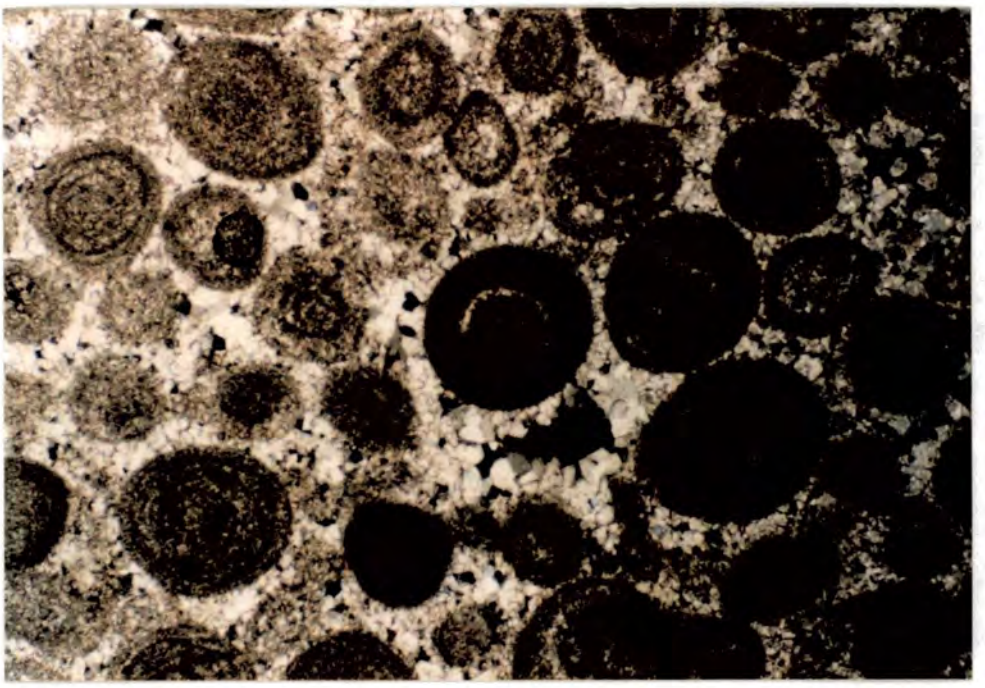

Fig. 4.5. Well-sorted calcitic oosparite. Ooids are in point-contact and have well-preserved concentric structure. Some ooids have suffered minor intra-ooid dissolution. [Half-stained thin section. XPL. G32. Width of View = 3mm]

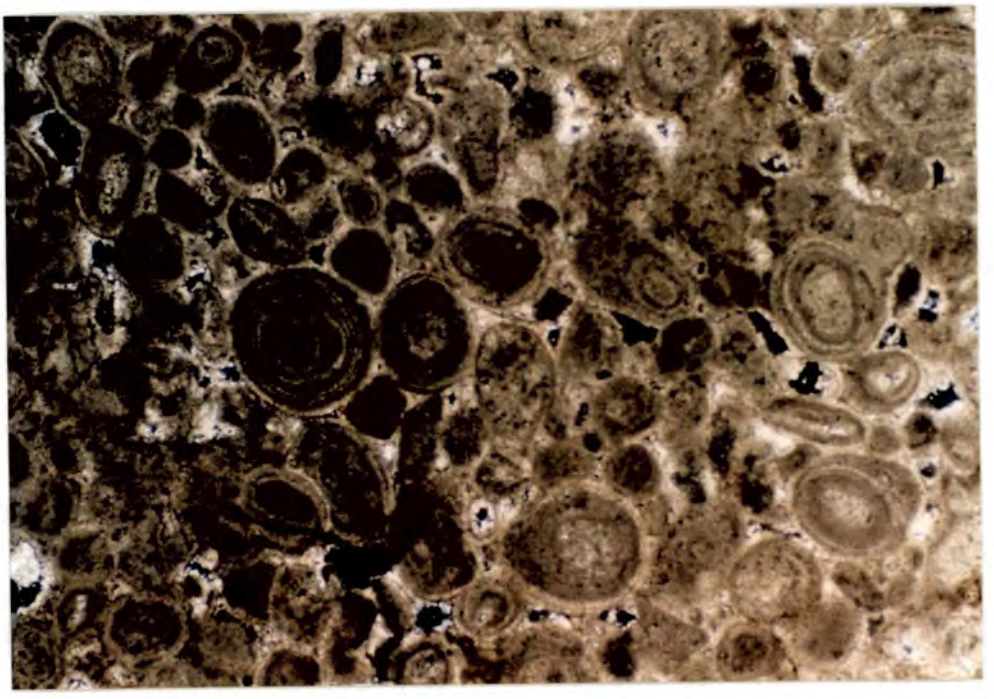

Fig. 4.6. Well-sorted ooids with well-preserved fabric in replacive dolomite. Some ooids are pisolitic with non-concentric structure. [XPL. A51. Width of View = 3mm]

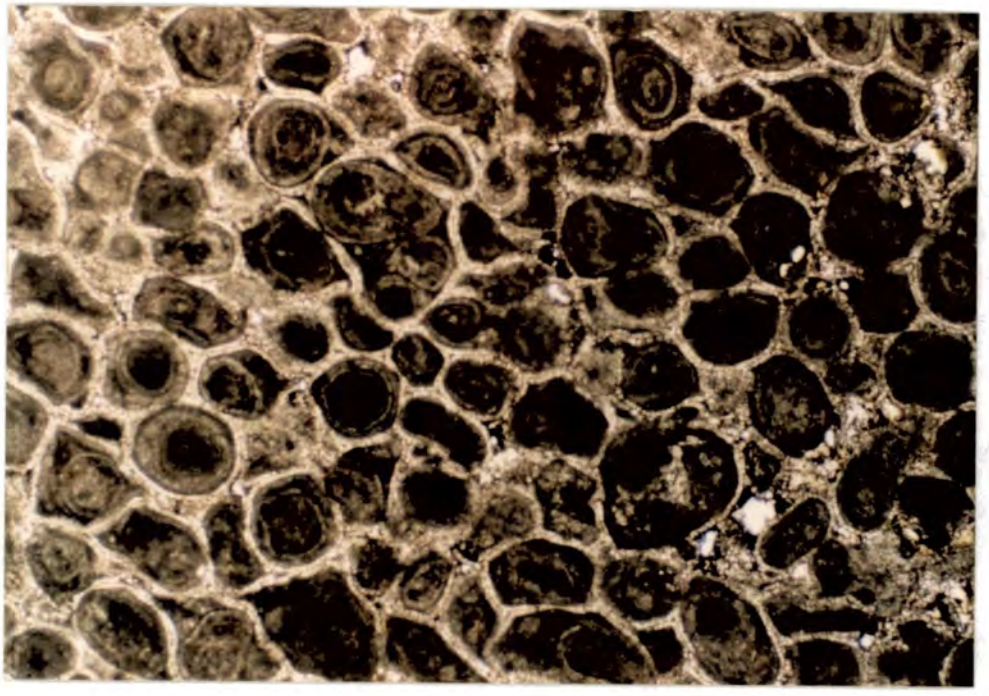

Fig. 4.7. Pisolitic fabric well-preserved in dolomite. Pisoids show polygonal 'fitted' fabric and development of intraclasts. [XPL. LR47. Width of View = 3mm]

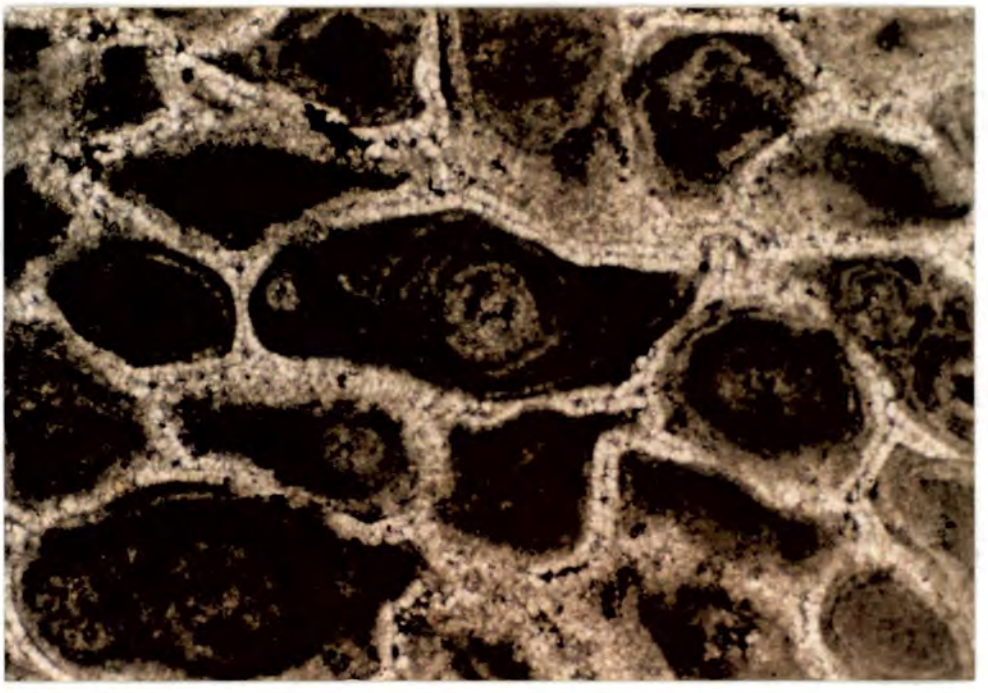

Fig. 4.8. Pisolite preserved in fabric-replacive dolomite. Fine-grained bridge structures link adjacent pisoids and are cemented by an isopachous fringing dolomitised cement. [XPL. LR47. Width of View = 1.4mm]

4.3.1.2 Pisoid petrography (Fig.s 4.7, 4.8)

The central part of each pisoid resembles the ooids with a typically indistinct nucleus, surrounded by a concentrically laminated cortex. However, the outer part of the cortex has irregular laminae and micritic bridge structures commonly link adjacent pisoids. Intraclasts are often present and are composed of several pisoids cemented together by micrite. These structures indicate that the pisoids were immobile during their later growth and that the later laminae grew more or less *in situ* (*cf.* the calcrete-coated grains of Wright, 1989). The growth of the pisoids was directed into the cavities, resulting in a polygonal 'mosaic' of pisoids against each other which appears to have been later enhanced by some dissolution and compaction (see Section 4.3.3). In general the pisoids do not appear to have vadose pendant or gravitational fabrics such as those described by Esteban & Pray (1983). The growth of the pisoids may have been microbially controlled in a beach caliche environment (Inden & Moore, 1983; Scholle & Kinsman, 1974) or in a supratidal environment with precipitation of aragonite muds (coniatolites, Purser & Loreau, 1973).

4.3.2 Oolite and pisolite cements

The ooids in the oosparites are cemented by an early fringing cement which passes into blocky calcite cement that occludes the intergranular porosity (Fig. 4.9). The early cement consists of bladed calcite crystals forming an irregular rim around the ooids. The cement is interpreted to be phreatic, and originally composed of calcite (see Harris *et al.*, 1985).

The pisolites contain micrite 'bridge' fabrics between pisoids and micrite-cemented intraclasts. The pisoids and intraclasts are cemented by a fringing, isopachous cement (Fig. 4.8). All the Lower Muschelkalk pisolites have been dolomitized and the cement consists of radially-oriented fibrous to bladed crystals of dolomite. The isopachous cement has been fractured during early compaction (see Section 4.3.3). The fractures are clean and well-preserved in the dolomite and may suggest that the dolomitization of the cements occurred before compaction. Early diagenetic dolomite cements have been recognised by Kaldi & Gidman (1982) from the Permian of England. Aissaoui (1988) suggested that early, periodic meteoric diagenesis could result in selective dissolution and partial dolomitization of Mg-calcite cements. Early meteoric diagenesis has clearly affected the Lower Muschelkalk oolites and pisolites and this may have resulted in the early dolomitization of the fringing cements before compaction and fracturing.

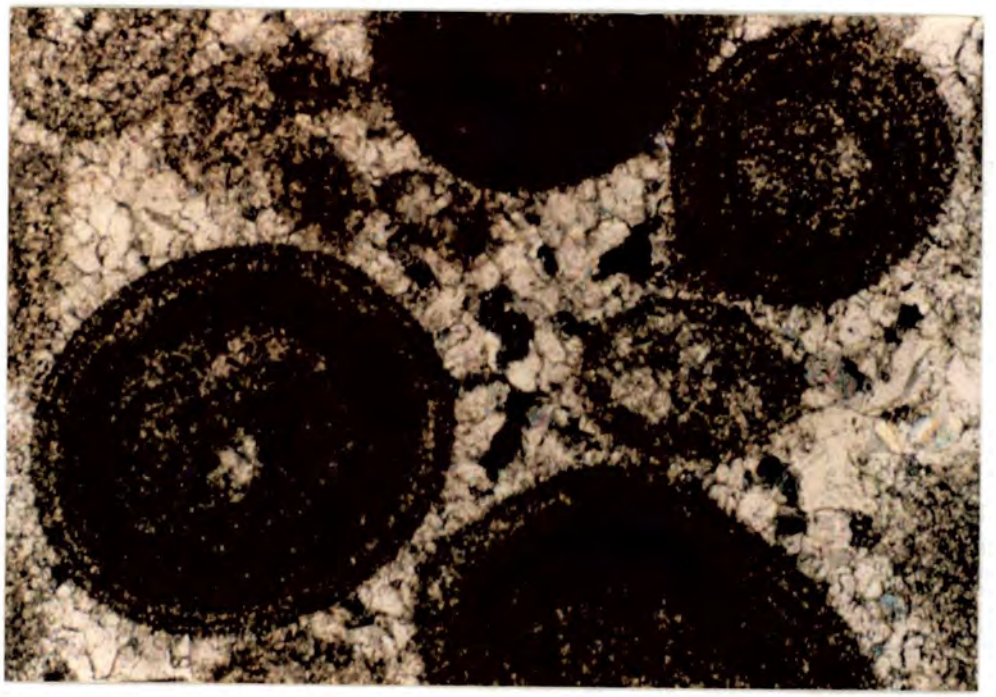

Fig. 4.9. Oosparite with isopachous bladed calcite cement passing into blocky calcite spar. [XPL. G32. Width of View = 1.4mm]

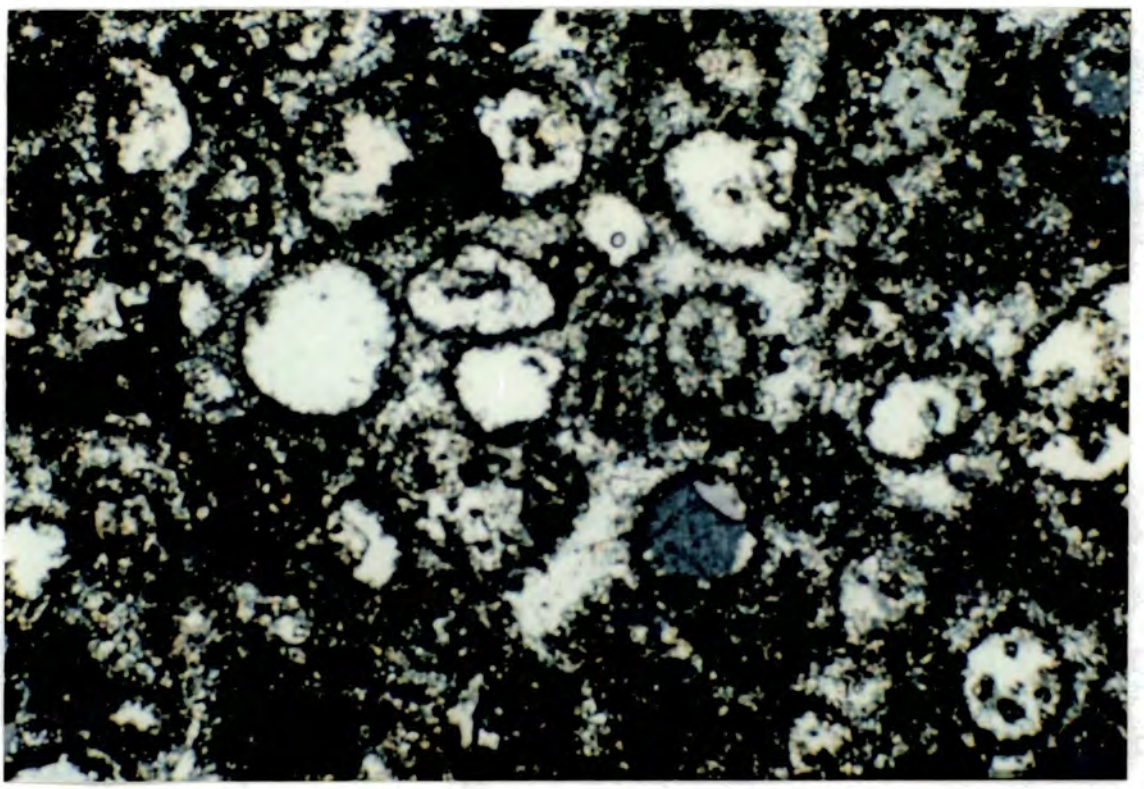

Fig. 4.10. Oomoldic porosity with near-total occlusion by calcite spar. Dolomite crystal rinds define the ooid shapes. See Fig.s 4.11 and 4.12. [Stained thin section. XPL. C16. Width of View = 1.4mm]

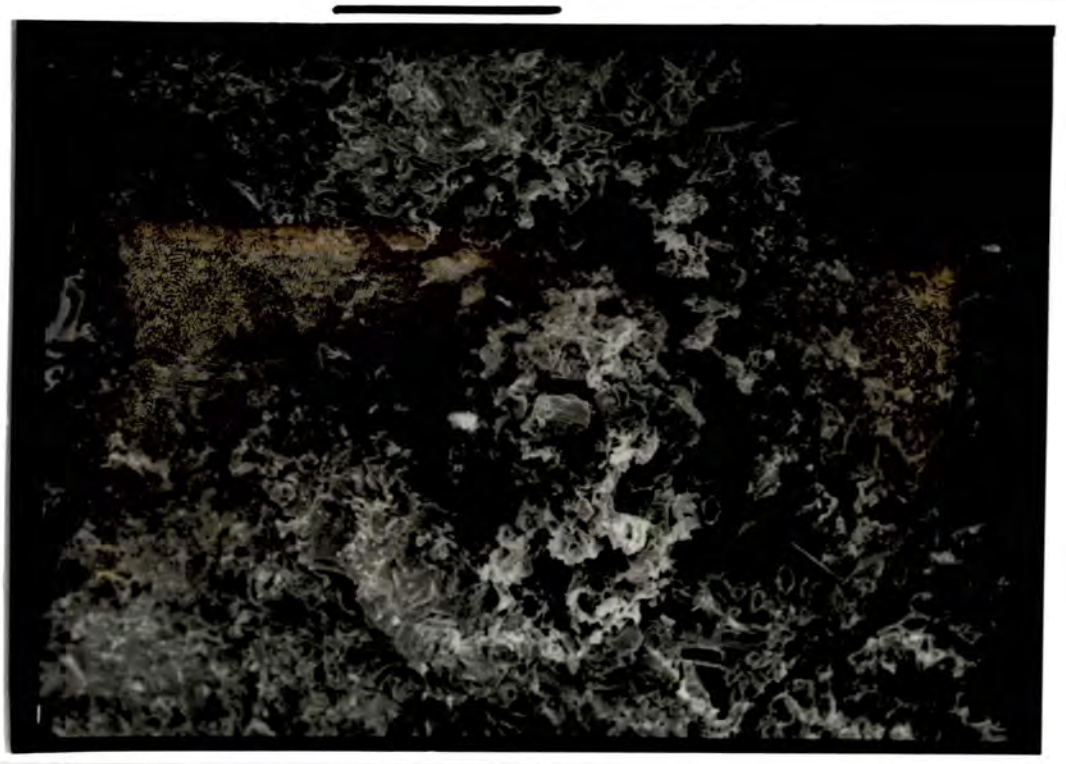

Fig. 4.11. SEM photograph of remnant porosity within oomoldic specimen. Most of the porosity has been occluded by calcite spar. See Fig.s 4.10 and 4.12. [C16. Scale bar = 100um]

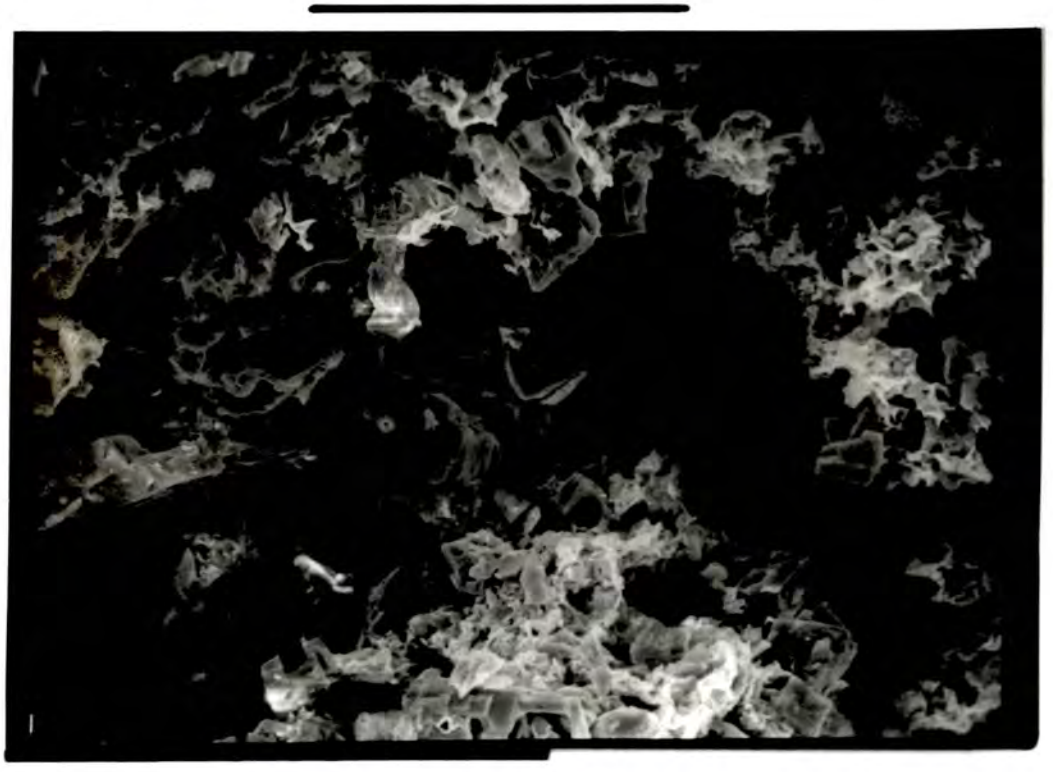

Fig. 4.12. Close-up of Fig. 4.11. Idiotopic dolomite rhombs occur within the oomoldic porosity. Dissolution of ooid occurred prior to dolomite growth. See Fig.s 4.10 and 4.11. [C16. Scale bar = 50um]

4.3.3 Dissolution and compaction structures in the oolites and pisolites

Dissolution and compaction structures are particularly common in the oolites and pisolites that are associated with karstic surfaces and are generally interpreted to result from meteoric diagenesis. The oolitic packstones are generally much less affected than the oolitic grainstones, reflecting the greater permeability of the mud-free grainstones.

4.3.3.1 Internal dissolution of ooids

The concentric lamellae of the ooids are commonly picked out by rings of microspar (Fig. 4.5) resulting from dissolution of the original ooid material and subsequent replacement. Very similar dissolution rings have been observed in Holocene aragonite ooids which have been subjected to meteoric diagenesis (Budd & Land, 1990).

Dissolution of the ooid cortex is very variable, but replacement is generally by clear calcite spar. In some cases only the outlines of the ooids are preserved in large poikilotopic calcite spar crystals (Fig. 4.10). The outlines are defined by dolomite crystal rinds which appear to have grown along micrite envelopes. Locally, two concentric dolomite rinds are present suggesting two phases of stagnation of ooid growth and micritization of the cortex rim. In some cases the dolomite crystals appear to have grown symmetrically inwards and outwards from the micrite envelope suggesting that the ooid dissolution occurred prior to dolomite growth. SEM observations also support this notion (Fig.s 4.11, 4.12). The last phase to precipitate appears to have been the enclosing poikilotopic calcite spar which occluded the oomoldic porosity. The calcite spar preserves ooid outlines with only minor physical compaction and thus was probably precipitated in the near-surface following dissolution of the aragonite cores (Fig. 4.13). This diagenetic sequence has been noted by James & Choquette (1984). Similar observations have been made by Kaldi & Gidman (1982) from the Permian of England.

4.3.3.2 Elephantine structures

Elephantine ('trunk to tail' or 'chain') structures have been noted by Harwood (1988), Wilkinson *et al.*(1984) and Conley (1977). The structures consist of zigzag chains of interlocking crescent-shaped ooid or peloid remnants. Conley (1977) described chains from a pisolite and suggested that the structures are the result of a high degree of pisomoldic porosity followed by local collapse at the narrow interconnections between pisomolds and subsequent cementation by calcite spar.

In the case of the Lower Muschelkalk, elephantine structures are developed in oolites and only locally does oomoldic porosity appear to have been an important part of the

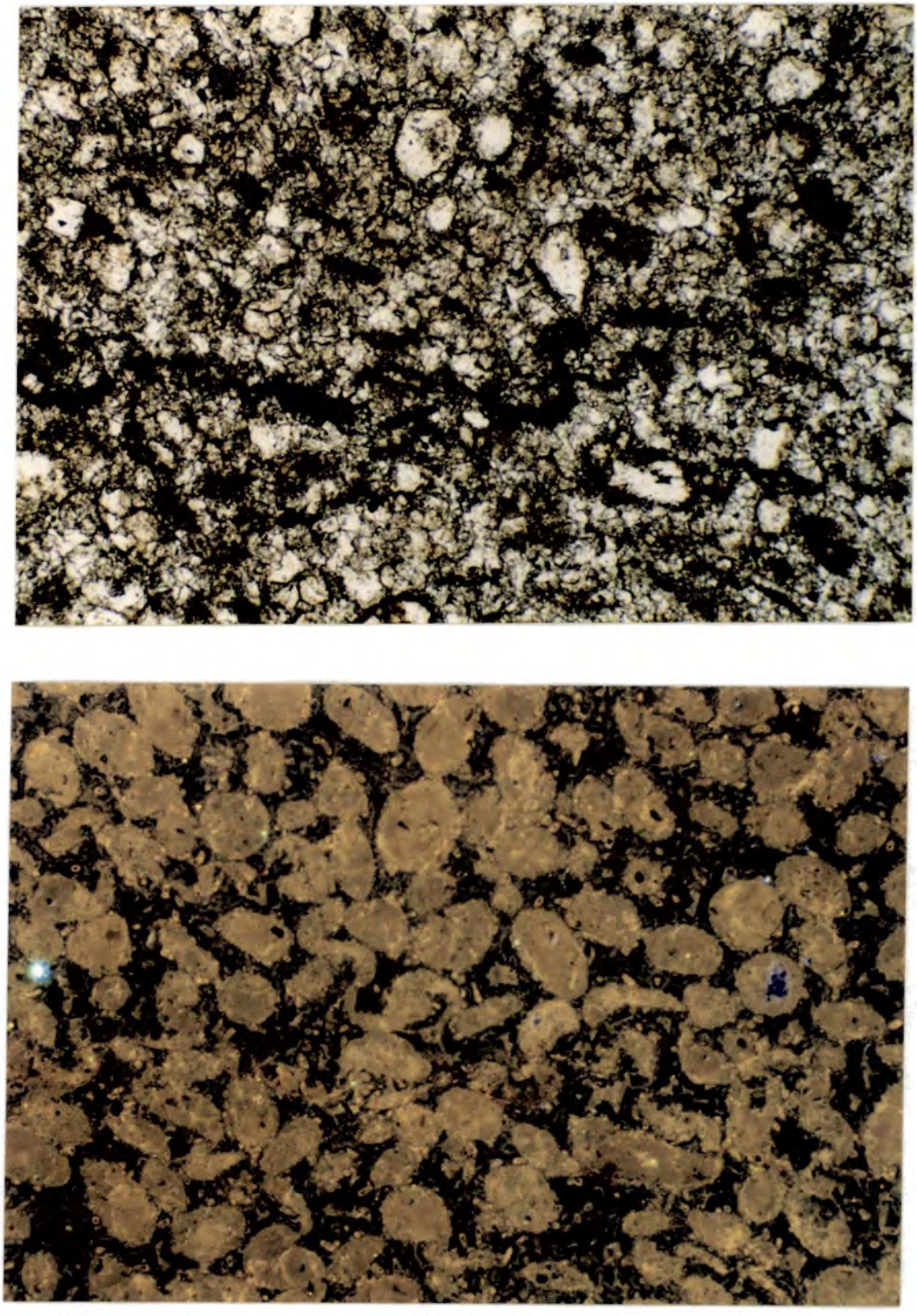

Fig. 4.13. Cathodoluminescence and PPL photomicrograph pair of oomoldic porosity occluded by calcite spar. The calcite spar locally preserves elephantine collapse structures indicating precipitation of spar after initial physical compaction. [VB6. Width of View = 3mm]

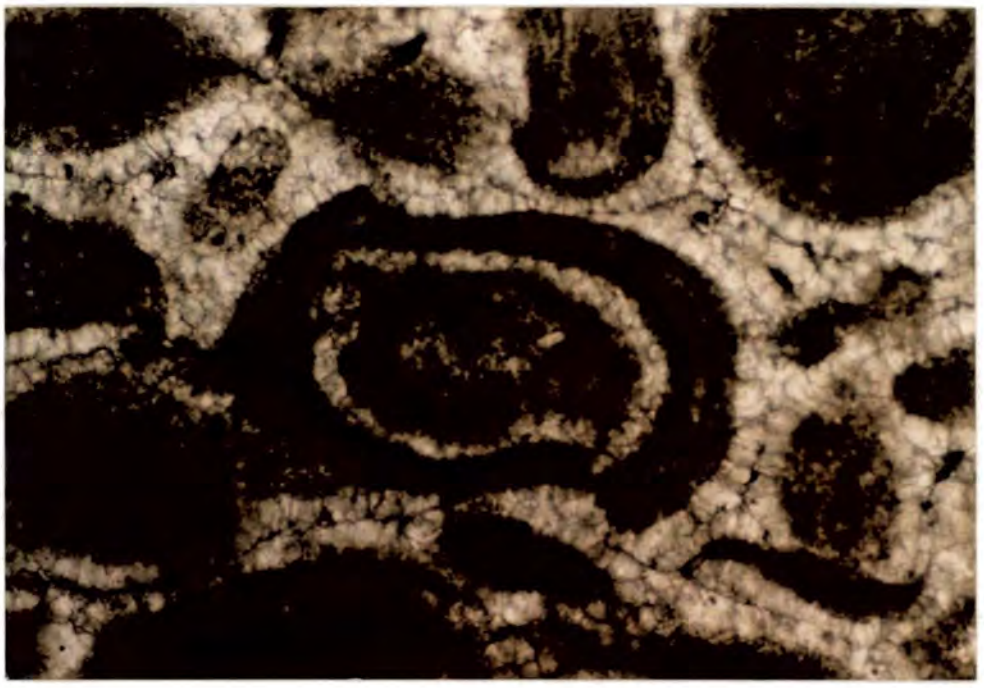

Fig. 4.14. Initial stage of development of elephantine structure in preserved in dolomitized oolite. [XPL. CV18. Width of View = 3mm]

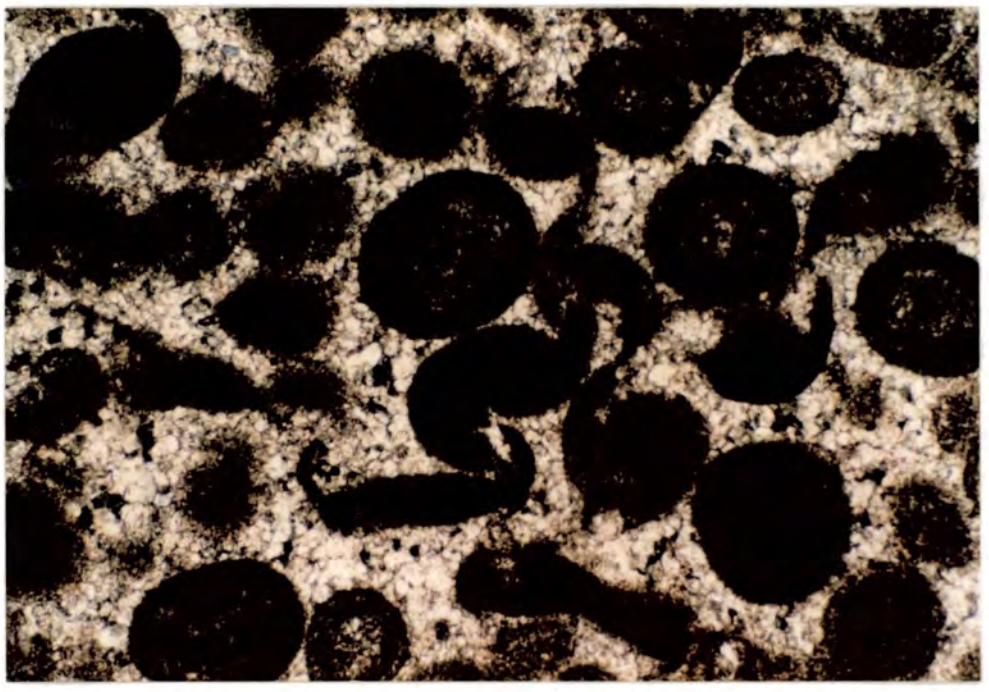

Fig. 4.15. Elephantine structures composed of distorted ooids. [XPL. G32. Width of View = 3mm]

process (Fig. 4.13). In many examples the original ooid fabric is still present and has not been replaced by spar (Fig.s 4.14, 4.15). Dissolution of the ooids appears to have been selective. In general the inner cortex has dissolved preferentially and the outer cortex has spalled off against adjacent ooids. The fracturing of the outer cortices has been initiated at the points of contact with neighbouring ooids and resulted in the flattening and interlocking of the ooid remnants as the inner parts dissolved (Fig. 4.16).

Analogous elephantine structures have been formed in peloidal grainstones.

4.3.3.3 Compaction structures in pisolites

The pisolites show clear signs of compaction. The fringing cement which surrounds the pisoids and intraclasts has behaved in a brittle fashion and cracked and overlapped itself as the rock compacted (Fig.s 4.8, 4.17). The compaction appears to have resulted from dissolution of the pisoid cortex, which probably consisted of aragonite. The fringing cement is commonly buckled around individual pisoids in an analogous fashion to the wrinkling of an apple skin as the fruit dries and shrinks underneath. The buckling might have occurred at the time of dolomitization of the ooid, however the high degree of fabric preservation suggests that the dolomitization conserved volume (see Section 5.5.1). Dissolution and compaction has resulted in the close-fitting mosaic fabric of the pisolites and the spastolithic shapes of some of the pisoids. Similar observations have been made by Hird & Tucker (1988) from Dinantian oolites of South Wales attributed to dissolution and compaction in undersaturated meteoric waters and referred to as 'vadose compaction'.

4.4 TERRIGENOUS COMPONENTS OF THE LOWER MUSCHELKALK

Quartz grains are a common component of the Lower Muschelkalk carbonates, particularly in the El Brull Unit, Olesa Unit and the Colldejou Unit. Sandstones are also present in the Valencia-Cuenca Basin, especially in the northwest where the sequence is thinner and more marginal (see Section 3.3).

4.4.1 Sandstone petrography

The sandstones occur as discrete sharp-based layers in the Valencia-Cuenca Basin (Section 3.3, Fig. 3.31). Towards the northwest the sandstones are thicker and composed of quartz, feldspar, lithic fragments of schist and quartzite and minor grains of tourmaline and muscovite (Fig.s 4.18, 4.19). The feldspar and lithic fragments are generally corroded and altered. Towards the southeast the sandstones have become more quartz-dominated. This lateral transition from lithic arkose to quartz arenite is in agreement with a northwest location for the source of the clastic material.

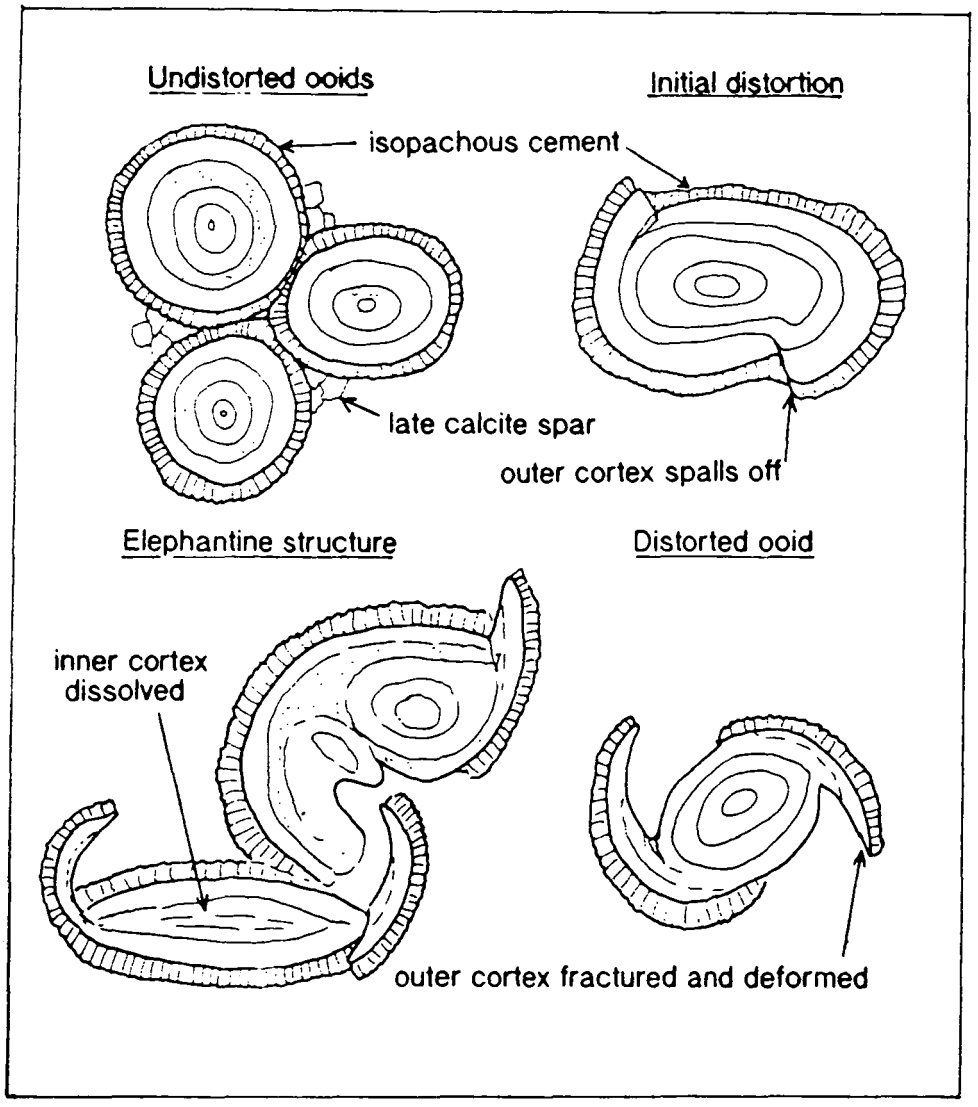

Fig. 4.16. Petrographical scheme for the distorted ooids.

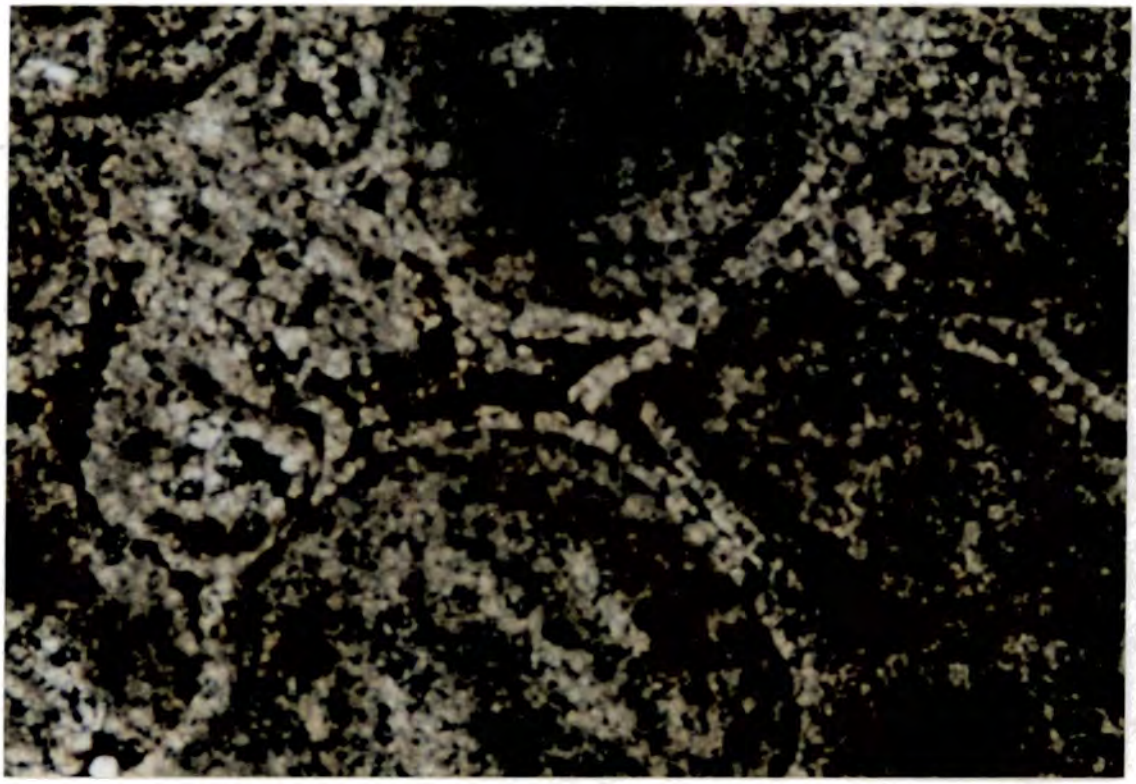

Fig. 4.17. Fractured fringe cement in a dolomitized pisolite. [XPL. F19. Width of View = 0.7mm]

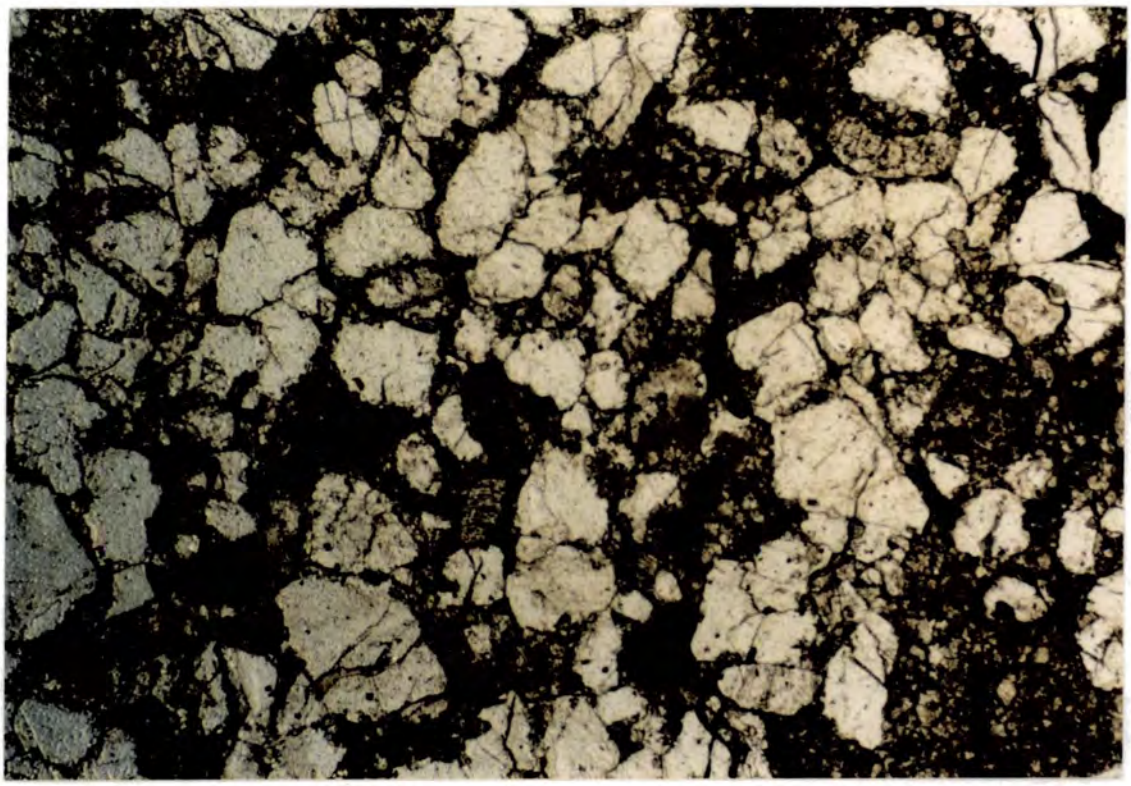

Fig. 4.18. Arkosic sandstone with dolomicrite matrix. [PPL. CV6. Width of View = 1.4mm]

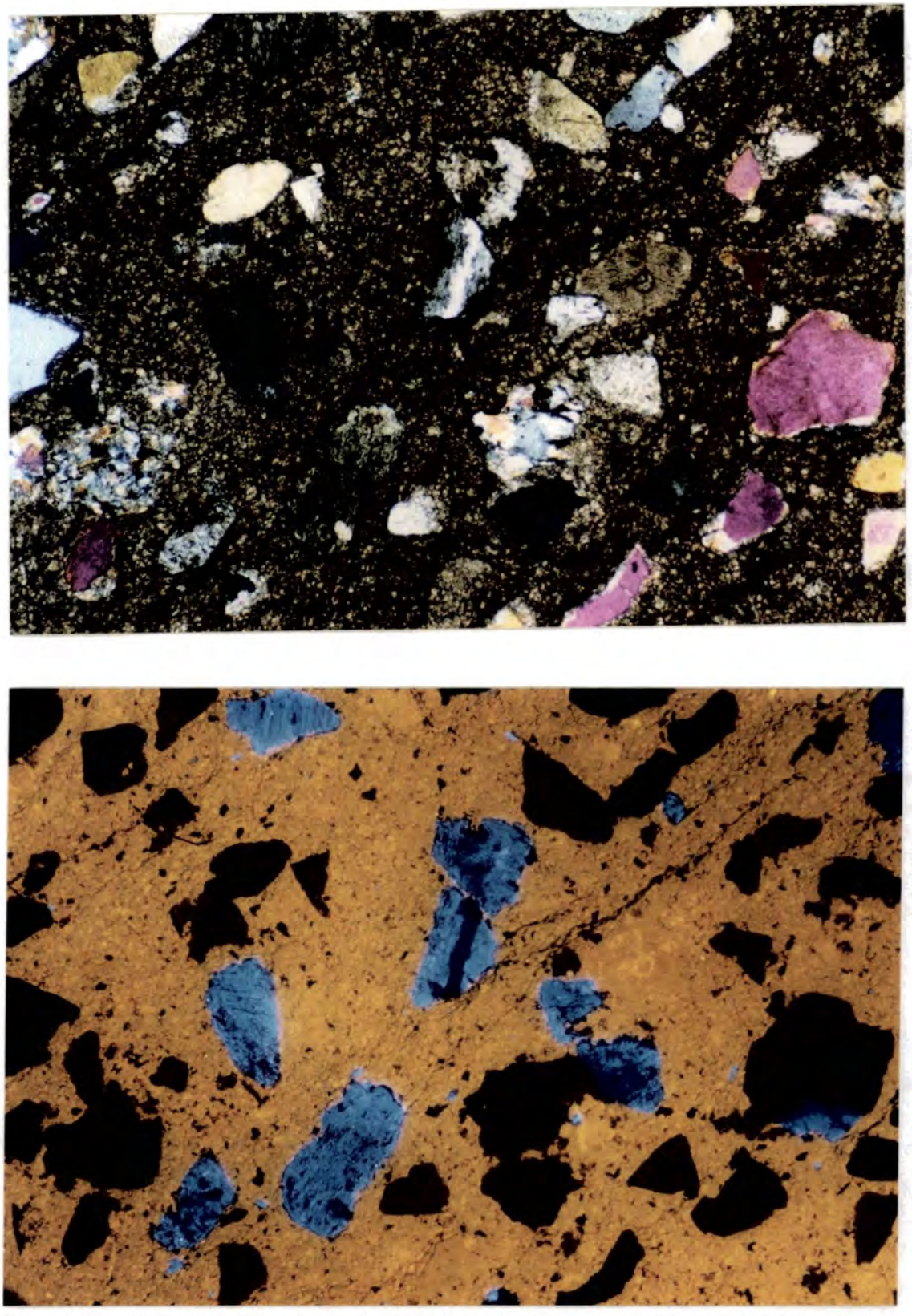

Fig. 4.19. XPL and CL photomicrograph pair of orange-luminescent dolomicrite forming the matrix to a sandstone containing lithic fragments, quartz grains, blue-luminescent feldspar grains and echinoderm fragments (*e.g.* right of centre). [Section is slightly thick. CV10. Width of view = 3mm]

The quartz grains have undulose extinction indicating an original metamorphic provenance, which is most likely to be the Paleozoic basement which would have been exposed in the Hesperic Massif to the west (Fig. 2.6).

The grain-size of the sandstones is generally medium-coarse sand and the rocks are grain-supported. The matrix is composed of dolomicrite which is often dedolomitized in irregular patches to inclusion-rich ferroan calcite spar (see Chapter 8). The calcite spar has a marked rhythmic zonation of orange and dull cathodoluminescence.

Carbonate grains occur with the siliciclastic grains in some of the sandstones. Echinoderm plates are the most common bioclasts, possibly reflecting the robust nature of the single calcite crystal skeletal fragments (Fig. 4.19). The presence of the bioclasts confirms that these are marine sandstones, rather than periods of fluvial deposition in the basin.

Ooids, peloids and echinoderm fragments occur in one of the sandstone layers at Chelva (Section 3.3.3). The ooids and micritic matrix have been dolomitized and the depositional fabric obscured. However, the concentric lamination of the ooids can be observed under cathodoluminescence (Fig. 4.20). Some of the quartz grains are coated form the nuclei to superficial ooids. The ooids and peloids are quite small (up to 0.3mm) and the quartz grains are larger (up to 0.4mm). The carbonate and quartz grains appear to have mixed after formation of the ooids suggesting that the ooid shoals were adjacent to clastic areas (?channels). Occasional strong tidal or storm currents may have resulted in the movement of ooids off-shoal into quiet-water conditions with lime-mud regions at the margins of the clastic channels.

4.4.2 Silt-grade quartz

Matrix-supported silt-grade quartz grains occur in many of the peritidal and lagoonal carbonates of the El Brull Unit, Olesa Unit and Colldejou Unit. These quartz grains may represent an aeolian admixture resulting from offshore sediment transport by dust-storms. Such dust-storms are an important factor in modern sediment accumulation in the Arabian Gulf and indicate predominantly arid conditions onshore (Kukal & Saadallah, 1973). Bioturbation has removed any lamination of clastic material in the sediment.

4.5 TEPEES AND PSEUDOANTICLINES

Tepees are early diagenetic arched-up, inverted V-shaped margins of expansion megapolygons which form in a wide variety of environments from processes involving early cementation and expansion of the surface sediment, fracturing of the resulting crust and filling of these fractures by sediment and further cement (Assereto

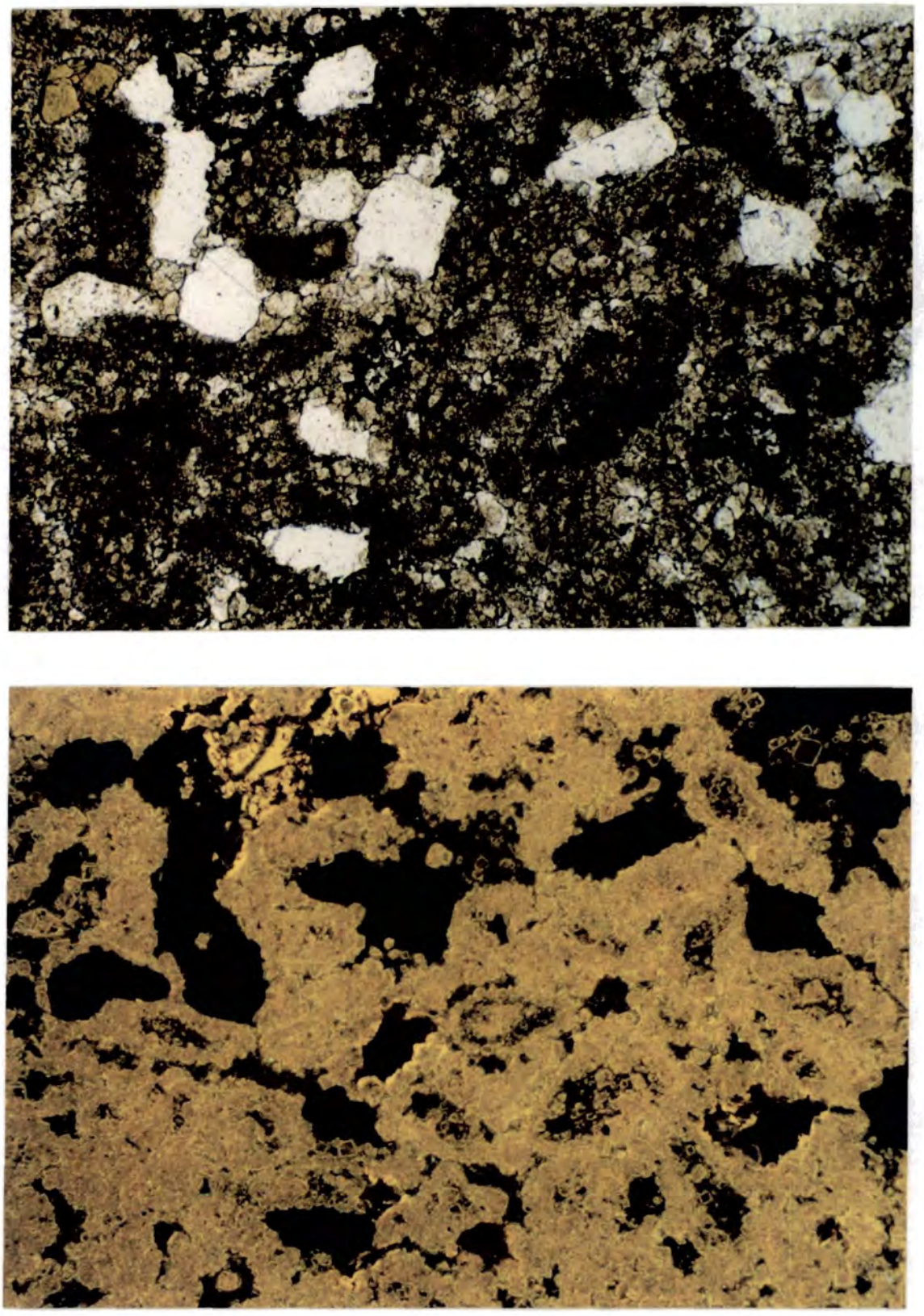

Fig. 4.20. PPL and CL pair of photomicrographs of mixed ooid, peloid and quartz grainstone. Most of the quartz grains are uncoated, but others form nuclei to superficial ooids. Brown (in PPL) crystal is of tourmaline. [CV11. Width of View = 1.4mm]

& Kendall, 1977; Kendall & Warren, 1987). Pseudoanticlines are similar bowed-up features but are more rounded and do not develop a breccia along their crests. Tepees have been recognised from a variety of Holocene environments and have been classified into four types: submarine, peritidal, lacustrine, and caliche (Kendall & Warren, 1987).

Tepees have been recognised in the El Brull Unit and Colldejou Unit of the Catalan Basin, and from the top of the Lower Muschelkalk (equivalent to the Colldejou Unit) in the Valencia-Cuenca Basin.

4.5.1 Tepees of the El Brull Unit

The tepees and pseudoanticlines of the El Brull Unit have been studied at Ciurana (Section 3.2.1.1) and occur at the top of metre-scale peritidal shale-carbonate cycles. The tepees are composed of 10-20cm thick crusts and have a maximum amplitude of about 20cm (Fig. 3.8). The tepees contain little sediment and cement in their fractures and may be classified as immature peritidal tepees (Kendall & Warren, 1987).

4.5.2 Tepees of the Colldejou Unit

The tepees at the top of the Colldejou Unit are generally better developed than those of the El Brull Unit. The three-dimensional tepee and pseudoanticline pattern may be observed at the Colldejou locality (Section 3.2.4.2). The tepees form linear ridges which intersect at approximately 120^{o} angles suggesting a relatively homogeneous stress field such as would occur in a near-horizontal depositional environment (Kendall & Warren, 1987). The megapolygons at the centre of rings of tepees have diameters of about 3-4m.

Pseudoanticlines are locally present and these may resemble microbial mounds (Fig. 4.21). However, laminae within the pseudoanticlines are continuous around the structure and near-isopachous showing that the ridge has resulted from lateral compression rather than from some microbial trapping of sediment.

Many of the tepees have brecciated cores containing angular clasts of laminated crusts cemented by silty dolomicrite and calcite spar (Fig. 4.22). The brecciation appears to have resulted from the lateral compression between the megapolygon edges. The tepee crusts generally consist of red-brown-yellow non-fossiliferous dolomicrite with 0.1-0.5mm laminae picked out by angular silt-grade quartz. Some of the laminae are crinkled and may be microbial with the original sediment crust having formed by cementation of a laminar stromatolite (*cf.* Kendall & Skipwith, 1969).

Fig. 4.21. Pseudoanticline at the top of the Colldejou Unit. Colldejou locality.

Fig. 4.22. Tepee with brecciated core. Note undisturbed bed under the tepee. Colldejou locality.

Locally the tepees contain abundant cement-fill and are highly altered; they may be classified as mature peritidal tepees (Kendall & Warren, 1987). The cements and alteration of the tepee crust show a complex diagenetic history. The tepee crust consists of dedolomitic calcite which in patches is clearly after coarse-grained zoned rhombic dolomite crystals suggesting dolomite growth or recrystallization in the subsurface followed by dedolomitization (Fig. 8.5). The crust also contains two phases of vadose calcite cement: an early, brown, pendant speckly-luminescent cement which may be after dolomite; and a later more widely-developed clear, limpid non-isopachous cement which is generally non-luminescent but red-luminescent in some patches. Locally the second cement overgrows the first. Small (1mm across) nodules of radiating length-slow chalcedony are also present. The petrography suggests the following sequence of events:

i) growth of tepee in fine-grained ?aragonite/dolomite crust.

ii) mature tepee develops with associated recrystallization, brecciation and growth of early pendant calcite (or ?dolomite) cement.

iii) burial and dolomitization of tepee and cements in the subsurface. Growth of zoned dolomite rhombs.

iv) Uplift and dedolomitization of tepee and cements and associated growth of meteoric vadose calcite cements in the near-surface. Formation of chalcedonic quartz.

The two phases of vadose cementation may reflect early and late near-surface meteoric diagenesis (see Section 4.10).

4.5.3 Tepees synthesis

The presence of peritidal tepees indicates a shallow water-table and climatic extremes along the margin of a strand-line of a shallow water-body (Kendall & Warren, 1987). The greater maturity of the Colldejou Unit tepees with respect to the El Brull Unit tepees may reflect a longer time of formation and/or a more supratidal than intertidal setting. The Colldejou Unit tepees occur directly below the sabkha evaporite deposits of the Middle Muschelkalk and have locally been affected by recrystallization and dedolomitization.

4.6 PALEOKARSTS OF THE LOWER MUSCHELKALK

Several types of paleokarst are generally recognised (Esteban & Klappa, 1983; James & Choquette, 1984; papers in James & Choquette, 1988). Wright (1982) distinguished i) Paleokarstic surfaces, representing dissolution at the air-rock interface (uncovered karst), at the soil-rock interface (covered karst) or at the water-rock interface, and ii) subsurface paleokarst (caves *etc.*) which have resulted from underground drainage.

Fig. 4.23. Paleokarstic surface developed upon massive oolite at the top of the Vilella Baixa Unit overlain by laminated dolomicrites of the Lower Member of the Colldejou Unit. Horizon with vuggy porosity occurs 1.3m below karst. Vilella Baixa locality.

Fig. 4.24. Paleokarstic surface developed on an undolomitized dasycladacean packstone at the top of the Lower Member of the Colldejou Unit. Overlying dolomicrite fills the karstic morphology. Torre de Fontaubella locality.

The Lower Muschelkalk of northeast Spain contains well-exposed examples of subsurface paleokarst and also evidence of paleokarstic surfaces, as would be expected for sediments deposited at or near sea-level. It should be noted that calcrete development and karstification have been widespread in northeast Spain during and since the Pleistocene (see figures of Esteban & Klappa, 1983; Calvet & Julia, 1983) and these essentially modern processes have locally obscured and/or reworked the paleokarsts. The modern calcretes and karsts may be associated with dedolomitization (Chapter 8). The paleokarsts were generally most easily recognised at fresh outcrops in quarries and road-cuts where there were no obvious dissolution features linking the karst to the modern soil surface.

4.6.1 Paleokarstic surfaces

Paleokarstic surfaces are quite common in the upper part of the Vilella Baixa Unit and the lower member of the Colldejou Unit.

4.6.1.1 Paleokarstic surfaces of the Vilella Baixa Unit

These paleokarstic surfaces are generally developed on the oolite horizons that occur at the top of the mud-shoal cycles of the upper Vilella Baixa Unit in the central and southern Catalan Coastal Ranges (see Section 3.2.3). The tops of the oolites are irregular with a relief of 5-20cm and are sharply overlain by the mudstones of the next cycle (Fig. 3.19). The oolites are commonly reddened towards the top and display evidence of meteoric diagenesis such as dissolution, pisolitic fabrics and oomoldic porosity occluded by calcite spar (see Section 4.3.3.1). The paleokarstic surfaces are interpreted to have resulted from the temporary exposure of an oolite shoal. There is no evidence of a paleosol or calcrete, suggesting that the paleokarstic surfaces were uncovered and developed at the air-rock interface.

Paleokarstic surfaces are commonly developed at the top of the Vilella Baixa Unit. At Vilella Baixa (see Section 3.2.3.4 and Fig. 3.21) a mud-shoal cycle forms the top of the Vilella Baixa Unit and is overlain by the transitional Lower Member of the Colldejou Unit. A paleokarstic surface is developed on the oolite at the top of the mud-shoal cycle (Fig. 4.23). Some 1.3m below the paleokarst there is a layer with large laminoid vuggy porosity. The vugs are 10-20cm high and form a sinuous pattern linked to the paleokarstic surface by dissolution pipes. The vuggy layer is similar to that described by Wright (1982) from the Carboniferous of South Wales and Land (1973) from the Pleistocene of Jamaica and may represent the paleowater-table. However, no clear evidence of vadose diagenesis is found above the vuggy layer and thus the interpretation cannot be confirmed.

At Colldejou and Falset the top of the Vilella Baixa Unit is directly and sharply overlain by the upper member of the Colldejou Unit (Section 3.2.4.2 and Fig. 3.24). The uppermost layer of the Vilella Baixa Unit is an oolite which exhibits signs of minor karstification including reddening-upwards and an irregular upper surface. About 0.5m below the paleokarstic surface the oolites have been dissolved and replaced by poikilotopic calcite spar which preserves uncompacted ooid outlines (Section 4.3.3.1). The calcite spar is interpreted as a meteoric phreatic cement associated with the karst. These early meteoric-cemented oolites have resisted subsequent dolomitization presumably as a result of their relatively stable mineralogy and coarse grain-size combined with relatively low permeability (see Section 6.3.4.2). However, the actual paleokarstic surface and the directly underlying oolite/pisolite has been well-preserved by later dolomitization (Section 5.5.1.2).

4.6.1.2 Paleokarstic surfaces of the Lower Member of the Colldejou Unit

Several exposures of the transitional Lower Member of the Colldejou Unit contain lenticular beds up to 1.0m thick which pinch out laterally. At Torre de Fontaubella one such lenticular dasycladacean packstone horizon is well-exposed at the top of the Lower Member (Fig. 4.24). The upper surface of the packstone layer is reddened and partially recrystallised to neomorphic spar which may be associated with meteoric waters (Magaritz, 1975). The overlying dolomicrite appears to fill the morphology in the packstone layer and laminae are truncated against it. The morphology of the packstone layer is interpreted to be the result of subaerial exposure and karstic processes and represents original topography at the time of deposition of the overlying dolomicrites. The packstone layer is undolomitized suggesting that there was early cementation and mineralogical stabilization by meteoric waters which prevented dolomitization owing to decreased permeability and reactivity (Section 5.10.1).

4.6.1.3 Synthesis of Lower Muschelkalk paleokarstic surfaces

Paleokarstic surfaces are concentrated in the upper part of the Vilella Baixa Unit and the Lower Member of the Colldejou Unit, and represent horizons of contemporaneous meteoric diagenesis. This early input of meteoric water has had an important influence on later diagenesis. The meteoric diagenesis is interpreted to have resulted in early-cemented layers which resisted subsequent dolomitization. The early dissolution of aragonite ooids and bioclasts may also have been accompanied by a general stabilization of the mineralogy by removal of aragonite from the Lower Muschelkalk sediments below the paleokarstic surfaces. The mineralogical differences may have affected subsequent dolomitization and resulted in geochemical differences between the Upper Member of the Colldejou Unit and the underlying sediments (see Section 6.3).

4.6.2 Subsurface Paleokarsts

The subsurface paleokarsts of the Lower Muschelkalk have been studied by Ramon & Calvet (1987) and Ramon (1985) and are recognised in the El Brull Unit, Olesa Unit and Vilella Baixa Unit. The subsurface paleokarsts are best developed in the northern Catalan Coastal Ranges at Centelles and El Brull and can be traced laterally to Olesa and Palleja. A subsurface paleokarst also occurs at Pontons where it is associated with Pb-Zn-Ba mineralization (see Section 4.7.1).

4.6.2.1 Subsurface Paleokarst of the northern Catalan Coastal Ranges

The subsurface paleokarsts of the northern Catalan Coastal Ranges consist of a number of laterally extensive dissolution surfaces subparallel to bedding. The thickness and degree of dissolution is variable but the paleokarsts are most marked towards the northeast. The paleokarst at Centelles is particularly well-developed and is described here (Fig. 3.16). For descriptions of the similar karst at El Brull and the smaller examples at Puig Gracios, Olesa and Palleja see Ramon (1985) and Ramon & Calvet (1987).

At Centelles two of the subsurface paleokarsts are well-exposed and are about 3m apart. The lower paleokarst is parallel to bedding and developed within limestones. The underlying limestone shows signs of dissolution and is covered by a 10cm layer of red marl. The lower paleokarst is connected via dissolution pipes to the better developed upper paleokarst. The upper paleokarst has a relief of 0.2-2.5m and is covered by silty marl (Fig. 4.25). The marl separates limestones below from dolomites above. The marl is hematitic and red-coloured towards the base of the paleokarst and within the dissolution pipes. The red marl becomes limonitic and ochre-coloured towards the top reflecting hydration of the hematite. The base of the overlying dolomite is irregular but relatively smooth in comparison to the underlying limestone. The marl contains rounded clasts of limestone up to 1m across and a few dolomite clasts towards the top. The larger blocks show bedding and have clearly been rotated.

No vadose cements, calcrete fabrics or exposure features have been identified in the marl fill and the presence of minor roof-collapse structures indicates that dissolution occurred after burial (Wright, 1982). The karst is interpreted as a meteoric phreatic subsurface paleokarst.

4.6.2.2 Identification of the exposure surface related to subsurface paleokarst

The exposure surface related to the subsurface paleokarst system is not readily identifiable. The two principal possibilities are: (a) the top of the Lower Muschelkalk

Fig. 4.25. Subsurface paleokarst at Centelles. Paleokarst deepens to the left of the view and is covered by orange-red marl containing blocks of dolomite and limestone. Karst separates dolomite above from limestone below. Centelles locality.

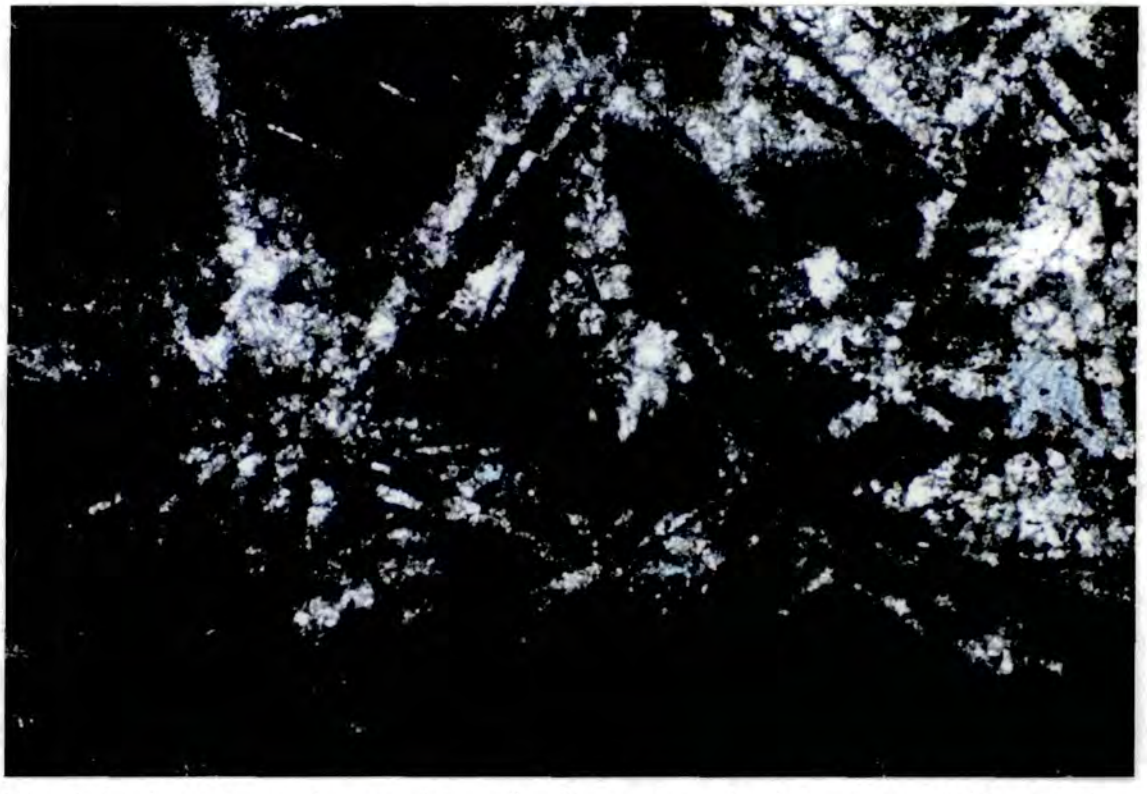

Fig. 4.26. Stellate calcite pseudomorph after gypsum in dolomicrite. [XPL. LR38. Width of view = 3mm]

where there is a sharp contact with the Middle Muschelkalk and locally a laminated crust which has been identified as a caliche deposit (Esteban *et al.*, 1977); and (b) the unconformity at the base of the Paleogene sediments. There is of course the possibility of overprinting of a later karst system on an earlier one; however, the paleokarsts appear to show only one phase of dissolution.

The base-Paleogene unconformity is angular and truncates the Muschelkalk in the northern Catalan Coastal Ranges (Fig.s 2.11, 3.1; Section 2.4) coinciding with the area of most highly developed subsurface paleokarst. Prominent subsurface paleokarsts are only found where the early Paleogene unconformity is at or below the top of the Triassic.

The sediment thickness between the paleokarst and the exposure surface represents a minimum estimate for the depth to the base of the meteoric phreatic lens. The subsurface paleokarst at Centelles is *ca.* 15m below the Paleogene unconformity but would have been about 35m below the top of the Lower Muschelkalk (*n.b.* the top of the Lower Muschelkalk is missing owing to the Paleogene unconformity). The meteoric phreatic lens in low-relief settings, such as the Lower Muschelkalk carbonate ramp, is often very thin or brackish (Tucker & Wright, 1990). The semi-arid climate during the Muschelkalk would also preclude extensive meteoric phreatic lens development. Hence, the most feasible exposure surface for the widespread development of the subsurface paleokarst system of the northern Catalan Coastal Range is considered to be the major unconformity at the base of the Paleogene.

4.6.2.3 Implications for the timing of dolomitization

The silty marl overlying the paleokarst at Centelles separates dolomite above from limestone below. At first sight the marl appears to have acted as an aquiclude to dolomitizing fluids suggesting that dolomitization occurred after karstification. However, closer examination implies that this is not the case.

Interstratal karst is a type of subsurface karst which develops along lithological boundaries, particularly where a permeable unit overlies limestone (Wright, 1982). The limestone dissolves preferentially and a karstic surface is formed along the lithological boundary. It is well known that limestones are several orders of magnitude more soluble in meteoric waters than dolomites (Choquette & James, 1988). The subsurface paleokarsts of the northern Catalan Coastal Range are interpreted as the result of migration of meteoric waters, at the time of the formation of the base-Paleogene unconformity, through overlying less soluble dolomite into more soluble limestones with concomitant interstratal karst formation. The meteoric water probably passed through the dolomite via thin dissolution pipes (Choquette &

James, 1988). In other words, the subsurface paleokarst exploited the solubility contrast between dolomite and limestone along the pre-existing dolomite front.

Clasts of dolomite also occur in the upper part of the marl fill implying dolomitization was pre-karstification. There is also abundant petrographic evidence that dolomitization occurred pre-burial and certainly before Paleogene uplift and erosion (see Section 5.10).

4.7 HYDROTHERMAL MINERALIZATION OF THE LOWER MUSCHELKALK

Hydrothermal mineralization locally occurs in both the Catalan Coastal Ranges and in the Valencia-Cuenca Basin. The mineralization is often associated with baroque dolomite which usually occurs as a fracture-lining cement and also locally as a baroque dolomite mosaic (see Section 5.8).

4.7.1 Catalan Coastal Ranges

Minor ore mineralization is locally present at a small number of localities in the central and northern Catalan Coastal Ranges (Sacrista *et al.*, 1980; Andreu *et al.*, 1987). The mineralization is always related to subsurface paleokarsts and breccia-fills similar to that at Centelles (Section 4.6.2). Breccia-hosted Pb-Zn-Ba mineralization commonly occurs in carbonate rocks and is thought to be the result of meteoric karstification and subsequent ore mineral emplacement as a separate and later event (Sangster, 1988). The consideration of the ore mineralization process is beyond the scope of this study. However, Neogene volcanism is quite common the north of the study-area (to the east of Centelles) and associated hydrothermal fluids may be responsible. Baroque dolomite cement is more common at those localities which have hydrothermal mineralization (see Section 5.8.2.1).

4.7.2 Eastern Iberian Ranges

A minor amount of hydrothermal mineralization has been recognised towards the base of the Lower Muschelkalk at two localities in the eastern Iberian Ranges (Chelva and Albarracin). The principal mineral was a coarse-grained, zoned iron-rich magnesite (or Breunnerite; Deer *et al.*, 1966) with subsidiary quartz, dolomite and calcite. The mineralogy was confirmed by XRD and ICPAES elemental analysis. The minerals occur in bedding-parallel sharp-sided veins up to 20cm across. Magnesite does occur as a primary sedimentary mineral, however the monomineralic nature of the layers and the sedimentary environment suggest that these are hydrothermal alteration/precipitation products.

4.8 SULPHATES AND ASSOCIATED PROCESSES

Sulphate minerals occur in the Lower Muschelkalk of the subsurface of the Ebro Basin (Jurado, 1988) and their former presence in the Catalan Coastal Ranges and eastern Iberian Ranges is indicated by the presence of pseudomorphs after gypsum and anhydrite and collapse breccias. This topic is also discussed in Section 8.4 because of the association of sulphate dissolution and dedolomitization.

This section will concentrate on pseudomorphs after sulphates which are common in the Lower Muschelkalk, particularly within the peritidal facies of the Colldejou Unit and El Brull Unit.

4.8.1 Pseudomorph shapes

Two principal pseudomorph shapes have been observed.

4.8.1.1 Stellate pseudomorphs with pointed terminations

These are the most common pseudomorphs and generally occur in the peritidal dolomicrites of the Colldejou Unit and El Brull Unit. Subtidal mudstones and wackestones of the Vilella Baixa Unit also contain stellate pseudomorphs. The pseudomorphs vary in size and complexity from 0.5mm lens-shapes to 5mm stellate clusters. The pseudomorphs are interpreted to be after early diagenetic gypsum (Fig. 4.26).

4.8.1.2 Lath-shaped square-ended pseudomorphs

Lath-shaped pseudomorphs are generally associated with partially dolomitized bioturbated wackestone facies in the Vilella Baixa Unit (Fig.s 4.27, 4.28). The pseudomorphs occur in the dolomitized areas between limestone 'burrows' (see Section 5.5.2). The pseudomorphs are interpreted to be after anhydrite which probably grew during late diagenesis from hypersaline brines that may be associated with dolomitization. Lath-shaped porosity, probably resulting from anhydrite dissolution occurs within some dolomitized grainstones (Fig. 4.29) confirming that these sulphates were not related to the depositional environment.

Lath-shaped and rectangular pseudomorphs are common in the Lower Muschelkalk of the Valencia-Cuenca Basin. The pseudomorphs are locally present in dolomicrite-cemented sandstones and are associated with dolomite cement (see Section 5.9.3.3). These pseudomorphs usually consist of ferroan calcite.

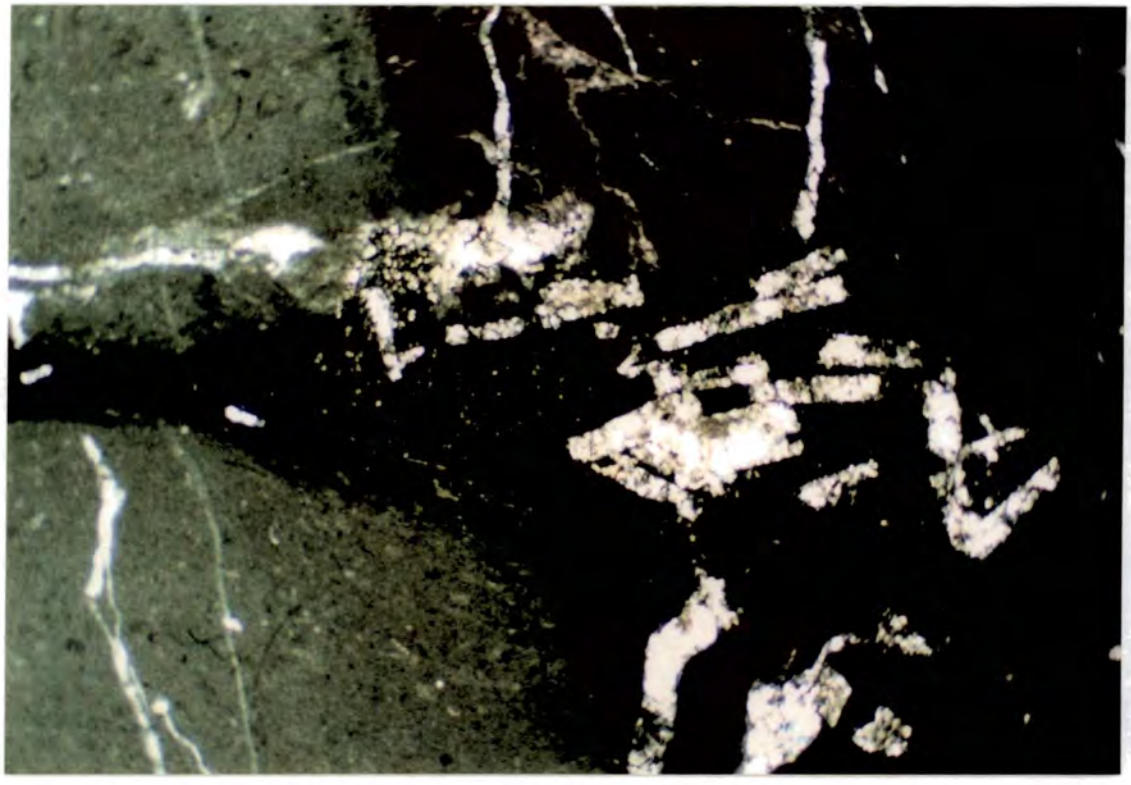

Fig. 4.27. Square-ended pseudomorphs after anhydrite within dolomitized part of a bioturbated lime mudstone. [Half-stained. PPL. CB12. Width of view = 14mm]

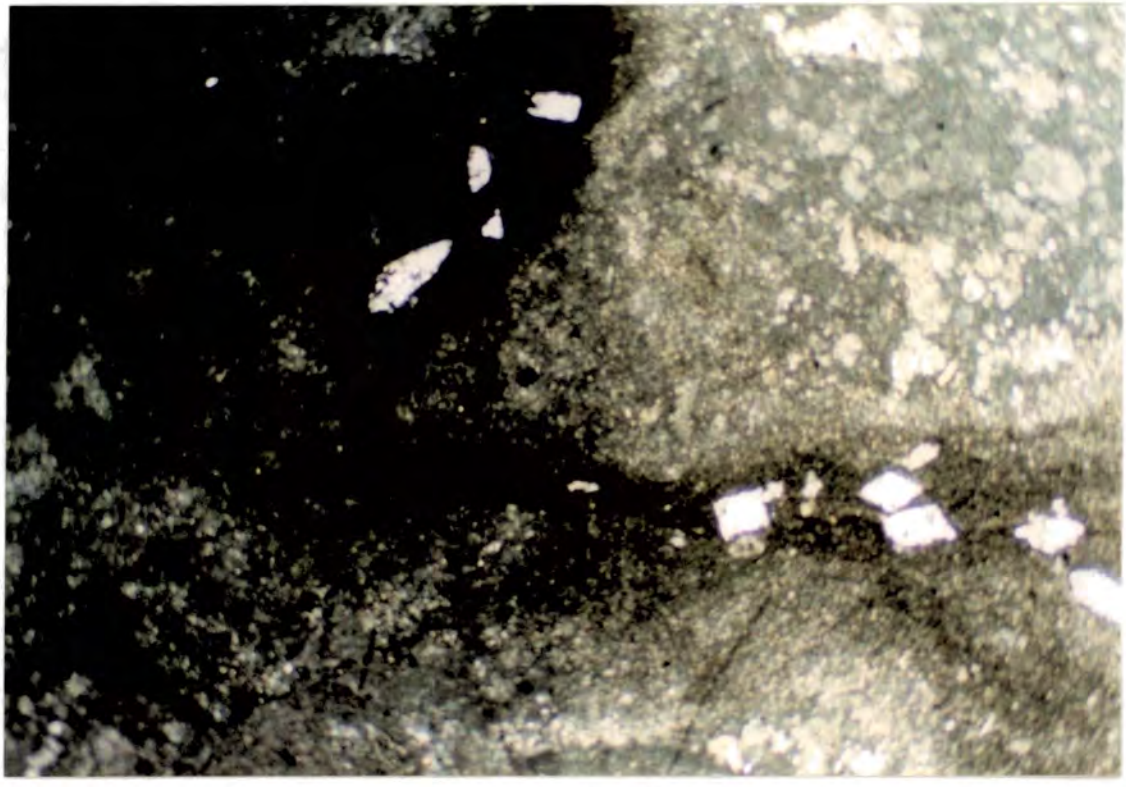

Fig. 4.28. Pseudomorph after anhydrite within dolomitized part of a lime packstone. [Half-stained section. XPL. OM17. Width of view = 14mm]

4.8.2 Pseudomorph mineralogy

Most of the pseudomorphs are composed of a replacive cement, however some have been unreplaced and are porous. There are two main cement associations.

4.8.2.1 Calcite spar

Clear, blocky calcite spar is the most common cement of the stellate pseudomorphs. The calcite generally has a marked rhythmic zonation of bright and dull orange cathodoluminescence. The pseudomorphs locally have geopetal fills of calcite crystal silt and pendant vadose cements (Fig. 4.30, 4.31). The calcite spar has a meteoric stable isotope signature and is thought to be related to dedolomitization processes (see Section 8.7).

These pseudomorphs are interpreted to have formed as a result of near-surface sulphate dissolution and meteoric calcite precipitation in locally vadose conditions.

4.8.2.2 Dolomite/calcite/quartz/fluorite

The pseudomorphs after anhydrite and a few of those after stellate gypsum contain a more varied mineralogy than in Section 4.8.2.1. The pseudomorphs are commonly lined by zoned red cathodoluminescent baroque dolomite crystals which locally form the entire pseudomorph. However more typically the pseudomorph centres are composed of non-luminescent calcite spar.

Some non-luminescent calcite spar stellate pseudomorphs contain lath-shaped clear quartz crystals which may be after anhydrite, suggesting replacement of the sulphate before rehydration to gypsum (see Section 4.9.2). A minor amount of fluorite is associated with this quartz in a few examples (Fig. 4.32). The fluorite has a bright blue cathodoluminescence and as a result of several minutes observation under CL changes colour in plane-polarised light from colourless to purple, a phenomenon noted by Lee & Harwood (1989) and Dickson (1980).

Fluorite is commonly considered to be a low-temperature hydrothermal mineral and fluid inclusion data on fluorite have given homogenisation temperatures as low as 83°C (Deer *et al.*, 1966). Baroque dolomite also indicates elevated temperatures of 60-150°C (Radke & Mathis, 1980) and has been associated with sulphate replacement by other workers (Machel, 1987; Sections 5.8, 5.9.3.3).

4.8.3 Pseudomorph synthesis

The great majority of pseudomorphs are associated with peritidal facies of the Colldejou Unit and El Brull Unit and are considered to indicate early diagenetic

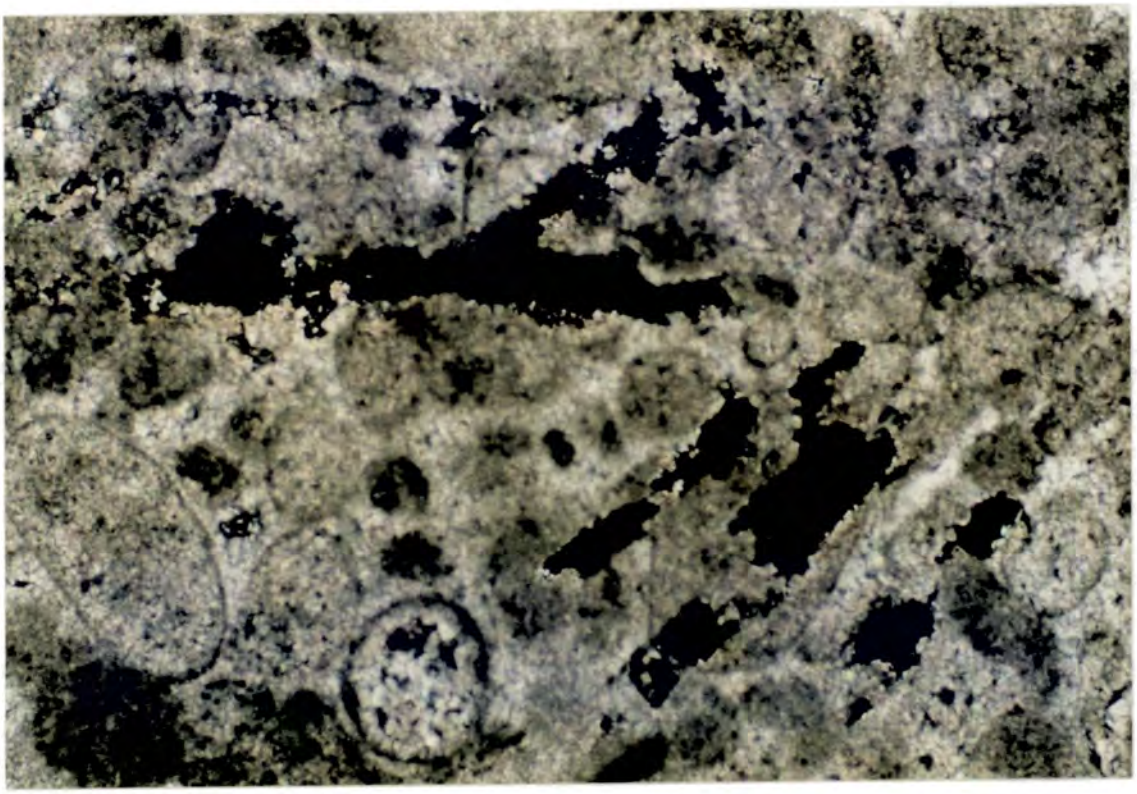

Fig. 4.29. Lath-shaped porosity within dolomitized grainstone. [XPL. F38. Width of view = 1.4mm]

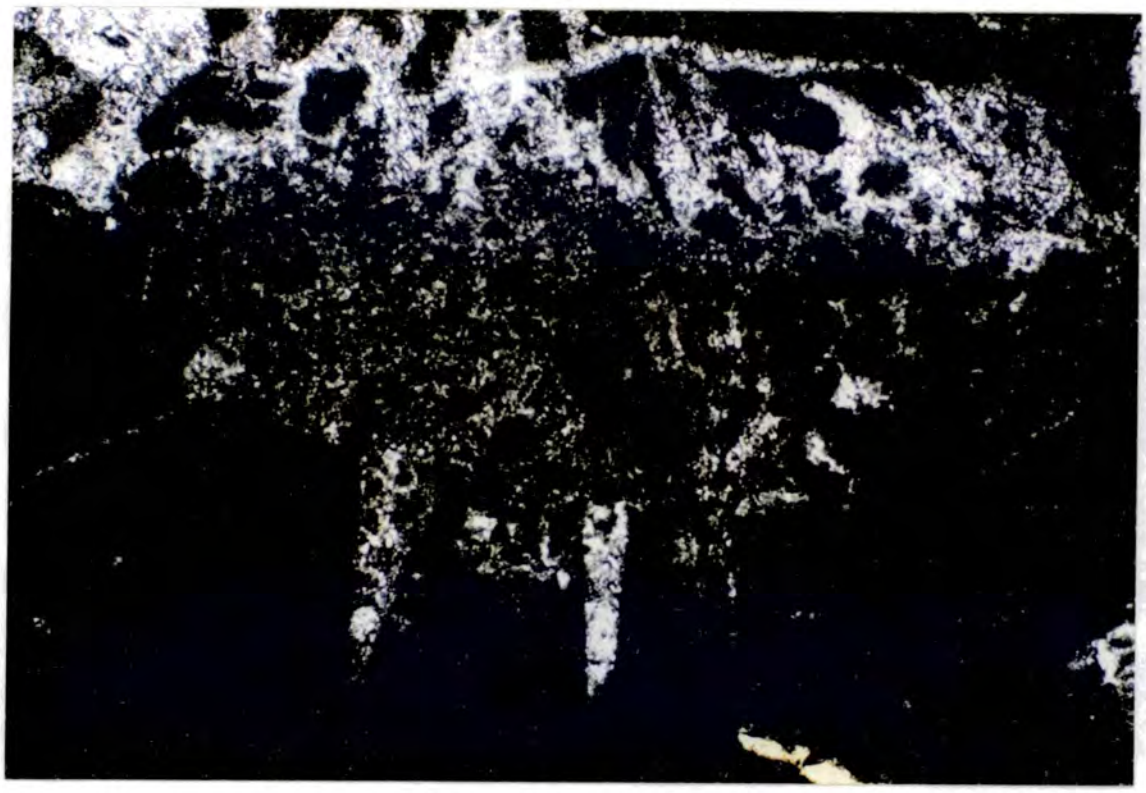

Fig. 4.30. Geopetal structure within calcite pseudomorph after sulphate. [PPL. F13. Width of view = 3mm]

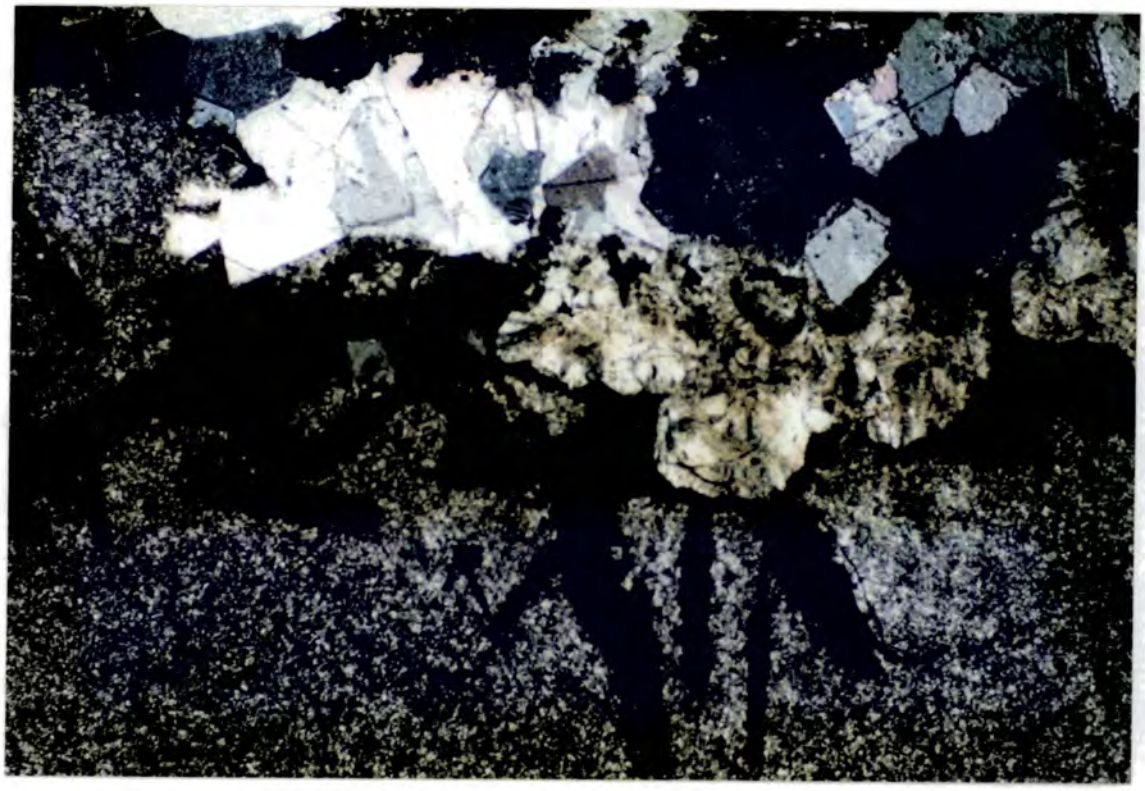

Fig. 4.31. Pendant equant calcite spar and fibrous speleothemic calcite cement within pseudomorph after sulphate. [XPL. A32. Width of view = 3mm]

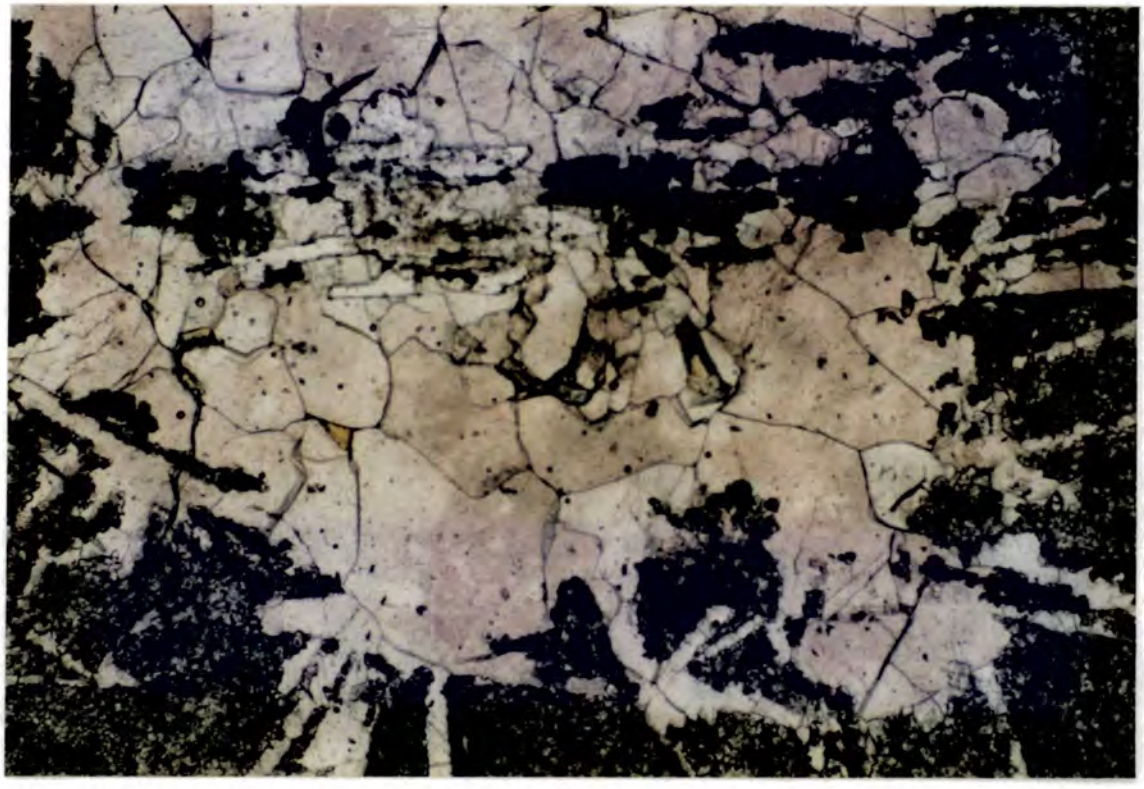

Fig. 4.32. Pink-stained calcite with clear elongate quartz and dark purple fluorite within pseudomorph after sulphate. [PPL. A31 Width of view = 3mm]

growth of stellate gypsum. The gypsum would have dehydrated to anhydrite on burial, as observed in the Lower Muschelkalk of the subsurface of the Ebro Basin (Jurado, 1988).

Other pseudomorphs, particularly those after anhydrite and those of the normal marine facies of the Vilella Baixa Unit, are later diagenetic and may be related to hypersaline brines and dolomitization (see Section 5.10.1.2).

Sulphate dissolution and pseudomorphic cementation appears to have taken place under a range of diagenetic conditions. The majority of calcitic pseudomorphs appear to have formed during near-surface and even vadose meteoric conditions. However, other pseudomorphs appear to have been formed at elevated temperatures and in association with some hydrothermal activity. The hydrothermal activity which emplaced the small amounts of Pb-Zn-Ba ore minerals is probably also responsible for the quartz and fluorite and may be related to Tertiary igneous activity (see Section 4.7).

4.9 SILICIFICATION OF THE LOWER MUSCHELKALK

Non-detrital diagenetic quartz is quite common in the Lower Muschelkalk and occurs in dolomitized and undolomitized sections. There are two main associations: i) Nodular and replacive silica unassociated with the former presence of sulphates; and ii) Limpid elongate quartz crystals forming the central parts of some pseudomorphs after sulphates. The two types may occur in close proximity (*e.g.* same thin section) but this is not always the case.

4.9.1 Chert nodules and replacive chalcedonic quartz

4.9.1.1 Chert Nodules

Smooth-surfaced subspherical chert nodules occur in the Olesa Unit and Vilella Baixa Unit and are up to 20cm across (Fig. 4.33). The nodules tend to be concentrated in bedding parallel layers and occur in dolomitized and undolomitized strata suggesting no simple relationship to the dolomitization process (*cf.* Knauth, 1979). The nodules are commonly zoned on a mm-scale into alternating light and dark bands which appear to result from varying degrees of silicification of the carbonate host. The zonation is concentric and this may suggest a phreatic origin. Most nodules have very sharp outer margins. However, others, particularly the zoned examples, have diffuse edges (Fig. 4.34). In partially dolomitized hosts the intergranular calcite appears to be more readily silicified than the euhedral dolomite resulting in an outer zone of dolomite rhombs with interstitial chalcedonic quartz (Fig. 4.35). This observation implies that dolomite rhombs within chert nodules may not imply contemporaneity of

Fig. 4.33. Chert nodule and veins within undolomitized Lower Muschelkalk. Capcanes locality.

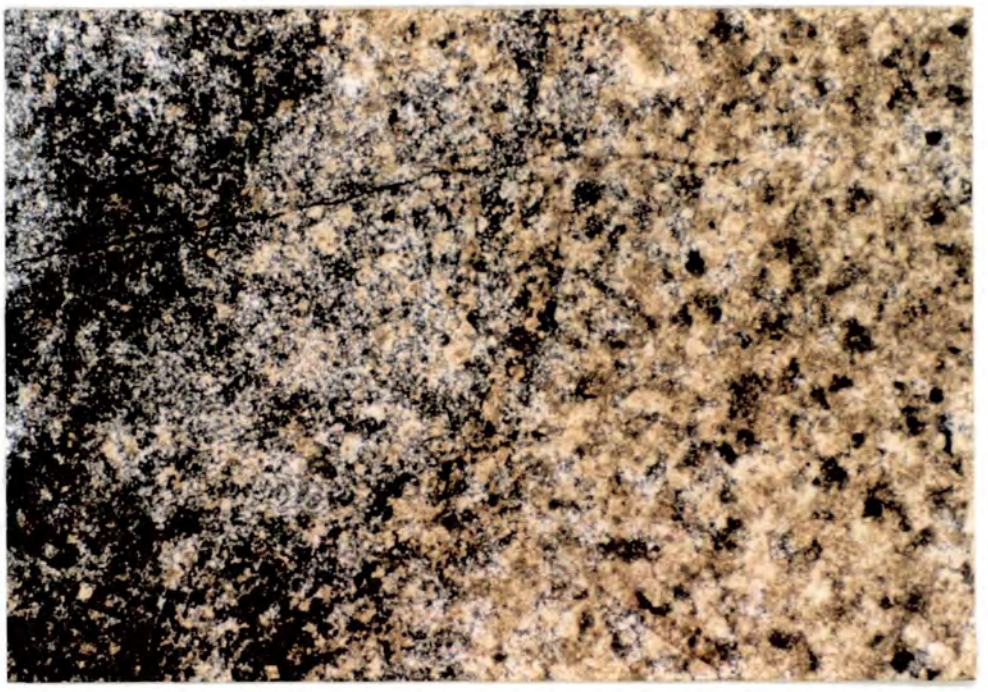

Fig. 4.34. Diffuse margin of chert nodule in dolomite. [XPL. CT50. Width of view = 3mm]

dolomitization and silicification (*cf.* Knauth, 1979). Kuslansky & Friedman (1981) reported a similar phenomenon: partial silicification of crinoid fragments could result in single calcite rhombs preserved within the chert, and these could be misinterpreted as the products of dedolomitization.

The silica in the nodules generally consists of brown (in plane-polars), fibrous chalcedonic quartz commonly grading centripetally to microcrystalline quartz with isolated pockets of larger quartz crystals. No inclusions of anhydrite or other sulphates have been identified and these nodules are not interpreted to be replacements of sulphate nodules (*cf.*Milliken, 1981; Maliva, 1987).

The chert nodules appear to be late diagenetic features post-dating dolomitization. A few examples are cut by late luminescent calcite spar veins. No compactional features are observed around the nodules suggesting that nodule formation was post-compaction.

Some small nodules, *ca.* 1mm across, of radiating chalcedonic quartz are associated with paleokarstic surfaces (Section 4.6.1) and these may be early diagenetic.

4.9.1.2 Chert veins and lenses

Locally chert occurs as veins and lenses which may be pseudomorphing burrows. The chert is not concentrically zoned but consists of inclusion-rich microcrystalline quartz overlying more transparent inclusion-poor quartz. This way-up zonation is consistent and may reflect a vadose origin.

4.9.1.3 Selective replacement by silica

Bioclasts in the Lower Muschelkalk are locally selectively replaced by silica. Dasycladacean algal thalli appear to be prone to silicification (*cf.* dedolomitization, Section 8.3.3). Calcitic echinoderm fragments have been replaced centripetally resulting in a rim of radial fibrous chalcedony (Fig. 4.36).

4.9.2 Limpid quartz forming pseudomorphs after sulphates

Some calcite pseudomorphs after sulphates contain elongate 'skeletal' crystals of clear quartz pseudomorphing laths of anhydrite (Section 4.8.2.;*cf.* Tucker, 1976). The anhydrite was probably produced by burial dehydration of originally stellate gypsum prior to subsequent silicification.

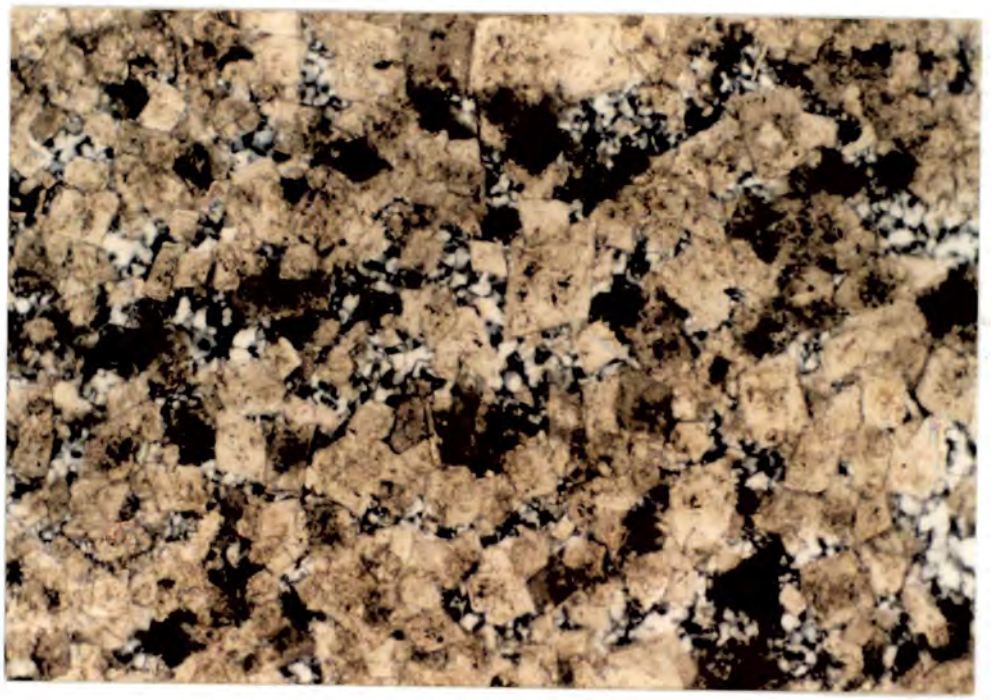

Fig. 4.35. Chalcedonic quartz between dolomite rhombs. [XPL. CT49. Width of view = 1.4mm]

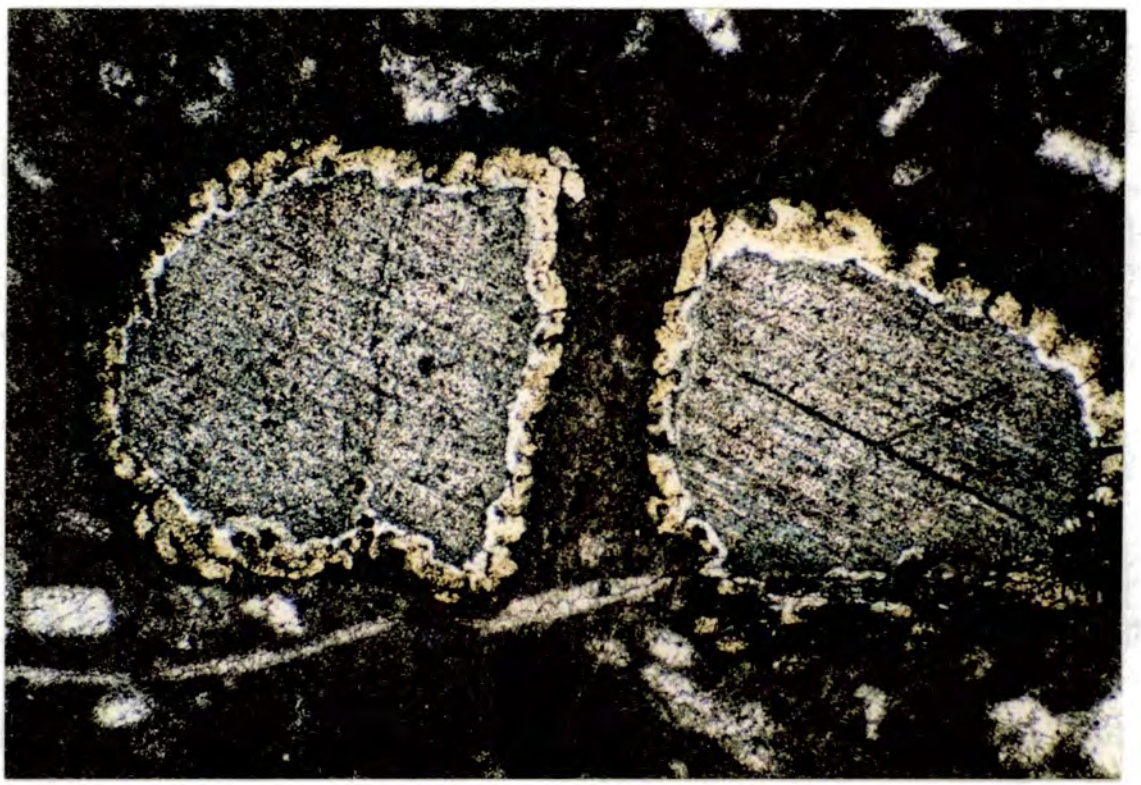

Fig. 4.36. Centripetal selective replacement of echinoderm fragments by chalcedonic quartz. [Stained section. PPL. CA24. Width of view = 3mm]

4.9.3 Silicification Synthesis

Silicification has occurred in limestones and dolomites and in some cases is associated with the former presence of sulphates.

The nodules and veins consist of chalcedonic and microcrystalline quartz and may exhibit vadose and phreatic zonation. They appear to be late uplift-related diagenetic features. Small nodules are related to paleokarstic surfaces and in some cases to dedolomitization. Subtle mineralogical and/or kinetic factors have locally controlled the silicification process resulting in fabric-selective replacement.

Clear quartz crystals are locally associated with sulphate dissolution and pseudomorph formation. These pseudomorphs have been interpreted as late diagenetic features but associated with elevated hydrothermal temperatures (Section 4.8.3).

No isotope studies have been carried out on these chert nodules. However, most of the Phanerozoic nodular cherts analysed by Knauth & Epstein (1976) have a meteoric-water isotope signature. Meteoric-derived groundwaters are generally considered to be important to the silicification process (Knauth, 1979; Milliken, 1979).

The silicification of the Lower Muschelkalk is generally considered to be late diagenetic and related to uplift and meteoric-derived groundwaters. In a few cases there may have been hydrothermal fluid involvement. The meteoric diagenesis may have taken place during early Paleogene uplift or may be related to modern uplift and erosion (see Section 8.6, the equivalent discussion for dedolomitization). Supratidal/sabkha deposits, like those of the Middle Muschelkalk, have been proposed as a possible source of silica (Moore *et al.*, 1972). Nicholls & Silberling (1980) noted similar silicification features in localities with very similar depositional and diagenetic settings to the Lower Muschelkalk.

4.10 SYNTHESIS OF METEORIC DIAGENESIS

The meteoric diagenesis of the Lower Muschelkalk can be considered as occurring in two phases: i) Early meteoric diagenesis penecontemporaneous to deposition; and ii) Late near-surface meteoric diagenesis associated with uplift and erosion during the early Paleogene or end-Tertiary to Recent.

4.10.1 Early penecontemporaneous meteoric diagenesis

The principal result of the early meteoric diagenesis was the formation of paleokarstic surfaces within the upper Vilella Baixa Unit and the lower member of the Colldejou Unit. The paleokarstic surfaces are associated with oomoldic porosity, pisolitic

fabrics, sparitization, dissolution features and early calcite cementation. The dissolution of molluscan aragonite skeleta and subsequent replacement by calcite spar is also probably related to early meteoric diagenesis. The early calcite spar is clear and dull to non-luminescent under cathodoluminescence. Early aragonite dissolution and mineralogical stabilization of the Lower Muschelkalk below the upper member of the Colldejou Unit is interpreted have been an important control on subsequent dolomitization (see Chapter 7).

4.10.2 Late meteoric diagenesis

Paleogene uplift and erosion resulted in meteoric diagenesis and the formation of a system of subsurface paleokarsts in the northern Catalan Coastal Range where the base-Paleogene unconformity is close to and truncates the Lower Muschelkalk. Elsewhere in the Catalan Coastal Ranges the late meteoric diagenesis may be related to early Paleogene uplift and erosion and/or the modern erosion surface. This has resulted in dedolomitization, silicification, calcite veining, sulphate dissolution and associated collapse breccias and pseudomorphs. The late meteoric diagenesis occurred after the main dolomitization process (Chapter 7). Most of the calcite spar associated with the late meteoric diagenesis is zoned under cathodoluminescence into bright and dull rings and has a meteoric isotope signature (see Section 8.5.4.3).

CHAPTER 5: DOLOMITIZATION FIELD RELATIONS AND PETROGRAPHY

5.1 INTRODUCTION

Dolomitization has been an important field of research for many years and the topic of several recent reviews (Morrow, 1982a,b; Land, 1985; Machel & Mountjoy, 1986; Hardie, 1987; Tucker & Wright, 1990) and symposia (Zenger *et al.*, 1980; Shukla & Baker, 1988). A large number of dolomitization models have been proposed and each has several variants (Fig. 5.1). Seawater dolomitization models are currently gaining in popularity and these invoke dolomitization by essentially unaltered seawater (Fig. 5.2). The principal requirements for any model of large-scale dolomitization are a source of Mg^{2+}, an efficient fluid-flow system over the envisaged time-span, and reaction conditions amenable to precipitation of dolomite or dolomitization of pre-existing calcium carbonate (after Morrow, 1982b).

5.2 DOLOMITIZATION OF THE LOWER MUSCHELKALK

The dolomitization of the Lower Muschelkalk is widespread and has resulted in two principal dolomite facies, referred to as 'white dolomites' and 'grey dolomites' by Calvet *et al.* (1990) and Calvet & Ramon (1987). The white dolomites form the Upper Member of the Colldejou Unit and generally consist of dolomicrites which preserve fine-scale peritidal sedimentary structures (*e.g.* Section 4.5.2). Dolomicrites with similar features are also locally present in the El Brull Unit.

The grey dolomites occur below the Upper Member of the Colldejou Unit and are very variable in thickness but generally extend down through the Vilella Baixa Unit. The base of the grey dolomites is a bedding-discordant dolomite front. The grey dolomites replace lagoonal to marine limestones to form massive commonly coarse-grained crystal mosaics with a variable degree of fabric preservation.

The **white dolomites** of the Upper Member of the Colldejou Unit and similar facies of the El Brull Unit will be referred to as the **peritidal dolomites.** The **grey dolomites** will be referred to as **fabric-replacive dolomites.**

The Lower Muschelkalk also locally contains minor amounts of baroque dolomite as a cement and replacive mosaic.

This chapter will concentrate on field observations and petrography of the Lower Muschelkalk dolomites of the Catalan Basin and then make comparisons with the Valencia-Cuenca Basin localities.

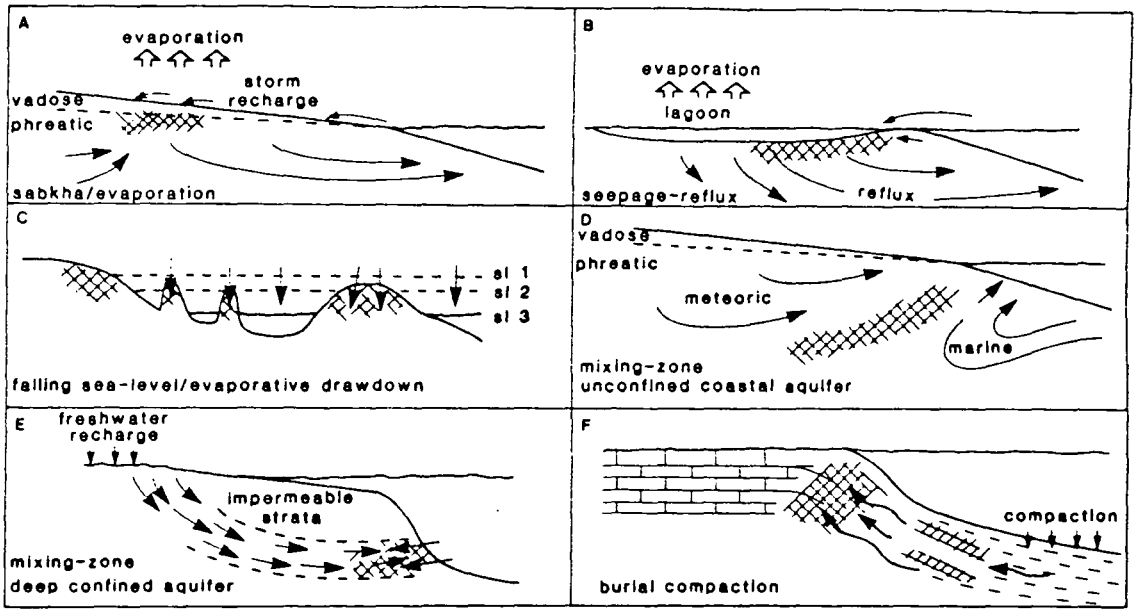

Fig. 5.1. Dolomitization models (excluding seawater models)

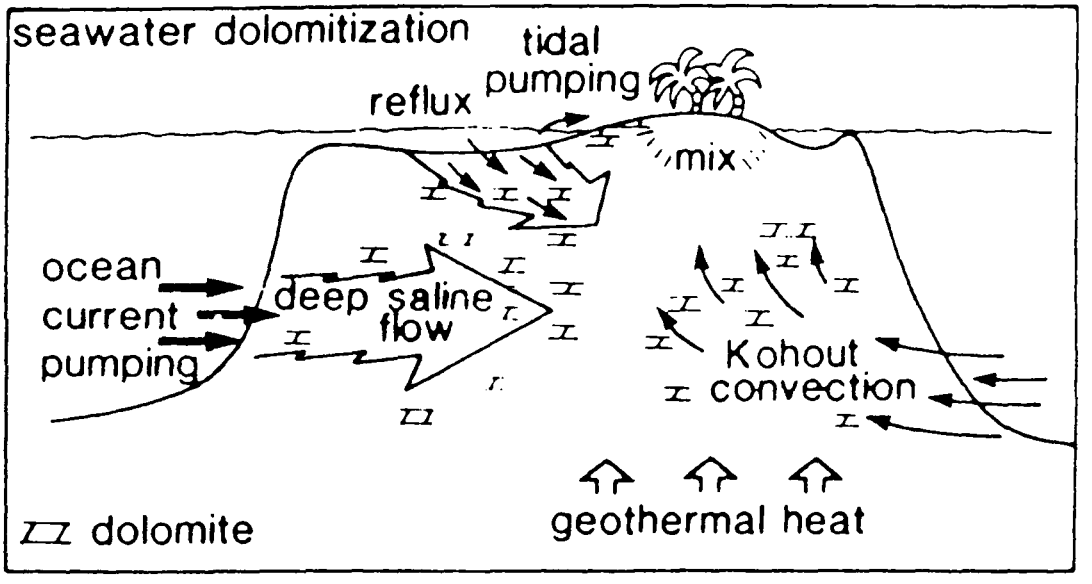

Fig. 5.2. Seawater dolomitization models for a carbonate platform: ocean current pumping, reflux of slightly hypersaline lagoon waters, tidal pumping along shoreline and Kohout convection. [from Tucker & Wright, 1990]

5.3 DOLOMITIZATION GEOMETRY OF THE LOWER MUSCHELKALK

The peritidal dolomite that forms the upper member of the Colldejou Unit and some horizons of the El Brull Unit is pervasive and laterally extensive. However in contrast the thickness of the fabric-replacive dolomite is variable.

The upper boundary of the fabric-replacive dolomite is generally a sharp contact with the peritidal dolomicrites of the Upper Member of the of the Colldejou Unit. However, the lower boundary of the fabric-replacive dolomites is a bedding-discordant dolomite front (Section 5.4.1). The extent of the fabric-replacive dolomite is shown in Fig. 5.3. Broadly, the Catalan Basin consists of a northern area where the dolomite front occurs in the Vilella Baixa Unit; a central area of near-total dolomitization; and a southern area with a much reduced thickness of fabric-replacive dolomite. Data from Jurado (1988) indicate that dolomitization of the Lower Muschelkalk of the subsurface of the Ebro Basin is virtually ubiquitous and limestone is only present in a few borehole localities in the southeast, towards the Catalan Basin.

The transitions between these areas of differing extent of dolomitization are sharp and some localities with extensive fabric-replacive dolomitization occur within a few kilometres of others with abundant limestone (*e.g.* Falset and Capcanes). However, the gradient of the dolomite front need not be any greater than that observed at outcrop (Section 5.4.1) at about 1:100. However, in part, the boundaries of the different areas do appear to follow the traces of Tertiary strike-slip faults (see Section 2.2) and movement on these may have juxtaposed areas and be partially responsible for the rapid transitions.

5.3.1 Conclusions from dolomite geometry

The general arrangement of the dolomitization of the Lower Muschelkalk is one of peritidal dolomite overlying fabric-replacive dolomite which has a sharp bedding-discordant contact with the underlying limestone. The extent of dolomitization is variable within the Catalan Basin but there is an increase in dolomite towards the northwest into the Lower Muschelkalk of the subsurface of the Ebro Basin. The dolomite geometry indicates that the dolomitizing fluid-flow system must have had at least a component of downwards movement and that the dolomitization was more effective towards the northwest. The steep gradients of the dolomite front suggest that there were some local variations in the fluid-flow system such that nearby areas have markedly different degrees of dolomitization.

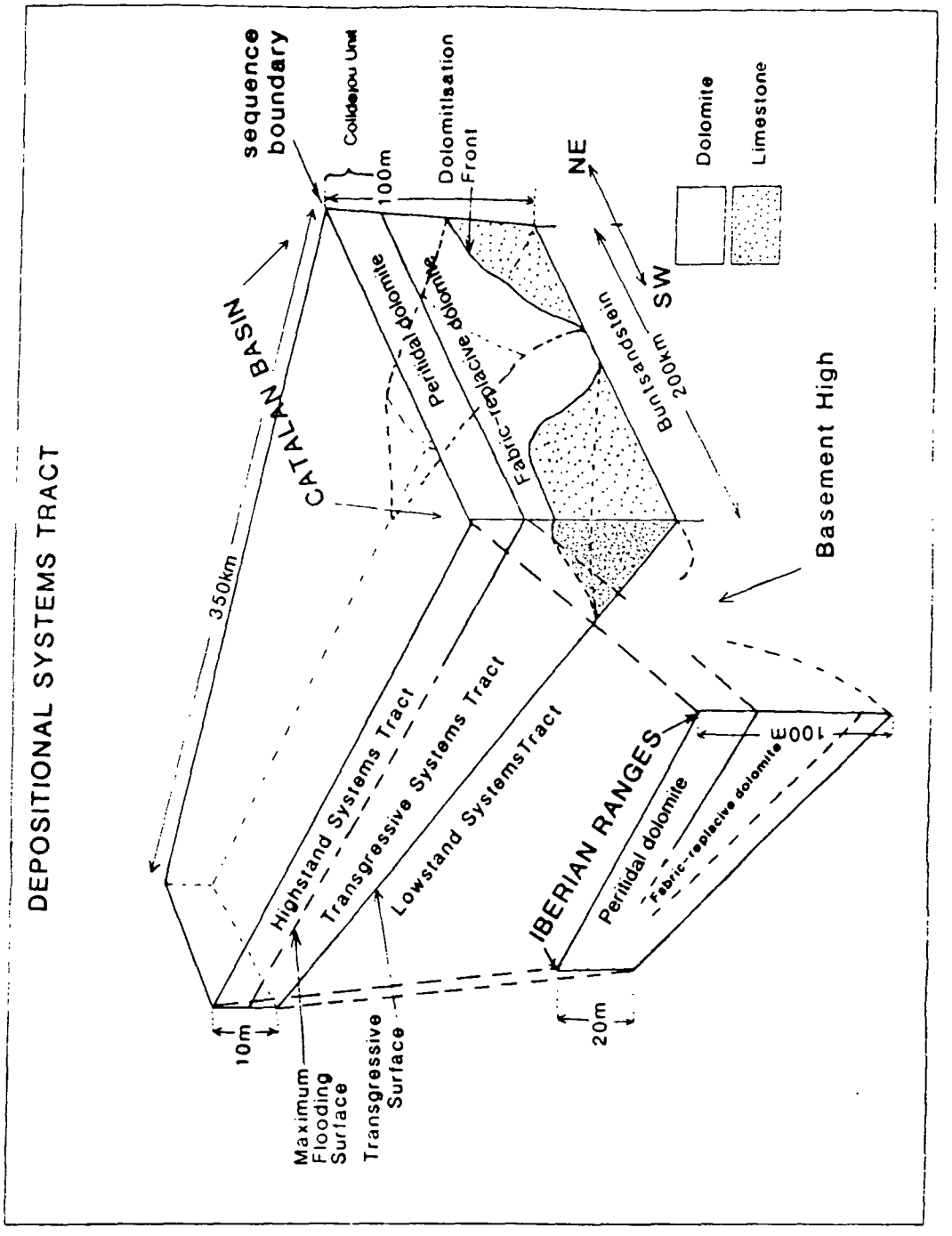

Fig. 5.3. The geometry of the peritidal dolomite and fabric-replacive dolomite of northeast Spain.

The pervasive nature and stratigraphic control of the peritidal dolomite suggest that this dolomitization is at least in part controlled by depositional processes and/or the original mineralogy.

5.4 DOLOMITE FIELD RELATIONSHIPS

5.4.1 Fabric-replacive dolomite front

The dolomite front is exposed at several localities and separates limestone below from dolomite above. In the northern Catalan Coastal Ranges the dolomite front typically occurs in bioturbated wackestones of the Vilella Baixa Unit and is well-exposed at Palleja (Fig. 5.4).

At Palleja the dolomite front is clearly discordant to bedding and cuts across a 1m thick bed. The gradient of the dolomite front is irregular but across the whole outcrop is about 1:100.

The dolomite front cuts across massive bioturbated limestones (Fig. 5.5). The limestones have an irregular mottling consisting of grey elongate lenses and tubular patches, probably outlining former burrows, with a yellow-weathering dolomitic limestone between. The minor dolomite associated with the bioturbation is discussed in Section 5.5.2.1.

The dolomite front consists of a 10cm-wide red dolomite layer with apophyses extending about 10cm into the underlying limestone. The apophyses tend to finger into the yellow-weathering limestone between the burrows, probably reflecting a permeability contrast. The dolomite above the front is buff-coloured and massive with poor preservation of the bioturbation. Vuggy, calcite spar-lined porosity is common in the dolomite particularly along the 10cm-wide red dolomite front.

The dolomite front in the northern Catalan Coastal Ranges is locally marked by a paleokarst (Section 4.6.2). The paleokarst is overlain by laterally discontinuous red marl which separates dolomite above from karstified limestone below. The paleokarst is interpreted to have developed along the pre-existing dolomite front (see discussion in Section 4.6.2.2).

5.4.2 Fabric-replacive dolomite and Peritidal dolomite Contact

The contact between the fabric-replacive dolomite and the peritidal dolomite of the Upper Member of the Colldejou Unit is generally very sharp and obvious at outcrop, particularly where the transitional Lower Member of the Colldejou Unit is absent (see Fig. 3.24).

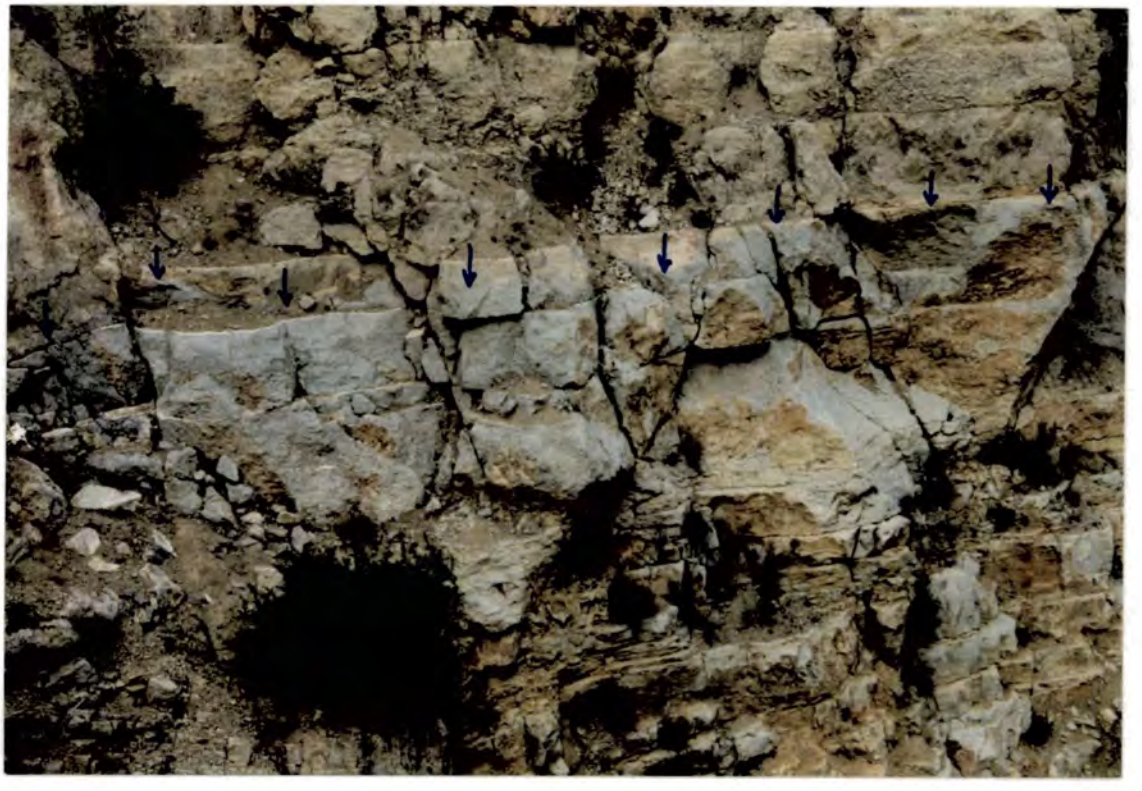

Fig. 5.4. Discordant dolomitization front separating upper buff dolomite from grey limestone. Width of view *ca.* 20m. Palleja locality. [See Section 5.4.1]

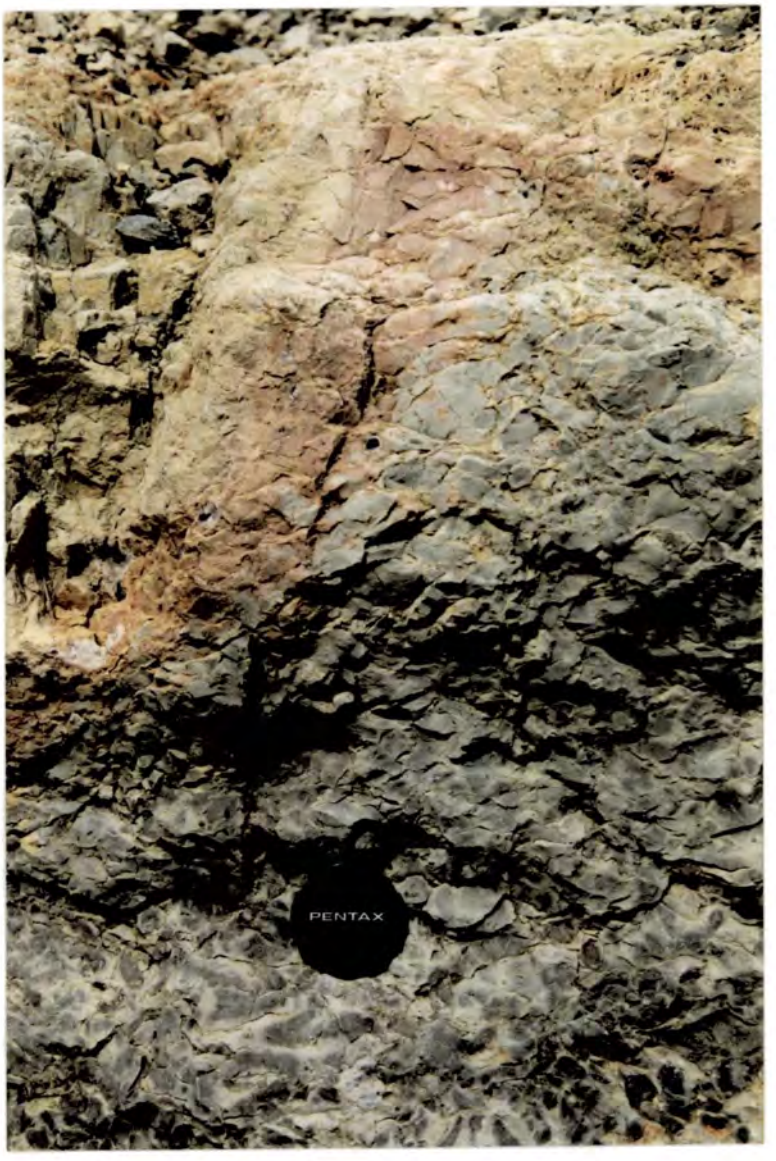

Fig. 5.5. Dolomite front developed in massive bioturbated limestones. Palleja locality. [See Section 5.4.1]

The contact typically consists of a bed-parallel surface separating massive fabric-replacive dolomitized grainstones or packstones of the uppermost Vilella Baixa Unit from laminated, fine-grained peritidal dolomites of the Upper Member of the Colldejou Unit. The contact is locally microkarstic (see Section 4.6.1.1). In thin section the contact is sharp between dolomicrites and well-preserved dolomitized ooids (Fig. 5.6). Ooids are locally truncated along the contact owing to microkarstic erosion or later stylolitic dissolution. The basal 10cm of the peritidal dolomicrite contains a few dolomitized echinoderm fragments.

The transitional Lower Member of the Colldejou Unit is locally undolomitized (see Section 3.2.4.1). However, where dolomitized there is generally good fabric preservation of the fine-grained sediments and there are few dolomite microspar mosaics which characterise the fabric-replacive dolomite.

5.4.3 Analogous dolomite relationships

A similar relationship between coextensive 'supratidal dolomite' and underlying 'secondary dolomite' has been described by Nicholls (1974) from the Triassic of north-central Nevada. Further examples of the association between 'primary' dolomite and underlying 'secondary' dolomite after normal marine limestones with a locally abrupt contact between are described from the Ordovician-Silurian, Silurian-Devonian, and Triassic of the Great Basin by Nicholls & Silberling (1980).

Nicholls & Silberling (1980) suggested that the term eogenetic should be used for the 'secondary' dolomitization which they considered to result from processes related to the upper surface of the 'secondary' dolomite or to the sediment deposited upon that surface. Nicholls & Silberling (1980) considered that many models (*e.g.* brine-reflux or mixed meteoric-marine) of dolomitization could fit the observed relationship. Nicholls & Silberling (1980) presented a field-based and petrographic study and did not provide any geochemical data.

5.5 CATALAN BASIN FABRIC-REPLACIVE DOLOMITE PETROGRAPHY

The fabric-replacive dolomite exhibits a wide range of petrographic textures from fabric-preservative fine-grained dolomicrites to coarse-grained fabric-destructive xenotopic and idiotopic dolomite mosaics. For descriptions and definitions of dolomite fabrics see Sibley (1982), Gregg & Sibley (1984) and Sibley & Gregg (1987).

5.5.1 Fabric Preservation

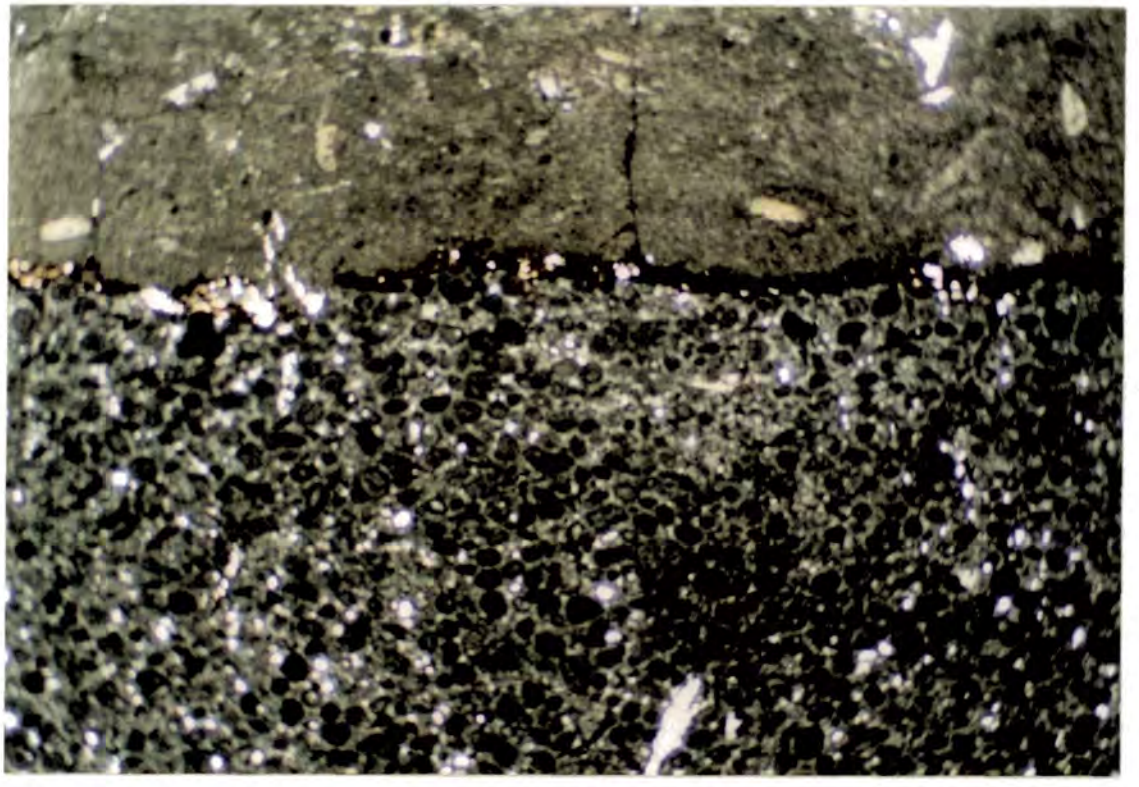

Fig. 5.6. Sharp contact between dolomitized oolite and peritidal dolomicrite with scattered echinoderm fragments. See Section 5.4.2. [PPl. F19. Width of view = 14mm]

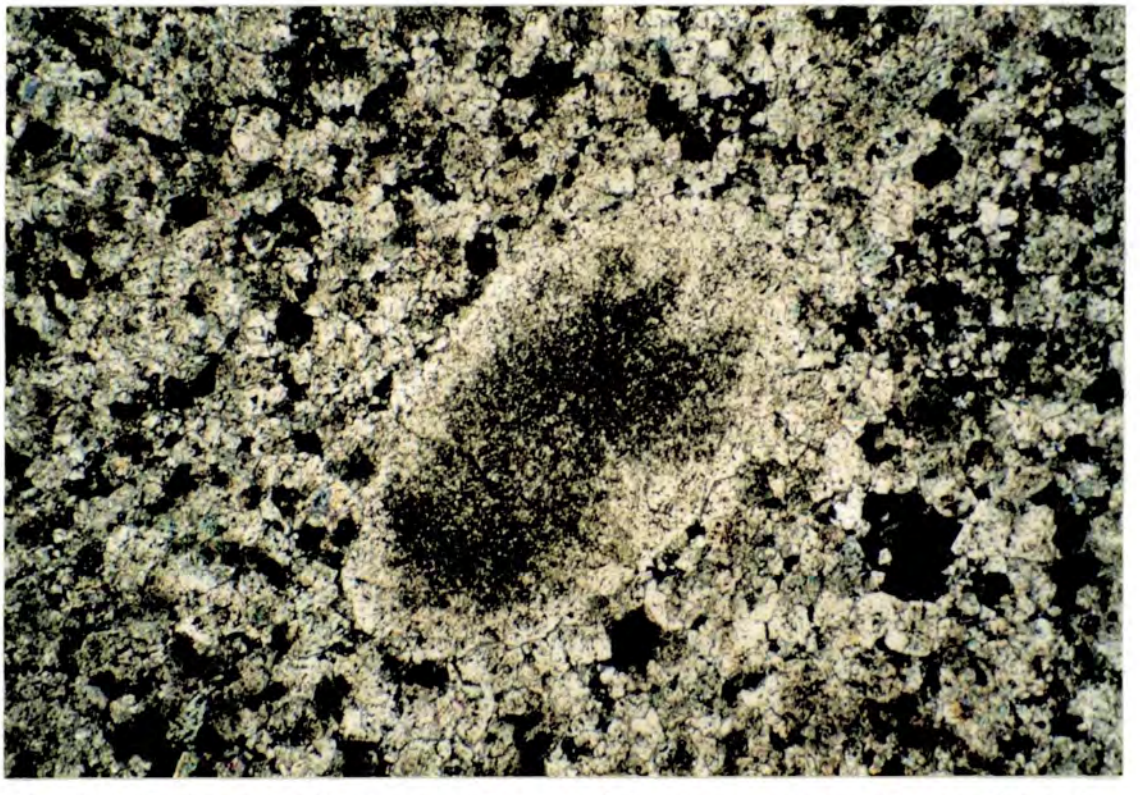

Fig. 5.7. Echinoderm fragment with syntaxial cement preserved in hypidiotopic fabric-replacive dolomite mosaic. [XPL. A16. Width of view = 3mm]

The degree of fabric preservation is very variable in the fabric-replacive dolomite. Fabric retention is thought to improve with the number of available nucleation sites, such that a fine-grained precursor, particularly if composed of high-Mg calcite, is likely to be replaced pseudomorphically (Sibley, 1982). The degree of fabric preservation also provides an insight on the dolomitization reaction. Fabric preservation requires a volume-for-volume replacement, whereas fabric destruction can be a volume-for-volume reaction, but may also be closer to mole-for-mole with consequent development of a porous, sucrosic fabric.

5.5.1.1 Bioclast Preservation

Bioclastic limestones of the Lower Muschelkalk, *e.g.* in the Olesa Unit, have generally been replaced by fabric destructive dolomite mosaics. However, where preserved at all, the following generally show good retention of skeletal detail: dasycladacean algae (Fig. 8.10); solenoporacean algae; ostracods; and echinoderm fragments. In contrast, all the molluscan fragments, such as gastropods and bivalves, are not recognisable at all in the dolomite.

The control on bioclast preservation appears to be original skeletal mineralogy. The well-preserved bioclasts were originally high-Mg calcite, whereas the molluscs were aragonitic. This observation has been confirmed experimentally by Bullen & Sibley (1984). However, an exception are the dasycladacean algae, the modern equivalents of which are aragonitic (Bathurst, 1975). Triassic dasycladacean algae, like red algae, may have been composed of high-Mg calcite. The molluscan fragments were generally replaced by calcite spar during early meteoric diagenesis (Section 4.2) and thus recognition of any such replaced bioclast in the dolomite is unlikely.

Echinoderm fragments are commonly the only recognisable bioclast in dolomite mosaics. The single crystal nature of echinoderm fragments leads to pseudomorphic replacement because only a few nucleation sites are required (Tucker & Wright, 1990). Syntaxial cements on echinoderm fragments are also commonly preserved in the dolomite (Fig. 5.7).

5.5.1.2 Oolitic and pisolitic fabrics

Oolite and pisolite petrography is discussed in Section 4.3.1, and the fabrics are commonly well-preserved in pseudomorphic dolomite (Fig.s 4.6, 4.7, 4.8, 4.17). The retention of concentric cortex fabric may suggest that the dolomite is after original aragonite without a fabric-destructive low-Mg calcite intermediate step. Oolites have commonly undergone early meteoric diagenesis (Section 4.3.3) which resulted in oomoldic porosity occluded by early calcite, and these horizons are undolomitized

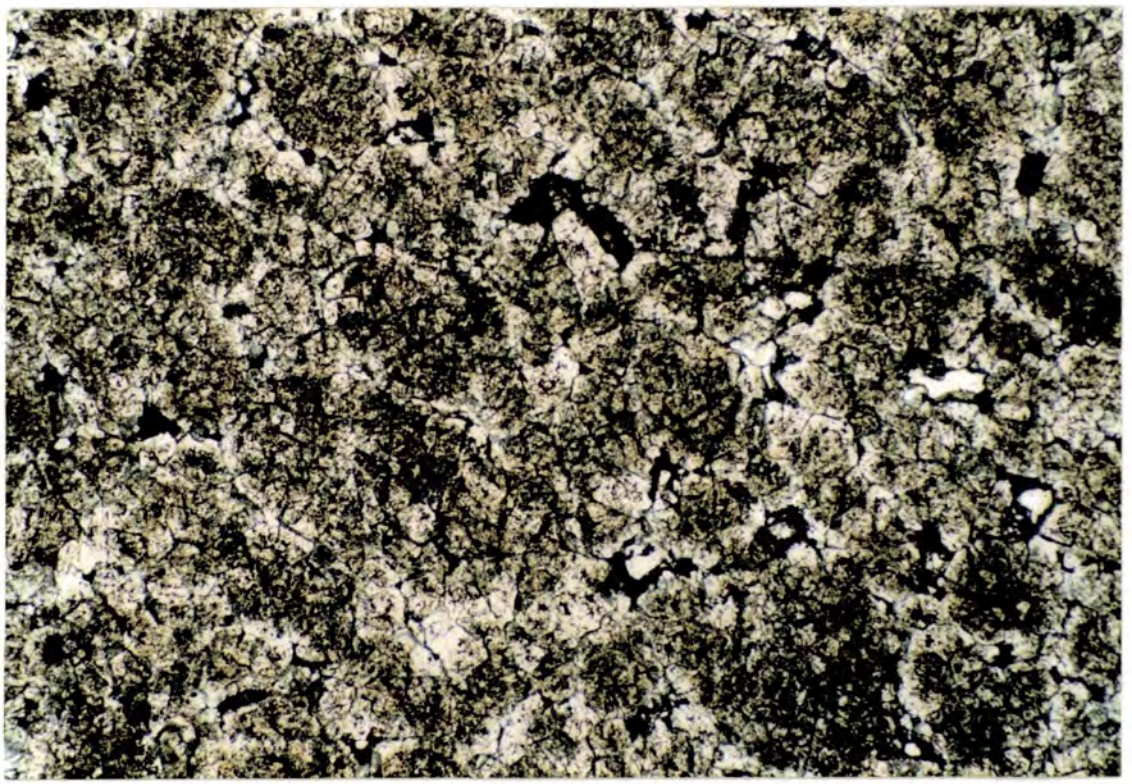

Fig. 5.8. Poorly preserved ooids in fabric-replacive dolomite mosaic from a cross-bedded oolite horizon. [PPL. A26. Width of view = 3mm]

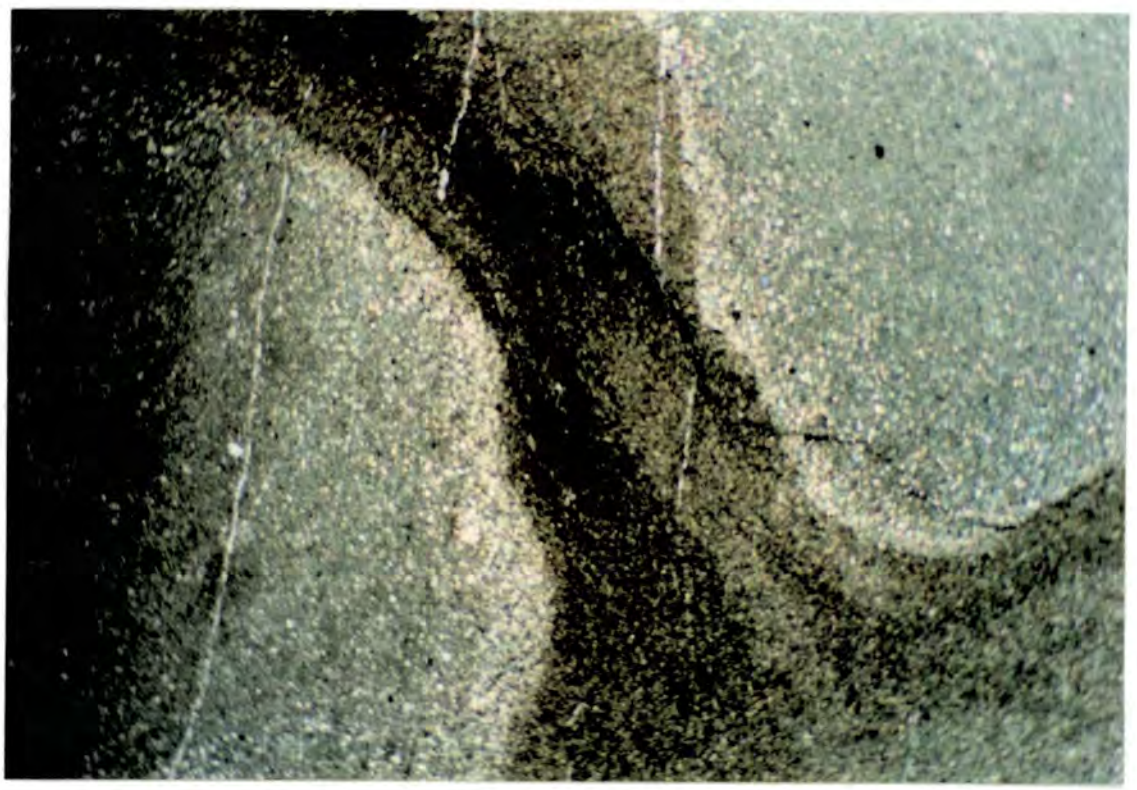

Fig. 5.9. Partially dolomitized bioturbation fabric with dolomite rhombs occurring at margins of undolomitized 'burrow'. [XPL. HP15. Width of view = 14mm]

(Fig. 4.10). The meteoric coarse-grained, low-Mg calcite would tend to resist dolomitization whereas the original aragonite (and any high-Mg calcite cements) would have been preferentially dolomitized (Tucker & Wright, 1990).

In some instances, oolites have been dolomitized without fabric preservation. Macroscopic features, such as clear cross-lamination, are commonly retained but only a ghost of the original grainstone fabric is preserved in a coarse dolomite mosaic (Fig. 5.8). Locally there has been no fabric preservation at all and the prior existence of an oolite can only be inferred.

5.5.2 Bioturbation Fabric

Bioturbation is common in the lime mudstones and wackestones of the Olesa Unit and Vilella Baixa Unit and can also be recognised in the fabric-replacive dolomite. The dolomite front in the northern Catalan Coastal Ranges generally occurs in this facies (see Section 5.4.1).

5.5.2.1 Undolomitized bioturbation fabric

The bioturbated limestones below the dolomite front consist of grey, elongate, 0.5mm to 2cm wide, locally branching, oval to circular cross-section irregular tubes. These appear to represent former burrows similar to *Planolites*. Between the burrows is a yellow-weathering marly limestone (Fig. 5.5). In thin section the burrows consist of homogeneous micritic calcite, whereas between the burrows there are many non-sutured dissolution seams which wrap around the burrow shapes. Dissolution seams appear to have preferentially formed in the relatively impure clay-rich limestone between the burrows. In some cases, small idiotopic dolomite crystals are present between the burrows, and these have probably formed as a result of local dissolution and recrystallisation of high-Mg calcite and release of magnesium, as discussed in Wanless (1979).

5.5.2.2 Partially dolomitized bioturbation fabric

Near the dolomite front (Section 5.4.1) the material between the burrows has been entirely dolomitized to a fine-grained idiotopic dolomite mosaic which overprints the dissolution seams (Fig. 5.9). The burrows are undolomitized. The contact between the limestone and dolomite varies from sharp to transitional with a zone of small idiotopic dolomite rhombs. At the dolomite front the dolomite tends to 'finger' between the limestone burrows. The dolomitized portions locally contain lath-shaped pseudomorphs after anhydrite. The anhydrite was presumably related to the dolomitization (Fig.s 4.27, 4.28).

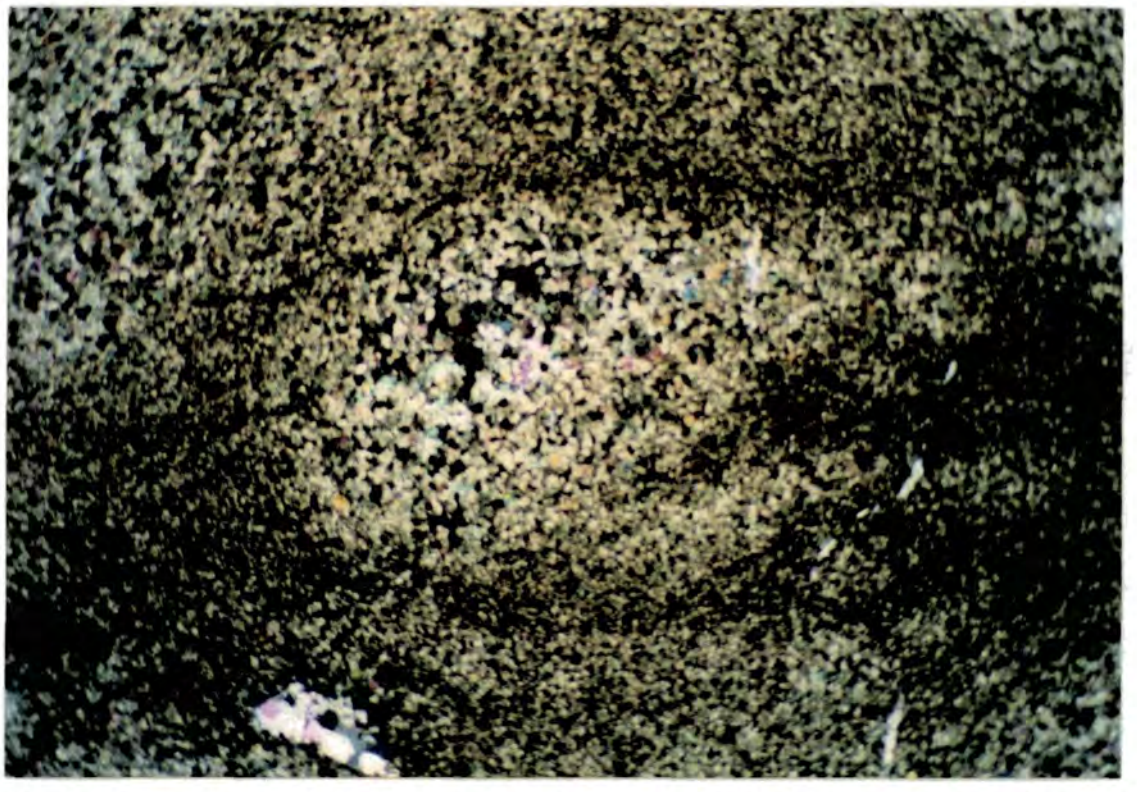

Fig. 5.10. Dolomitized bioturbation fabric revealed by contrasts in the dolomite mosaic developed in former 'burrow' and 'interburrow'. [XPl. C6. Width of view = 14mm]

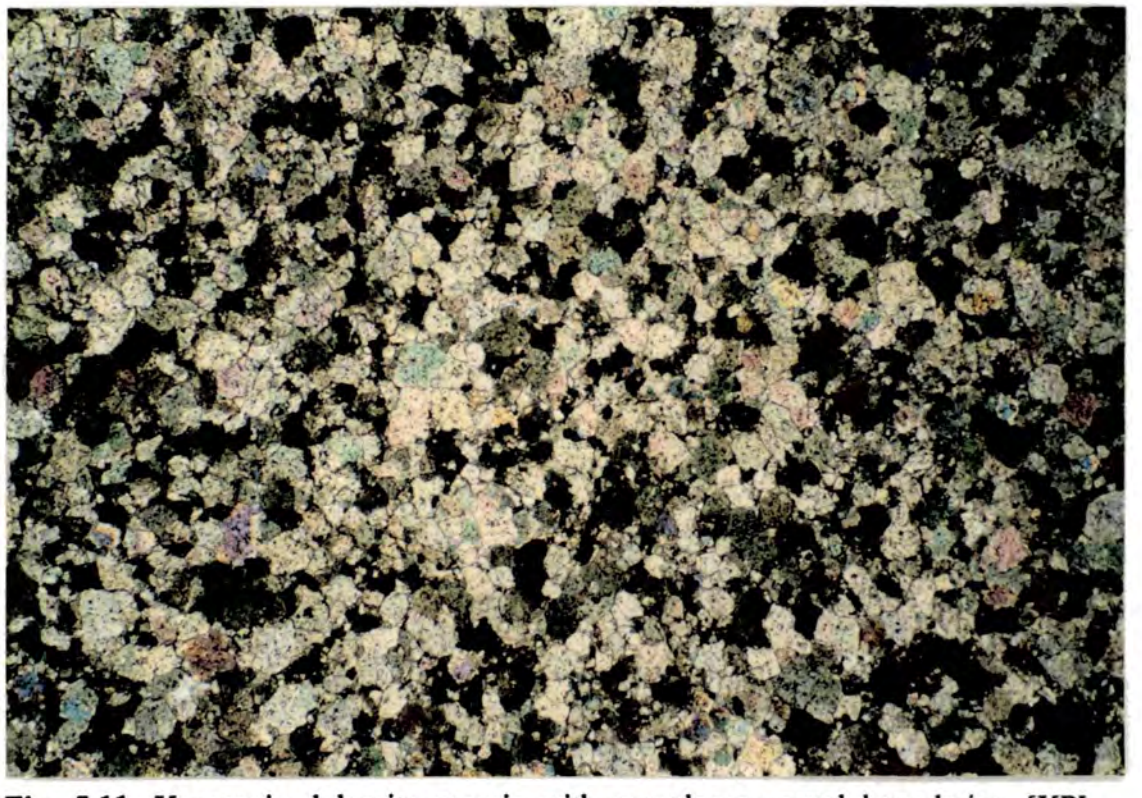

Fig. 5.11. Xenotopic dolomite mosaic with non-planar crystal boundaries. [XPL. A23. Width of view = 3mm]

The dolomitization is probably related to a greater permeability around the burrows than through them, and possibly to the greater reactivity of the interburrow carbonate owing to the presence of any early-formed pressure-dissolution-related dolomite.

5.5.2.3 Totally dolomitized bioturbation fabric

Above the dolomite front the bioturbated fabric is recognisable owing to differences in the dolomite mosaic. The interburrow material consists of fine-grained idiotopic dolomite mosaic whereas the dolomite of the burrow is coarser and xenotopic (Fig. 5.10). The grainsize difference probably reflects a greater number of nucleation sites in the interburrow than in the burrow (Sibley, 1982).

5.5.3 Dolomite mosaics

Dolomite mosaics are common in the fabric-replacive dolomite. The mosaics vary range from fine to coarse-grained, idiotopic to xenotopic, and tight to porous. Some mosaics preserve some of the original fabric, such as echinoderm fragments, ghosts of ooids, and bioturbation, as mentioned above (Fig. 5.7, 5.8, 5.10). However, most mosaics have no fabric preservation (Fig. 5.11). In general, mudstones and wackestones appear to have been replaced by fine-grained mosaics, whereas grainstones have resulted in coarse mosaics, probably owing to the difference in the density of nucleation sites (Sibley, 1982).

Idiotopic dolomite mosaics commonly have a porosity that is partially or fully occluded by poikilotopic calcite cement that is zoned under cathodoluminescence (Fig.s 5.12, 5.13). The idiotopic rhombs are also commonly zoned with a dusted inclusion-rich core with dull to speckly cathodoluminescence, and a limpid, dull to bright luminescent rim (Section 8.3, Fig.s 5.14, 5.15)). Such zoned dolomite rhombs have been noted by many workers (*e.g.* Land, 1980; Sibley, 1980, 1982) and reflect changing conditions during dolomite growth. Gregg & Sibley (1984) suggested that idiotopic mosaics should form preferentially below about 50-100°C. However, the close occurrence of different dolomite mosaic types suggests that the precursor mineralogy, fabric and grainsize may also be controls.

The abundance of coarse fabric-destructive dolomite mosaics commonly tends to decrease upwards through the fabric-replacive dolomite. The thickness of the dolomite body at most is only 60m and thus extrinsic factors, such as burial and recrystallisation temperature, are unlikely to have had an effect. The different dolomite fabrics may be due to different original mineralogies and/or different dolomitizing fluid chemistry. Early diagenetic recrystallisation of high-Mg calcite to low-Mg calcite would, in general, have affected the lower parts of the section more

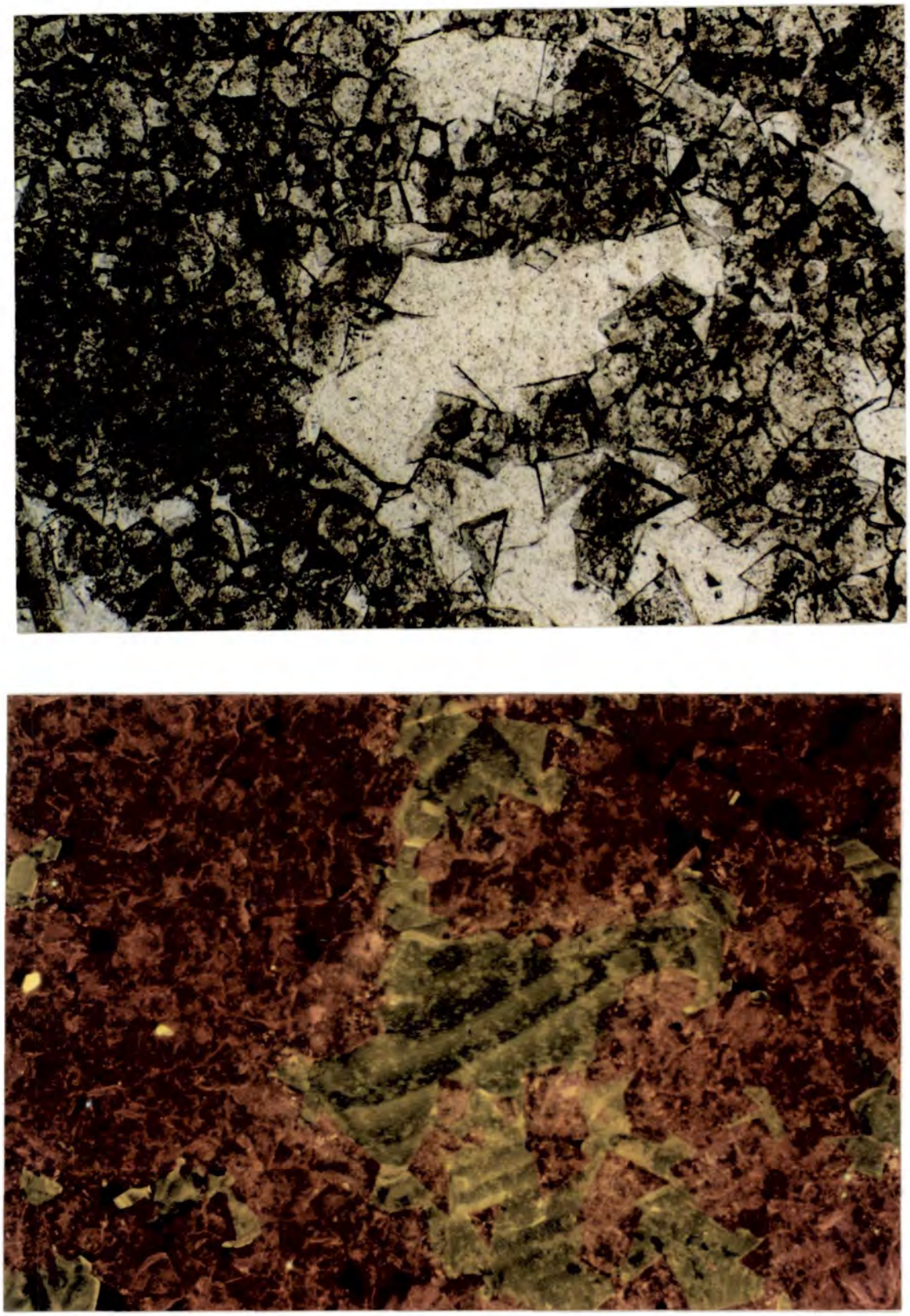

Fig. 5.12. PPL and CL photomicrograph pair of red-luminescent idiotopic dolomite mosaic with dull, zoned poikilotopic calcite spar. [CB34. Width of view = 1.4mm]

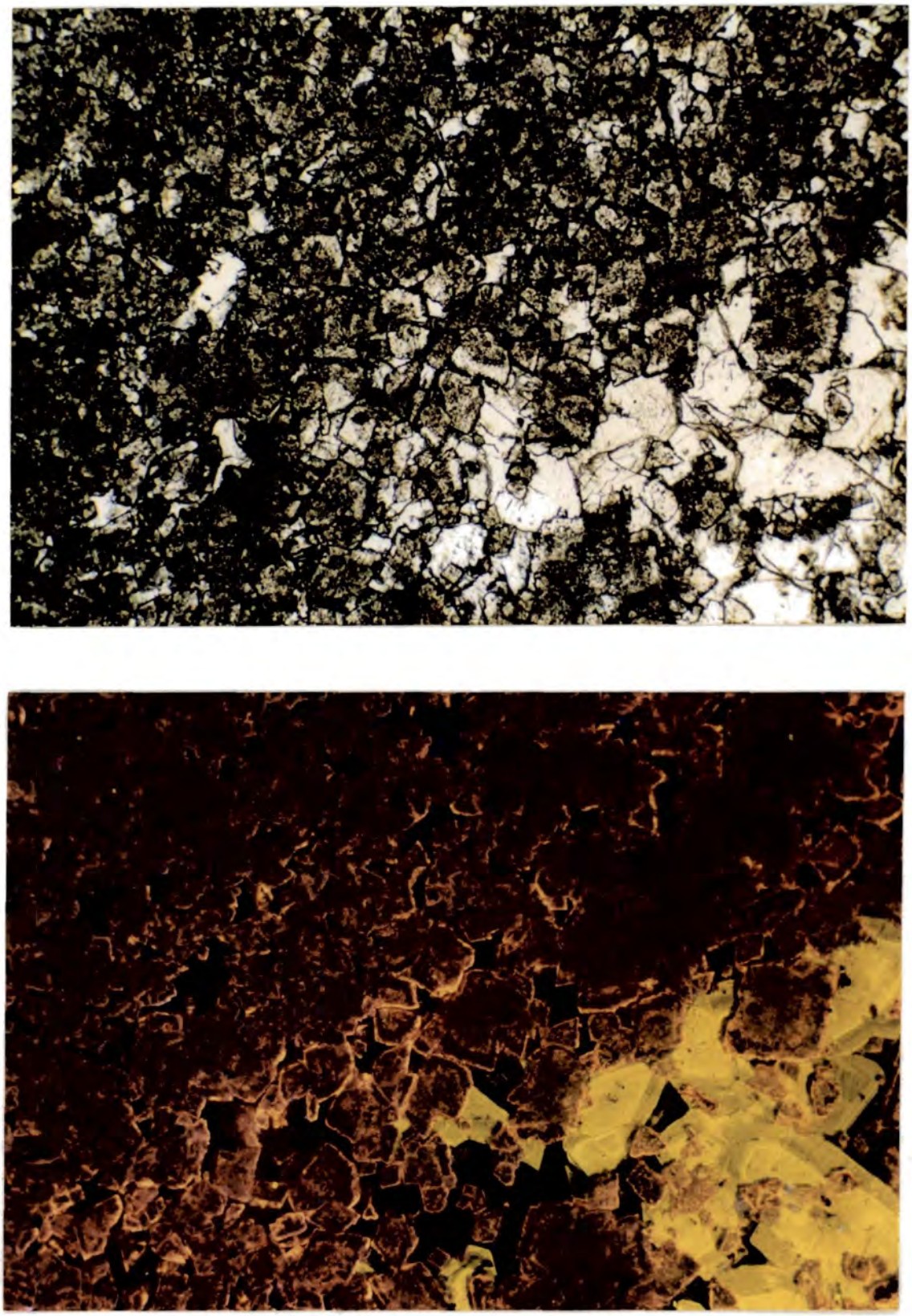

Fig. 5.13. PPL and CL photomicrograph pair of zoned poikilotopic calcite spar enclosing red-luminescent hypidiotopic dolomite which grades into a xenotopic mosaic. [CB34. Width of view = 1.4mm]

than the upper, owing to greater length of time available and more prolonged exposure to meteoric/brackish conditions, and this may have partly controlled the dolomite textures.

5.5.4 Synthesis of fabric-replacive dolomite petrography

The fabric preservation of the fabric-replacive dolomite is very variable and appears to be in part a function of the original mineralogy. High-Mg calcite bioclasts are typically well-preserved. Aragonite ooid fabrics may be well-preserved if unaffected by early meteoric diagenesis and replacement by calcite spar. Dolomite mosaics are common. The occurrence of fabric-destructive mosaics may be related to a predominantly low-Mg calcite precursor. The low-Mg calcite would have resulted in part from early meteoric diagenesis.

5.6 PERITIDAL DOLOMITE OF THE CATALAN BASIN

The peritidal dolomite occurs in the Upper Member of the Colldejou Unit and similar facies are locally present in the El Brull Unit (Sections 3.2.1 & 3.2.4.2) and these have been interpreted as intertidal to supratidal deposits. Modern peritidal environments are well-known as sites of modern dolomite formation.

5.6.1 Modern occurrences of peritidal dolomite

The modern formation of dolomite has been studied in several peritidal and evaporitic settings, *e.g.* intertidal-supratidal sediments of the Trucial Coast sabkhas (Patterson & Kinsman, 1982; Hardie, 1987); Sugarloaf Key, Florida (Carballo *et al.*, 1987); Andros Island tidal flats, Bahamas (Shinn, 1983); and Ambergris Cay, Belize (Mazzulo *et al.*, 1987). Several dolomitization models (Fig.s 5.1, 5.2) have been proposed, *e.g.* evaporative pumping (Hsu & Siegenthaler, 1969) and flood recharge (Patterson & Kinsman, 1982) in the Arabian Gulf sabkhas; tidal pumping at Sugarloaf Key (Carballo *et al.*, 1987); and small-scale meteoric-marine mixing-zones (Gebelein, 1977). Dolomite may be forming as a replacement of early-precipitated aragonite (Patterson & Kinsman, 1982) possibly with a high-Mg calcite intermediate step (McKenzie, 1981) or as more recent evidence suggests, as a directly precipitated cement (Carballo *et al*, 1987; Lasemi *et al.*, 1989).

However, not all modern peritidal carbonates contain dolomite and some ancient peritidal deposits consist of limestone, *e.g.* the Jurassic Purbeck sequence of Dorset, England (West, 1975). Nevertheless, dolomitization of ancient peritidal lime-mud to sabkha cycles is very common (Wilson, 1975).

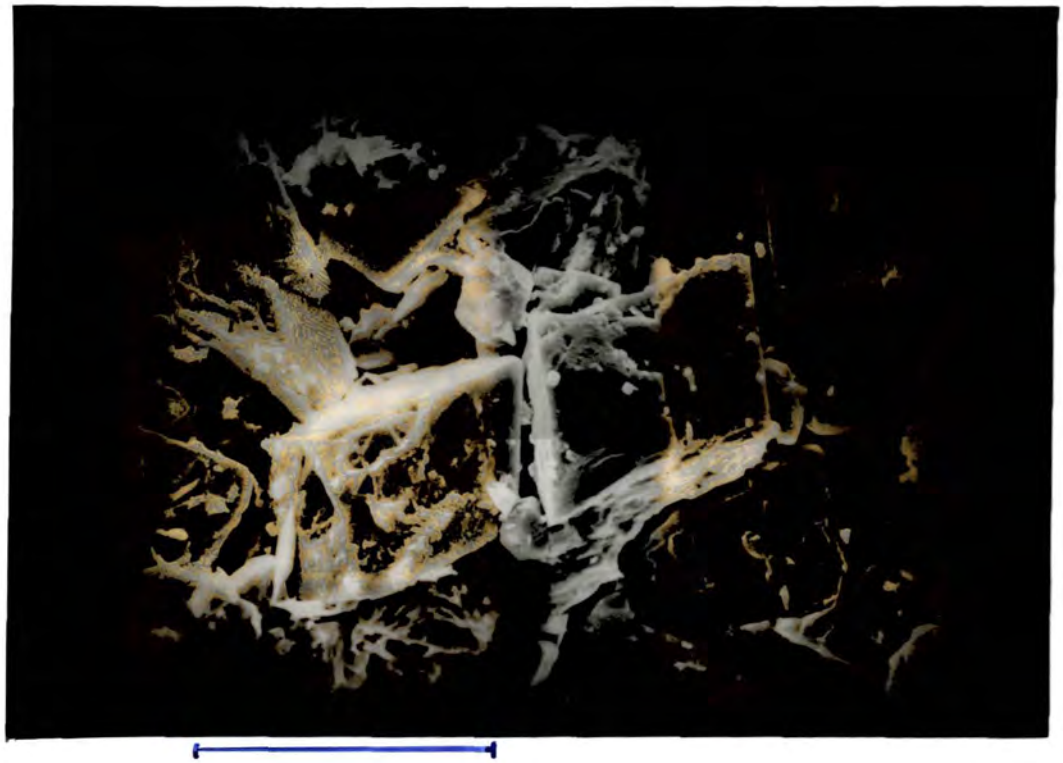

Fig. 5.14. SEM photograph of a fracture surface of idiotopic dolomite rhombs. [C16. Scale bar = 20um]

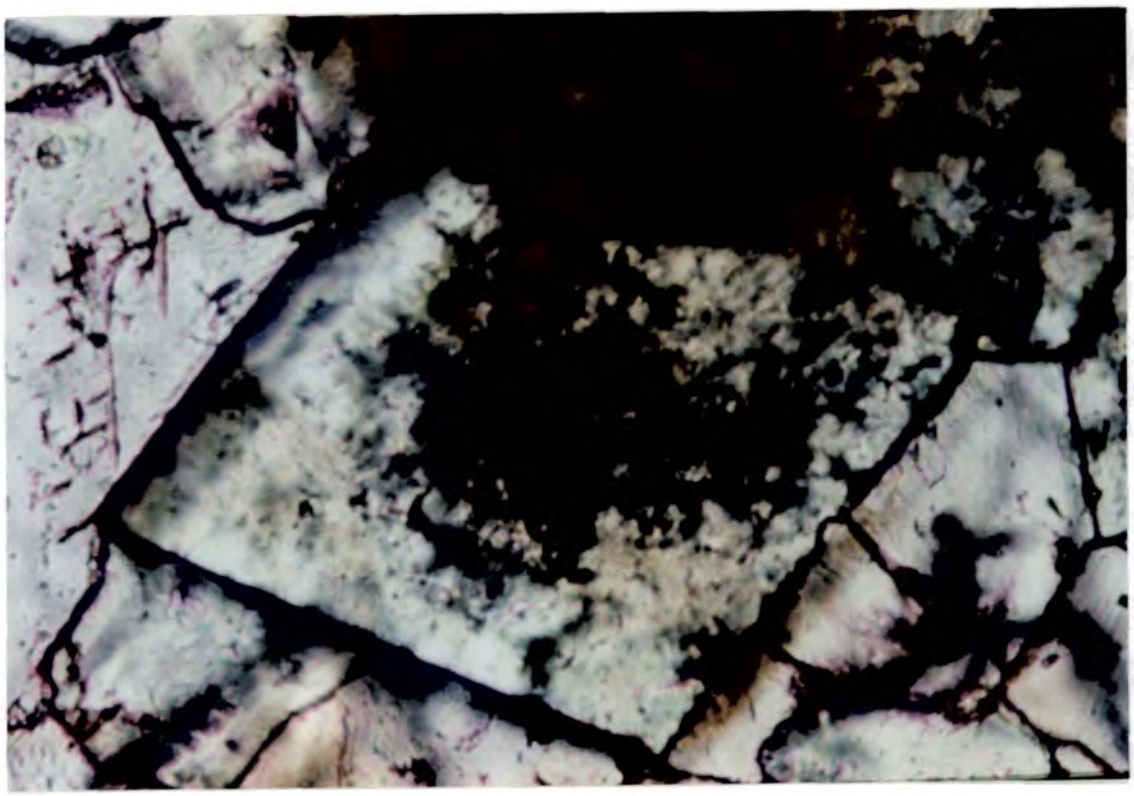

Fig. 5.15. Zoned euhedral dolomite rhomb. [Stained section. VB66. Width of view = 0.4mm]

Modern evaporitic dolomite tends to be calcium-rich, poorly to moderately ordered and generally only forms part of the sediment. Data from McKenzie (1981), plotted in Fig. 5.16, indicate that in the coastal sabkhas of Abu Dhabi most of the sediment consists of about equal amounts of dolomite, aragonite and calcite (low-Mg and high-Mg).

5.6.2 Peritidal dolomite in the Lower Muschelkalk

The peritidal dolomite is clearly at least in part related to the depositional environment and unlike the fabric-replacive dolomite shows clear stratigraphic control. The peritidal dolomite occurs in the Upper Member of the Colldejou Unit and similar facies are locally present in the El Brull Unit. The main features of the peritidal dolomite have already partly been described in Chapter 3 and 4.

5.6.2.1 Peritidal dolomite of the El Brull Unit

The El Brull Unit was described in Section 3.2.1 and commonly contains laterally extensive horizons of laminated dolomicrite interbedded with limestones. The peritidal dolomite is best exposed in the northern and southern Catalan Coastal Ranges because in the central Catalan Coastal Ranges the fabric-replacive dolomite front extends down into the El Brull Unit and has obscured the sedimentary features.

5.6.2.2 Peritidal dolomite of the Upper Member of the Colldejou Unit

The Upper Member of the Colldejou Unit (see Section 3.2.4.2) consists of pervasively dolomitized fine-grained sediment. The laminated peritidal dolomite contrasts with the generally massive fabric-replacive dolomite.

5.6.3 Peritidal dolomite petrography

The peritidal dolomite facies contains sedimentary features indicative of an intertidal to supratidal environment, such as: scarce, restricted fauna; pseudomorphs after evaporites and collapse breccias (Section 8.4); parallel lamination resulting from a lack of bioturbation; planar and domal stromatolites; and tepees (Section 4.5).

The petrography of the peritidal dolomite is not as variable as the fabric-replacive dolomite and generally consists of fine-grained, homogeneous laminated dolomicrite (Fig.s 3.24, 5.6). The peritidal dolomite locally contains angular dolomicrite intraclasts, which may represent small fragments of early reworked dolomitic supratidal crusts (Shinn, 1983). The intraclasts have a slight grain-size contrast with respect to the dolomicritic matrix. Dolomicritic peloidal packstones are also locally present (Fig. 5.17).

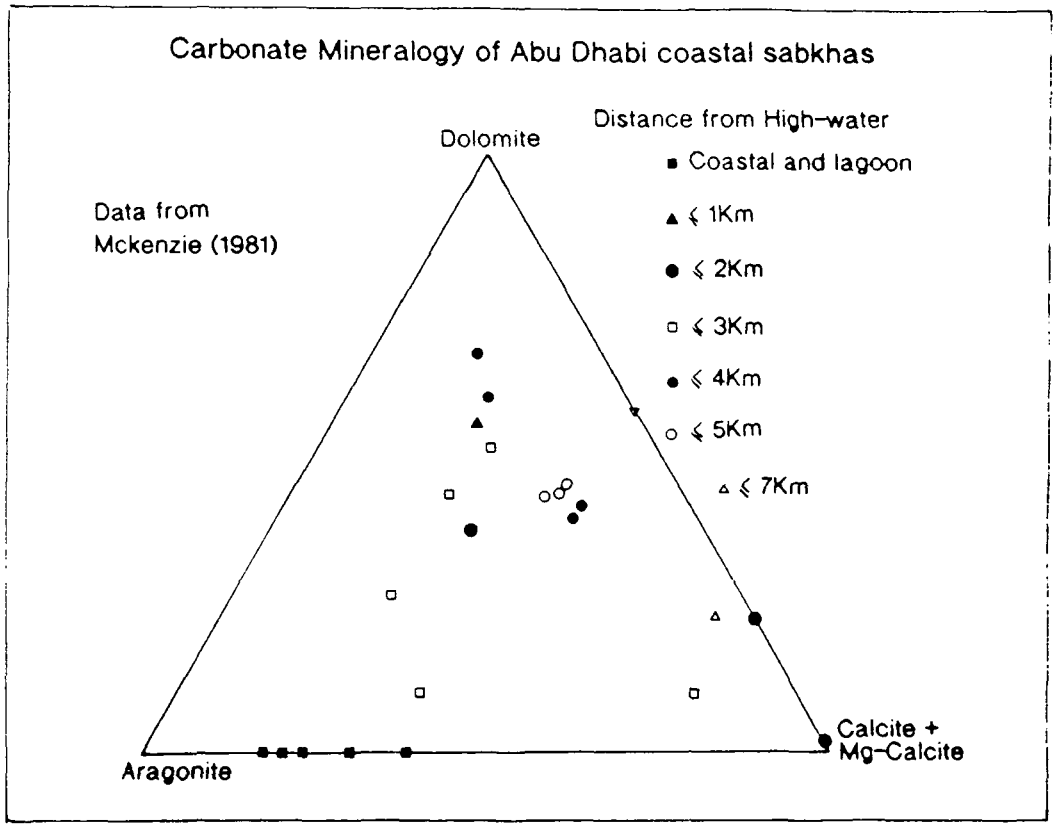

Fig. 5.16. Carbonate mineralogy of Abu Dhabi coastal sabkhas.

Locally the peritidal dolomites have been bioturbated. However, in contrast to the fabric-replacive dolomite, this is not shown by a difference in grainsize but merely by the pattern of clay-lined solution seams in the dolomicrite, suggesting that bioturbation was occurring in at least a partly dolomitized sediment.

5.6.4 Synthesis of peritidal dolomite observations

The depositional setting of the peritidal dolomite is considered to be intertidal to supratidal and by analogy with modern environments would originally have been composed of mainly aragonite, high-Mg calcite and possibly some penecontemporaneous dolomite. The preservation of sedimentary structures such as fine laminae, intraclasts, peloids and bioturbation, show a high degree of fabric retention during subsequent recrystallisation and any further dolomitization, and which may be related to a small amount of low-Mg calcite in the original sediment. The pervasive nature of the peritidal dolomite and the strong stratigraphic control show that the depositional environment and resulting unstable mineralogy was highly conducive to complete dolomitization during diagenesis.

5.7 SEM PETROGRAPHY OF THE CATALAN BASIN DOLOMITES

Dolomicrites were examined using SEM techniques. Fracture faces, although readily prepared, did not show the grain boundaries and shapes clearly. Acid-etched fragments of polished thin sections were found to be the most useful specimens (see Appendix 5; Lasemi *et al.*, 1989).

Dolomicrite samples were chosen from the peritidal dolomite (the Upper Member of the Colldejou Unit) and from the fabric-replacive dolomite (subtidal mudstones and wackestones of the Vilella Baixa Unit) from a number of localities from the Catalan Coastal Ranges . The optical microscopical features of the dolomicrites were very similar.

SEM petrography showed that the dolomicrites of the peritidal dolomite were consistently more fine-grained and more homogeneous than the dolomicrites of the fabric-replacive dolomite. Discrete rhombic dolomite crystal boundaries were common in the fabric-replacive dolomite but only rare in the peritidal dolomite (Fig.s 5.18, 5.19).

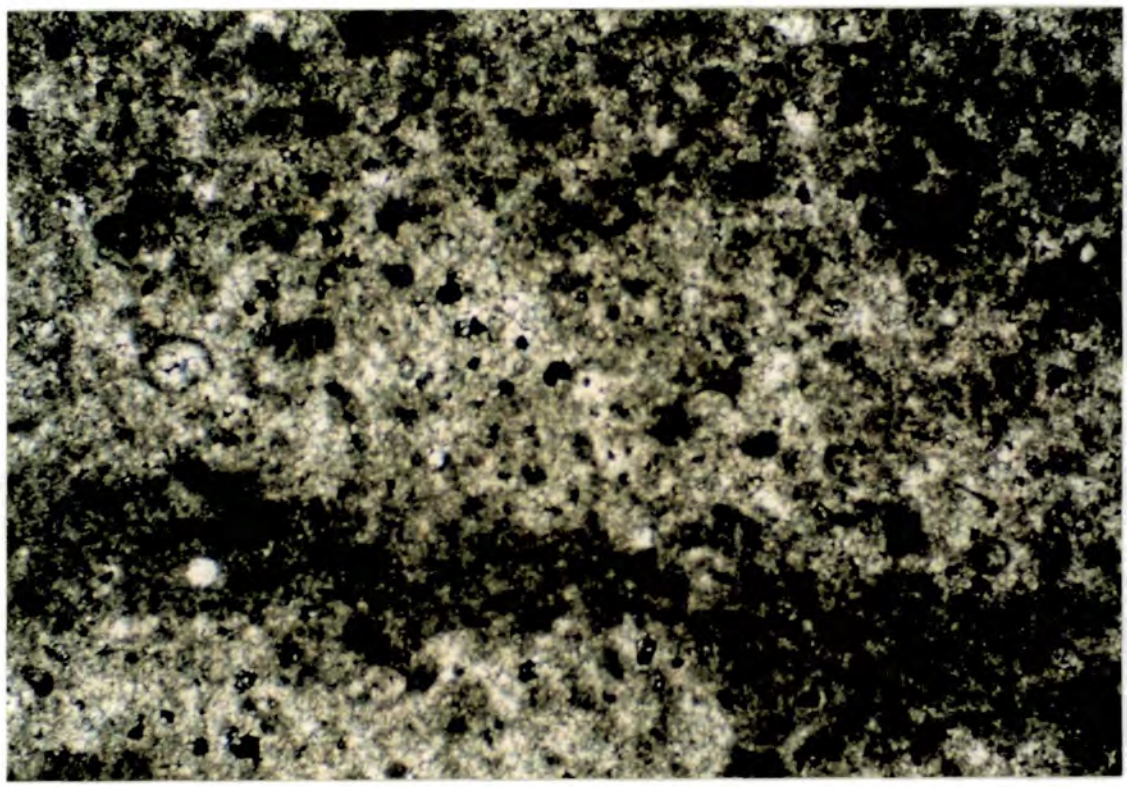

Fig. 5.17. Peloidal fabric in peritidal dolomicrite. [XPL. A50. Width of view = 3mm]

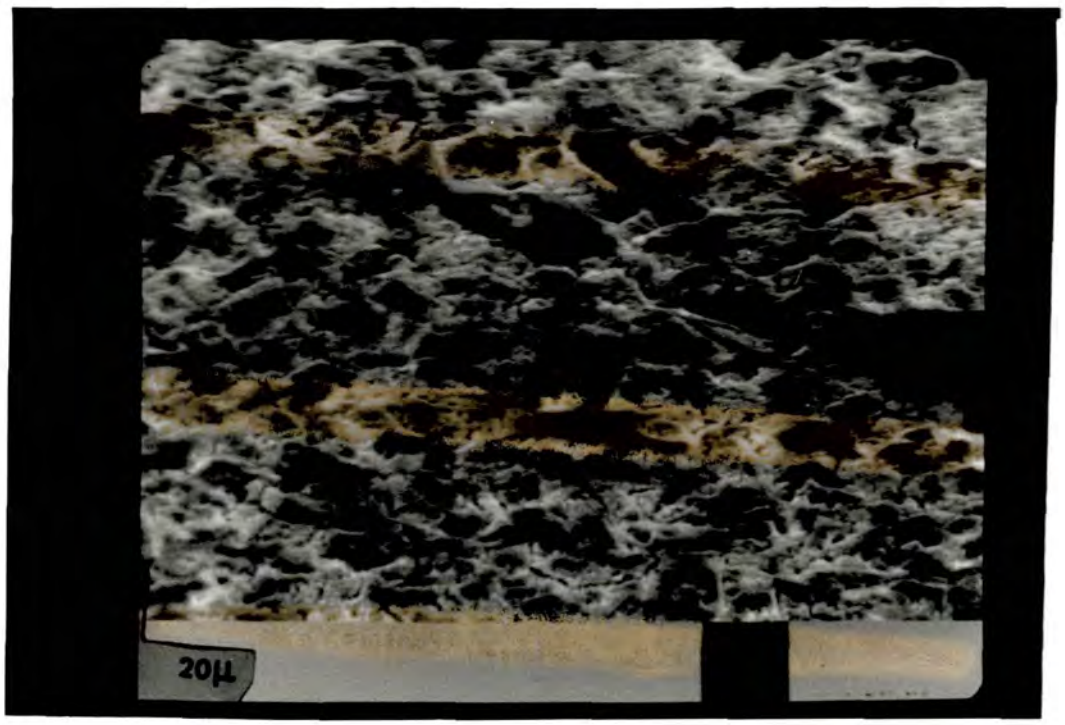

Fig. 5.18. SEM photograph of etched, polished surface of fabric-replacive dolomicrite showing rhombic crystal boundaries. See Fig. 5.19. [Sample C4]

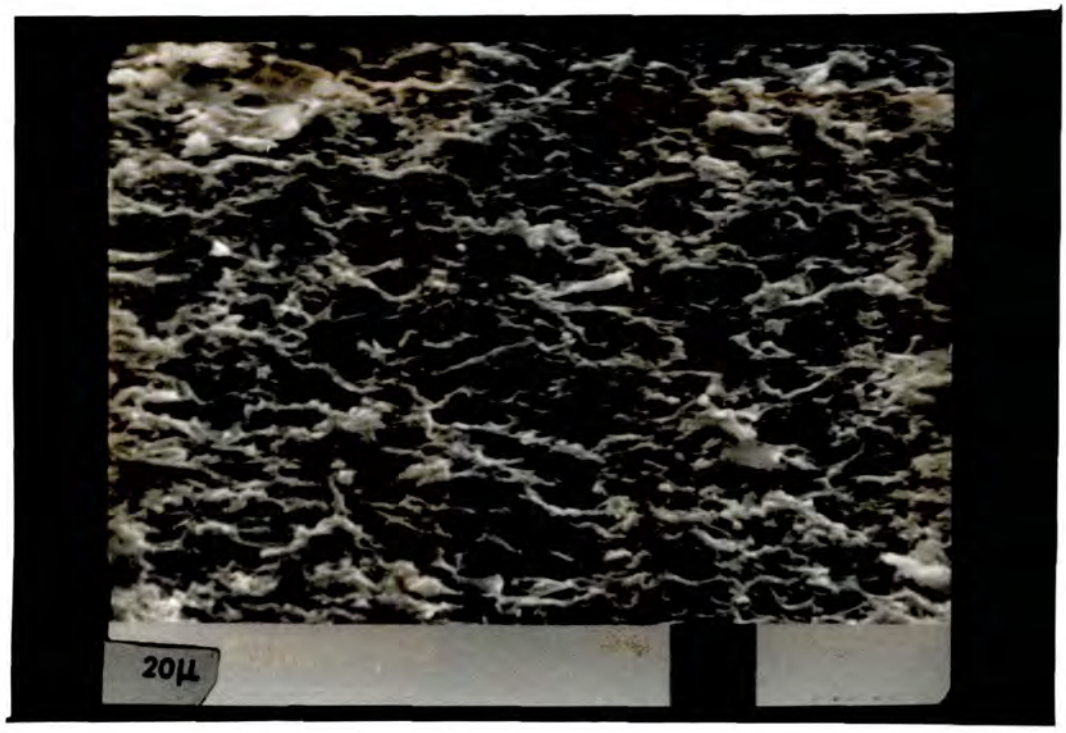

Fig. 5.19. SEM photograph of etched, polished surface of peritidal dolomicrite showing no clear crystal boundaries and generally pitted surface. See Fig. 5.19. [Sample F9]

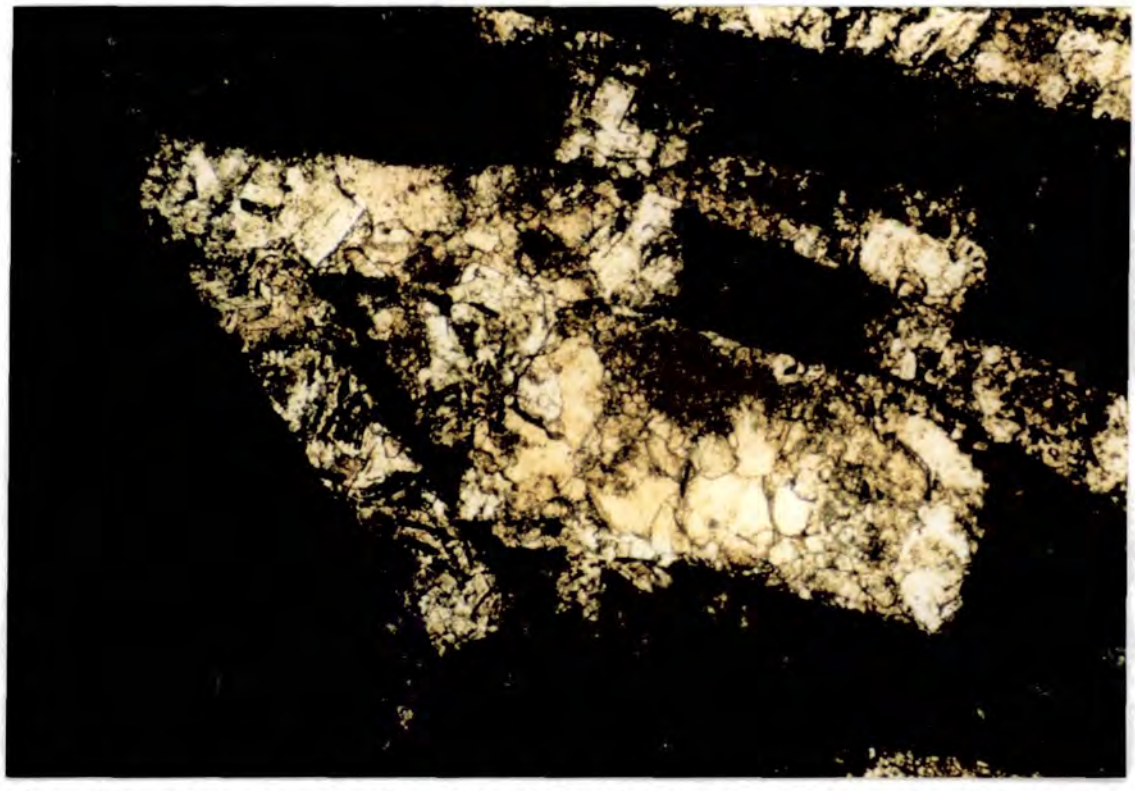

Fig. 5.20. Baroque dolomite with pink-stained calcite cements in lath-shaped pseudomorph. [Stained section. PPL. CB12. Width of view = 3mm]

5.8 BAROQUE DOLOMITE OF THE CATALAN BASIN

5.8.1 Introduction

Baroque dolomite is a particular variety of the mineral characterised by a warped crystal lattice resulting in curved crystal faces and undulose extinction (Radke & Mathis, 1980). Baroque dolomite commonly forms in association with epigenetic sulphide mineralization and also with hydrocarbons. Radke & Mathis (1980) suggest that baroque dolomite forms within the oil window at elevated temperatures of 60-150°C. Machel (1987) suggests that chemical compaction and thermochemical sulphate reduction at elevated temperatures may produce baroque dolomite.

5.8.2 Baroque dolomite in the Lower Muschelkalk

Baroque dolomite is not common in the Lower Muschelkalk of the Catalan Basin and occurs mainly as a cement phase and in one location as a replacement mosaic.

5.8.2.1 Baroque dolomite cement

Baroque dolomite cement occurs in association with some of the pseudomorphs after sulphates (see Section 4.8.8.2). Limpid baroque dolomite cement crystals line the margin of the pseudomorphs which commonly contain calcite spar towards the centre (Fig. 5.20). The baroque dolomite crystals commonly exhibit a zonation of bright red and dull red cathodoluminescence with many individual zones. This complex zonation contrasts with the simple patterns shown by the fabric-replacive dolomite rhombs. Baroque dolomite cement occurs in fractures in limestones and dolomites and in both cases the matrix appears unaffected (Fig. 5.21). Under cathodoluminescence some baroque dolomite crystals show evidence of dissolutional stages prior to renewed growth (Fig. 5.22).

The baroque dolomite is more common at those localities which are associated with the Pb-Zn-Ba mineralization (see Section 4.7).

5.8.2.2 Baroque dolomite mosaic

A baroque dolomite mosaic has been noted at one locality in the Catalan Basin (Masroig). The dolomite mosaic is coarse-grained and fabric-obliterative and forms about 4m of the section. Some of the grains have a speckly centre and have straight extinction and may be pseudomorphic replacement of echinoderm fragments. The pre-existing fabric was not revealed by cathodoluminescence or fluorescence microscopy (*cf.* Dravis & Yurewicz, 1985). Pb-Zn mineralization does not occur at this locality.

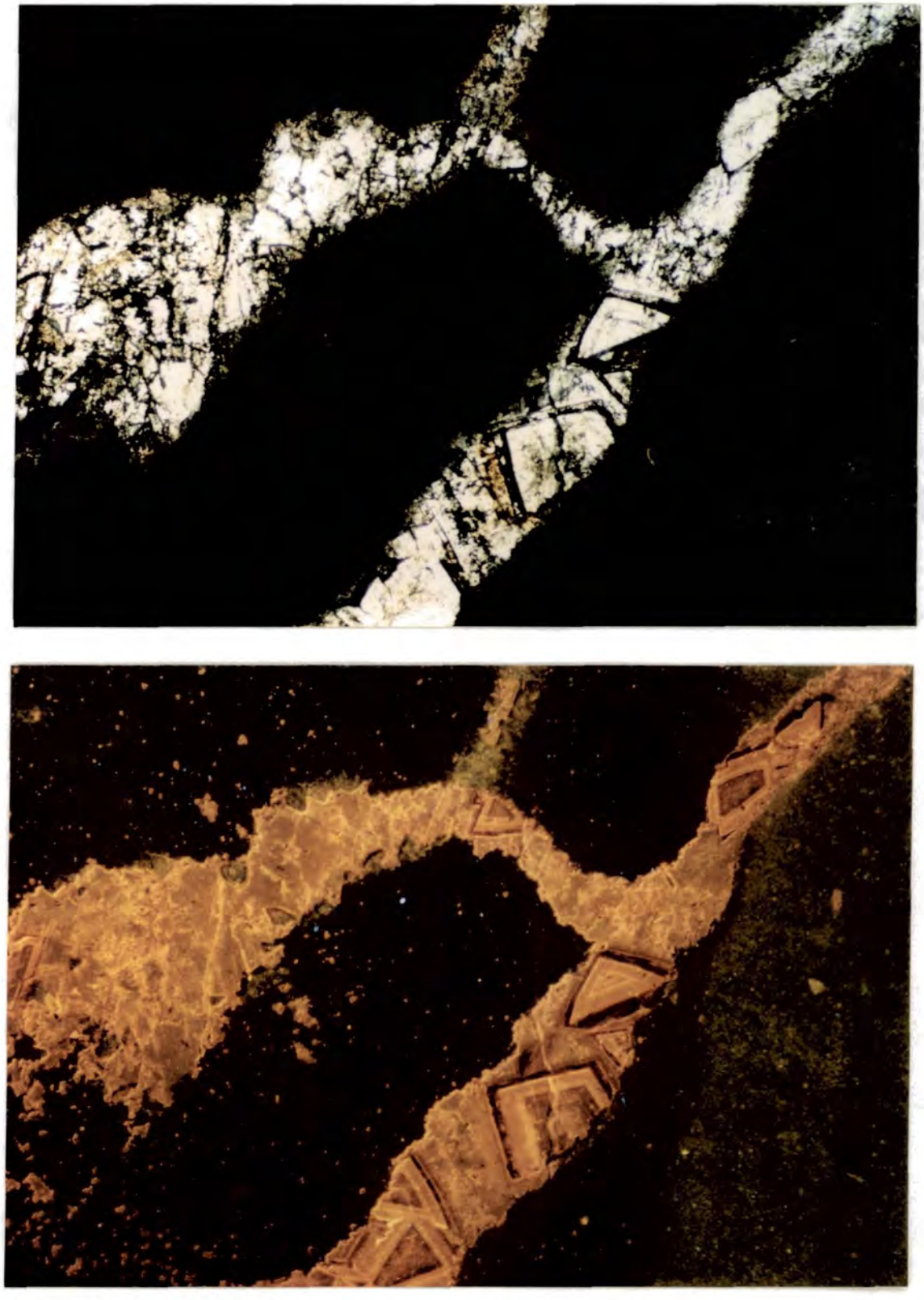

Fig. 5.21. PPL and CL photomicrograph pair of baroque dolomite cement in fractured limestone. [Half-stained section. CB12. Width of view = 3mm]

5.8.3 Baroque dolomite conclusions

Baroque dolomite generally occurs at localities affected by Pb-Zn mineralization and is considered to be associated with the same hydrothermal system. The baroque dolomite mainly occurs as a late cement lining fractures and dissolved sulphates. The former presence of sulphates may be associated with the baroque dolomite precipitation and sulphide emplacement (Beales & Hardy, 1980; Machel, 1987).

5.9 DOLOMITIZATION OF THE LOWER MUSCHELKALK OF THE VALENCIA-CUENCA BASIN

5.9.1 Introduction

The Lower Muschelkalk of the Valencia-Cuenca Basin is extensively dolomitized. In the southeast of the basin the depositional facies are similar to the Catalan Basin, but towards the northwest the section thins and becomes more marginal and peritidal-dominated (see Section 3.3). The quality of the outcrop is generally poorer in the Iberian Ranges then in the Catalan Coastal Ranges and there has locally been fabric-destructive dedolomitization.

5.9.2 Previous Work

There has been some previous work on the dolomitization of the Muschelkalk of the Iberian Ranges, notably by Freeman (1972). Freeman did not discriminate between Upper Muschelkalk and Lower Muschelkalk and some of his field observations may relate to the Upper Muschelkalk which was not examined in this study. The localities visited by Freeman are not readily identifiable from his paper but exposures in the same general area as his southeastern outcrops were examined. Freeman suggests a novel model of uplift-related dolomitization resulting from the percolation of meteoric waters through the overlying Keuper evaporites and shales. Freeman examined modern salina waters derived from the Keuper and found that despite the abundance of calcium sulphates, these locally contained Ca/Mg ratios less than unity. Freeman suggested that the Keuper was releasing 'dehydrated seawater' and that loosely bound magnesium ions in chlorite were the source for the dolomitization. Freeman used field sketches to show that dolomitization was apparently joint-controlled and that some dolomite drusy cement was precipitated 'post mountain-building'.

However, observations made during this study do not support the model of Freeman (1972), which is considered to have several inherent problems. A simple mass-transfer calculation (see Appendix 2) shows that if chlorite loses an improbably high 20% of the ionic magnesium, then under ideal reaction, one volume of dolomite would

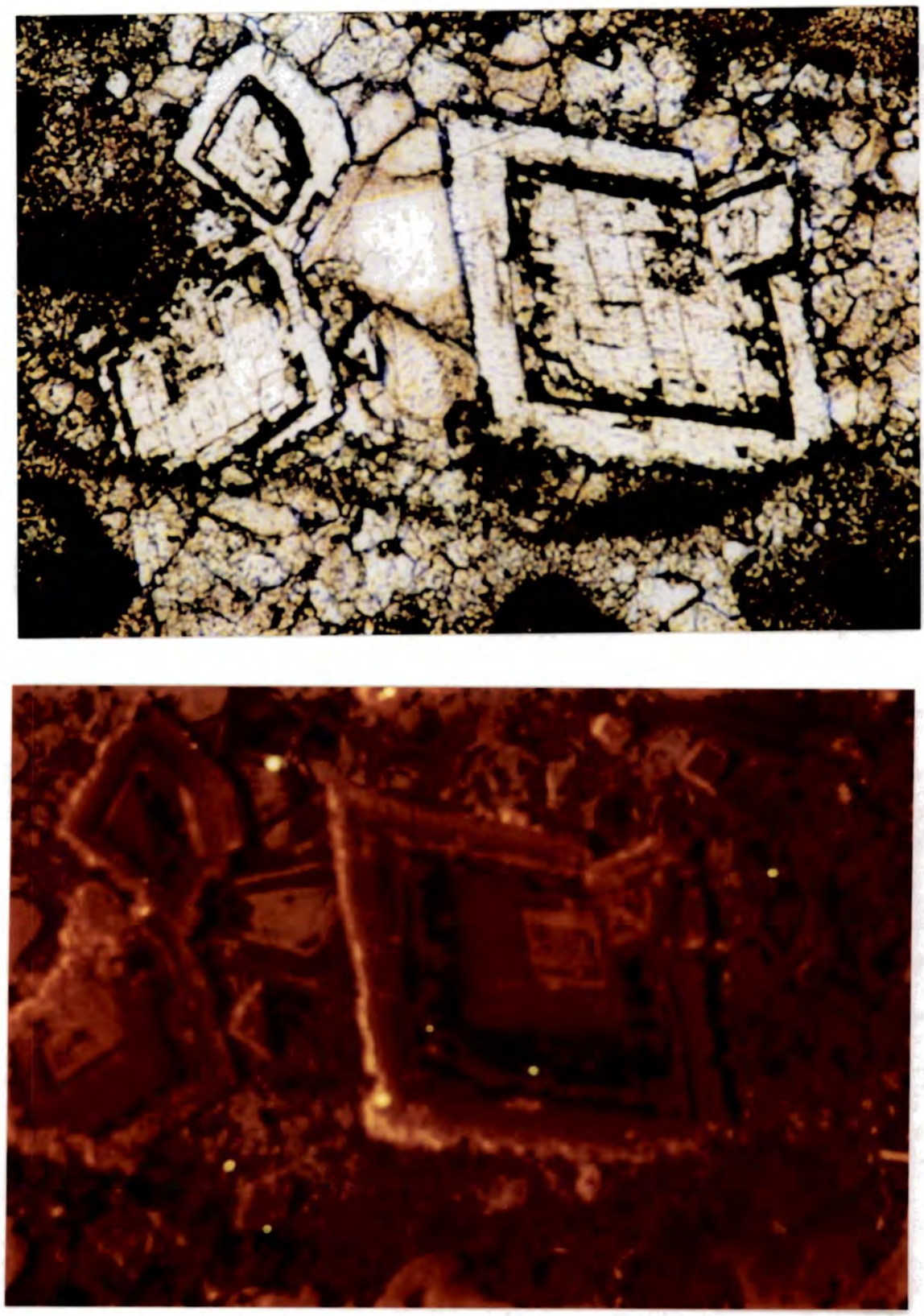

Fig. 5.22. PPL and CL photomicrograph pair of baroque dolomite cement crystals which show evidence of a dissolution phase prior to renewed growth. [Stained section. PT2. Width of view = 1.4mm]

require 5-25 volumes of pure chlorite (depending on the chlorite composition from Deer *et al.*, 1966). The Keuper is of similar thickness to the Muschelkalk in the Iberian Ranges (Virgili *et al.*, 1977) and does not contain enough chlorite for this to be a tenable source of magnesium for dolomitization. Freeman (1972) acknowledges that his measurements of modern brines will have been affected by evaporation, which by precipitation of gypsum will have lowered the Ca/Mg ratio. The magnesium may be derived from karstic dissolution of overlying dolomites (*e.g.* the Imon Formation).

Dolomitization in the Valencia-Cuenca Basin, on the basis of petrographic evidence in this study is clearly polyphase and the last episode of baroque dolomite precipitation cross-cuts earlier dolomite mosaics. This latest episode probably accounts for the dolomite cement observed by Freeman and interpreted as 'post mountain-building' which probably corresponds to burial diagenetic. However, evidence in this study indicates that the baroque dolomite grew in an already dolomitized Muschelkalk.

5.9.3 Valencia-Cuenca Basin Dolomite petrography

The three main dolomite types noted in the Lower Muschelkalk of the Catalan Basin are also present in the Valencia-Cuenca Basin, *i.e.* fabric-replacive dolomite, peritidal dolomite and baroque dolomite. However, in the Valencia-Cuenca Basin the peritidal dolomite and baroque dolomite are quantitatively more important than in the Catalan Basin. In addition, at one locality (Chelva) idiotopic dolomite rhombs occur in unusual pseudomorphs developed in a sandstone and is described in Section 5.9.3.4.

5.9.3.1 Fabric-replacive dolomite

The fabric-replacive dolomite decreases in abundance towards the northwest of the Valencia-Cuenca Basin and generally consists of fine to coarse-grained xenotopic dolomite mosaics which enclose pseudomorphically-replaced echinoderm fragments. Some of the mosaics preserve a bioturbated fabric similar to that described in Section 5.9.3.4.

5.9.3.2 Peritidal dolomite

The peritidal dolomite becomes more common towards the northwest of the Valencia-Cuenca Basin and distinction of any fabric-replacive dolomite becomes more difficult. The peritidal dolomite facies consists of laminated dolomicrites with small stellate pseudomorphs after gypsum with occasional thin dolomitized pisolite horizons.

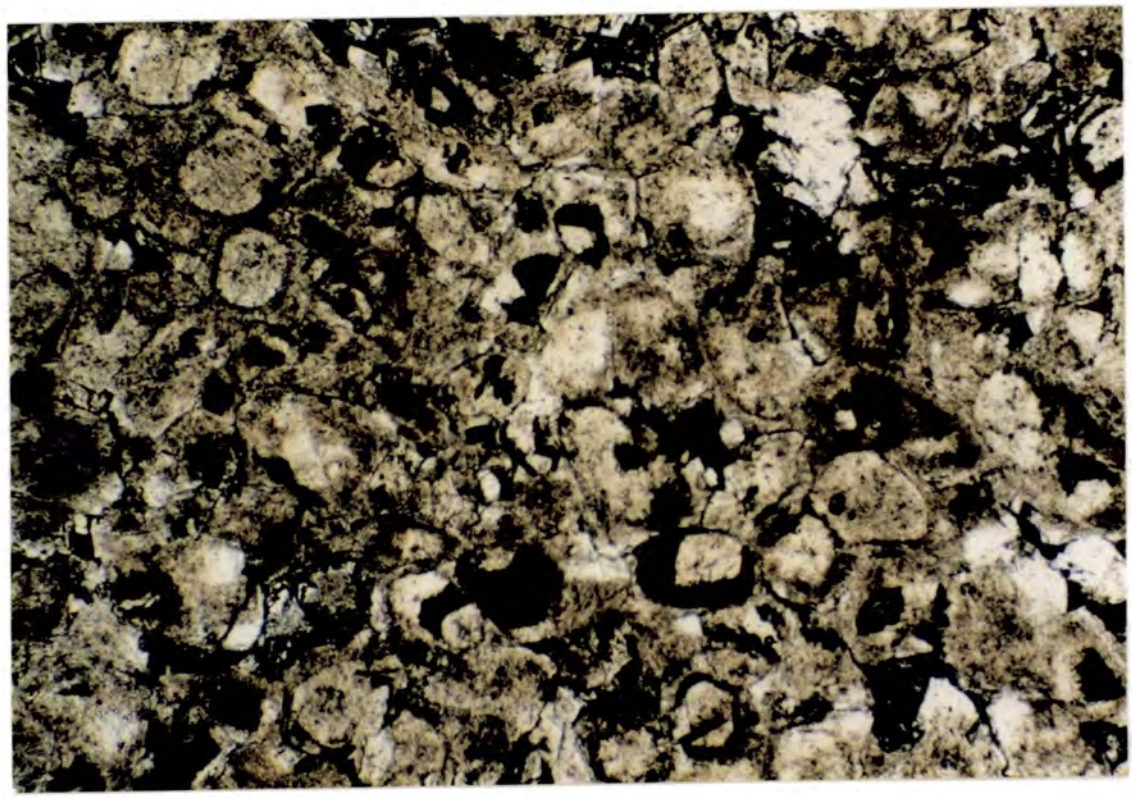

Fig. 5.23. Coarse baroque dolomite mosaic formed as a replacment after a cross-bedded oolite. Ghosts of ooids are present in the centres of some of the crystals. See Fig. 5.24. [PPL. ST6. Width of view = 3mm]

Fig. 5.24. Baroque dolomite mosaic with crystals showing undulose extinction (*e.g.* centre of photograph). [XPL. ST6. Width of view = 1.4mm]

5.9.3.3 Baroque dolomite

Baroque dolomite is more common in the Valencia-Cuenca Basin than in the Catalan Basin and occurs as mosaics, cross-cutting veins and cements.

The baroque dolomite mosaics occur at Serra (Section 3.3.2) and are coarse-grained replacements of cross-laminated oolites. Non-cathodoluminescent ghosts of ooids are present in the centres of coarse red-luminescent baroque dolomite crystals (Fig.s 5.23, 5.24).

Baroque dolomite veins (up to 1mm across) cross-cut fabric-replacive dolomite mosaics and thereby confirm that the baroque dolomitization was after the fabric-replacive (Fig.s 5.25, 5.26).

5.9.3.4 Euhedral dolomite associated with pseudomorphs

An unusual diagenetic fabric is developed in a dolomicrite-cemented sandstone horizon at Chelva. The dolomicrite contains rectangular to square-shaped pseudomorphs after ?anhydrite (Fig. 5.27). The quartz grains of the sandstones have not been replaced and occur within the pseudomorph implying non-displacive dolomite growth. The anhydrite has been replaced by fringing, isopachous dolomite cement, euhedral, zoned dolomite rhombs and interstitial ferroan calcite and iron oxy-hydroxides. Some of the cores of the dolomite rhombs have been replaced and altered to ferroan calcite (See Chapter 8). The quartz grains have remained dispersed within the pseudomorph indicating that there was no void stage. The dolomite is not baroque but may nevertheless have resulted from thermochemical sulphate reduction at depth (Beales & Hardy, 1980).

Similar pseudomorphs to these are present elsewhere in the Valencia-Cuenca Basin but without the dolomite cement lining and idiotopic rhombs and merely containing ferroan calcite (see Section 4.8.1.2).

5.9.3.4 Conclusions

Dolomitization of the Lower Muschelkalk of the Valencia-Cuenca Basin appears to be essentially similar to that of the Catalan Basin. However, the relationship between the peritidal dolomite and fabric-replacive dolomite is not as obvious in the Valencia Cuenca Basin and as the Lower Muschelkalk becomes thinner towards the northwest the distinction is difficult. The greater abundance of baroque dolomite in the Valencia-Cuenca Basin may be related to a greater hydrothermal activity in that region.

Fig. 5.25. Dolomite mosaic cut by dissolution seam, both of which are cut by a coarse baroque dolomite vein. [XPL. ST4. Width of view = 3mm]

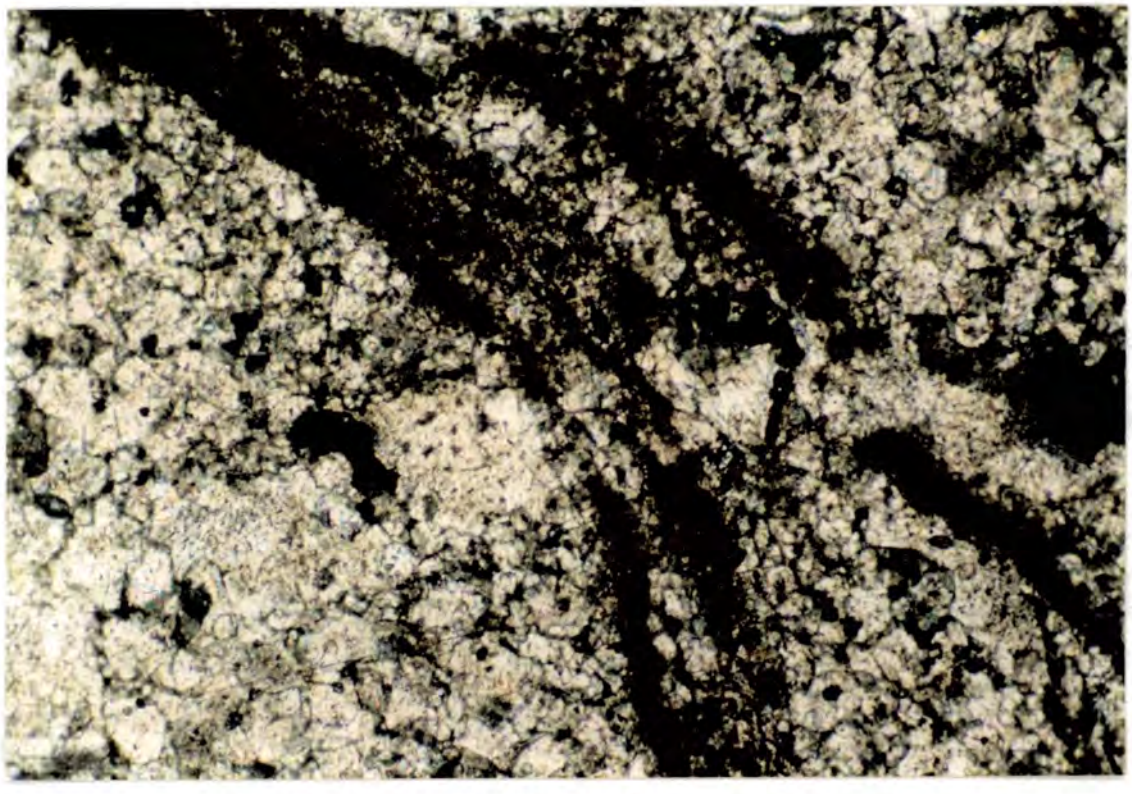

Fig. 5.26. Dolomite mosaic cut by dissolution seam, both of which are cut by a coarse baroque dolomite vein. [XPL. ST1. Width of view = 1.4mm]

5.10 RELATIVE TIMING OF DOLOMITIZATION

The timing of dolomitization is often difficult to ascertain, especially in situations involving overprinting and recrystallization of earlier formed dolomites. Recrystallization of dolomites has certainly occurred during the burial of the dolomites in the Lower Muschelkalk which may have affected the geochemical patterns (see Chapter 7), however field evidence and petrographical observations can be used to constrain the relative timing.

5.10.1 Relative timing of fabric-replacive dolomitization

5.10.1.1 Field evidence

The fabric-replacive dolomite clearly replaces near-normal marine limestones. The dolomite front at the base of the fabric-replacive dolomite is discordant to bedding and the dolomite is not restricted to a particular depositional facies. These features indicate that dolomitization occurred post-deposition and was not related to any particular depositional environment or mineralogy.

The relationship between subsurface paleokarsts and dolomitization was discussed in Section 4.6.2.3. The subsurface paleokarst appears to be related to the base-Paleogene unconformity and was developed along a pre-existing dolomite front, suggesting that dolomitization had already occurred prior to the early Paleogene uplift.

5.10.1.2 Petrography

Mechanical compaction features in oolites and pisolites, such as buckling and fracturing of cements (see Section 4.3.1), are commonly preserved in pseudomorphic fabric-replacive dolomite. However, this does not clearly constrain the timing of dolomitization. The cements may have been dolomitized and subsequently fractured or dolomitization may have pseudomorphed a pre-existing broken cement. The lack of dolomite cement between the broken ends of the cement fringe may suggest dolomitization pre-fracturing (*cf.* Kaldi & Gidman, 1982).

Chemical compaction features, such as stylolites, clearly cut across dolomite mosaics and show that fabric-replacive dolomitization occurred pre-stylolitization (Fig. 5.28). A minor amount of dolomite associated with the nodular/bioturbated fabrics in limestones throughout the Lower Muschelkalk may have resulted from non-sutured seam dissolution (Section 5.5.2.1; Wanless, 1979). This dolomite would have resulted from local remobilization of magnesium from high-Mg calcite and implies that locally the mineralogy had not been completely stabilised by meteoric diagenesis. Chemical

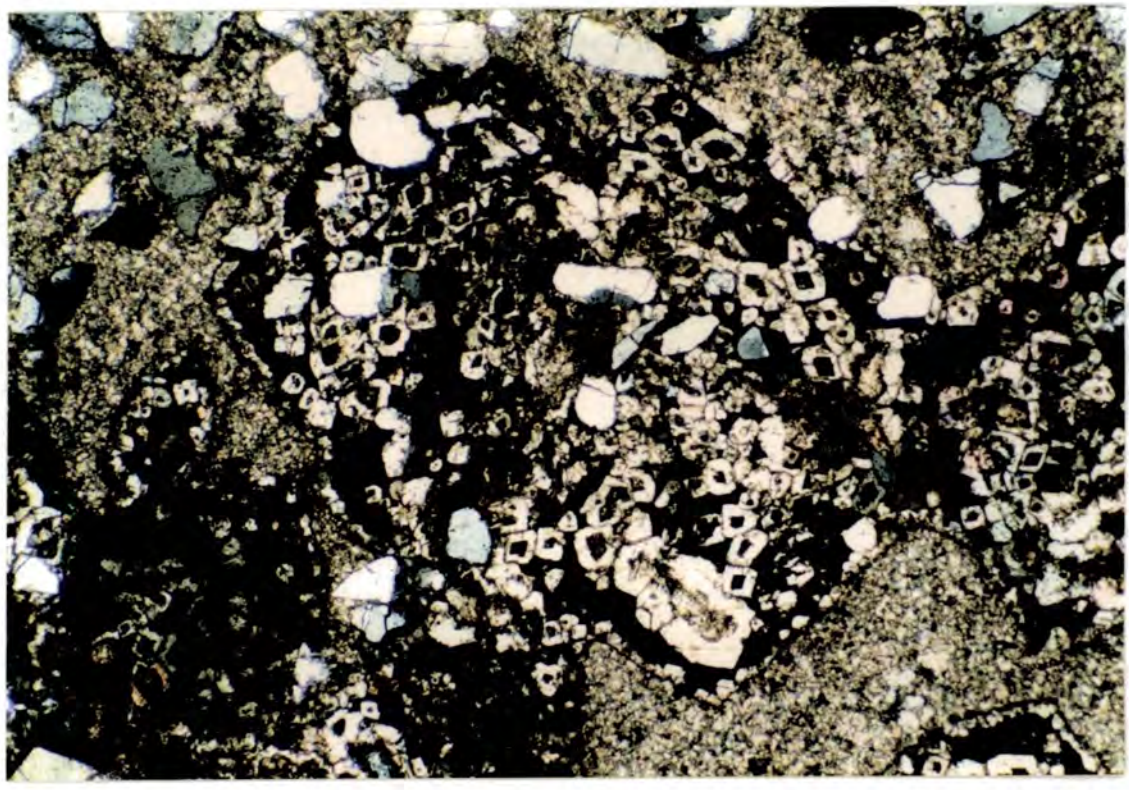

Fig. 5.27. Zoned dolomite rhombs within a rectangular pseudomorph after ?anhydrite which grew in a carbonate-cemented quartz sandstone. See Section 5.9.3.4. [XPL. CV8. Width of view = 3mm]

Fig. 5.28. Stylolite cross-cutting fabric-replacive dolomite mosaic. [XPL. LR21. Width of view = 3mm]

compaction probably begins in marine sediments within the first few hundred metres (Choquette & James, 1987). Meyers & Hill (1983) suggested that pressure dissolution in Mississippian shallow-marine grainstones and packstones began after tens to hundreds of metres of burial. Thus, the fabric-replacive dolomite is considered to be shallow-burial.

Lath-shaped pseudomorphs after anhydrite are locally associated with fabric-replacive dolomitization. This is particularly clear in partially dolomitized bioturbated wackestones where the pseudomorphs only occur in the dolomitized areas (see Fig.s 4.27, 4.28). The growth of calcium sulphate minerals from a hypersaline brine would enhance the dolomitization potential by increasing the Mg/Ca ratio of the fluid. The anhydrite precipitation is considered to be penecontemporaneous with the matrix replacive dolomitization. The pseudomorphs locally contain baroque dolomite cement which is considered to be a separate and later phase of dolomitization.

The preservation of fine concentric laminae in the cortices of ooids suggests that the dolomitization may have been pseudomorphing an aragonite precursor. However, the lack of identifiable molluscan debris suggests that their aragonite skeleta had been replaced by calcite spar prior to dolomitization. Fabric-replacive dolomitization probably occurred after the dissolution and replacement of some aragonite allochems but before in the case of others. The local early aragonite dissolution is probably related to meteoric diagenesis (see Section 4.10).

The contact at the top of the fabric-replacive dolomite is locally sharp and directly overlain by laminated peritidal dolomites (see Section 5.4.2). The contact locally appears to be a paleokarstic surface and may be associated with early meteoric-related ooid dissolution and mineralogical stabilization which prevented subsequent fabric-replacive dolomitization. The relationship indicates that fabric-replacive dolomitization occurred post-karstification and therefore during or after the deposition of the overlying peritidal dolomicrite.

5.10.2 Relative timing of peritidal dolomitization

5.10.2.1 Field evidence

The peritidal dolomite is clearly stratigraphically-controlled and related to particular depositional facies. The pervasive and ubiquitous nature of the peritidal dolomite suggests that the dolomitization may have at least begun during deposition by processes analogous to those envisaged for peritidal dolomites in modern environments. The depositional mineralogy would have consisted of fine-grained aragonite, high-Mg calcite and any penecontemporaneous dolomite.

5.10.2.2 Petrography

The peritidal dolomite is pervasively dolomitized and there are no relic limestones or partially dolomitized horizons. Thin oolitic layers that are locally present are also completely dolomitized. Therefore, after deposition and formation of any penecontemporaneous dolomite there was further dolomitization and stabilization of the mineralogy. In a similar way to the fabric-replacive dolomite the peritidal dolomite is pre-stylolitization. However, stylolites are not so common in the peritidal dolomite and this may be due to relatively early formation of a grain-supported fabric (Choquette & Steinen, 1980).

5.10.3 Relative timing of baroque dolomitization

Baroque dolomite occurs as cements and mosaics, and is more common in the Valencia-Cuenca Basin than in the Catalan Basin. The baroque dolomite veins clearly cross-cut fabric-replacive dolomite mosaics and stylolites (Fig.s 5.25, 5.26). The baroque dolomite mosaics are probably produced by recrystallization of pre-existing dolomite. The baroque dolomite cement lines late fractures and also occurs in association with local sulphate replacement, possibly by thermochemical sulphate reduction. Baroque dolomite is widely accepted to be a high-temperature form of the mineral and is more common at those localities which have Pb-Zn ores and hydrothermal minerals. The Pb-Zn ores in the northern Catalan Coastal Ranges exploit the subsurface paleokarst system which, as argued before may be related to the base-Paleogene unconformity. The baroque dolomite is a burial form and may be related to Tertiary hydrothermal systems.

5.10.4 Conclusions

The fabric-replacive dolomitization occurred during shallow-burial of a locally mineralogically-stabilized near-normal marine limestone, probably during or immediately after the deposition of the overlying peritidal dolomite.

The peritidal dolomite was probably at least in part formed during deposition and underwent complete stabilization and dolomitization in the near-surface.

The baroque dolomite is late, burial, fracture-related and cross-cuts the earlier dolomites, and occurs predominantly in association with ore deposits which may be related to Tertiary hydrothermal systems.

CHAPTER 6: GEOCHEMISTRY OF THE LOWER MUSCHELKALK

6.1 INTRODUCTION

The principal aims of the geochemical study were to investigate limestone diagenetic trends, geochemical distinctions between dolomite facies, geochemical trends that might be related to fluid flow, and elucidation of the geochemical environment of dolomitization.

Geochemical methods of studying limestones and dolomites are numerous and the techniques are reviewed in Tucker (1988). The principal methods used in this study have been: X-ray diffraction (XRD), for dolomite ordering and stoichiometry; Atomic Absorption Spectrophotometry (AAS) and Inductively Coupled Plasma Atomic Emission Spectrometry (ICPAES), to examine major and trace element concentrations; and carbon and oxygen stable isotope analysis. In addition, the above have been supplemented by cathodoluminescence (CL) and staining.

6.2 LIMESTONE AND CALCITE SPAR GEOCHEMISTRY

6.2.1 Introduction

The geochemical patterns resulting from limestone diagenesis are quite well understood, particularly in the meteoric environment. Modern marine carbonate sediments are porous and generally consist of aragonite, high-Mg calcite and minor low-Mg calcite. During subsequent lithification and diagenesis porosity is greatly reduced and the overall mineralogy becomes dominated by low-Mg calcite (Tucker & Wright, 1990). The mineralogical changes and trace element partitioning result in a decrease in strontium content, but increase in iron and manganese concentrations, and commonly more negative $\delta^{18}O$ and $\delta^{13}C$ values (Veizer & Demovic, 1974; Morrow & Mayer, 1977; Hudson, 1977; Pingitore, 1978; Dickson & Coleman, 1980; Allan & Matthews, 1982).

The conversion of aragonite to calcite is well-documented petrographically (*e.g.* Dodd, 1966, Longman, 1980) and has been studied experimentally (see Bathurst, 1975). The time-scale for aragonite-calcite stabilization is generally considered to be a few tens of thousands of years. Vacher *et al.* (1990) estimated that the half-life of aragonite-calcite reaction in a freshwater lens is about 6000-7000years. Lasemi & Sandberg (1984) used SEM studies to show that aragonite muds alter to microsparitic limestone as a result of both early calcitization and meteoric cementation. However, under some particular circumstances (*e.g.* in impervious shales) aragonite may persist into the burial diagenetic realm and occurs in ancient strata.

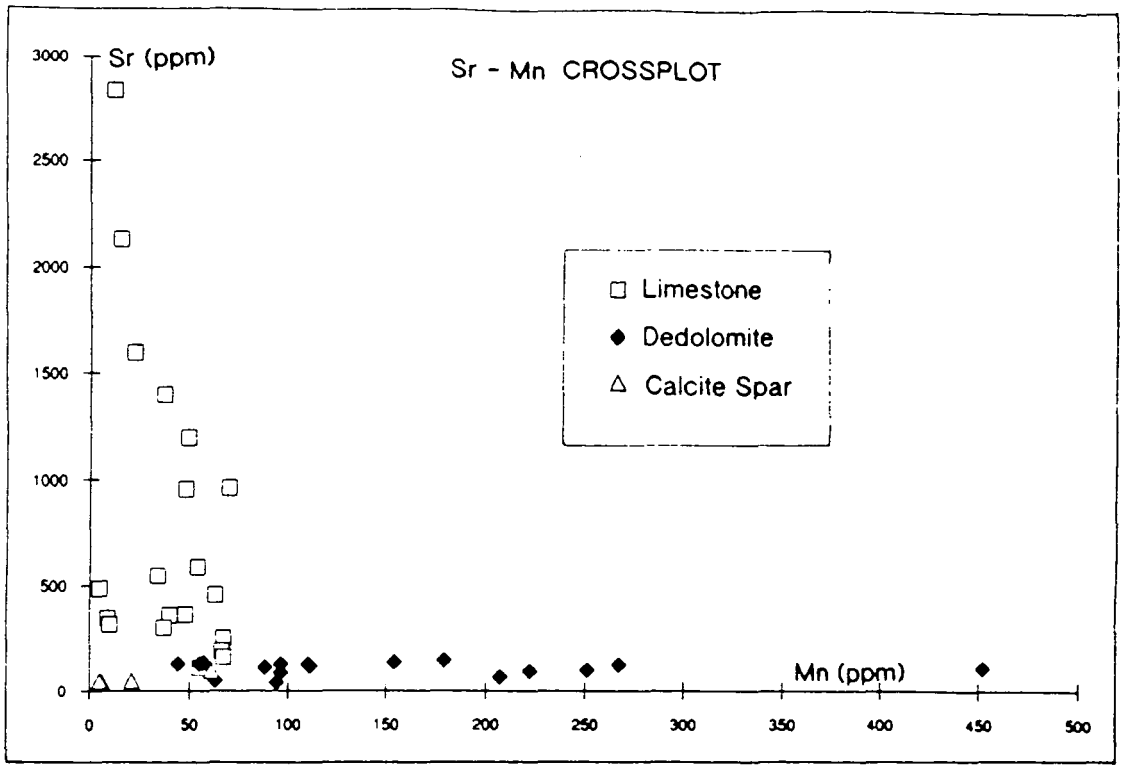

Fig. 6.1. Crossplot of strontium concentration against manganese concentration for limestone, dedolomite and calcite spar samples.

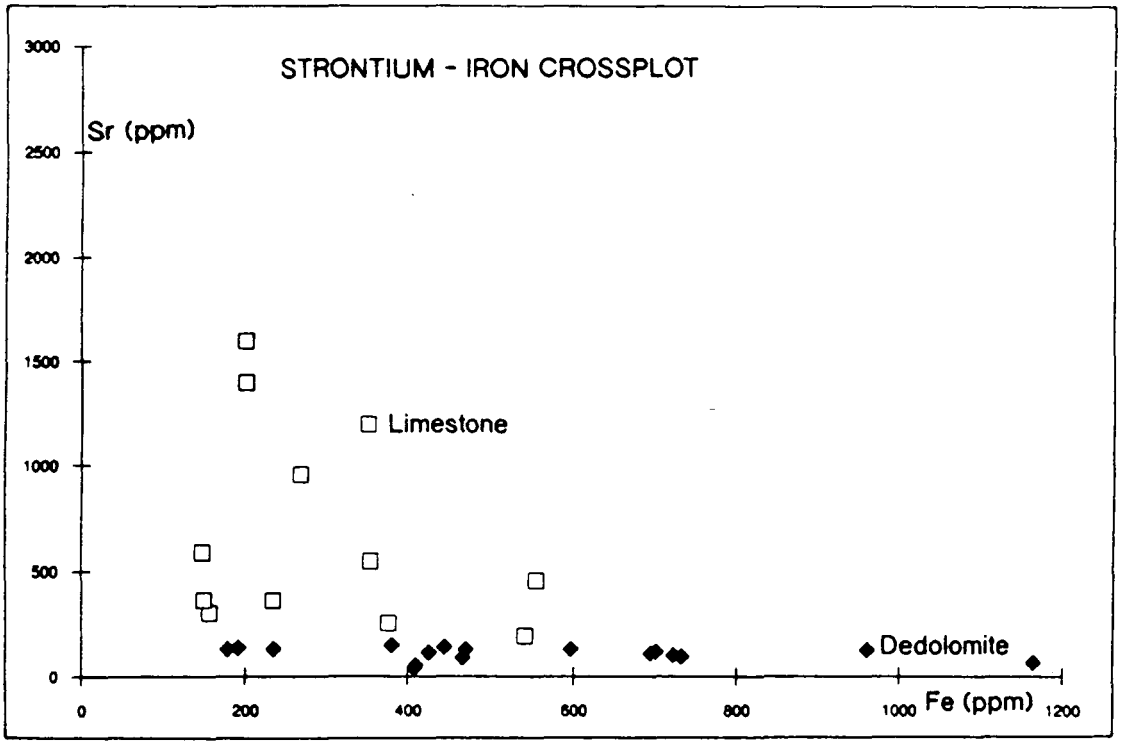

Fig. 6.2. Crossplot of strontium concentration against iron concentration for limestone, dedolomite and calcite spar samples.

6.2.2 Sampling

Analytical procedures for ICPAES and stable isotope analysis are outlined in Appendices 3 and 4. The samples were of three types: whole-rock samples of fine-grained, tight limestones mainly from the Vilella Baixa Unit; calcite allochem (brachiopod, echinoderm and ooid) microsamples; and late calcite spar from pseudomorphs after evaporites and associated veins. The results are tabulated in Appendix 6 and presented graphically here. *Note, all stable isotope data are given relative to PDB and trace elements are normalised to 100% carbonate* (see Appendix 3).

6.2.3 Whole-rock micrite samples

6.2.3.1 Trace element results

The calcium and magnesium data confirm that these are near-pure low-Mg calcite carbonates. Strontium concentrations vary from nearly 3000ppm to 100ppm and generally have lower iron and manganese concentrations at high strontium values (Fig.s 6.1, 6.2). The iron and manganese concentrations have a crude positive correlation and vary from 150-1200ppm iron and 10-100ppm manganese (Fig. 6.3). The trace element contents of the micrite samples contrast with the dedolomite and calcite spar samples (see Section 8.5).

6.2.3.2 Stable isotope results

The limestone samples vary from +1 to +3 $\delta^{13}C$ and -4.5 to -8 $\delta^{18}O$ (Fig. 6.4). The $\delta^{18}O$ values have a strong logarithmic relationship to strontium concentrations such that decreasing strontium correlates with more negative $\delta^{18}O$. This relationship contrasts with the dedolomite and calcite spar samples (Fig. 6.5; Section 8.5).

6.2.3.3 Whole-rock limestone interpretation

The strontium concentrations of the micritic limestones are similar to those of many Bermudan and Floridan limestones which have been subjected to meteoric alteration (Stehli & Hower, 1961 in Bathurst, 1975) and are also similar to many other ancient micrites. It is commonly accepted that the strontium concentration of a limestone decreases during diagenesis as a result of the low partition coefficient and the mineralogical change to low-Mg calcite from aragonite, whose structure can accommodate strontium. The model of Morrow & Mayers (1978) requires several thousand pore-volumes of meteoric water to reduce the strontium content of modern aragonite sediments to values of hundreds to thousands of ppm. However, experimental work by Katz *et al.* (1972) indicated that the aragonite-calcite inversion

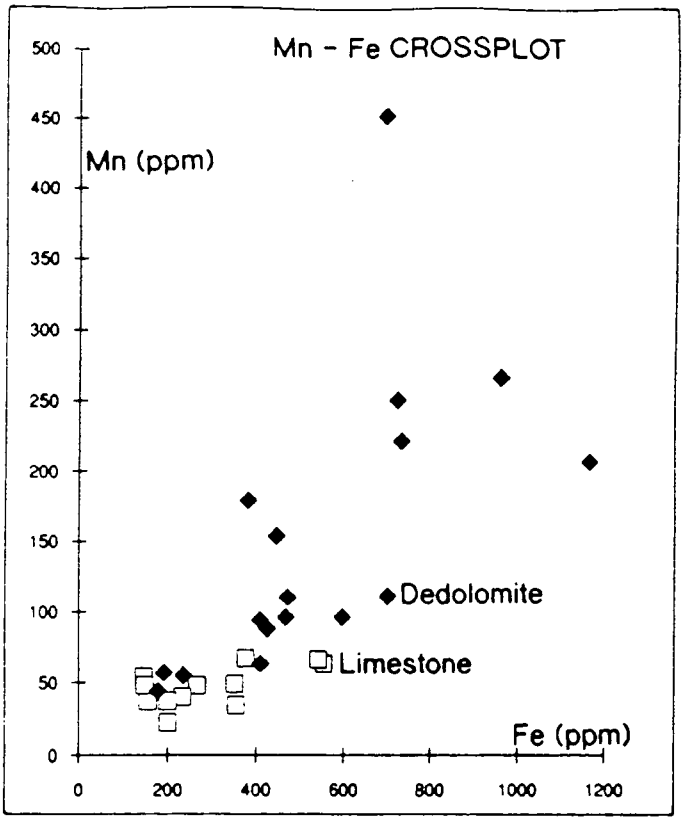

Fig. 6.3. Crossplot of manganese concentration against iron concentration for limestone and dedolomite samples.

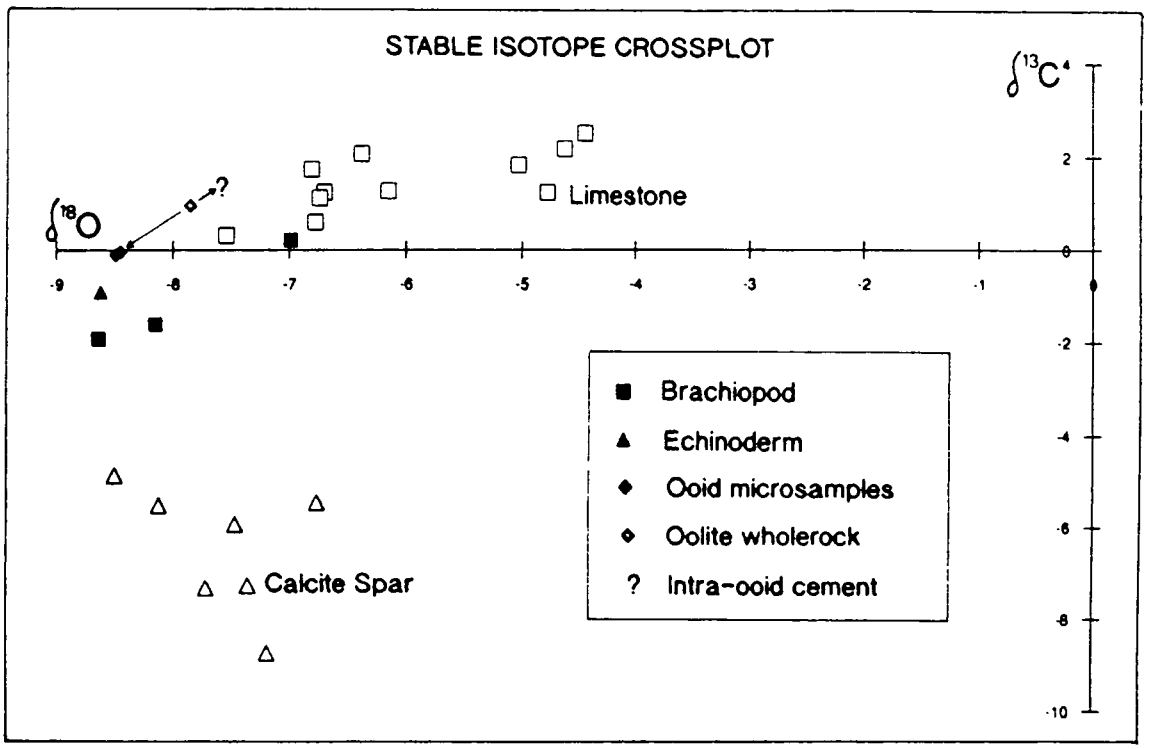

Fig. 6.4. Stable isotope crossplot for calcitic samples.

will lose strontium even in a system open to marine waters. Thus, the strontium depletion observed in the Lower Muschelkalk lime mudstones could have occurred in either meteoric or brackish groundwaters. Morrow & Mayers (1978) considered that the differences in strontium concentrations are more likely to arise from varying groundwater-rock ratio and groundwater composition than from variations in initial strontium concentrations.

The negative correlation between strontium and iron or manganese indicates enrichment of these two trace elements during diagenesis. Iron and manganese are generally incorporated from reducing, phreatic porewaters (James & Choquette, 1984). However, Pingitore (1978) suggested that the aragonite-calcite transformation would result in increasing manganese concentration in the calcite, particularly in an open system, as a result of the high partition coefficient into calcite.

The carbon and oxygen stable isotope data appear to lie on a diagenetic trend of more negative $\delta^{18}O$ value and slightly less positive $\delta^{13}C$ value similar to that shown by Hudson (1977). The minor positive correlation between $\delta^{18}O$ and $\delta^{13}C$ values may be related to diagenesis in a marine-meteoric mixing zone (Allan & Matthews, 1982).

The strong correlation between $\delta^{18}O$ value and strontium concentration confirms that these are diagenetic trends. However, the sample with the most undepleted $\delta^{18}O$ value contains about 3000ppm strontium, a concentration less than but comparable with a modern sediment, and thus the original isotopic composition of the fine-grained sediment would probably have been slightly more positive than -4.5 $\delta^{18}O$. Other values for Triassic marine precipitates are given for comparison in Fig. 6.6.

6.2.4 Calcite allochem and spar samples

6.2.4.1 Results

The allochem isotope data fall within -7 to -9 $\delta^{18}O$ and +1 to -2 $\delta^{13}C$. The spar samples consist of low-Mg calcite and plot in a different field around -7 to -9 $\delta^{18}O$ and -7 to -9 $\delta^{13}C$.

AAS analyses of an early poikilotopic calcite spar cemented oomoldic limestone are discussed in Section 6.3.4.3 and show that the precipitating fluids were reducing with high Fe^{2+}/Ca^{2+} and Mn^{2+}/Ca^{2+} ratios.

Calcite ooids which display strong concentric fabrics (*e.g.* Fig. 4.5) were analysed as was a whole-rock sample of the oolite. The different analyses allow estimation of the isotopic composition of the inter-ooid early calcite cement (Fig. 6.4).

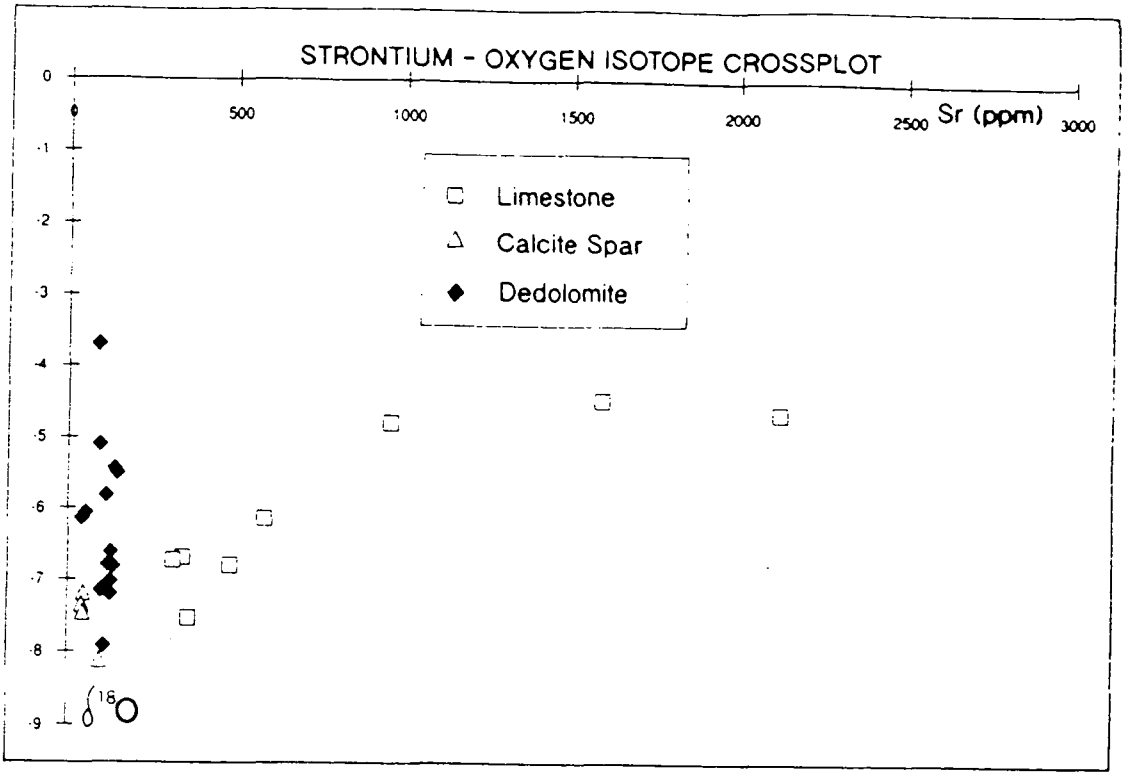

Fig. 6.5. Crossplot of $\delta^{18}O$ against strontium concentration.

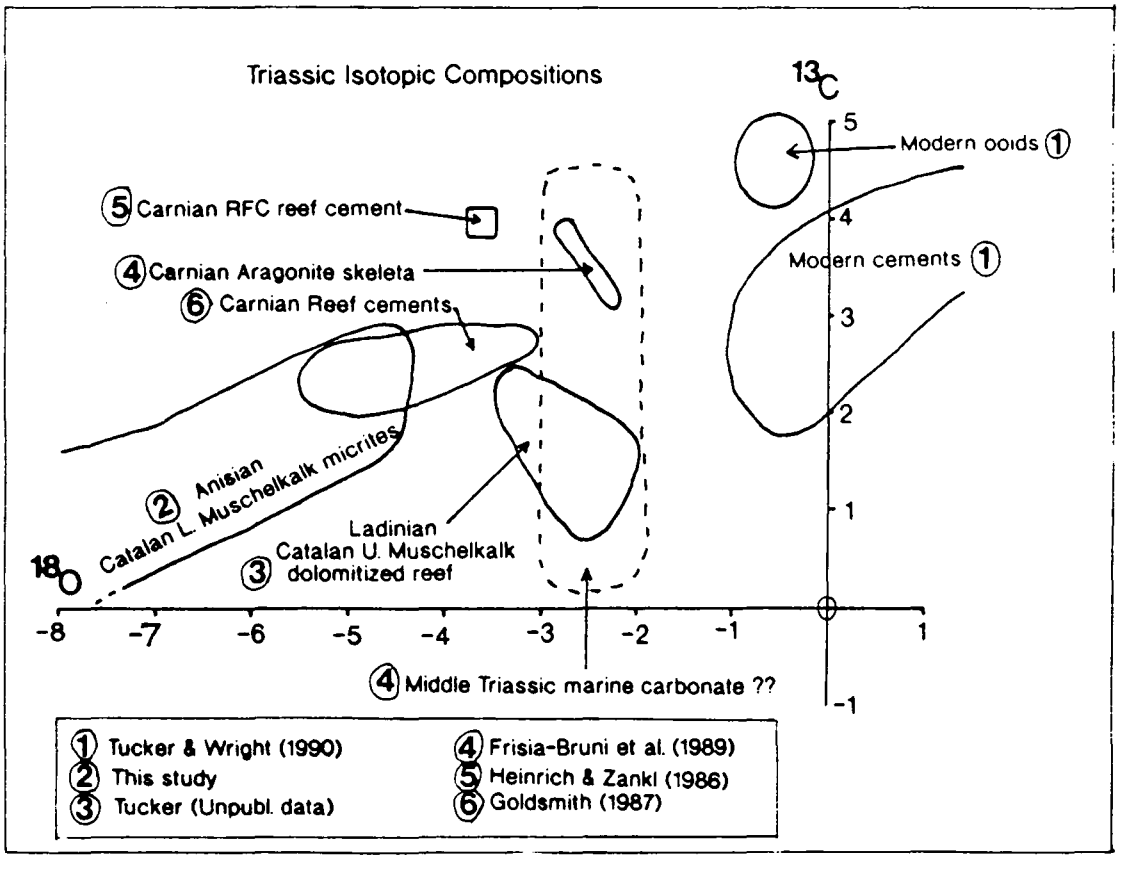

Fig. 6.6. Stable isotope plot of a range of Triassic carbonates for comparison with the Lower Muschelkalk analyses.

6.2.4.2 Interpretation

The allochems appear to plot on the same diagenetic trend as the micritic limestones. The brachiopod samples come from specimens which display good skeletal preservation and were non-luminescent under CL and thus should represent the best opportunity of estimating the seawater composition (Popp *et al.*, 1986). However, the brachiopods are clearly too negative to represent a marine composition and thus there has been isotopic alteration without skeletal deterioration, as noted by Dickson & Coleman (1989).

The ooid samples and whole-rock oolite sample suggest that the inter-ooid early calcite cement has an average isotopic composition of about -7 $\delta^{18}O$ and +1.5 $\delta^{13}C$. This may represent the early diagenetic calcite isotope signature. The calcite spar samples reflect the late diagenesis which is associated with dedolomitization (Chapter 8). The late calcite spar is substantially more depleted in ^{13}C than the early calcite possibly owing to more soil gas involvement in the late uplift-related diagenesis.

6.2.5 Limestone and calcite sample conclusions

The trace element and stable isotope analyses confirm that during diagenesis the micritic limestones have stabilized from a strontium-rich, ^{18}O-enriched and probably aragonitic precursor to a strontium-depleted, ^{18}O-depleted low-Mg calcite limestone. Most of this alteration could have taken place during early near-surface meteoric diagenesis in phreatic, reducing and possibly brackish environments. Strontium depletion and some of the absorption of iron and manganese may have occurred during deeper burial, and this may account for the very strontium-poor compositions of some of the limestone samples.

Estimates of the isotopic composition of sea-water are difficult. The least ^{18}O-depleted micrite samples (-4.5 $\delta^{18}O$) provide a minimum value for the sea-water composition. Brachiopod and other allochems have been affected by diagenesis and do not represent sea-water composition. The sea-water composition was probably around -3 $\delta^{18}O$.

Late meteoric diagenetic calcites have a distinct isotopic composition from the early calcite estimated from the ooid and oolite samples.

6.3 CATALAN BASIN FABRIC-REPLACIVE AND PERITIDAL DOLOMITE GEOCHEMISTRY

6.3.1 Introduction

The geochemistry of dolomite and dolomitization is much less well understood than for calcite and aragonite and the diagenesis of lime sediments. Dolomite is a highly ordered mineral and has not yet been synthesized in the laboratory under near-surface conditions. As a result of the uncertainty regarding the values of many fundamental geochemical parameters with respect to dolomite (*e.g.* fractionation factors), geochemical techniques are generally used qualitatively (Land, 1980). Reviews of dolomite geochemistry are given in Land (1980), Morrow (1982a), Land (1983), Machel & Mountjoy (1986) and Tucker & Wright (1990).

In this study geochemical techniques were used to characterise dolomite types and attempt to constrain the paleohydrology.

6.3.2 Techniques and sampling strategy

Analytical procedures for XRD, AAS, ICPAES and stable isotope analysis are given in the appendices together with tabulated results.

6.3.2.1 XRD samples

XRD was used to analyse about 20 whole-rock powders of coarse and fine-grained dolomites from two localities for dolomite crystal ordering and stoichiometry (Lumsden & Chimahusky, 1980; Hird, 1986; Tucker & Wright, 1990).

6.3.2.2 Elemental analysis

Elemental analysis was carried out by AAS and ICPAES. *Note, all elemental analyses are given normalised to 100% carbonate* (see Appendix 3).

i) AAS samples

AAS was used to analyse samples from two localities where the Lower Muschelkalk is almost completely dolomitized (Colldejou and Arboli). Whole-rock powders were prepared from nearly all the specimens from each locality. The samples were analysed for calcium, magnesium, iron, manganese, strontium and sodium. The analyses were performed in order to examine any trace element correlation with depositional facies or dolomite fabric.

ii) ICPAES samples

ICPAES was used to analyse whole-rock dolomite samples of the main dolomite facies from 22 localities in the Catalan Basin in order to investigate regional and stratigraphic trace element variations. In order to minimise differences due to depositional facies and within sample variation most of the specimens were allochem-free dolomicrites. ICPAES analysis measured 24 elemental concentrations for each sample. However the most useful analyses were of calcium, magnesium, strontium and manganese. Iron was analysed in only some of the samples.

6.3.2.3 Stable isotope samples

Eighty whole-rock dolomite samples were analysed for carbon and oxygen stable isotopes. Most of the samples were fine-grained dolomicrites but some coarse dolomite mosaics were also analysed. The analyses were performed in order to constrain the chemistry of the dolomitizing fluids and to compare with trace element trends. *Note, all stable isotope results are given in permil relative to PDB standard* (see Appendix 4).

6.3.3 XRD analysis

6.3.3.1 XRD results

The XRD data do not show much variation (Fig. 6.7). Stoichiometry is near to the ideal 50% in all the samples. Ordering varies from 0.55 to 0.95. The peritidal dolomites have on average a less ordered structure than the fabric-replacive dolomites.

6.3.3.2 XRD interpretation

Dolomites forming in modern peritidal settings are typically calcian and poorly ordered (Tucker & Wright, 1990) suggesting that the Lower Muschelkalk peritidal dolomites have undergone considerable stabilization. The formation of better ordered dolomite from a poorly ordered precursor has been documented from modern sabkhas (McKenzie, 1981) and tidal flats (Carballo *et al.*, 1987). Lumsden & Chimahusky (1980) also noted a trend towards more stoichiometric dolomite in older dolostones suggesting gradual recrystallization and stabilization. The peritidal dolomites of the Lower Muschelkalk would most closely correspond to the evaporite-related dolomicrites of Lumsden & Chimahusky (1980) which they considered to be syndepositional to early diagenetic.

6.3.4 Trace element analysis

6.3.4.1 Introduction

Trace element analyses of dolomites are common in the literature. However, there is considerable uncertainty regarding the values of trace element distribution coefficients of dolomite under near-surface and diagenetic conditions. Most distribution coefficients values are either extrapolated from high-temperature data (*e.g.* Katz & Matthews, 1977), theoretically modelled (*e.g.* Kretz, 1982) or calculated inversely from natural dolomites (*e.g.* Vahrenkamp & Swart, 1990). However, there is considerable agreement that Sr^{2+} has a distribution coefficient considerably less than 1 whereas Fe^{2+} and Mn^{2+} values are much greater than 1 (Vahrenkamp & Swart, 1990; Tucker & Wright, 1990). Hence, iron and manganese tend to be incorporated into the dolomite lattice during dolomitization whereas strontium tends to be depleted.

Paleohydrological fluid flow may in some cases be determined from trace element trends, particularly from strontium and manganese data (Land *et al.*, 1975; Land, 1983; Machel, 1988; Gregg & Shelton, 1989). Strontium variations have also been used as an aid to facies analysis and to discriminate dolomites that formed from aragonitic strontium-rich precursors as opposed to calcitic, strontium-poor precursors (Veizer & Demovic, 1974).

A large proportion of the trace sodium ions is not incorporated into the crystal lattice but occurs in interstitial sites and in fluid inclusions (Machel, 1988). Nevertheless, Na^{+} appears to have an effective distribution coefficient much less than 1 and has been used to indicate paleosalinity and paleoenvironment (Veizer *et al.*, 1977; Veizer *et al.*, 1978; Sass & Katz, 1982).

The whole-rock trace element samples showed uniform cathodoluminescence suggesting homogeneous iron, manganese, and by implication strontium, concentrations (Fraser *et al.*, 1989; Hemming *et al.*, 1989).

6.3.4.2 AAS results

Whole-rock samples were analysed from two localities, Arboli and Colldejou.

i) Arboli

The Lower Muschelkalk at Arboli is completely dolomitized (see Section 3.2.3.3). Paleokarstic surfaces are common at the tops of small-scale oolite-capped cycles in the Vilella Baixa Unit (Section 4.6.1.1).

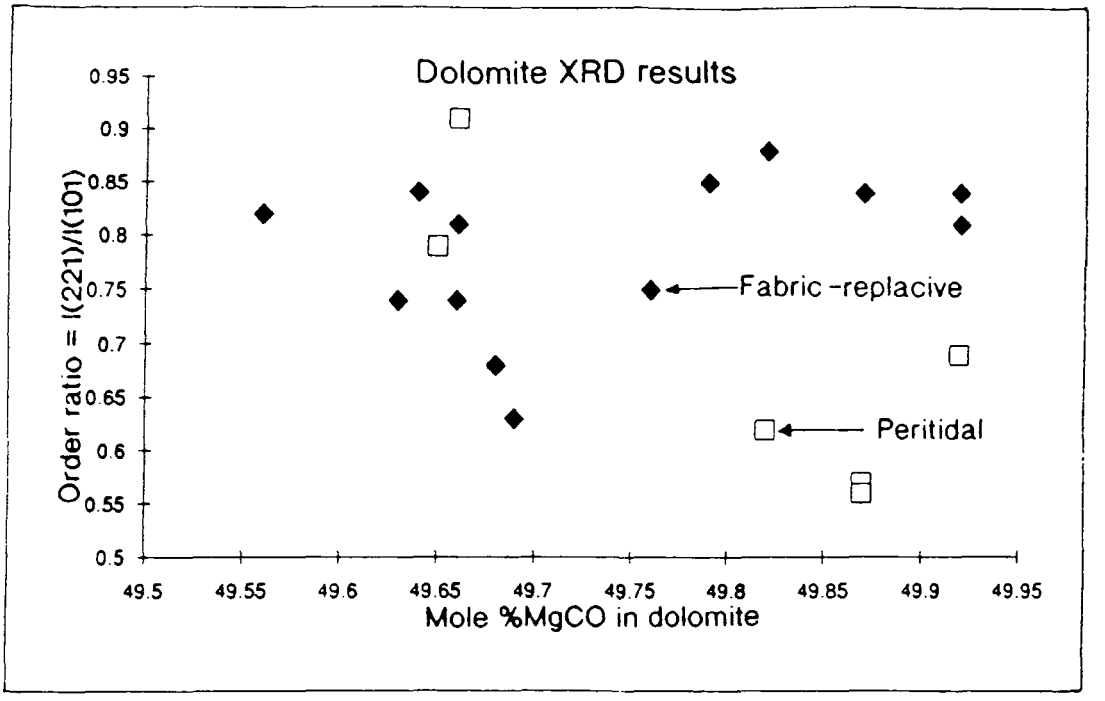

Fig. 6.7. Order ratio and stoichiometry for fabric-replacive and peritidal dolomites. Calculated from XRD data.

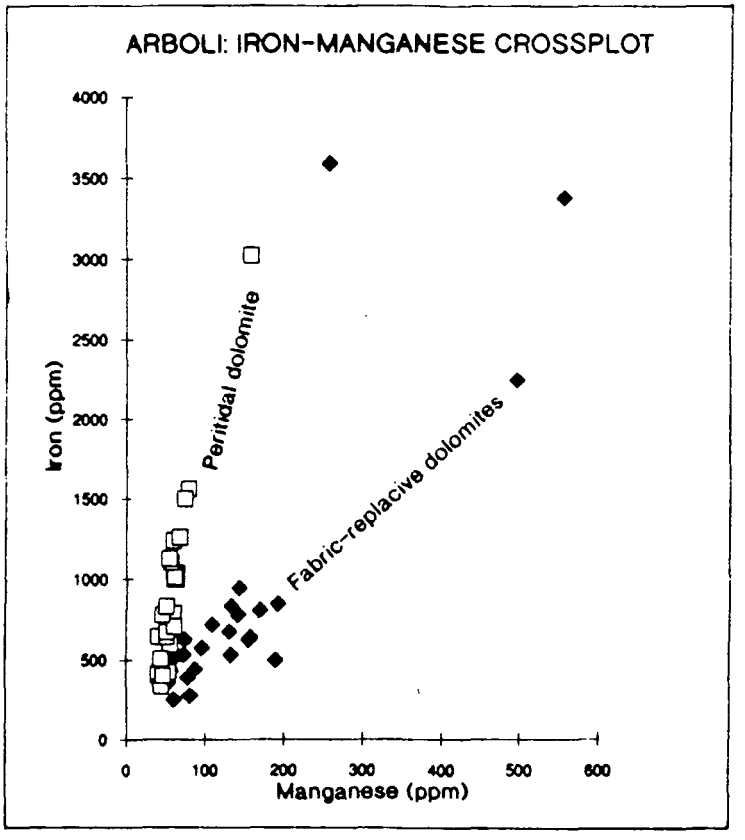

Fig. 6.8. Crossplot of iron and manganese concentrations (from AAS analyses) for peritidal dolomites and fabric-replacive dolomites from Arboli locality.

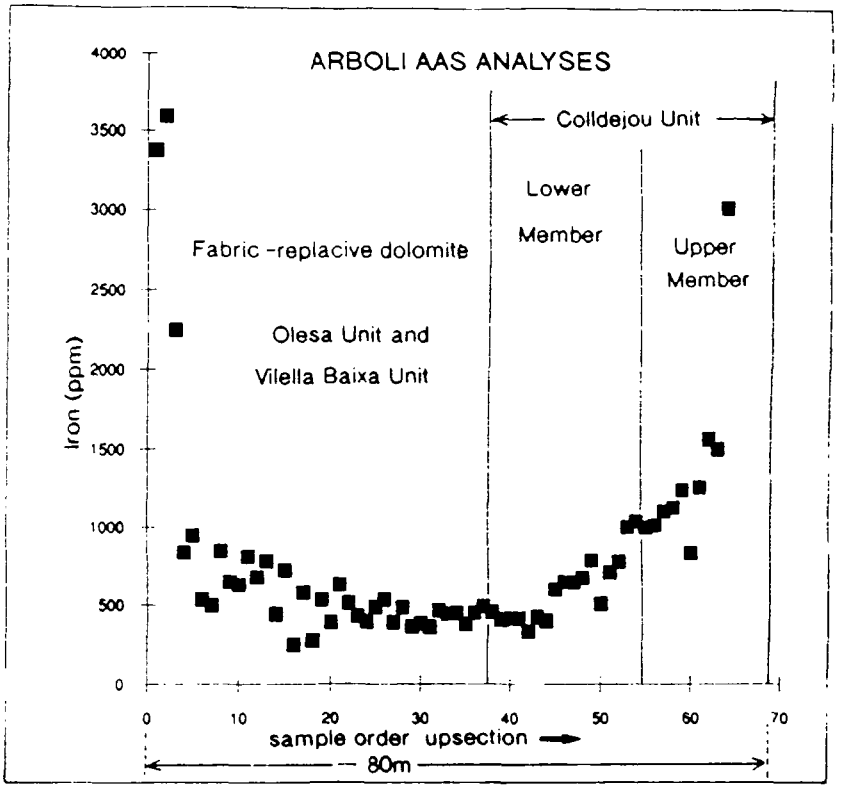

Fig. 6.9. AAS analyses for iron concentrations in Arboli locality dolomites plotted against stratigraphic position.

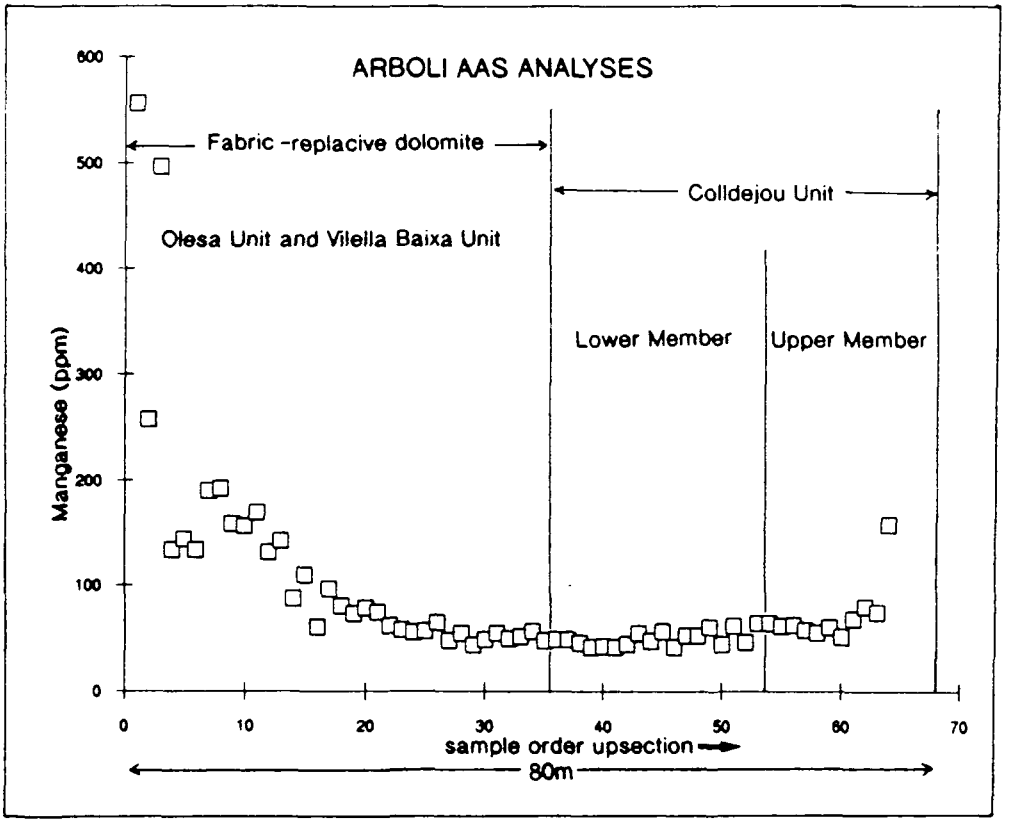

Fig. 6.10. AAS analyses for manganese concentrations in Arboli locality dolomites plotted against stratigraphic position.

Iron and manganese data are covariant (Fig. 6.8) and the concentrations gradually decrease upwards through the fabric-replacive dolomite and increase, iron more markedly than manganese, up through the overlying Colldejou Unit peritidal dolomites (Fig.s 6.9, 6.10). Iron contents range from 250 to 3500ppm and manganese from 50-500ppm. The stratigraphic variations in iron and manganese are quite smooth and there is no correlation with depositional facies. The iron-manganese crossplot emphasizes that the peritidal dolomites have a greater Fe/Mn ratio than the fabric-replacive dolomites.

Strontium and sodium data are very erratic and there are no clear stratigraphic trends. Strontium concentrations vary from 25-160ppm and sodium from 100-450ppm. The erratic behaviour of strontium in the fabric-replacive dolomite is decreased if only dolomicrites are considered. The strontium-sodium crossplot shows that the Colldejou Unit peritidal dolomites generally contain more strontium than the fabric-replacive dolomite, but there is no clear difference in sodium content (Fig. 6.11).

ii) Colldejou

At Colldejou the El Brull Unit and Olesa Unit are inaccessible and were not sampled so that the trace element data only refer to specimens from the Vilella Baixa Unit and Colldejou Unit.

The Lower Muschelkalk at Colldejou is nearly entirely dolomitized. The Lower Member of the Colldejou Unit is absent and the peritidal dolomites rest directly upon dolomitized oolites of the Vilella Baixa Unit. The contact has been interpreted as a paleokarstic surface (see Section 4.6.1.1). An oomoldic limestone with poikilotopic calcite spar occurs a few metres below the karst and is considered to be the product of early meteoric dissolution and later calcite spar cementation which has resisted subsequent dolomitization (Section 5.5.1.2).

The dolomites at Colldejou generally contain less manganese than at Arboli, and are more variable, ranging from 70-300ppm (Fig. 6.12). The oomoldic limestones contain abundant manganese (up to 1900ppm) and there is a pronounced peak at this level below the paleokarstic surface. The iron contents are approximately covariant with the manganese and vary from 350-2000ppm (Fig. 6.13). However, the iron content of the oomoldic limestone does not vary as markedly as the manganese.

The strontium and sodium data are quite variable and there is little stratigraphic correlation. However, mean values indicate that the peritidal dolomites contain more strontium (60 ppm) and sodium (274ppm) than the fabric-replacive dolomite (47ppm strontium, 158ppm sodium).

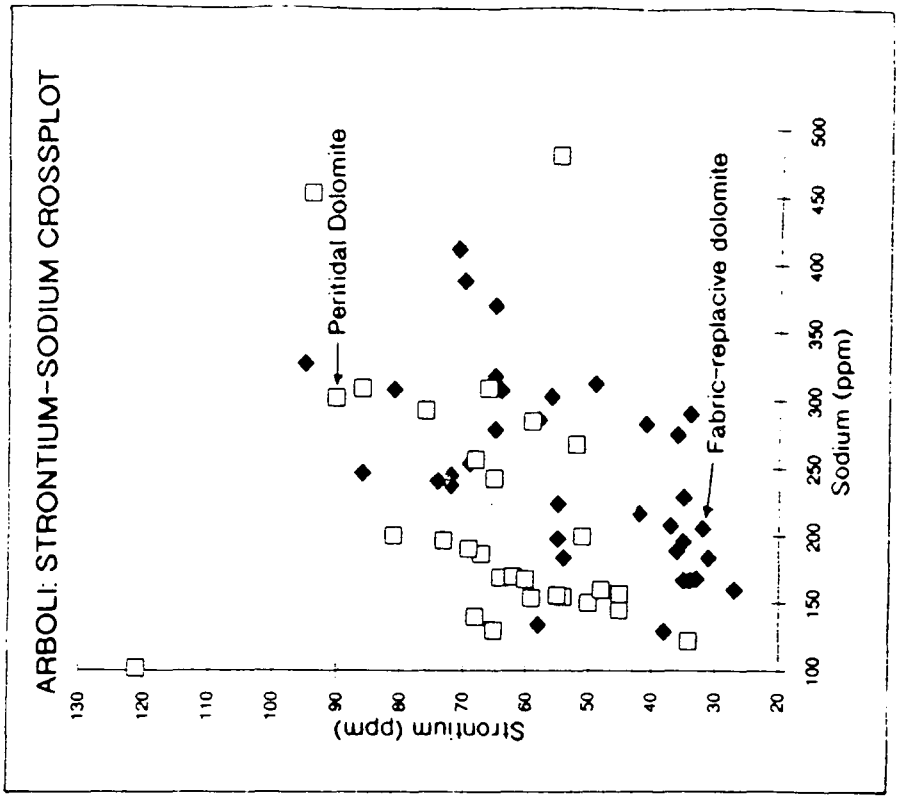

Fig. 6.11. Crossplot of strontium and sodium concentrations (from AAS analyses) for peritidal dolomites and fabric-replacive dolomites from Arboli locality.

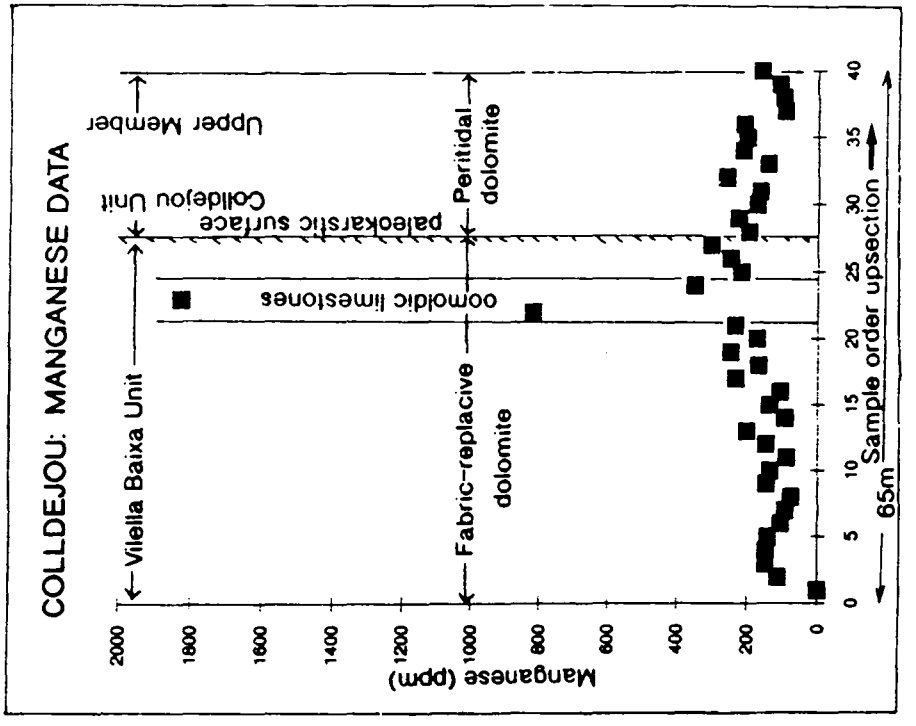

Fig. 6.12. AAS analyses for manganese concentrations in Colldejou locality dolomites plotted against stratigraphic position.

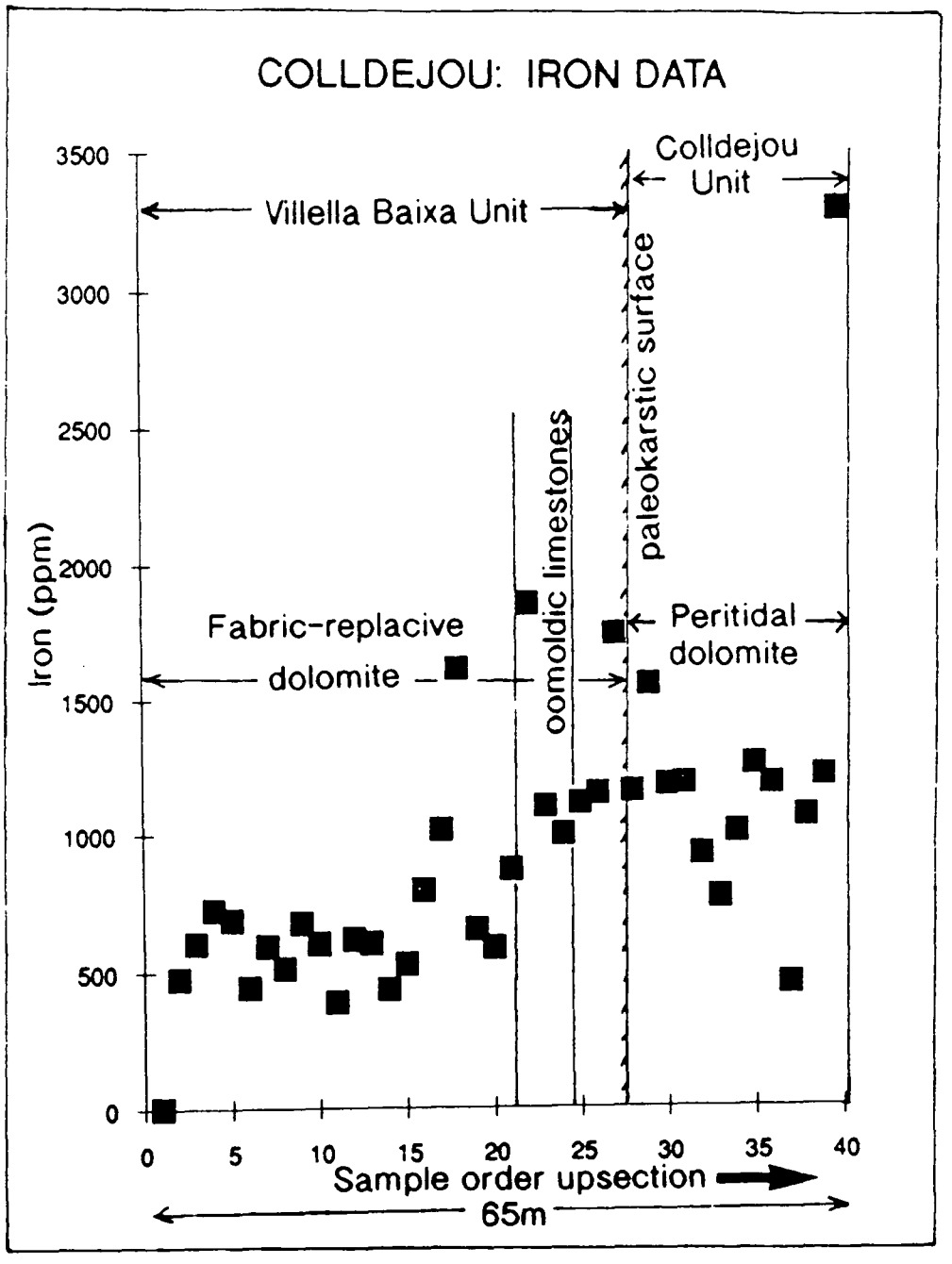

Fig. 6.13. AAS analyses for iron concentrations in Colldejou locality dolomites plotted against stratigraphic position.

6.3.4.3 AAS data interpretation

The iron and manganese data generally show covariance suggesting a common fluid source and the values are generally greater than for limestones in the Catalan Basin (see Section 6.2.3.1). The greater trace element contents have presumably resulted from dolomitization by a reducing (negative Eh) manganese and iron-rich groundwater.

The smooth change in manganese content in the fabric-replacive dolomite shows that the original limestone depositional facies (*i.e.* grainstone to mudstone) did not affect the incorporation of manganese. There is also no correlation between dolomite grainsize and trace element content.

At Arboli the general decrease in iron and manganese contents through the fabric-replacive dolomite and the marked increase in iron and minor increase in manganese up through the Colldejou Unit suggests a contrast in the behaviour of the two parts during dolomitization. The Colldejou Unit may already have contained early, penecontemporaneous dolomite whereas the precursor to the fabric-replacive dolomite probably consisted mostly of calcite owing to meteoric diagenesis (Section 4.10). Machel (1988) used the observation of Sass & Katz (1982) to show that the sense of trace element trends produced by fluid flow will in part depend upon the difference between the initial trace/Ca^{2+} ratio in the fluid and the trace/Ca^{2+} ratio in the precursor carbonate phase. The large-scale dolomite geometry in the Catalan Basin shows that the dolomitizing fluid had a downward component of movement (see Section 5.4.1). The observed iron and manganese trends could have resulted from the downward movement of a dolomitizing fluid through an iron and manganese-poor Colldejou Unit and then into a relatively iron and manganese-rich underlying Vilella Baixa Unit and Olesa Unit. In the Colldejou Unit iron and manganese would be preferentially incorporated into the growing dolomite resulting in a downstream decrease in trace/Ca^{2+}. However, in the underlying trace element-rich calcitic precursor the amount of iron and manganese released will offset the decrease due to the Heterogeneous Distribution Law and result in downflow increase in trace/Ca^{2+} (see analogous argument in Machel, 1988). The greater manganese and iron content of the fabric-replacive dolomite precursor could have resulted from a combination of lime mudstone deposition in reducing, locally poorly-oxygenated lagoonal waters and from early meteoric diagenesis. The Machel (1988) model depends upon a large number of assumptions and the most important relating to the Lower Muschelkalk dolomites is that any subsequent recrystallisation must be isochemical. The XRD data and low-strontium concentrations do indicate recrystallisation. However, many of the Catalan Basin limestones have maintained relatively high strontium concentrations

during burial and uplift and if the dolomites were subjected to the same diagenetic fluids then it suggests that the strontium-loss took place during dolomitization and not as a result of burial recrystallization.

The trends in iron and manganese in the dolomites at Colldejou are not as well-marked as at Arboli and the concentrations are lower. The distinction on the iron-manganese crossplot are also not as clear. Hence, these differences could have resulted from contrasting pore-fluid or substrate chemistries at the two localities.

At Colldejou the oomoldic dolomitic limestones have particularly high manganese and iron concentrations indicating precipitation from a reducing, Mn^{2+} and Fe^{2+}-rich, phreatic groundwater (Choquette & James, 1987). The coarse calcite spar contains outlines of ooids that under CL clearly preserve early physical compaction features such as elephantine structures (*e.g.* Fig. 4.13). Thus, if the oomoldic porosity did develop as consequence of the paleokarstic surface a few metres above, then subsequent calcite precipitation probably did not occur until there was further burial.

The strontium data suggest considerable depletion during dolomitization. The peritidal dolomites have higher strontium values than the fabric-replacive dolomite. The lower strontium values in the fabric-replacive dolomite could have arisen from early meteoric diagenesis and aragonite dissolution in the limestone precursor.

The more evaporitic depositional setting of the peritidal dolomites may have resulted in the greater sodium concentrations (Veizer *et al.*, 1978).

6.3.4.4 ICPAES results

Whole-rock samples from a large number of localities were analysed by ICPAES including some repeats of the AAS samples in order to check accuracy (see Appendix 3).

Similar trends to those at Arboli and Colldejou were also found at other localities (*e.g.* Pontons, Puig Gracios; Fig. 6.14). Iron and manganese concentrations are generally covariant in the range 200-1000ppm iron and 100-400ppm manganese. The peritidal dolomite iron and manganese contents usually decrease downwards or stay constant and then remain relatively constant or increase downwards through the fabric-replacive dolomite (*e.g.* Vacarisses, Olesa; Fig. 6.15).

The strontium values vary between about 50 and 100 ppm at any one locality and are usually fairly constant (*e.g.* Fig. 6.14) or greater in the peritidal dolomite than in the fabric-replacive dolomite (*e.g.* Fig. 6.15). There is also considerable regional

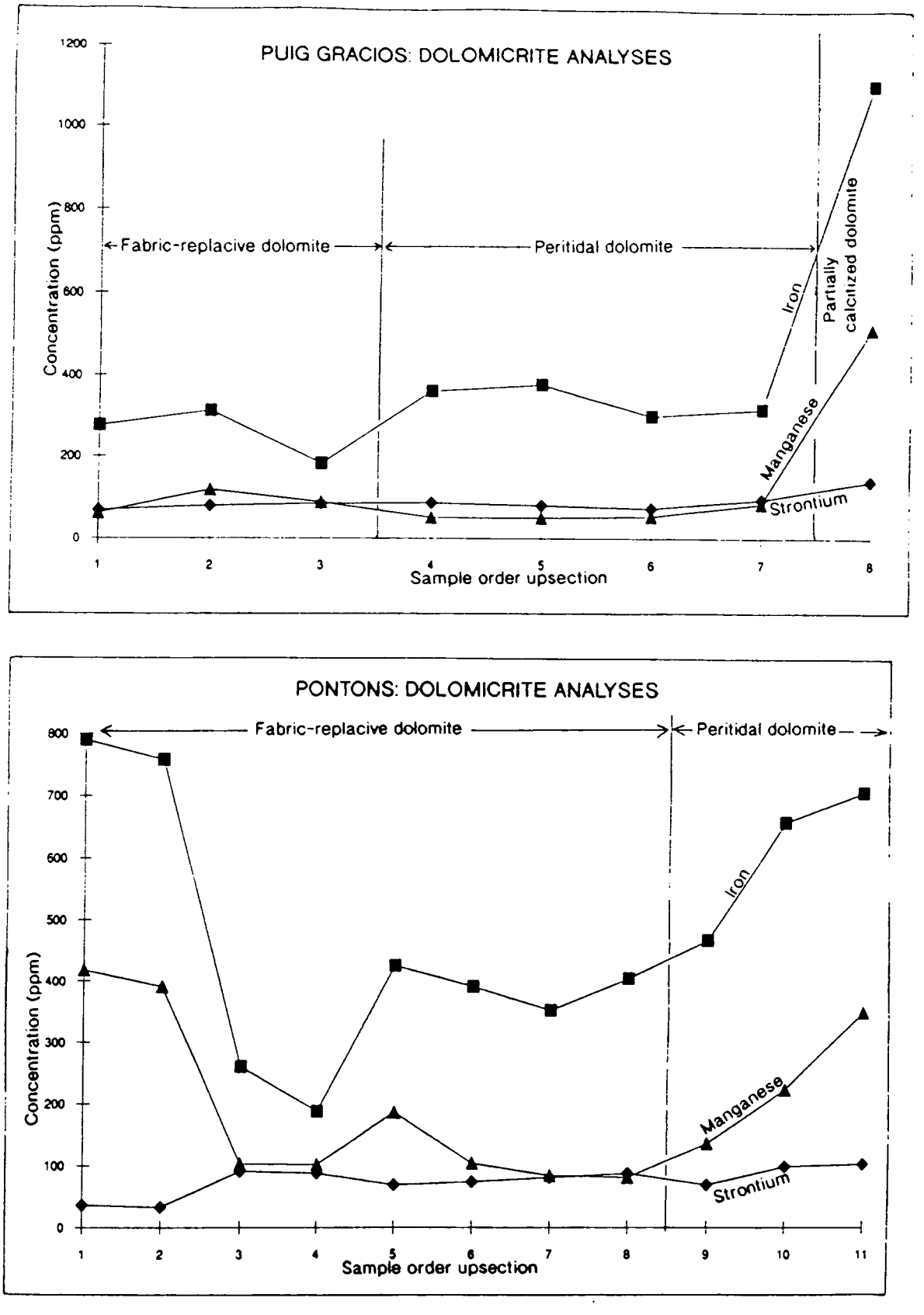

Fig. 6.14. Trace element trends (from ICPAES analyses) for bioclast-free dolomicrite samples from Pontons and Puig Gracios localities.

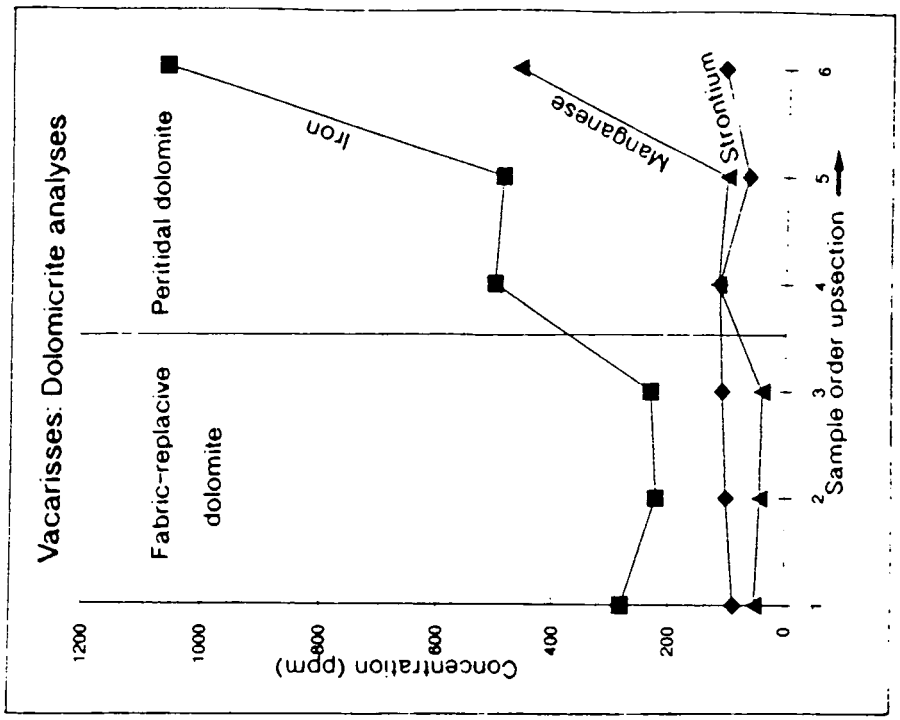

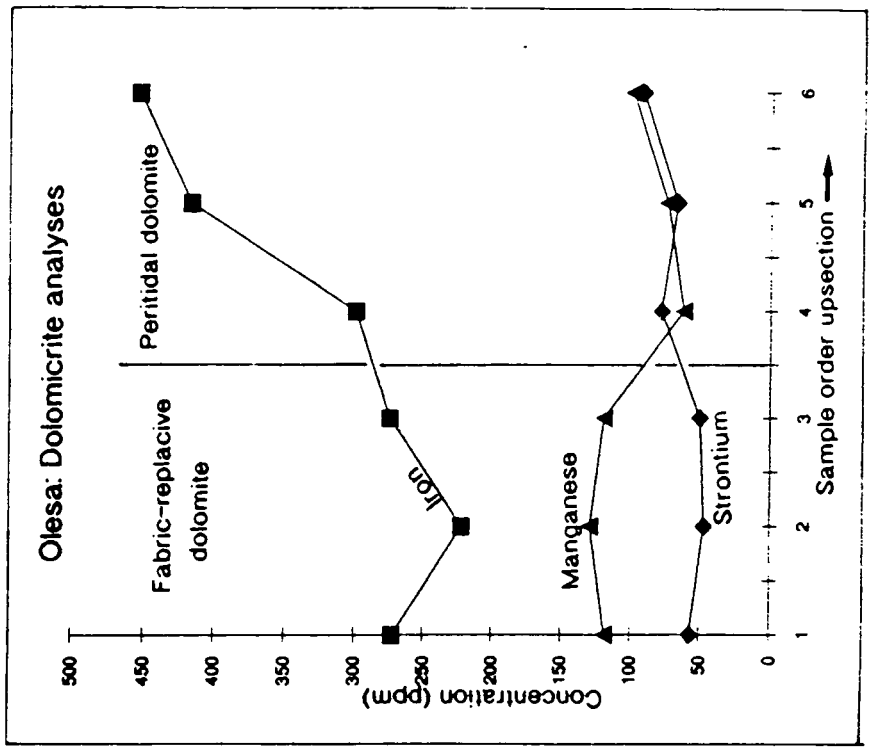

Fig. 6.15. Trace element trends (from ICPAES analyses) for bioclast-free dolomicrite samples from Olesa and Vacarisses localities.

variation in mean strontium composition of the peritidal dolomite or fabric-replacive dolomite samples between different localities (see Section 6.3.5.3).

6.3.4.5 ICPAES data interpretation

The ICPAES data generally confirm the observations of the AAS data. The majority of the variation in iron and manganese is stratigraphic rather than regional. No clear or consistent lateral variations in trace element concentrations were found. This suggests that the principal dolomitizing fluid-flow direction was downwards without a major lateral component (*cf.* Land *et al.*, 1975). The different iron and manganese trends may have arisen from different local fluid compositions and/or differing trace element contents in the precursors to the dolomites.

The peritidal dolomite generally contains more or similar amounts of strontium to the fabric-replacive dolomite. This may reflect differing amounts of aragonite in the precursor.

6.3.5 Stable isotope analysis

6.3.5.1 Stable isotopes: introduction

Stable isotope analyses of dolomites are common in the literature. As with trace elements, quantitative interpretation of stable isotope data is difficult owing to considerable uncertainty regarding the water-dolomite and calcite-dolomite fractionation factors and their temperature dependence (Land, 1980). Recent dolomites forming in modern peritidal settings tend to group around +1 to +4 $\delta^{18}O$ and +2 to +4 $\delta^{13}C$ whereas most ancient dolomites have negative $\delta^{18}O$ values and $\delta^{13}C$ between 0 and +6 (Tucker & Wright, 1990). Isotopic trends, and $\delta^{18}O$ values in particular, have been used to characterise dolomites thought to have been produced by different processes. For example, reflux dolomites associated with evaporated brines may be enriched in ^{18}O, whereas a covariant trend between $\delta^{18}O$ and $\delta^{13}C$ may be associated with mixing-zone dolomites (Zhao & Fairchild, 1987). Trends in $\delta^{18}O$, often combined with trace element data, have also been used to determine fluid flow directions (*e.g.* Suchecki & Hubert, 1984).

6.3.5.2 Stable isotopes: results

The stable isotope data for the fabric-replacive dolomite and peritidal dolomite show a broad range of oxygen isotope values from -2 to -7.5 $\delta^{18}O$ but relatively little variation in carbon isotope values which range from +1.5 to +3 $\delta^{13}C$ (Fig. 6.16).

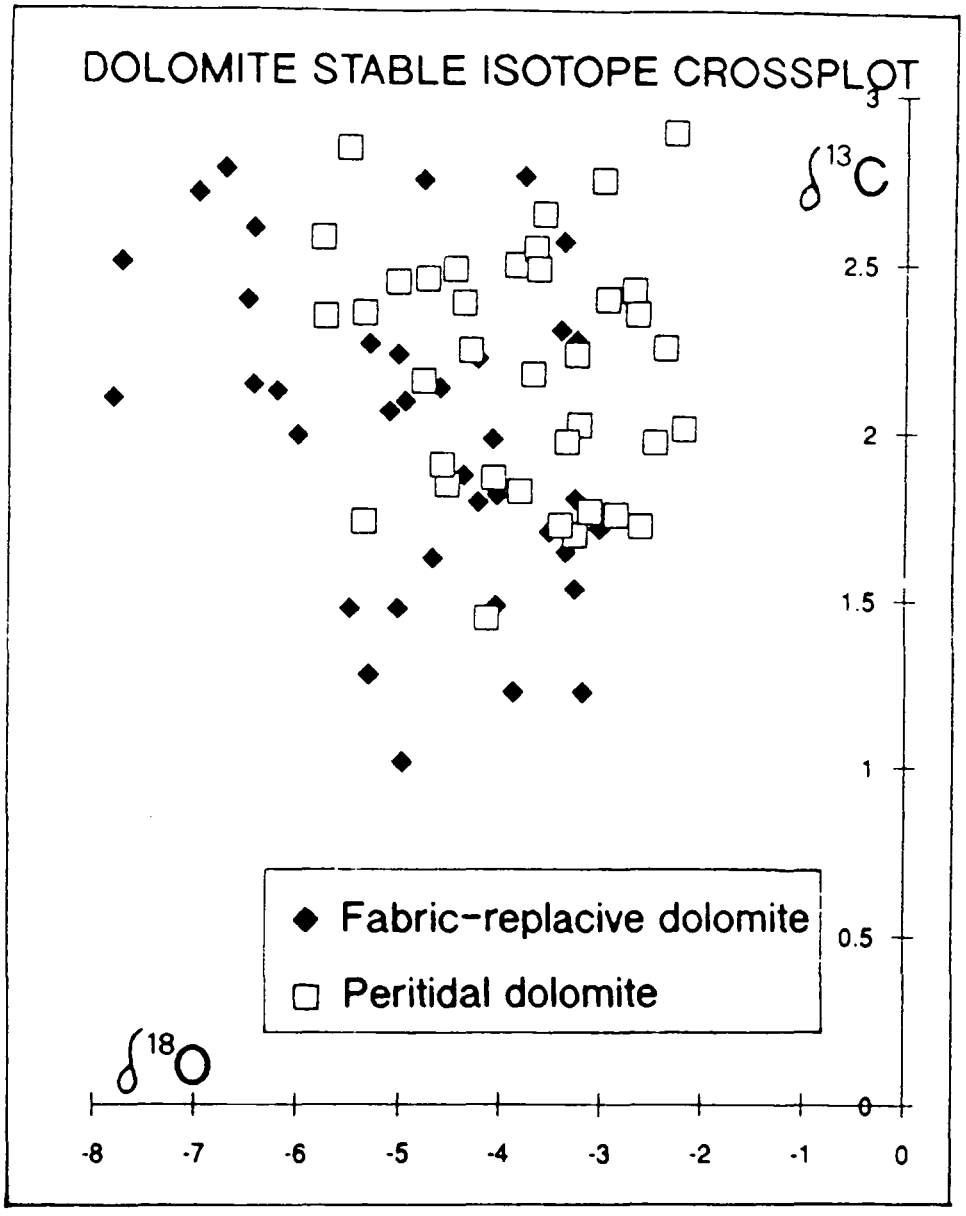

Fig. 6.16. Stable isotope crossplot for fine-grained fabric-replacive dolomite and peritidal dolomite samples from a number of localities (see Appendix 6).

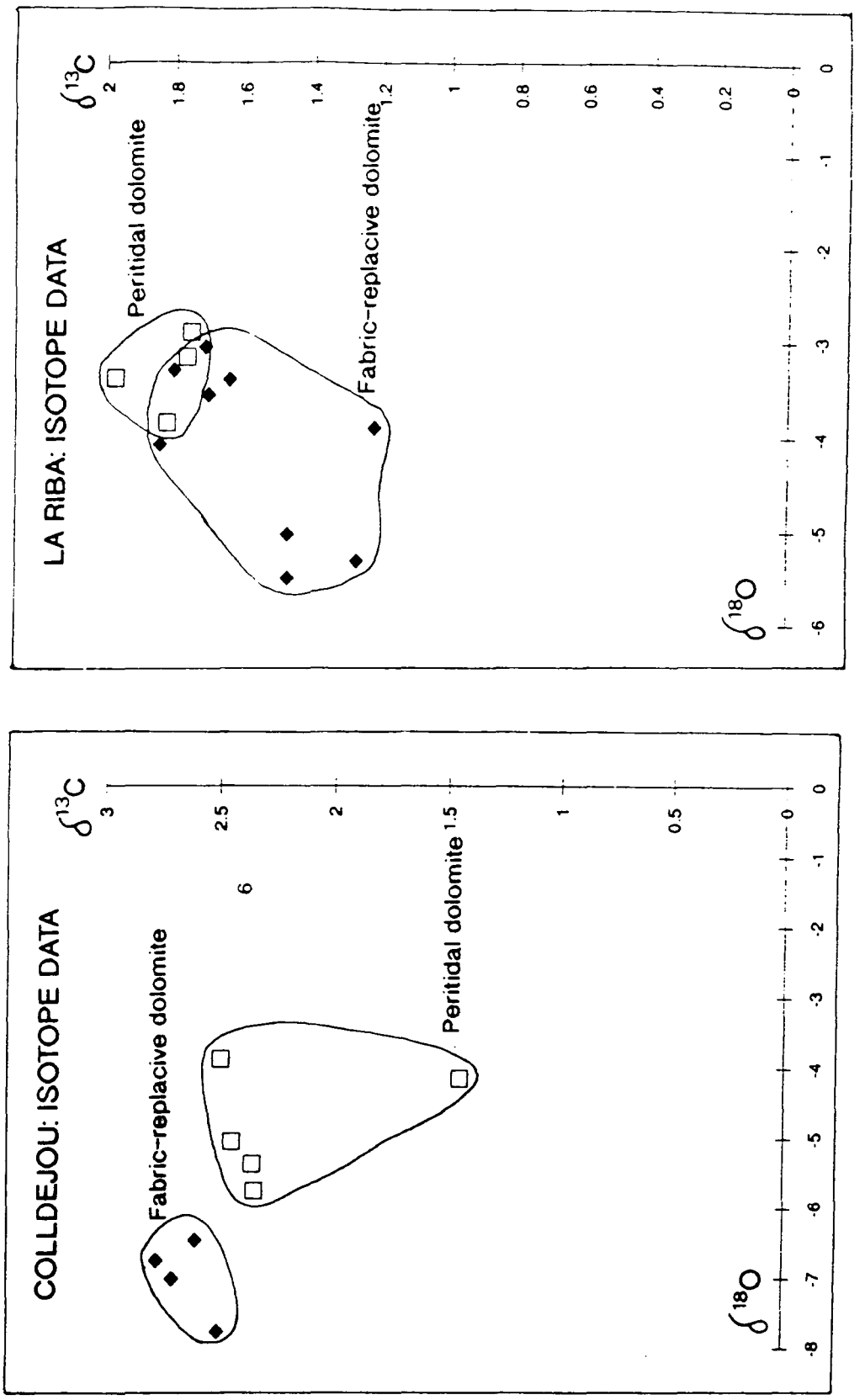

Fig. 6.17. Stable isotope crossplots of fine-grained fabric-replacive dolomite and peritidal dolomite samples from the same localities (la Riba and Colldejou).

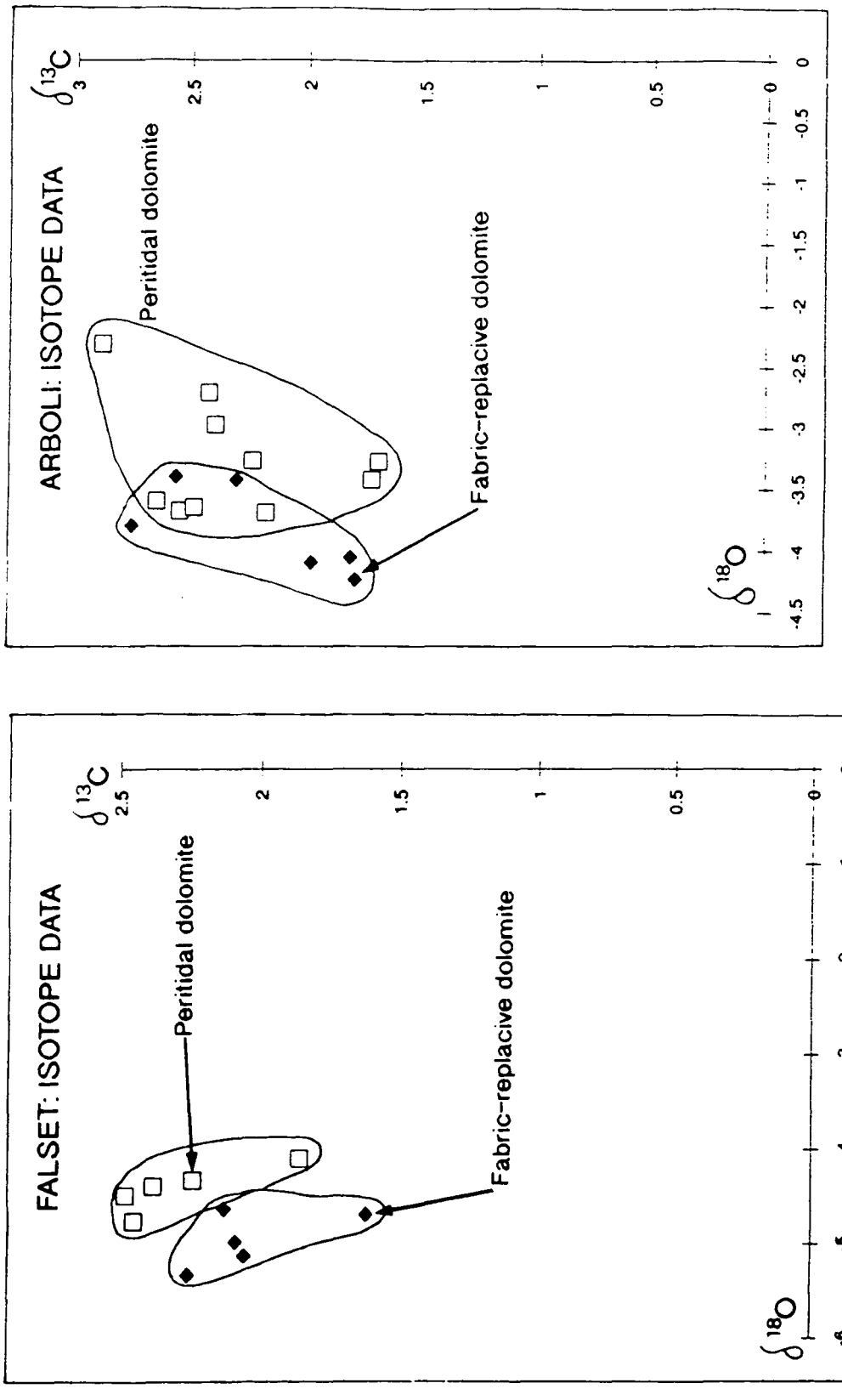

Fig. 6.18. Stable isotope crossplots of fine-grained fabric-replacive dolomite and peritidal dolomite samples from the same localities (Falset and Arboli).

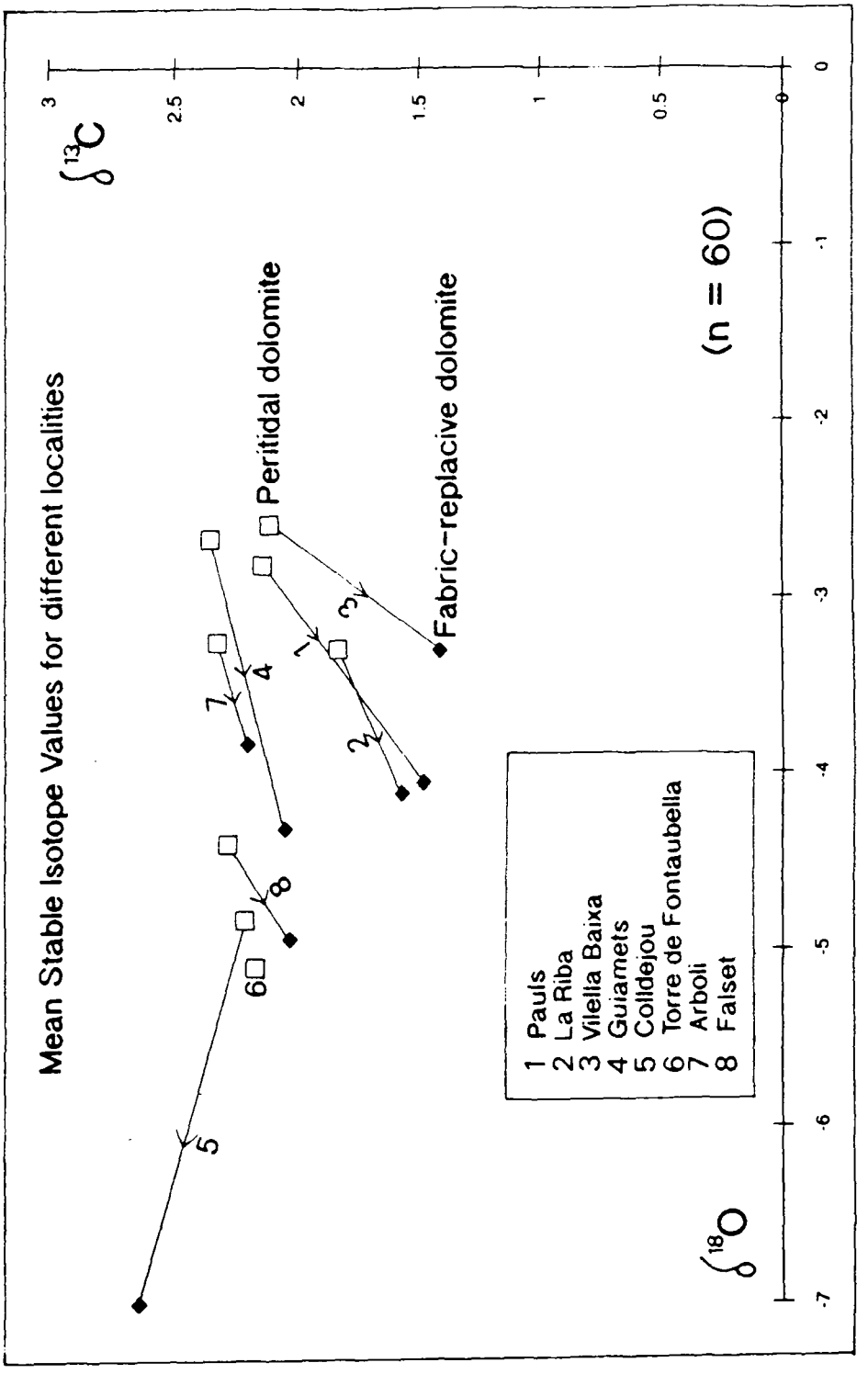

Fig. 6.19. Stable isotope crossplot of mean isotopic values for peritidal dolomite samples and fine-grained fabric-replacive dolomite samples at each locality.

Overall, there is little distinction between the fabric-replacive dolomite and peritidal dolomite on the stable isotope crossplot. The two groups have a considerable overlap with a slight tendency for the peritidal dolomites to have slightly more positive $\delta^{13}C$ and less negative $\delta^{18}O$. However, at any one locality the peritidal dolomites are generally less depleted in ^{18}O than the underlying fabric-replacive dolomite (Fig.s 6.17, 6.18). Carbon values are similar. The data are best displayed by plotting mean isotope compositions for the fabric-replacive dolomite and peritidal dolomite samples for each locality on the same diagram (Fig. 6.19). The magnitude of the difference between mean peritidal and mean fabric-replacive dolomites varies between different localities. At Colldejou the average fabric-replacive dolomite is over 2 permil lighter in ^{18}O than the peritidal dolomite whereas at Arboli the difference is only 0.6 permil. The fabric-replacive dolomites are generally slightly depleted in ^{13}C with respect to the peritidal dolomites.

Strontium and $\delta^{18}O$ values for peritidal dolomites and fabric-replacive dolomites from each localities generally plot in different areas (*e.g.* Fig. 6.20). A crossplot is shown in Fig. 6.21 for average strontium and $\delta^{18}O$ values for fabric-replacive dolomite and peritidal dolomite from a number of localities. The consistent depletion in ^{18}O between the peritidal dolomite and fabric-replacive dolomite is associated with a decrease in average strontium concentration. As with the isotope crossplot the magnitude of the difference varies between different localities.

6.3.5.3 Stable isotope interpretation

The dolomites of the Catalan Basin have broadly uniform carbon isotope values similar to the Lower Muschelkalk limestones. The inheritance of $\delta^{13}C$ values during diagenesis and dolomitization is common owing to the initial low carbon content of pore fluids (Tucker & Wright, 1990).

The oxygen isotope values show considerable variation and there is no simple overall distinction between the peritidal dolomites and the fabric-replacive dolomites. The regional variation in the average peritidal dolomite $\delta^{18}O$ values contrasts with the uniformity of the depositional facies suggesting that post-depositional diagenetic stabilization and complete dolomitization involved different fluid compositions in different areas. Different burial depths are not considered to be important for the peritidal dolomites and the facies-replacive dolomite owing to the maximum thickness of the Lower Muschelkalk being only about 100m.

The fabric-replacive dolomite $\delta^{18}O$ values are regionally variable but always on average depleted with respect to the peritidal dolomite at the same locality. The difference in $\delta^{18}O$ between the peritidal dolomites and fabric-replacive dolomite may

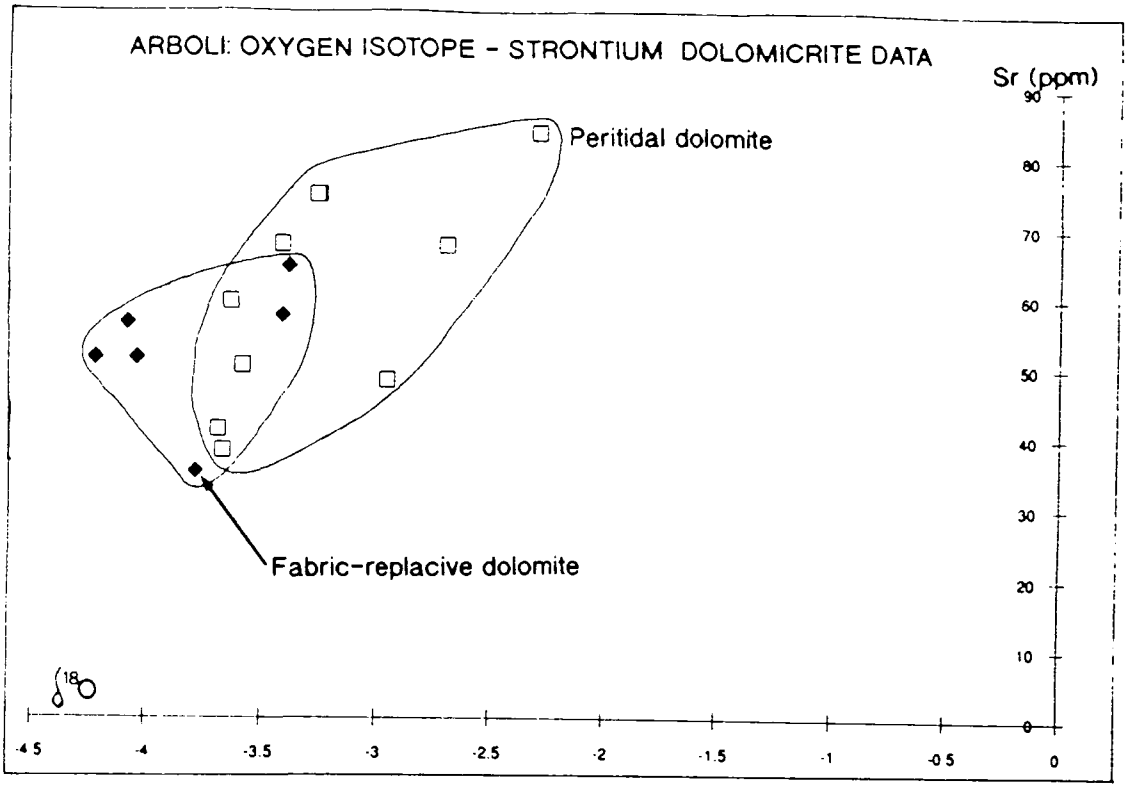

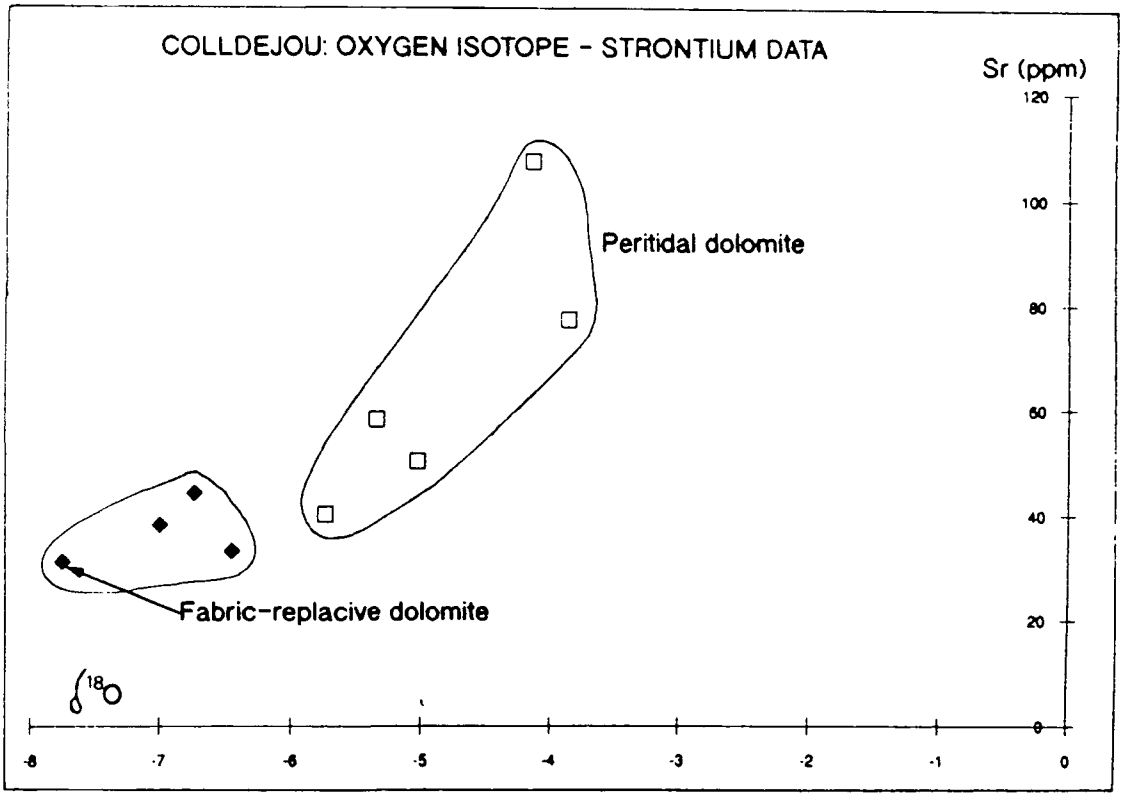

Fig. 6.20. Crossplot of strontium concentration (from ICPAES analyses) against $\delta^{18}O$ values for fine-grained fabric-replacive dolomite and peritidal dolomite samples from Colldejou and Arboli localities.

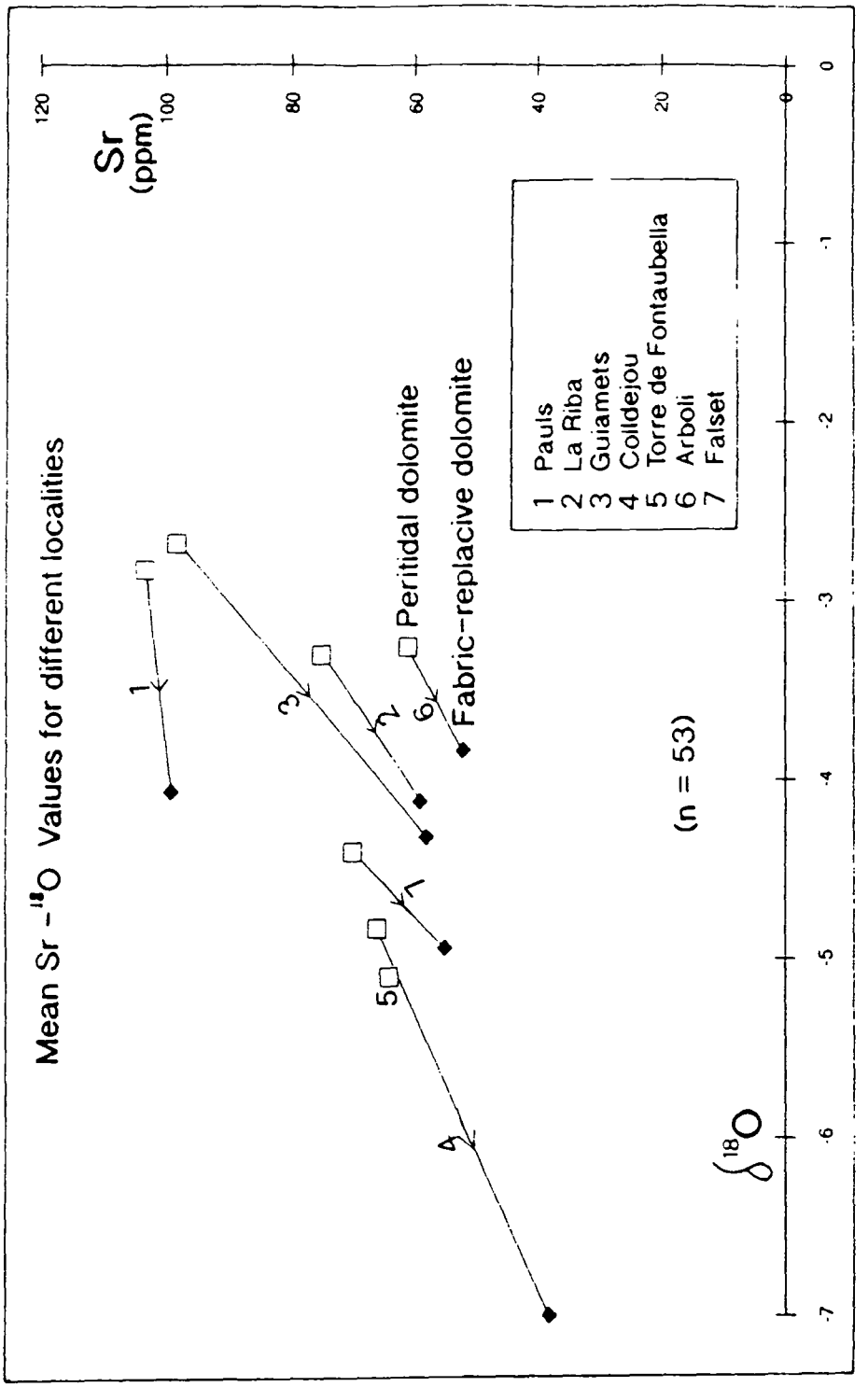

Fig. 6.21. Crossplot of mean strontium concentrations and $\delta^{18}O$ values for fine-grained fabric-replacive dolomite and peritidal dolomite samples from a number of localities.

be related to a different ^{18}O fractionation between aragonite-dolomite and calcite-dolomite. The fabric-replacive dolomite samples are always enriched in ^{18}O with respect to underlying undolomitized limestones.

The Sr-$\delta^{18}O$ crossplot confirms the consistent variation between peritidal dolomite and fabric-replacive dolomite at any given locality and that large variations occur between different localities in both fabric-replacive dolomite and peritidal dolomite. The consistent stratigraphic variation in $\delta^{18}O$ and strontium content could be the result of differences in the precursors to the dolomites. The precursor to the peritidal facies dolomites probably consisted of ^{18}O and strontium-rich aragonite, high-Mg calcite and early penecontemporaneous dolomite whereas the underlying limestones consisted of already partially stabilized, strontium and ^{18}O-depleted low-Mg calcite.

The geochemical variations between different localities do not appear to show any patterns that might be consistent with regional lateral fluid-flow. This may be due in part to the arrangement of the outcrops in the Catalan Basin which are not particularly extensive in the northwest-southeast direction. Nevertheless, it seems likely that the variations between localities may have been the result of local variations in the composition of the dolomitizing fluid.

6.3.6 Fabric-replacive dolomite and peritidal dolomite synthesis

Geochemical analysis in conjunction with petrographic and regional data (Section 5.3) suggest:

i) The dolomitizing fluid principally migrated downwards through the peritidal dolomite and into the fabric-replacive dolomite.

ii) The precursor to the peritidal dolomite was ^{18}O and strontium-rich with respect to the fabric-replacive dolomite precursor.

The geochemical analyses also indicate:

i) The source of the dolomitizing fluid was regional with local compositional variations. No lateral geochemical trends attributable to fluid-flow have been found.

ii) The dolomitizing fluid may have been enriched in manganese, iron, and ^{18}O and hence was reducing, phreatic, and may have been partially evaporitic.

iii) The dolomitizing fluid increased the overall iron and manganese contents of the dolomites with respect to the precursors and may also have lead to downflow decreasing or increasing trends depending on the substrate chemistry.

iv) The dolomitizing fluid decreased strontium contents overall, but maintained the initial contrast in strontium concentrations such that the peritidal dolomite contains on average more strontium than the fabric-replacive dolomite at the same locality.

6.4 CATALAN BASIN BAROQUE DOLOMITE GEOCHEMISTRY

6.4.1 Introduction

Baroque dolomite is not common in the Catalan Basin and occurs as cements in fractures and pseudomorphs after evaporites and as a mosaic at one locality. Only the mosaic was suitable for sampling and this was analysed for trace elements by ICPAES and stable isotopes, as described in Appendix 3 and Section 6.4.3.

6.4.2 Baroque dolomite cement

The cathodoluminescence zonation observed in the baroque dolomite cements (Section 5.8.2.1) indicates fluctuating chemical conditions during growth, probably related to changing redox potential (Fraser *et al.*, 1989). The cathodoluminescent character of the surrounding matrix dolomite appears unaffected by the presence of the baroque cement which locally occurs in undolomitized limestones. This indicates little interaction between matrix and pore-fluid, probably as a result of the low permeability and indurated nature of the matrix. The presence in the limestone indicates that the dolomitizing fluid may have been saturated with respect to calcite.

6.4.3 Baroque dolomite mosaic

6.4.3.1 Introduction

The baroque dolomite mosaic occurs at Masroig and is described in Section 5.8.2.2. The mosaic is replacive and locally contains non-baroque dolomitized echinoderm fragments and therefore may be geochemically distinct from the baroque dolomite cements. However, as noted in the Valencia-Cuenca Basin (see Section 5.9.3.3) the baroque dolomite cements and mosaics probably show similar trends with respect to the other dolomites (see Section 6.5).

Five samples of baroque dolomite mosaic were analysed for stable isotopes and two for trace elements as well. Non-baroque dolomicrites and dolosparites were also analysed from the same locality (see Appendix 6).

6.4.3.2 Analytical results

The two baroque dolomite samples contain similar amounts of manganese and strontium to the non-baroque samples (*ca.* 65ppm manganese, 50ppm strontium). The baroque dolomites contain about 450ppm iron.

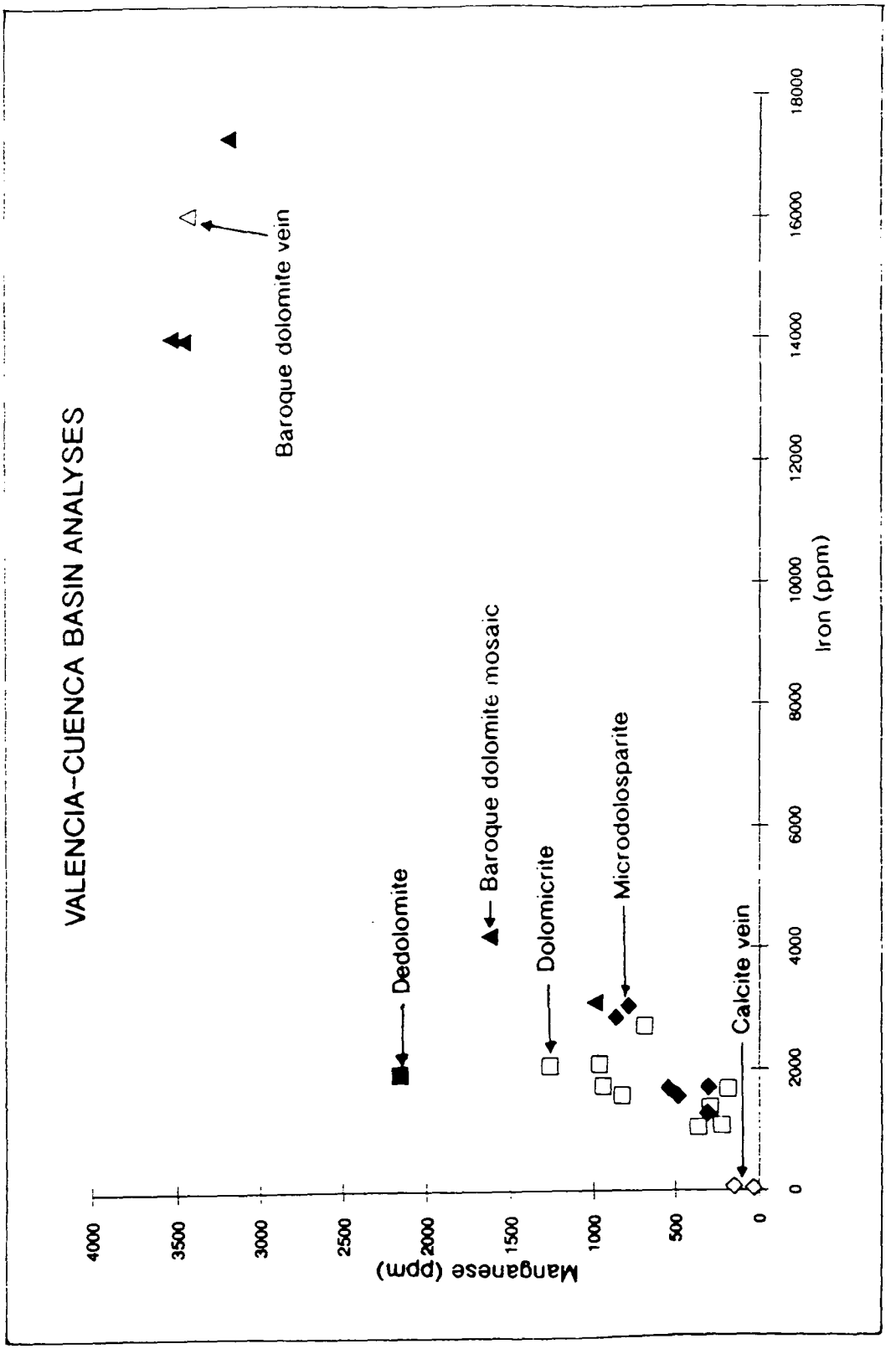

Fig. 6.22. Crossplot of manganese and iron concentrations (from ICPAES analyses) for the Valencia-Cuenca Basin samples.

The baroque dolomite stable isotope compositions plot around +0.7 to +2.3 $\delta^{13}C$, -6 to -7.5 $\delta^{18}O$ which is similar to the non-baroque dolomites. However, on average the baroque dolomites are more depleted in ^{18}O.

6.4.3.3 Interpretation

In comparison to most of the Catalan Basin peritidal and fabric-replacive dolomites, these baroque dolomites are particularly depleted in ^{18}O suggesting elevated temperatures of precipitation and burial-related pore-fluids. They are similar in composition to the baroque dolomites of the Valencia-Cuenca Basin (Section 6.5). The similarity between the baroque dolomites and the non-baroque samples at Masroig indicates that there may have been some interaction between the burial dolomitizing fluid and the matrix without the formation of baroque crystals. Alternatively, the non-baroque dolomicrites and dolosparites, which do not appear to be recrystallised, may have already possessed a $\delta^{18}O$ value similar to that produced in the baroque dolomite. The Valencia-Cuenca Basin data support this view because there it is clear that non-baroque dolomites have not been affected by adjacent burial baroque dolomitization (Section 6.5).

The similarity in $\delta^{13}C$ value may indicate a local source of carbonate for the baroque dolomite, probably related to stylolitization and pressure-dissolution of the non-baroque dolomites.

6.4.4 Catalan Basin baroque dolomite conclusions

The fluid which precipitated the baroque dolomite cements does not appear to have affected the surrounding dolomites and limestones but has been confined to the pervious fractures and porosity created by evaporite dissolution (see Section 5.8.2.1).

In comparison to the much better developed baroque dolomites of the Valencia-Cuenca Basin, the baroque dolomite mosaic at Masroig is unusual because it is isotopically and compositionally indistinct from adjacent non-baroque dolomites.

6.5 VALENCIA-CUENCA BASIN LOWER MUSCHELKALK GEOCHEMISTRY

6.5.1 Introduction

Twenty eight whole-rock and vein samples from five localities in the Valencia-Cuenca Basin were prepared for analysis of stable isotopic composition and trace element contents by ICPAES. The samples were chosen to represent a range of lithologies:

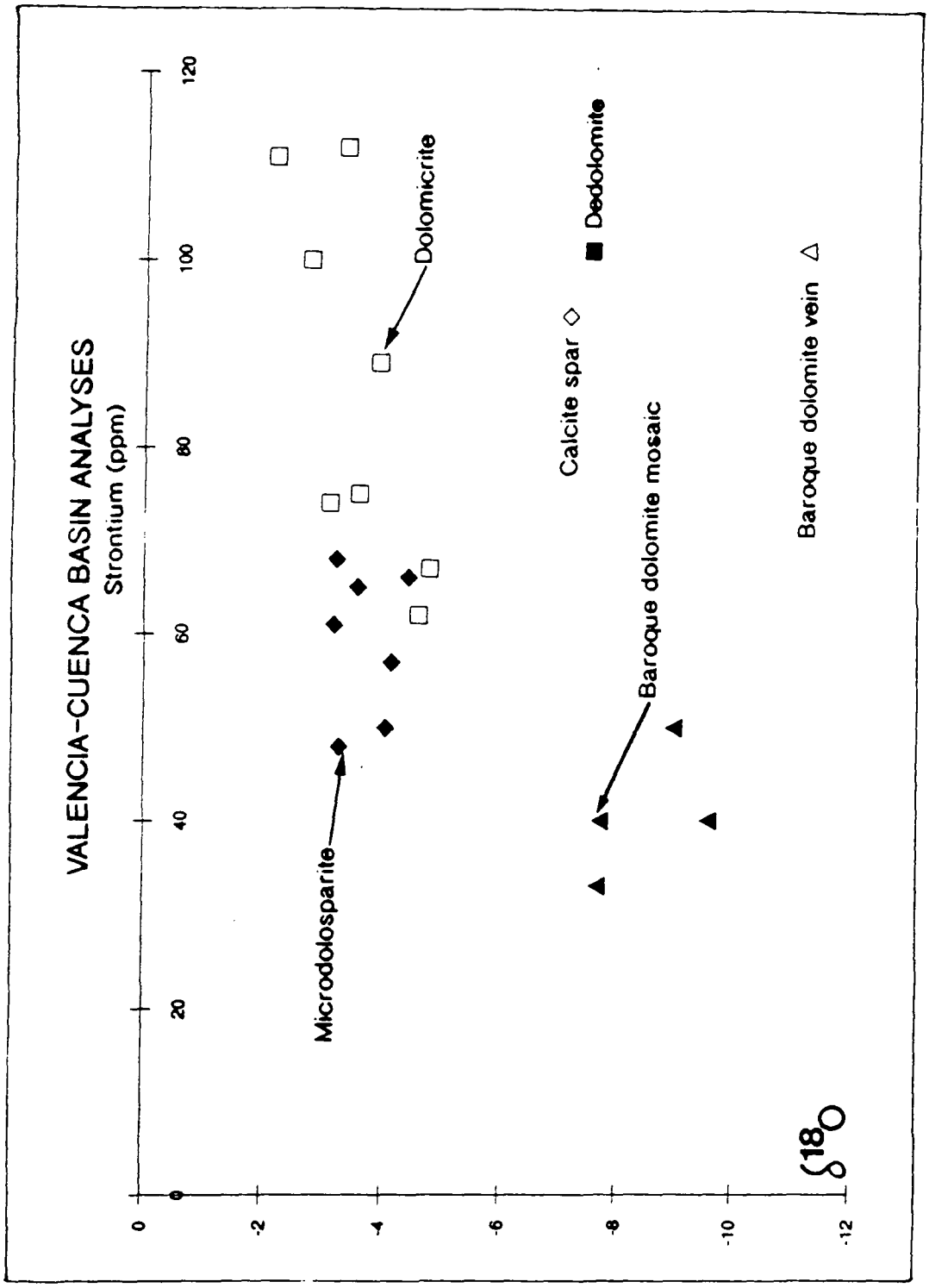

Fig. 6.23. Crossplot of strontium concentrations (from ICPAES analyses) and $\delta^{18}O$ values for the Valencia-Cuenca Basin localities.

i) Unfossiliferous dolomicrites, considered to be equivalent to the peritidal dolomite of the Catalan Basin (8 samples)
ii) Fossiliferous microdolosparites, considered to be equivalent to the fabric-replacive dolomite of the Catalan Basin (7 samples)
iii) Baroque dolomite (4 mosaic samples and 1 vein cement sample)
iv) Late calcite spar veins (2 samples)
v) Dedolomite (1 sample)

The baroque dolomite mosaics are clearly replacements after oolitic and bioclastic packstones (see Fig.s 5.23, 5.24). The bioclasts include non-baroque dolomitized echinoderm fragments suggesting that the precursor to the baroque mosaic had already been dolomitized (see Section 5.9.3.3).

6.5.2 Trace element results

The microdolosparites and dolomicrites contain similar amounts of iron (1000-3000ppm) and manganese (250-1300ppm; Fig. 6.22). However, the dolomicrites are enriched in strontium (60-110ppm) with respect to the microdolosparites (50-70ppm strontium; Fig. 6.23).

The baroque dolomites are particularly ferroan (3000-18,000ppm iron) and manganoan (1000-4000ppm manganese). The strontium contents of the baroque dolomite mosaics (30-50ppm strontium) are considerably less than the baroque dolomite vein (100ppm strontium).

The calcite veins have low iron and manganese contents with respect to the dolomites and are relatively enriched in strontium (about 100ppm). The dedolomite sample is manganoan and ferroan and has a similar strontium content to the calcite vein spar.

6.5.3 Stable isotope results

The dolomicrites and microdolosparites plot in overlapping groups on the isotope crossplot and vary from -2 to -5 $\delta^{18}O$ and +1 to +2.5 $\delta^{13}C$, similar to most of the Catalan Basin dolomites. Generally, there are not enough data points to compare dolomicrite and microdolosparite samples from the same locality. However, it is noteworthy that at Albarracin the dolomicrite is less depleted in ^{18}O than the four microdolosparites (see Appendix 6).

The baroque dolomite mosaics are much more depleted in ^{18}O and vary from -7.5 to -10 $\delta^{18}O$ and 0 to +1 $\delta^{13}C$. The baroque dolomite vein sample is even more depleted in ^{18}O and slightly more depleted in ^{13}C.

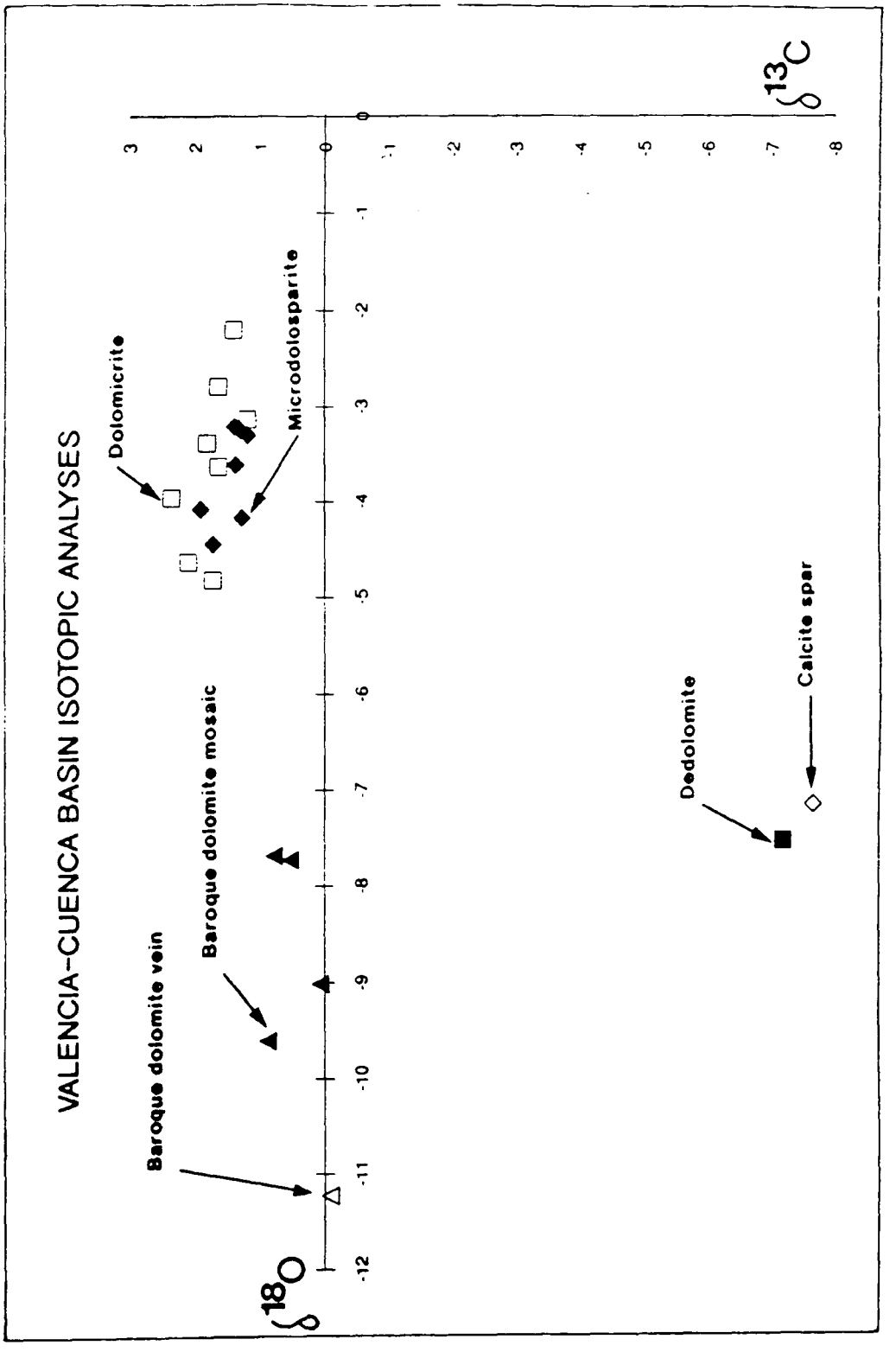

Fig. 6.24. Stable isotope crossplot for the Valencia-Cuenca Basin samples.

The calcite spar and dedolomite samples have similar isotopic compositions and are particularly depleted in ^{13}C at about -7.5 $\delta^{13}C$.

The Sr-$\delta^{18}O$ cross-plot discriminates the main groups of samples (Fig. 6.23).

6.5.4 Interpretation

The dolomicrites and microdolosparites have similar isotopic and elemental compositions to the peritidal dolomite and fabric-replacive dolomite of the Catalan Basin and display similar relationships in strontium concentrations and $\delta^{18}O$ values suggesting a more aragonitic, evaporitic precursor to the dolomicrites than to the microdolosparites. The dolomicrites are more ferroan and manganoan than most of the Catalan Basin dolomites. However, as discussed in Section 6.3.4.5, the iron and manganese contents are probably related to local variations in dolomitizing fluid composition. The dolomicrites and microdolosparites do not appear to have been affected by the fluids which precipitated the adjacent baroque dolomite cements and mosaics.

The isotopic and trace element composition of the baroque dolomites suggests precipitation at elevated temperatures from strongly reducing, Fe^{2+} and Mn^{2+}-rich groundwaters. The differences in composition between the baroque mosaics and the baroque vein may be due to contamination of the baroque dolomite mosaics by original non-baroque grains such as echinoderm fragments. The similar $\delta^{13}C$ value of the baroque dolomite suggests that the carbonate source was mostly local and probably related to pressure dissolution and stylolitization of the surrounding dolomite. The relatively high strontium-content of the baroque vein may be due to release of strontium owing to sulphate dissolution and reduction associated with the reducing conditions and the baroque dolomitization (Machel, 1987; Section 5.9.3.9). Ferroan calcite pseudomorphs after anhydrite are present in the Lower Muschelkalk of the Valencia-Cuenca Basin (Section 4.8).

The calcitic specimens have similar trace element and isotopic compositions to the late, uplift-related calcite spars and dedolomites of the Catalan Basin which are discussed at length in Chapter 8.

6.5.5 Conclusions

The geochemical analysis of samples from the Valencia-Cuenca Basin supports the field and petrographic observations which suggest that the dolomites of the Valencia-Cuenca Basin are similar to the Catalan Basin and probably resulted from the same processes.

The dolomicrite and microdolosparite samples are geochemically indistinct from the peritidal dolomite and fabric-replacive dolomite of the Catalan Basin and show the same relationships to each other. The dolomicrites and microdolosparites were not affected by adjacent baroque dolomite precipitation suggesting that the process may not have been long-lived and was highly permeability-dependent.

The baroque dolomites of the Valencia-Cuenca Basin have similar $\delta^{13}C$ values but in general are more depleted in ^{18}O than the baroque dolomite mosaic of the Catalan Basin. The baroque dolomite vein sample does not involve any replacement and is therefore probably most indicative of the fluid composition. The isotopic and trace element composition of the baroque vein suggests precipitation at elevated temperatures from strongly reducing, manganoan and ferroan porewaters with carbonate ions derived from local pressure dissolution of dolomite and possibly some involvement of sulphate replacement.

The calcite samples are similar in isotopic and trace elemental composition to the late calcite spars and dedolomites of the Catalan Basin and are considered to have formed in the same way (Chapter 8).

CHAPTER 7: SYNTHESIS OF THE DOLOMITIZATION OF THE LOWER MUSCHELKALK

7.1 INTRODUCTION

The previous chapters have described the field relations, petrography and geochemistry of the dolomites of the Catalan Basin and Valencia-Cuenca Basin. The same principal types of dolomite facies occur in both basins. However the peritidal dolomite and baroque dolomite are more important in the Valecia-Cuenca Basin. The relationship between the peritidal dolomite and fabric-replacive dolomite is much better displayed in the Catalan Basin than in the Valencia-Cuenca Basin.

This chapter will review the salient conclusions of the previous chapters and attempt to propose a coherent dolomitization model which will then be discussed.

7.2 DOLOMITE FIELD RELATIONS AND PETROGRAPHY

7.2.1 Peritidal dolomite

Peritidal dolomite facies occur as discrete layers in the El Brull Unit and more importantly in the Upper Member of the Colldejou Unit of the Catalan Basin (see Section 3.2.4.2). In the Valencia-Cuenca Basin the peritidal dolomite is the most important dolomite facies, particularly towards the more marginal, northwestern parts of the basin where the whole Lower Muschelkalk is dominated by peritidal deposits (see Section 3.3). In each case, the depositional environment was intertidal to supratidal (see Section 3.6). Dolomitization of the peritidal facies is pervasive and stratigraphically controlled suggesting formation was a consequence of the depositional environment and the unstable depositional mineralogy.

The dominant peritidal dolomite lithology is very fine-grained dolomicrite which may have been deposited with a similar mineralogy to the modern sediments of the coastal sabkhas of the Arabian Gulf, *i.e.* aragonite, penecontemporaneous calcian dolomite, and relatively minor calcite (see Section 5.6.1). However, dolomitized oolite horizons are locally present and dolomitized bioclasts suggest further post-depositional dolomitization which resulted in the pervasive nature and stabilized geochemistry of the peritidal dolomite (see Section 3.3.3).

The peritidal dolomite contains abundant pseudomorphs after stellate gypsum indicating the presence of hypersaline pore-fluids penecontemporaneous with deposition.

7.2.2 Fabric-replacive dolomite

The fabric-replacive dolomite occurs below the peritidal dolomite of the Upper Member of the Colldejou Unit in the Catalan Basin and occurs towards the southeast of the Valencia-Cuenca Basin where the Lower Muschelkalk is thicker and contains more open marine facies (see Section 3.3.6). The upper contact of the fabric-replacive dolomite with the peritidal dolomite is commonly sharp. However, where the Lower Member of the Colldejou Unit is present the contact is more transitional in both depositional facies and dolomite texture. The lower contact of the fabric-replacive dolomite is clearly discordant to bedding on an outcrop and regional scale resulting in considerable thickness variations of the fabric-replacive dolomite which locally extends to the base of the Lower Muschelkalk. The fabric-replacive dolomite was clearly not controlled by the depositional environment and replaced a variety of open-marine and lagoonal mudstone to grainstone sediments. The petrography of the fabric-replacive dolomite is very variable and ranges from fabric-destructive to fabric-retentive, and from fine to coarse-grained mosaics with idiotopic to xenotopic crystals (see Section 5.5). The proximity of different textures, *e.g.* in the dolomitized bioturbated fabric (see Section 5.5.2) and the interfingering nature of the dolomite front indicate that the dolomitization was in part controlled by permeability contrasts in the precursor lime sediments. Horizons containing abundant coarse-grained early diagenetic calcite spar crystals, *e.g.* where occluding oomoldic porosity, are commonly undolomitized. Thus, the fabric-replacive dolomite is much less pervasive than the peritidal dolomite and much more variable petrographically. This indicates that the precursor to the dolomite was much more variable in mineralogy, grain-size and permeability and that some horizons were already stabilized owing to early meteoric diagenesis via paleokarstic surfaces (see Section 4.6.1).

The fabric-replacive dolomite contains pseudomorphs after stellate gypsum and also after rectangular anhydrite. The pseudomorphs, in contrast to those of the peritidal dolomite, appear to be unrelated to the depositional environment and indicate post-depositional hypersaline diagenetic pore-fluids. The orientation of the dolomite front indicates downward migrating dolomitizing fluids.

7.2.3 Baroque dolomite

The baroque dolomite occurs mainly as a cement lining fractures and within some pseudomorphs after evaporites (see Section 5.8). Baroque dolomite mosaics are rare in the Catalan Basin but more common in the Valencia-Cuenca Basin (Section 5.9.3.3), where they appear to be replacements after earlier fabric-replacive dolomite. Cross-cutting baroque dolomite veins clearly indicate that the baroque dolomite was precipitated after the fabric-replacive dolomite and peritidal dolomite. In both the

Catalan Basin and Valencia-Cuenca Basin the baroque dolomite appears to be related to local hydrothermal mineralization (see Section 4.7). The baroque dolomite locally lines fractures within unaffected limestone, showing that the lithified limestone was resistant to recrystallisation by the hydrothermal fluids which precipitated the baroque dolomite.

7.3 GEOCHEMISTRY

7.3.1 Peritidal dolomite and fabric-replacive dolomite

The geochemical analyses are consistent with stabilization and pervasive dolomitization of a mineralogically unstable ^{18}O-rich, strontium-rich precursor to the peritidal dolomite and dolomitization of the underlying partially meteoric stabilised ^{18}O-depleted, strontium-poor normal marine and lagoonal precursor to the fabric-replacive dolomite by a downward migrating dolomitizing fluid. The dolomitization was regional with local pore-fluid variations which resulted in the geochemical variations of the peritidal dolomite and fabric-replacive dolomite between different localities. The dolomitizing fluid resulted in ^{18}O-enrichment of the fabric-replacive dolomite with respect to its precursor, meteoric-stabilized limestones.

7.3.2 Baroque dolomite

The geochemical analyses of the baroque dolomite indicate that it is distinct from the fabric-replacive dolomite and peritidal dolomite and consistent with precipitation from strongly reducing Fe^{2+} and Mn^{2+}-rich fluids. Elevated temperatures resulted in the depleted $\delta^{18}O$ values of the baroque dolomite. The $\delta^{13}C$ value is similar to those of the peritidal dolomite and fabric-replacive dolomite suggesting that the carbonate ions were provided by local stylolitic dissolution. The close proximity of unaffected fabric-replacive dolomite and peritidal dolomite to the baroque dolomite confirm that the baroque dolomitization did not result in extensive recrystallization and geochemical resignaturing of the surrounding dolomite or limestone. The exceptions to this observation are the baroque dolomite mosaics which are petrographically distinct from the fabric-replacive dolomite mosaics.

7.4 DOLOMITIZATION MODEL

The intertidal to supratidal facies of the El Brull Unit and Colldejou Unit of the Catalan Basin and the similar facies of the Valencia-Cuenca Basin are considered to have been deposited as fine-grained ^{18}O-rich, strontium-rich aragonite probably with some unstable calcian penecontemporaneous dolomite which formed in a similar way to the evaporative dolomite of the Arabian Gulf coastal sabkhas. The peritidal facies contained hypersaline pore-fluids which precipitated stellate gypsum.

The lowermost Middle Muschelkalk which overlies the Lower Muschelkalk consists of sabkha-style nodular evaporites and shales as well as laminated evaporites which suggest deposition within bodies of more permanent hypersaline water (see Section 2.4.4). It is suggested that hypersaline fluids migrated downwards due to density contrasts with the underlying groundwater from the Middle Muschelkalk and resulted in the complete dolomitization of the peritidal dolomite, and shallow-burial, pre-stylolitic fabric-replacive dolomitization of the partially meteoric-stabilized underlying limestones. The hypersaline fluids preferentially dolomitized the unstable mineralogies and were in part controlled by the permeability contrasts within the limestone. The hypersaline fluid locally precipitated replacive gypsum and minor anhydrite. The thickness of the fabric-replacive dolomite is variable owing to the considerable thickness and facies variations of the Middle Muschelkalk evaporites. The overall similarity of the petrography of the peritidal dolomite is due to the generally fine-grained, homogeneous aragonite-dominated precursor, whereas the heterogeneous nature of the mineralogy, grain-size and permeability of the underlying limestones resulted in the variety of petrographic textures of the fabric-replacive dolomite (*cf.* Dawans & Swart, 1988). The complete dolomitization of the Lower Muschelkalk in much of the Ebro Basin is consistent with the increase in thickness of the Middle Muschelkalk towards the northwest of the Ebro Basin and Valencia-Cuenca Basin (Jurado, 1988).

Local variability within the Middle Muschelkalk resulted in different initial trace element concentrations within the dolomitizing fluid giving rise to the regional geochemical variations within the peritidal dolomite and fabric-replacive dolomite. The consistent geochemical contrasts between the peritidal dolomite and fabric-replacive dolomite are due to consistent differences in the average mineralogy of the precursors.

Subsequent burial probably resulted in some geochemical stabilization and changes in crystal ordering and stoichiometry of the peritidal dolomite and fabric-replacive dolomite. This stabilization appears to have been essentially isochemical and preserved the dolomite fabrics and geochemical contrasts between the dolomite facies.

The baroque dolomite was the consequence of separate and only locally important dolomitization by late highly-reducing hydrothermal fluids which migrated principally through fractures within the lithified limestones and dolomites. The cations and anions for the dolomite cement were derived by local pressure dissolution and the depleted $\delta^{18}O$ signature was due to the elevated temperatures. The baroque dolomite was associated with hydrothermal mineralization and local sulphate reduction and formation of pseudomorphs after sulphates.

7.5 DISCUSSION

Density-driven reflux of hypersaline waters produced by evaporation has often been suggested as a mechanism for dolomitization. The evaporated seawater would have a greater Mg^{2+}/Ca^{2+} ratio owing to the precipitation of calcium sulphate evaporites and this is considered to favour dolomitization (Folk & Land, 1975). The reflux model was initially applied by Adams & Rhodes (1960) amongst others to the Permian Reef Complex of West Texas. A modern reflux setting was suggested by Deffeyes *et al.* (1965) to be operative below a hypersaline lake on Bonaire Island. However, later studies showed that there was little reflux for most of the time and there was no dolomite below the lake (Murray, 1969). Nevertheless, the reflux model has commonly been applied to ancient dolomites, particularly those associated with sulphates *e.g.* Sears & Lucia (1980), Smith (1981), Bein & Land (1983), Theriault & Hutcheon (1987). Reviews of the reflux models of dolomitization are given in Tucker & Wright (1990) and Machel & Mountjoy (1986).

Criticisms of the reflux model have generally been based on the lack of evidence for reflux at Bonaire Island, on the feasibility of producing the required fluid flow by a density contrast mechanism and whether sufficient flux of magnesium could be provided to result in the extent of the observed dolomite.

Simms (1984) suggested that the lack of observable reflux on Bonaire was due to tidal dispersion in the groundwaters beneath the hypersaline lake which maintained the normal salinities in the underlying limestones. Simms (1984) also showed that reflux into a carbonate platform is theoretically possible with only slightly hypersaline platform-top waters, and suggested that plumes of such waters would migrate downwards displacing the less dense internal waters of the platform. Simms envisaged the Bahama platform as a possible locality for this mechanism. In the case of the Middle Muschelkalk, evaporation clearly reached gypsum precipitation and thus the density contrast is likely to have been greater. Simms (1984) indicated that reflux will only be possible where the underlying groundwaters are less dense than the hypersaline waters near the surface. The groundwaters in a ramp setting like the Muschelkalk of northeast Spain are likely to have been meteoric-derived waters or seawater, or a mixture of both, depending upon the extent and position of the meteoric lens. In either case, the hypersaline fluid will be more dense and should be capable of downward reflux and subsequently be carried away laterally by the groundwater flowpath back to the sea.

The presence of permeability barriers between the evaporating lagoons and sabkhas of the Middle Muschelkalk and the Lower Muschelkalk is a possible problem for the dolomitization model and a general problem for reflux models (Machel & Mountjoy,

1986). However, the permeability of the sabkha deposits during deposition is obviously greater than their ancient lithified equivalents which commonly form impermeable seals. Trenches cut in modern sabkhas (*e.g.* fig. 39 and fig. 41B of Shinn, 1983) appear to rapidly fill with groundwater indicating at least lateral permeability in the sediments. It does not seem improbable that dense hypersaline waters would be able to find a downwards migration path avoiding low permeability horizons.

A simple calculation based on the composition of modern seawater and assuming that all the calcium in any volume of seawater produces calcium sulphate and the magnesium is available for dolomitization of calcium carbonate shows that the volume ratio of dolomite to gypsum would be 4.5:1 and dolomite to anhydrite would be 7:1. Magnesium bearing evaporite minerals are not common (Holser, 1979a) and if any calcium from the seawater were included in the dolomite then these ratios would be even higher. The thickness of sulphates in the Middle Muschelkalk is difficult to estimate from surficial outcrop owing to dissolution. However, graphic logs from Marzo & Calvet (1985) and Jurado (1988) indicate evaporitic shales and sulphate horizons commonly form much of the 50-300m thickness of the Middle Muschelkalk of the Catalan Basin and Ebro Basin. No data were available for the Valencia-Cuenca Basin, although the Middle Muschelkalk facies are very similar. Thus, the thickness of sulphates indicates there was clearly enough seawater to provide the magnesium for the dolomitization. The Middle Muschelkalk contains more clastics and relatively few sulphates in the northern part of the Catalan Basin (Marzo & Calvet, 1985) corresponding to the region of only partial fabric-replacive dolomitization of the Lower Muschelkalk. The variability of Middle Muschelkalk evaporite facies does appear to be related to the degree of dolomitization.

The applicability of this model of dolomitization to other ancient dolomites is clearly not universal. However, the similar arrangement of dolomite facies described by Nicholls & Silberling (1980) from a number of different examples from the Great Basin of the USA, the reflux model of Asquith (1979) for the Mississippian Red River Group and of Longman (1982) for Ordovician dolomites of the Williston Basin indicate that similar situations have arisen at several times in the geological record. The dolomite facies observed in the Lower Muschelkalk of northeast Spain are also present in the Muschelkalk of Hungary (Torok, 1990) and a similar diagenetic sequence has been postulated (Torok, 1990 pers. comm.).

7.6 DOLOMITIZATION AND SEQUENCE STRATIGRAPHY

It is useful to consider the dolomitization model in terms of the sequence stratigraphic framework for the Muschelkalk (see Section 3.7). The Middle Muschelkalk is the

Lowstand Systems Tract (LST-2) to the second depositional sequence and is considered to be the major source of dolomitizing brines which migrated downwards through the Highstand Sytems Tract (HST-1) and into the Transgressive Systems Tract (TST-1) to produce the peritidal dolomites and fabric-replacive dolomites respectively. The association of brine-reflux dolomitization with lowstands of relative sea-level is quite common in the literature, particularly in semi-isolated evaporite-related intra-cratonic basins, *e.g.* the Zechstein of northeast England (Smith, 1981) and Poland (Peryt & Magaritz, 1990), the Middle Devonian basins of western Canada (Kendall, 1989) and the nothern Delaware Basin and the Permian Reef Complex (Melim & Scholle, 1989; Kendall & Harwood, 1989). These examples are all carbonate shelves with well-defined shelf-edge breaks and differ somewhat from the homoclinal ramp setting of the Lower Muschelkalk. However, climate appears to be the most important factor in determining the feasibility of brine-reflux dolomitization during lowstands. The climate during the Lower Muschelkalk of northeast Spain was semi-arid (see Section 2.3) and similar to the paleoclimates of the other examples mentioned above. During a more humid climate, karstification may be the more important process that is associated with sequence boundaries.

CHAPTER 8: CALCITIZATION OF LOWER MUSCHELKALK DOLOMITES

8.1 INTRODUCTION

The replacement of dolomite by calcite is commonly termed dedolomitization and has been recognised on the basis of a variety of petrographic textures (Evamy, 1967; Braun & Friedman, 1970; Zenger, 1973; Theriault & Hutcheon, 1987). Many workers consider that dedolomitization is a near-surface phenomenon related to uplift and proximity to meteoric groundwaters, so that the presence of dedolomite in the subsurface may indicate an unconformity (Goldberg, 1967; Braun & Friedman, 1970; Al-Hashimi & Hemingway, 1973; Franck, 1981).

Experimental observations by De Groot (1967) suggested that dedolomitization requires :

i) High initial Ca^{2+}/Mg^{2+} ratio in the dedolomitizing fluid.

ii) High rate of fluid flow, to maintain i).

iii) Carbon dioxide partial pressure much less than 0.5atm.

iv) Temperature not greater than 50°C.

Conditions iii) and iv) indicate that the process should be restricted to the near-surface.

More recently, experimental work by Stoessel *et al.* (1987) suggested that at elevated pressure (300bars) dedolomitization can occur at higher temperatures (100-200°C). Dedolomites have now been recognised in the burial diagenetic realm (*e.g.* Budai *et al.*, 1984) and several other settings, including: contact metamorphism (Wood & Armstrong, 1975); schizohaline marine-meteoric mixing zone (Magaritz & Kafri, 1981); and freshwater aquifer systems (Longman & Mench, 1978; Plummer & Back, 1980; Back *et al.*, 1983). Calcitization has also been related to the later stages of early, reflux dolomitization (Theriault & Hutcheon, 1987).

A common observation is that ferroan dolomite is preferentially calcitized relative to non-ferroan dolomite and this has been attributed to a greater metastability of the ferroan dolomite under near-surface conditions (Franck, 1981).

Dedolomitization of the Lower Muschelkalk of the Catalan Basin has occurred at several localities. Calcitization has affected several dolomite facies and produced a wide variety of textures. Field relations and geochemistry indicate that this is a near-surface, uplift-related process. Meteoric-derived groundwaters and local dissolution of evaporite minerals produced a fluid capable of dedolomitization and calcite precipitation.

Fig. 8.1. Red, porous calcitized dolomite layer in vertical-bedded fabric-replacive dolomite. Layer probably acted as conduit for calcitizing fluid. Pauls locality.

Fig. 8.2. Porous, coarse-grained dedolomitized dasycladacean algal packstone layer Pauls locality.

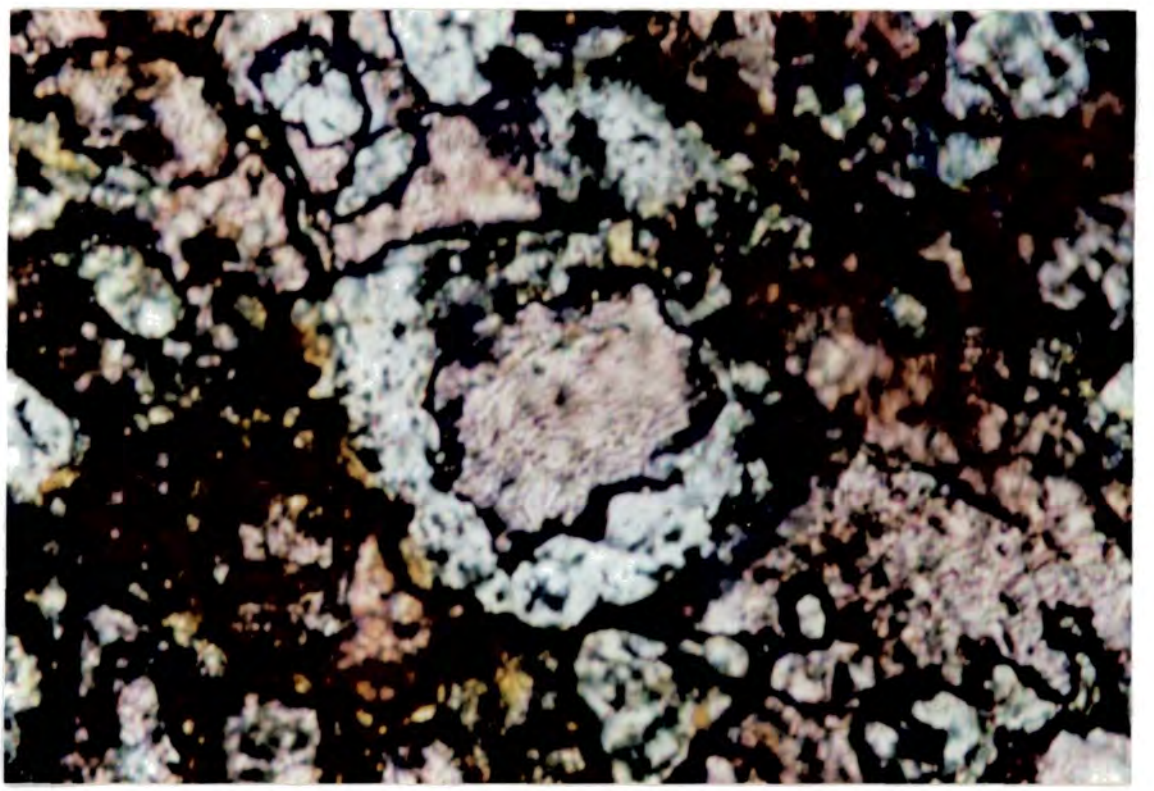

Fig. 8.3. Corroded limpid dolomite rim with calcite spar core. [Stained thin section. PPL. Sample VB60. Width of view = 0.4mm]

8.2 DEDOLOMITE FIELD RELATIONS

Dedolomites were recognised in the field as discrete, laterally continuous (on outcrop scale) calcitic horizons, up to 1m in thickness, within dolomitic successions. The calcitized layers are commonly bedding-parallel with sharp boundaries and have a reddened 'rusty' appearance (Fig. 8.1). Calcitization has affected the dolomite irrespective of the dolomite facies and position in the succession; however, the top and basal parts of the Lower Muschelkalk appear to have been particularly prone to dedolomitization. The dedolomites appear to be locally associated with modern calcretes, other soils, karstic levels and collapse breccias. Some dedolomite horizons are coarse-grained with an irregular intergranular porosity (Fig. 8.2) whereas others are fine-grained and tight.

8.3 DEDOLOMITE PETROGRAPHY

Several calcitization textures occur in the Lower Muschelkalk and can be considered in two groups: coarse-grained dedolomite; and fine-grained dedolomite.

8.3.1 Coarse-grained dedolomite

8.3.1.1 Dolomite crystal rims with calcite spar cores

Rounded to rhombohedral limpid dolomite crystal rims exhibit embayed internal and external margins, up to 0.5mm in diameter, with cores of clear, calcite spar (Fig.s 8.3, 8.4). The rims have a dull red cathodoluminescence with a dull pink luminescent external margin. In many examples the core is a single non-cathodoluminescent calcite crystal which is syntaxial with the dolomite rim. Some of the rims are discontinuous with the gaps filled by calcite spar. Calcite veins, up to 2mm across, with minor quartz cement cross-cut the fabric. Some areas are iron-stained and the calcite spar crystals are rimmed by brown iron oxides.

8.3.1.2 Hollow dolomite crystal rims

Rounded to rhombohedral limpid dolomite crystal rims, up to 0.5mm in diameter, as described in Section 8.3.1.1 but with hollow cores. This texture commonly occurs in association with dolomite rims with calcite cores (Fig. 8.5).

8.3.1.3 Zoned rhombohedral calcite crystals

Rounded calcite crystals, up to 0.5mm in diameter, with clear limpid rims and speckled 'dirty' cores (Fig. 8.5). The calcite crystals are zoned under CL with very

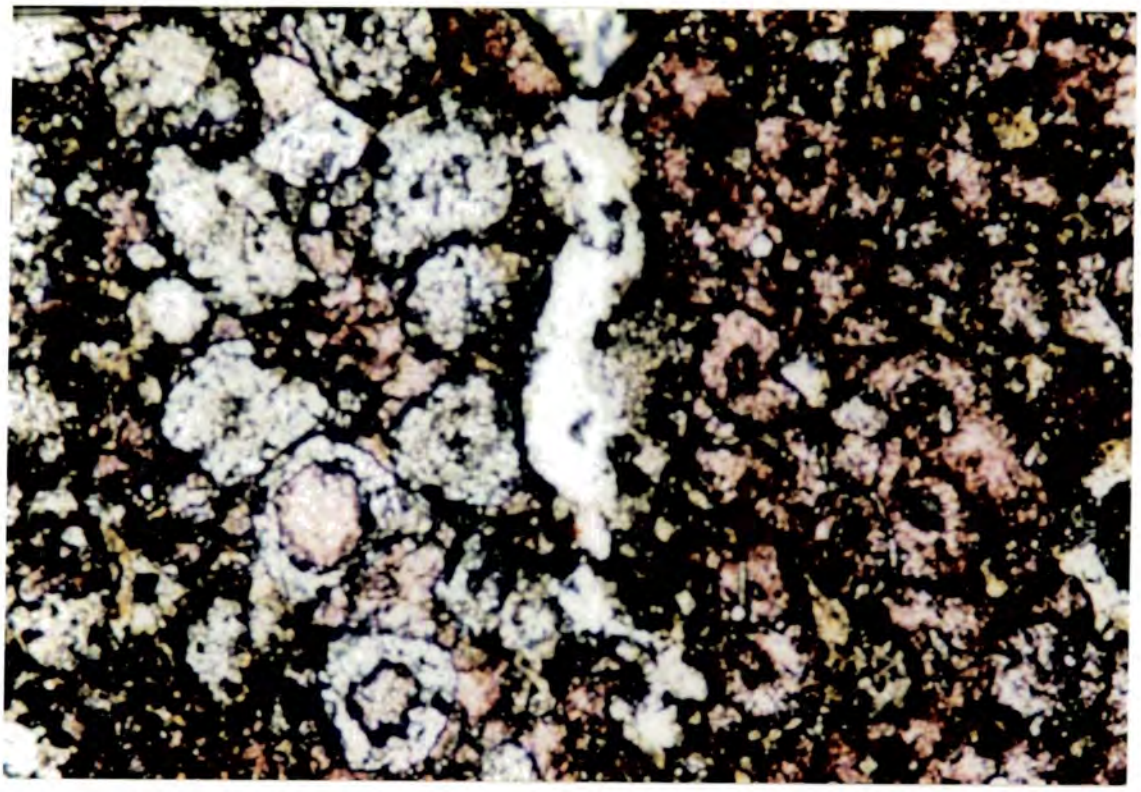

Fig. 8.4. Corroded dolomite rhombs, dolomite rims with calcite spar cores and zoned rhombohedral calcite crystals. [Stained thin section. PPL. Sample VB60. Width of view = 0.8mm]

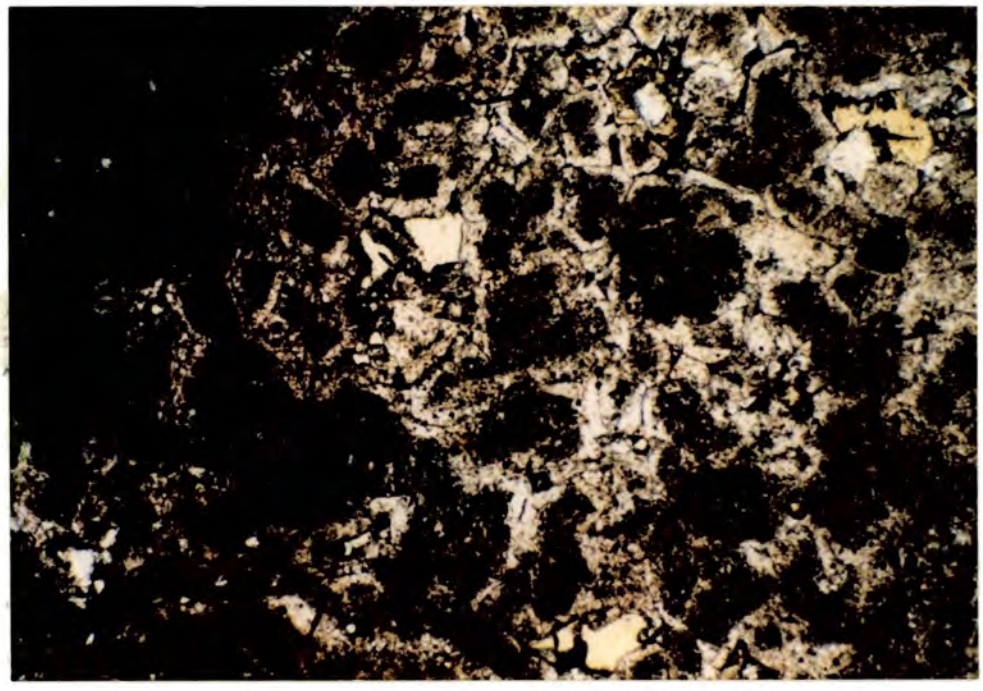

Fig. 8.5. Zoned rhombohedral calcite crystals with intergranular porosity from layer with tepees at the top of the Colldejou Unit at Arboli locality. [only left of section stained. PPL. Sample A66. Width of view = 0.4mm]

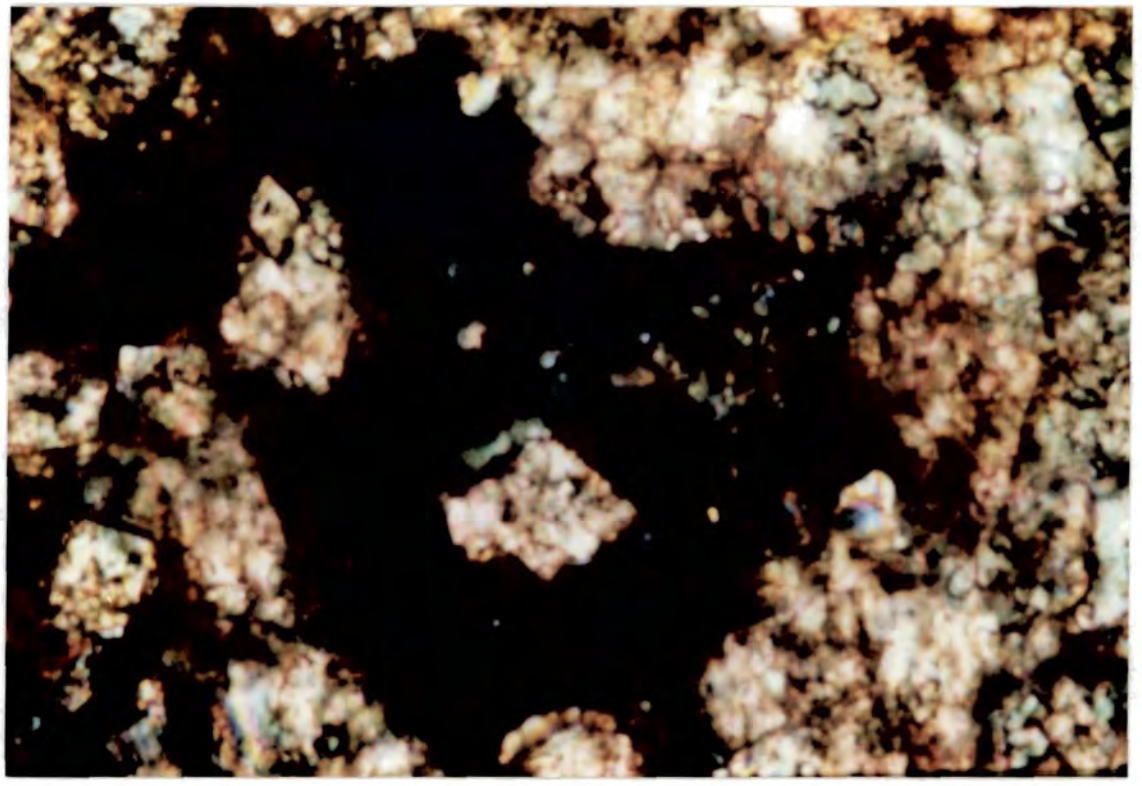

Fig. 8.6. Rhombohedral calcite. [Stained thin section. XPL. Sample VB90. Width of view = 0.4mm]

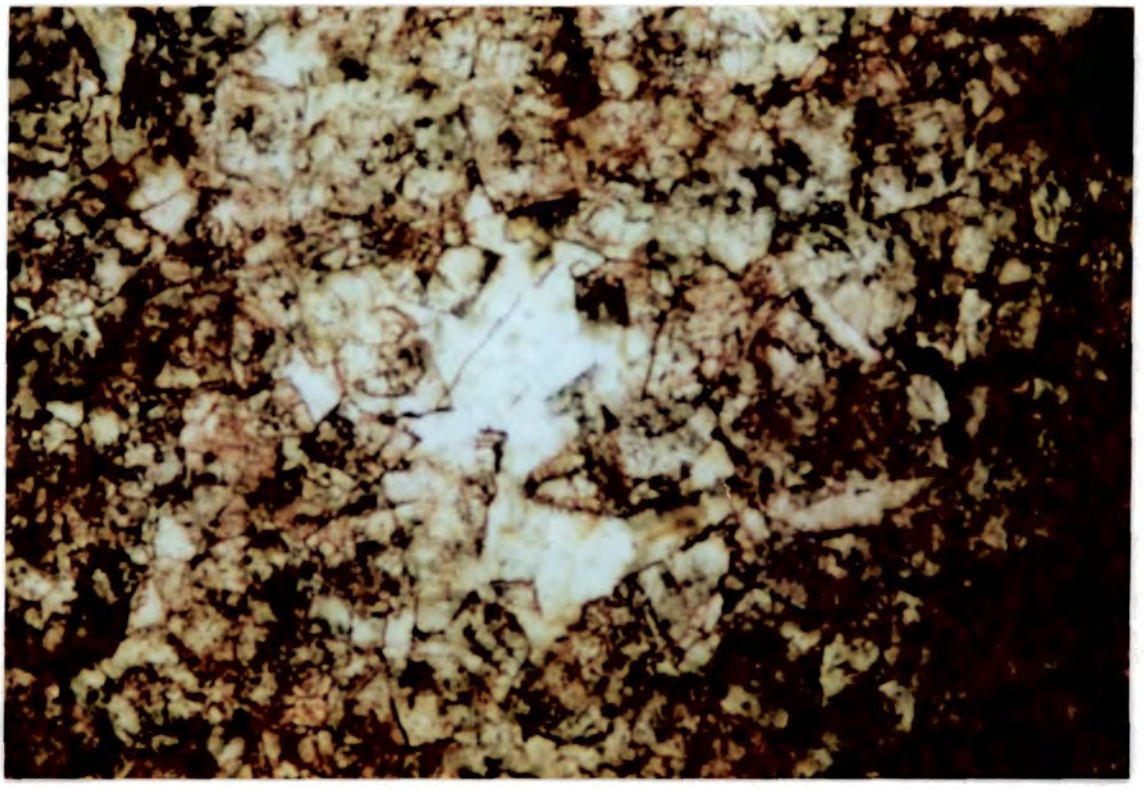

Fig. 8.7. Rhombohedral calcite with intergranular clear calcite spar. [Stained thin section. PPL. Sample VB6. Width of view = 0.8mm]

dull to non-luminescent cores and dull red cortices. These zoned crystals are surrounded by a calcite microsparite 'matrix' with crystals up to 0.1mm, and commonly occur with crystals displaying dolomite crystal rim fabrics. Some of the grains are coated by iron oxides and associated with calcite spar veining.

8.3.1.4 Rhombohedral calcite

Sparry calcite mosaic which in crossed polars exhibits rhombohedral outlines (Fig. 8.6). Much of the calcite is poikilotopic and encloses smaller rhombohedral calcite grains (Fig. 8.7). The calcite is inclusion-rich and is dull red to non-cathodoluminescent. Small, irregular relic dolomite grains are also present.

8.3.2 Fine-grained dedolomites

8.3.2.1 Dolomite crystal rims with micritic calcite cores

Angular, rhombohedral dolomite crystal rims which have a bright red luminescence under CL, enclose micritic calcite cores (Fig. 8.8). 'Fingers' of dolomite commonly project from the rim towards the core and in one case dolomite is present at the centre of the rhomb to leave an annulus of micritic calcite, indicating that these are calcitized dolomite rhombs and not merely skeletal growth of dolomite (as noted by Harwood, 1988). The micritic calcite is dull red cathodoluminescent and is locally microsparitic and similar to the dolomite crystal rims with calcite spar core texture described above.

8.3.2.2 Micritic calcite with relict dolomite grains

Fine-grained featureless micritic calcite with small, rounded crystals of dolomite grade into regions of inclusion-rich microsparitic calcite. The crystal boundaries are commonly picked out by brown iron oxides and there is an irregular vuggy porosity (with pores up to 2mm across). The calcite has a dull red cathodoluminescence.

8.3.3 Selective dedolomitization of bioclasts

At one locality (Pauls; Appendix 1) a particular 0.5m-thick dasycladacean algal packstone horizon exhibited a varying degree of calcitization and could be compared with completely unaltered algal packstone.

8.3.3.1 Dolomicritic algal packstone (Fig. 8.10)

Dasycladacean algal thalli, up to 4mm across, form the bioclasts in the packstone which has a dolomicritic matrix. The internally chambered structure of the algal thalli is preserved in the dolomicrite.

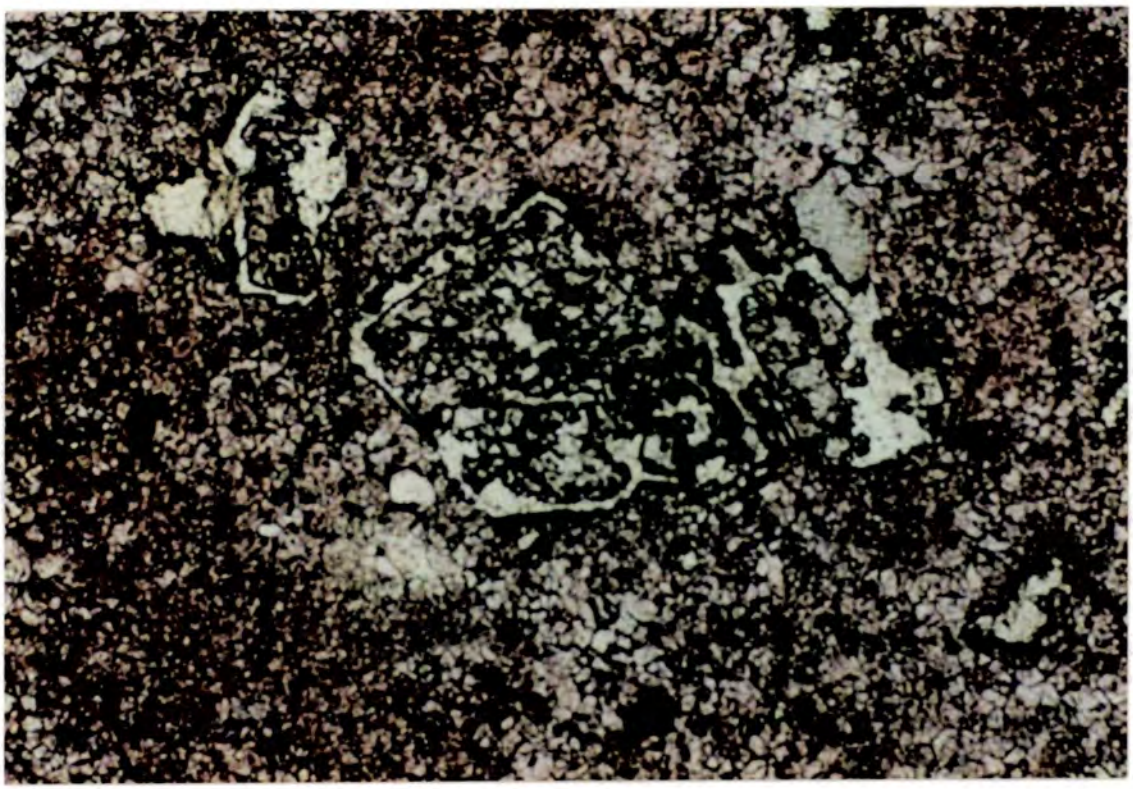

Fig. 8.8. Angular 'skeletal' dolomite enclosing microsparitic calcite. [Stained thin section. PPL. Sample LR31. Width of view = 0.8mm]

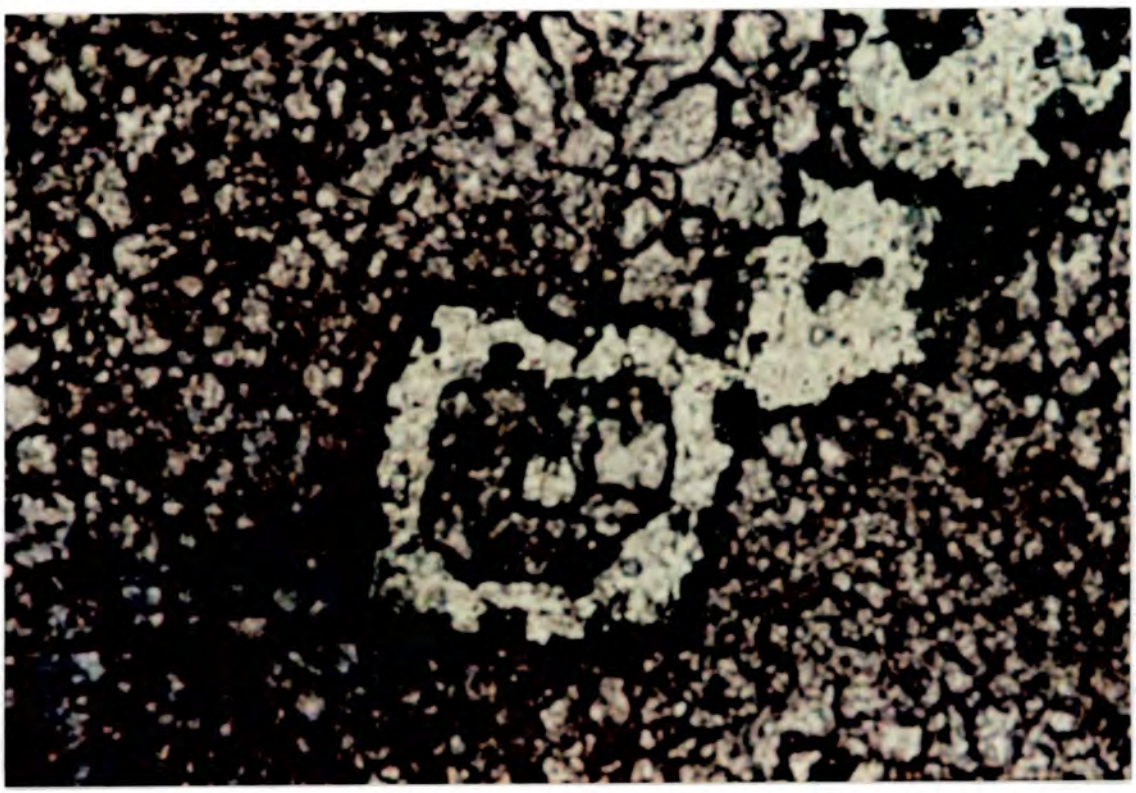

Fig. 8.9. Corroded dolomite rhomb with inner cortex replaced by microsparitic calcite. [Stained thin section. PPL. Sample. TF4. Width of view = 0.8mm]

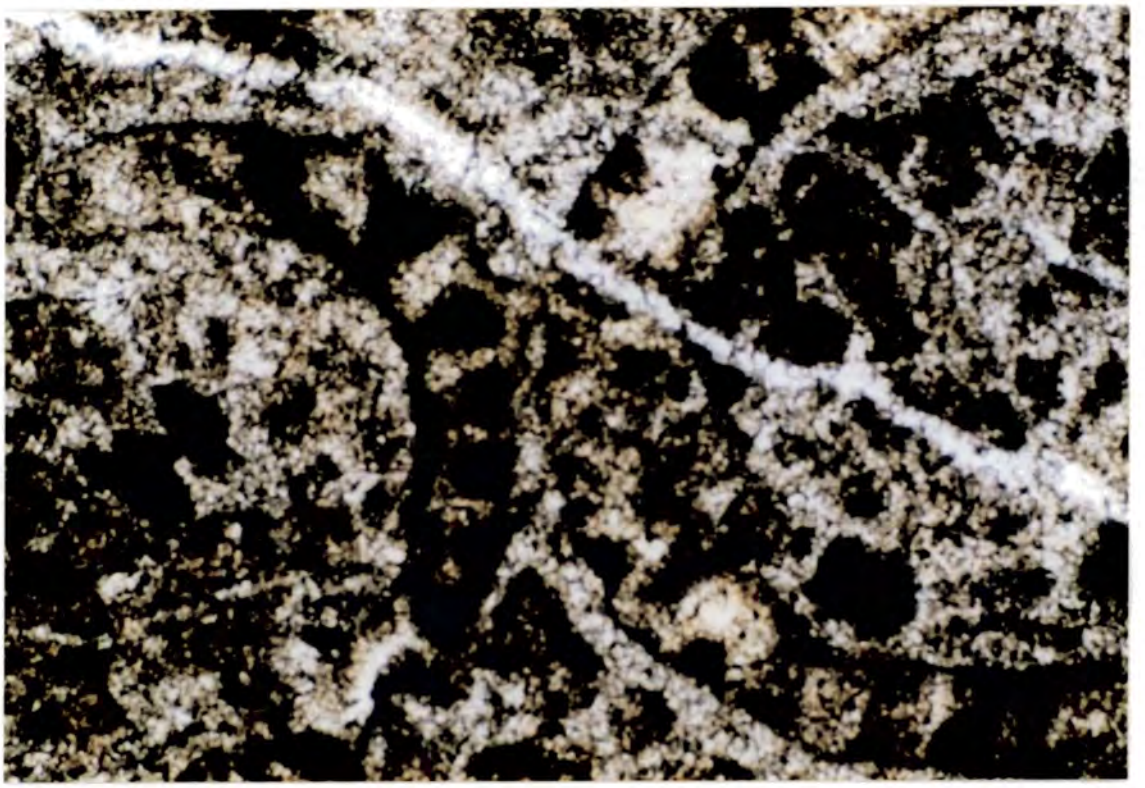

Fig. 8.10. Dasycladacean algal thalli with skeletal structure preserved in dolomicrite. Minor calcitization has occurred within the algal material. [Stained thin section. PPL. Sample VB31. Width of view = 3mm]

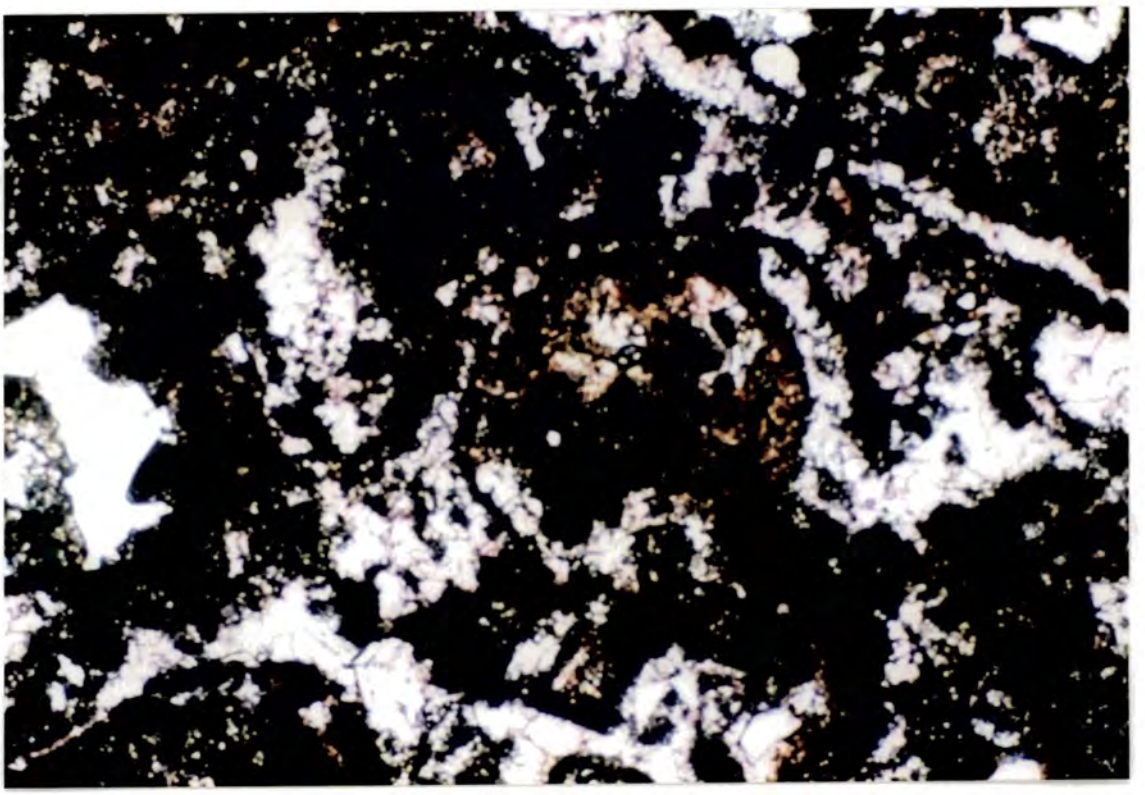

Fig. 8.11. Extensively calcitized dasycladacean algal packstone. Outline of algal thalli visible at centre. [Stained thin section. PPL. Sample PA63. Width of view = 3mm]

8.3.3.2 Partial calcitization

The algal bioclasts are preferentially calcitized and replaced by coarse calcite spar which is non-cathodoluminescent. Small relic grains of dolomite persist within the calcite spar and minor calcitization of the dolomicritic matrix has also occurred. Patches and veins of calcite spar, with minor quartz cement, cut across the fabric.

8.3.3.3 Extensive calcitization (Fig 8.11)

Calcitization has affected the dolomicrite matrix as well as the bioclasts to produce a reddened 'rusty' rock with the development of vuggy, intergranular porosity. The dasycladacean algal fragments are only preserved as outlines in the clear non-cathodoluminescent calcite spar. The dolomicrite matrix has been altered to cloudy, dull red-cathodoluminescent calcite spar with abundant small, rounded dolomite crystals. Some calcite crystals are coated by iron oxides which also occur in discrete veins.

8.3.4 Synthesis of dedolomite petrography

Dedolomitization has resulted in a wide variety of textures and these are summarised with their interpreted origins in Fig. 8.12. Many workers have observed the preferential calcitization of the cores of dolomite rhombs (Evamy, 1967; Franck, 1981). Dolomite rhombs in the Lower Muschelkalk of the Catalan Basin are commonly zoned with a ferroan, inclusion-rich, non-stoichiometric core and a clear, limpid, stoichiometric rim (see Section 5.5.3; Fig. 5.15). Hence, the core of the dolomite rhomb will generally be less stable than the rim leading to preferential replacement of the former by calcite. Small inclusions of low magnesium calcite may have been present in the core, as observed by Sibley (1982), and these may have acted as nuclei for the replacement calcite. The calcitizing fluid probably enters the rhombs via microfractures, oriented parallel to the cleavages, some of which have been widened by dissolution to produce calcite spar-filled cracks in the dolomite rims.

The rounding of the angular edges of the precursor dolomite rhombs is presumably related to the greater reactivity of the edges of the rhomb in comparison to the faces suggesting that the kinetics of the replacement reaction are partly controlling the dedolomite texture.

The occurrence of dolomite crystal rims, hollow dolomite rims and zoned calcite crystals in the same hand specimen indicates replacement as opposed to dissolution of the dolomite cores and/or rims, and subsequent calcite spar precipitation must have

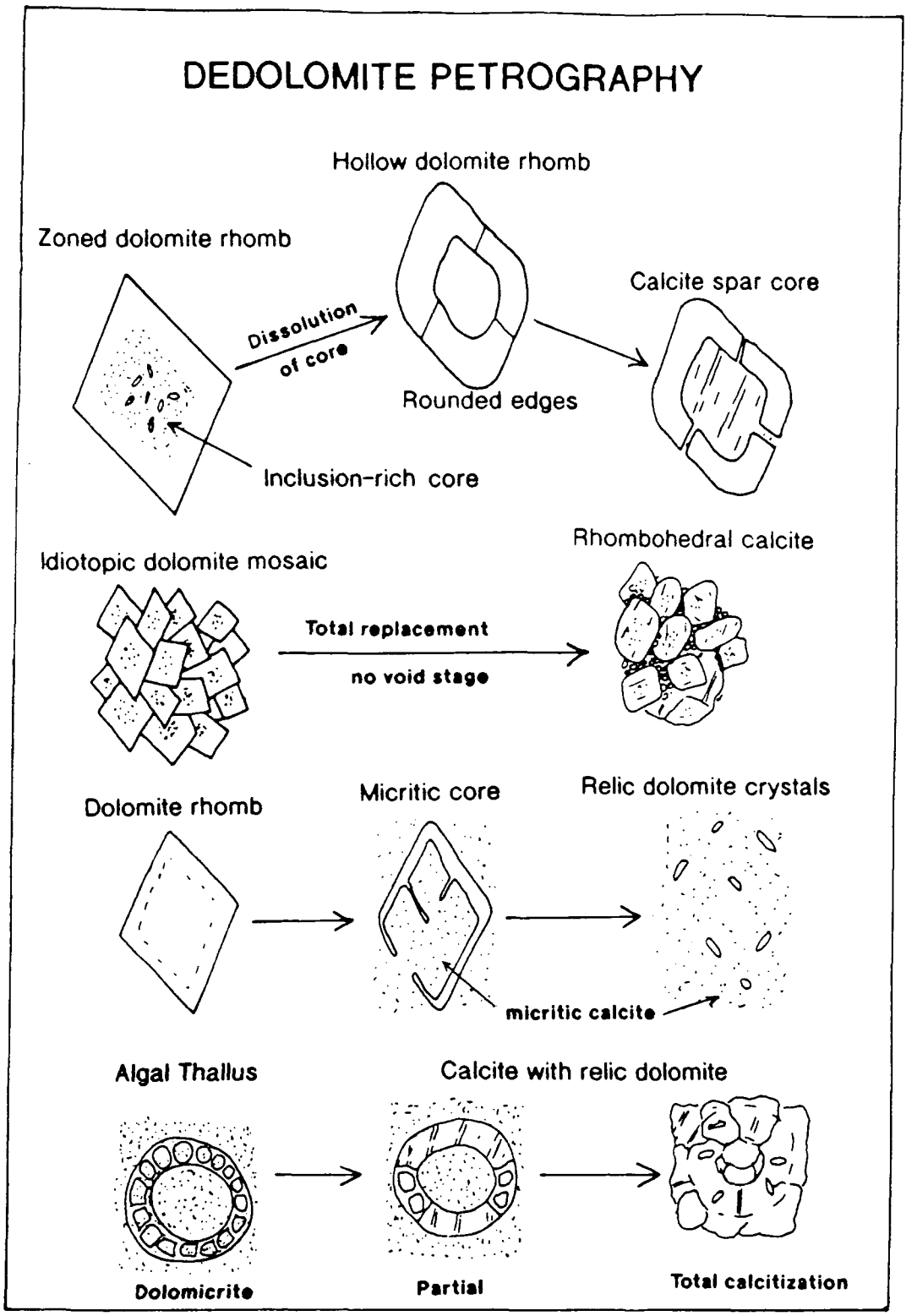

Fig. 8.12. Interpretative scheme for the dedolomite petrography.

been controlled by very local variations in the chemistry of the precursor or calcitizing fluid. The critical control on dissolution/crystallisation may have been kinetic.

The dolomite precursor to the rhombohedral calcite is presumably an idiotopic dolosparite with relatively little or no zonation in the dolomite rhombs (see Section 5.5.3).

The fine-grained dedolomites reflect different stages of the gradual replacement of dolomite by micritic calcite without a void stage and/or spar growth. Low magnesium calcite inclusions commonly occur in the cores of dolomite rhombs (Sibley, 1982) and a large number and irregular orientation of these may have promoted the formation of a micritic calcite core as opposed to a calcite spar core.

The preferential and selective calcitization of the bioclasts in the algal packstone must be related to a stability contrast between the dolomicrite of the bioclast and that of the matrix. Trace element data on whole rock crushes show that the dolomitized algal packstones are more ferroan than 'typical' dolomite mudstones suggesting that the iron content of the dolomitized algal bioclasts is greater than the dolomicrite of the matrix and that this is controlling the calcitization. The dedolomitized algal packstones are pervasively reddened and 'rusty' owing to the presence of iron oxides and hydroxides which are interpreted as the byproduct of the calcitization of ferroan dolomite by an oxidizing fluid (Fran_k, 1981).

8.4 SULPHATE MINERALS AND ASSOCIATED PROCESSES

Dedolomitization is thought to require a high Ca/Mg ratio in the calcitizing fluid (De Groot, 1967) and mass balance considerations imply that a source of calcium ions is required for the process. Gypsum and anhydrite dissolution will provide a Ca-rich solution and this has often been considered a necessary part of the dedolomitization reaction (*e.g.* Lee & Harwood, 1989). Stoessel *et al.* (1987) concluded that the sulphate ions are not involved in the dedolomitization reaction and that significant calcium ion concentration is the prime requisite.

8.4.1 Lower Muschelkalk Sulphates in the subsurface of the Ebro Basin

Jurado (1988) studied the Triassic from the subsurface of the Ebro Basin using cores and wire-line logs from a large number of boreholes (see Section 3.4). Sulphate minerals, principally anhydrite have been recognised within dolomitized Lower Muschelkalk and occur in two forms:

i) Stellate rosettes of anhydrite (after gypsum?) in a dolomicrite matrix (seen in core samples).
ii) Discrete layers of anhydrite up to 3m thick (seen in core and recognised from log response).

8.4.2 Surficial evidence for the former presence of sulphates

Although sulphates do not occur in the Lower Muschelkalk at the surface there is considerable evidence for their former existence.

8.4.2.1 Pseudomorphs after sulphate minerals

The petrography of pseudomorphs after gypsum and anhydrite is discussed in detail in Section 4.8. Evaporite dissolution and pseudomorph formation appears to have occurred in two phases, the second and most important of which is probably related to uplift during the Neogene into locally meteoric vadose conditions (see Section 2.6). Only this uplift-related evaporite dissolution is considered to be related to calcitization.

Pseudomorphs after stellate gypsum, up to 5mm across, are common, particularly within the dolomicrites. The calcite of the pseudomorphs commonly has a marked rhythmic zonation of bright and dull cathodoluminescence. Some pseudomorphs also contain elongate clear quartz crystals that appear to pseudomorph the former evaporite mineral (see Section 4.8). Pendant calcite cements and geopetal crystal silt fills occur in some of the pseudomorphs suggesting that some precipitation occurred in the vadose environment.

8.4.2.2 Collapse breccias

Collapse breccias are locally present within the Lower Muschelkalk in the El Brull Unit and the Colldejou Unit and form discrete layers up to 1m thick (*e.g.* La Riba, Fig. 3.23, and Malpaso, Fig. 3.29). The clasts in the breccias are poorly sorted, angular and generally composed of laminated dolomicrite with abundant pseudomorphs after evaporites.

8.4.3 Sulphate mineral synthesis

Comparison between the sulphate-bearing Lower Muschelkalk of the subsurface of the Ebro Basin and the Lower Muschelkalk exposed in the Catalan Coastal Ranges indicates that sulphate dissolution occurred during uplift. Dissolution and replacement of stellate gypsum/anhydrite has resulted in calcite-quartz pseudomorphs and

dissolution of discrete evaporite layers has produced collapse breccias. The cathodoluminescent zonation of the calcite cement within the pseudomorphs indicates that it precipitated from fluids of fluctuating redox potential and this may be related to seasonal-controlled variation in meteoric-derived groundwaters and/or periodic stagnation of the flow system (Barnaby & Rimstidt, 1989). The presence of the quartz cement suggests that the precipitating fluid was at least in part meteoric in origin and the system may have been open with respect to carbon dioxide and thus near-surface (Knauth, 1979). Moore *et al.* (1972) suggested that supratidal sediments, like those of the Middle Muschelkalk, may act as sources of silica.

The sabkha-style evaporites of the Middle Muschelkalk and the evaporitic shales of the evaporite-lutite-carbonate complex (see Section 2.4), stratigraphically above and below the Lower Muschelkalk respectively, are generally poorly exposed, but have been considerably affected by meteoric precipitation and run-off and are clearly undergoing weathering and dissolution.

8.5 DEDOLOMITE GEOCHEMISTRY

Geochemical aspects of dedolomitization have been of interest to many workers. Experimental approaches have been taken by De Groot (1967) and Stoessel *et al.* (1987) in order to investigate the conditions favourable for calcitization.

Field-based studies have also commonly involved geochemical analysis (*e.g.* Al-Hashimi & Hemingway, 1973; Magaritz & Kafri, 1981; Budai *et al.*, 1984; Lee & Harwood, 1989) to distinguish different dedolomite phases and to constrain the composition and source of the calcitizing fluid.

Mass balance and mass transfer calculations have been used to measure the overall conditions (such as reaction and fluid flow rates) for dedolomitization within carbonate aquifer systems (Back *et al.*, 1983; Plummer & Back, 1980).

8.5.1 Analytical aims and sampling

Field relations and associated petrography (Section 8.3.4) suggest that dedolomitization was associated with dissolution of sulphates by near-surface oxidising groundwaters. Carbon and oxygen isotopic compositions and trace element concentrations were determined for the dedolomites to compare with the unaltered dolomite. Calcite spar samples (from pseudomorphs after gypsum and associated veins) were also analysed for comparison with the dedolomites and to test the above model by constraining the origin and composition of the calcitizing fluid. In several

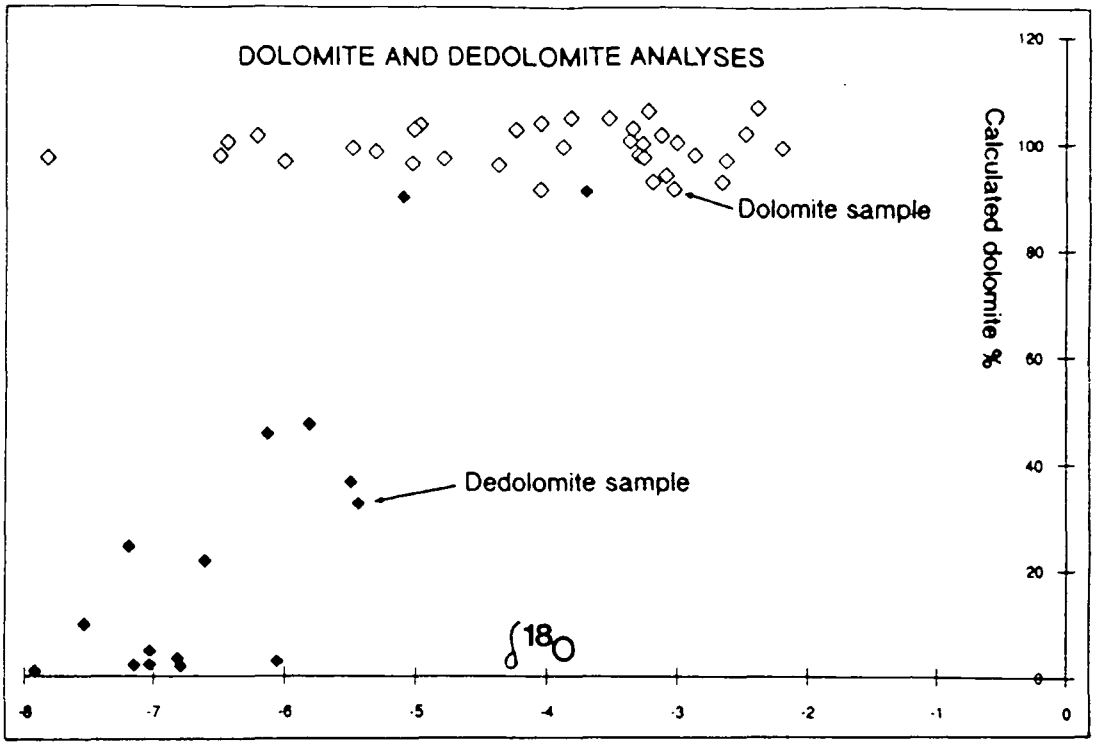

Fig. 8.13. Plot of calculated dolomite percentage in sample against oxygen isotope composition showing affect of residual dolomite.

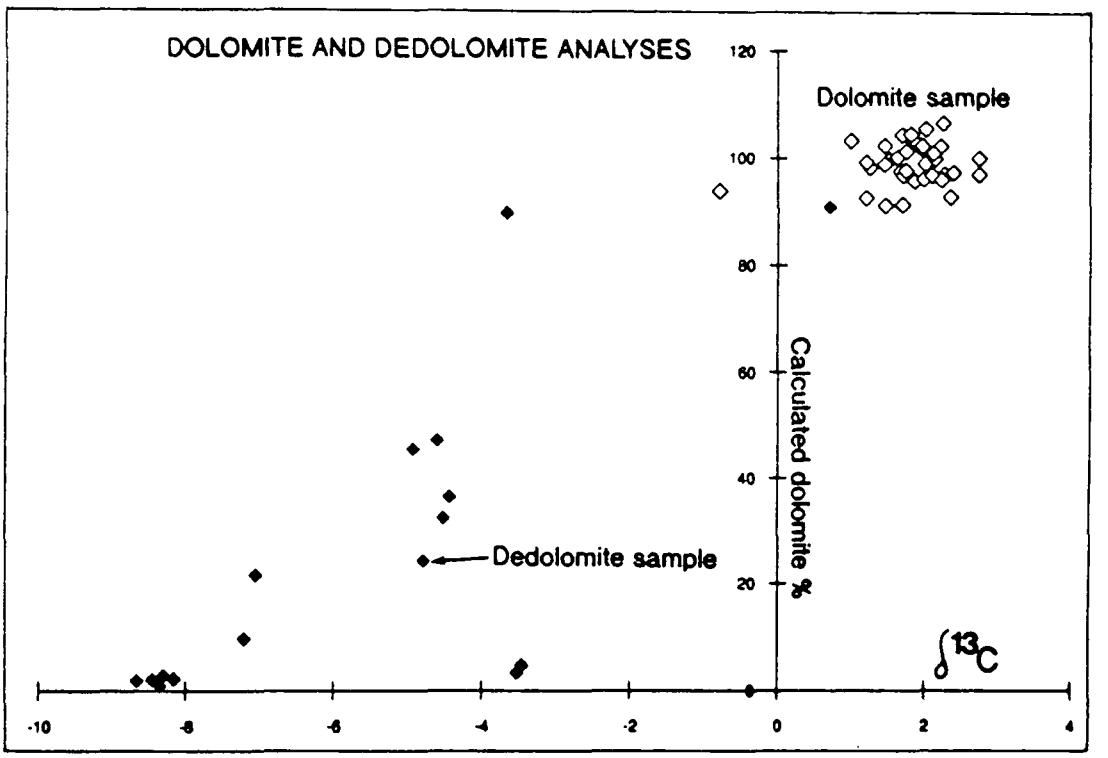

Fig. 8.14. Plot of calculated dolomite percentage in sample against carbon isotope composition showing affect of residual dolomite.

cases, particularly the fine-grained dedolomites, separation of small, individual dolomite crystals from the calcite was not possible. For analytical methods see Appendices 3 and 4.

8.5.2 Carbon and oxygen isotopic analysis

Carbon and oxygen stable isotopic analyses of the dedolomite and calcite spar samples were compared with analyses of dolomite samples from the same five localities. Dedolomite and calcite spar samples are also compared to Lower Muschelkalk limestones in Fig.s 6.4 and 6.5.

8.5.2.1 Effect of contamination by residual dolomite

As mentioned in Section 8.5.1 sampling of pure calcite from dedolomites was difficult. However, trace element data (see Section 8.5.5) was available for these samples and allowed the effect of contamination by residual dolomite to be quantified (see Appendix 3).

i) Oxygen isotope data

The 'pure' dedolomites (less than 10% calculated dolomite) have oxygen isotope values of between -6 and -8 $\delta^{18}O$ (Fig. 8.13). The effect of contamination by residual dolomite is shown by the trend towards more positive $\delta^{18}O$ values with increasing dolomite content, approaching the majority of dolomite analyses which plot between -3 and -5 $\delta^{18}O$.

ii) Carbon isotope data

The 'pure' dedolomites cluster around -8 to -9 $\delta^{13}C$ (with two exceptions which plot around -3.5$\delta^{13}C$) and there is a trend from these values towards those of the dolomites (+1 to +3 $\delta^{13}C$) with increasing calculated dolomite percentage, indicating that this trend is due to remnant dolomite within the sample (Fig. 8.14).

The two conspicuously heavier 'pure' dedolomite samples with carbon isotope value of about -4 $\delta^{13}C$ (VB77 and VB78) have fine-grained rhombohedral calcite fabrics and were collected only a few metres apart at the same locality (Vilella Baixa).

8.5.2.2 Comparison of dolomite and dedolomite analyses

An isotope crossplot of dolomite, dedolomite and calcite spar analyses is shown in Fig. 8.15. The dedolomitization has produced calcite of -6 to -8 $\delta^{18}O$ and -8 to -9 $\delta^{13}C$ representing a depletion of about 2 to 5 permil in ^{18}O and 3 to 5 permil in ^{13}C

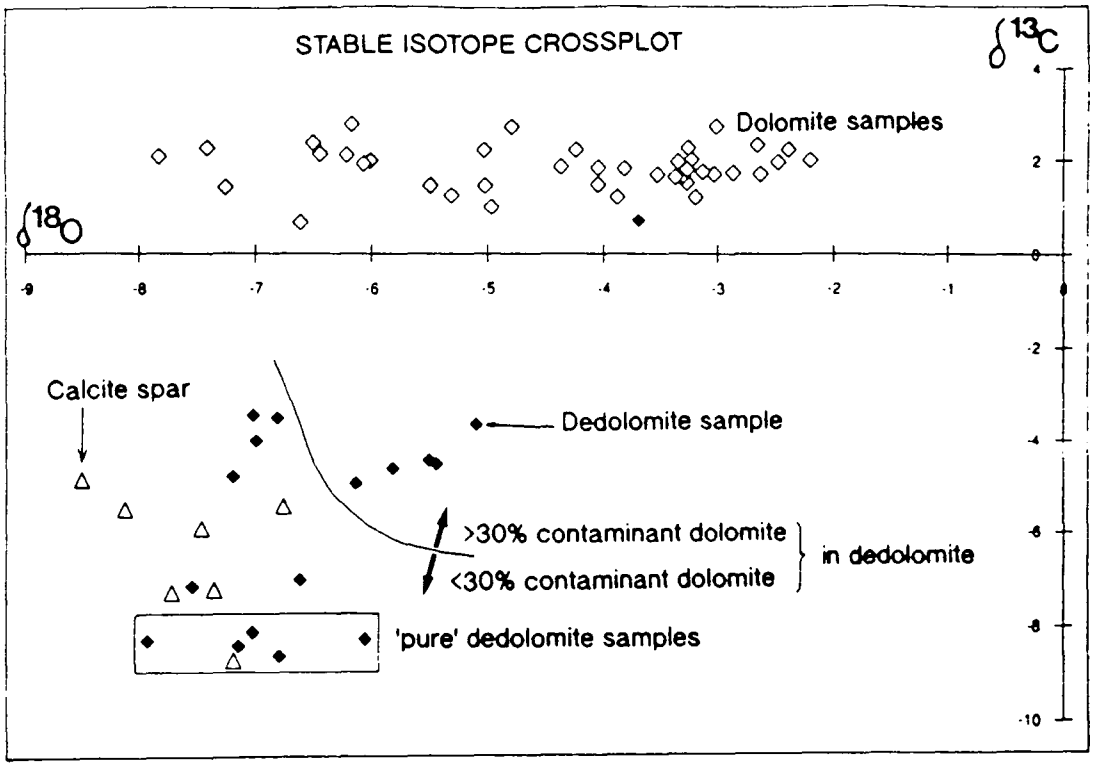

Fig. 8.15. Stable isotope crossplot for dolomite, dedolomitic calcite and associated calcite spar samples.

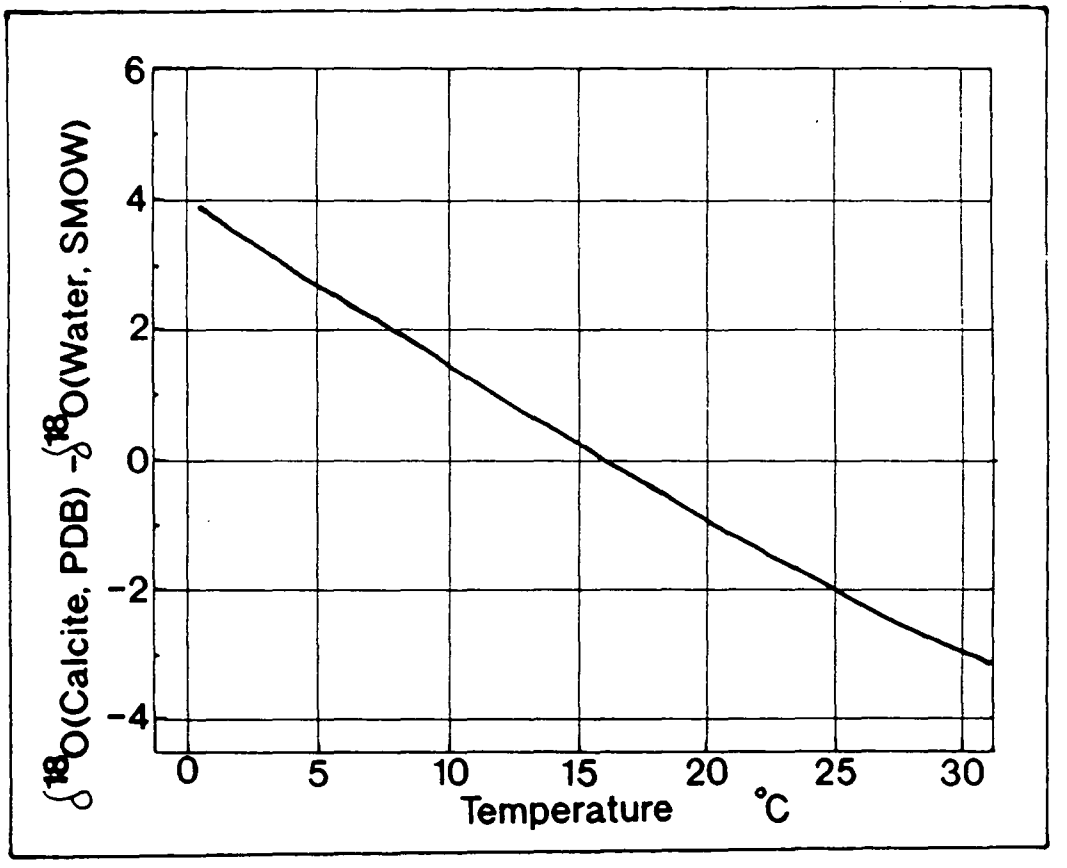

Fig. 8.16. Oxygen isotopic fractionation between calcite and water at sedimentary temperatures (adapted from fig. 1-2 from Anderson & Arthur, 1983).

from precursor dolomite.

The two aberrant 'pure' dedolomites have less negative $\delta^{18}O$ of around -7 permil and the ^{13}C is relatively enriched at about -4 $\delta^{13}C$.

The isotopic compositions of the calcite spar samples from the veins and pseudomorphs after evaporites are also plotted on Fig. 8.15 and these plot in the range -6.5 to -9 $\delta^{18}O$ and -4.5 to -9 $\delta^{13}C$ and overlap the dedolomite field. Trace element data are only available for four of the seven spar samples but do suggest that there may have been some contamination of the calcite by matrix dolomite during sampling of the small pseudomorphs. The contaminant dolomite may be responsible for the less negative $\delta^{13}C$ values of some of the calcite spar samples.

8.5.2.3 Discussion of the stable isotope results

The observed isotopic shift during dedolomitization towards lighter $\delta^{18}O$ and $\delta^{13}C$ values in the replacive calcite with respect to the precursor dolomite has been noted by several workers in dedolomites from a variety of diagenetic settings (*e.g.* Magaritz & Kafri, 1981; Budai *et al.*, 1984; Theriault & Hutcheon, 1987).

The similar isotopic compositions of the calcite spar and the uncontaminated dedolomite samples suggest precipitation from fluids of comparable isotopic composition. The average oxygen isotopic value of the dedolomite and calcite spar is about -7 $\delta^{18}O$ and calcite of this composition should be in equilibrium with water of about $\delta^{18}O_{smow}$ = -5 at 25°C (using Fig. 8.16). This value compares well with data of Fig. 8.17, from Yurtsever (1975) in Anderson & Arthur (1983) which shows that the mean annual $\delta^{18}O_{smow}$ value for precipitation in northeast Spain should be about -4 $\delta^{18}O_{smow}$. Thus the oxygen isotopic composition of the calcite spars and dedolomites is broadly consistent with precipitation from modern meteoric water at the latitude of northeast Spain. The variation in oxygen isotope value of the calcite spars and the 'pure' dedolomites results from local differences in fluid composition and/or different reaction conditions. The oxygen isotope composition of meteoric water in the area will vary as a result of seasonal temperature/precipitation fluctuations. Near-surface processes such as evaporite and limestone/dolomite dissolution (releasing ^{18}O from sulphate and carbonate ions) will also alter the isotopic composition of the meteoric-derived groundwater.

The carbon isotope composition of the dedolomitic calcite of about -8 $\delta^{13}C$ is depleted with respect to any of the limestone or dolomite in the area (Fig.s 8.15 and 6.4). Salomons (1975) found a consistent decrease in $\delta^{13}C$ of between 2 and 6 permil,

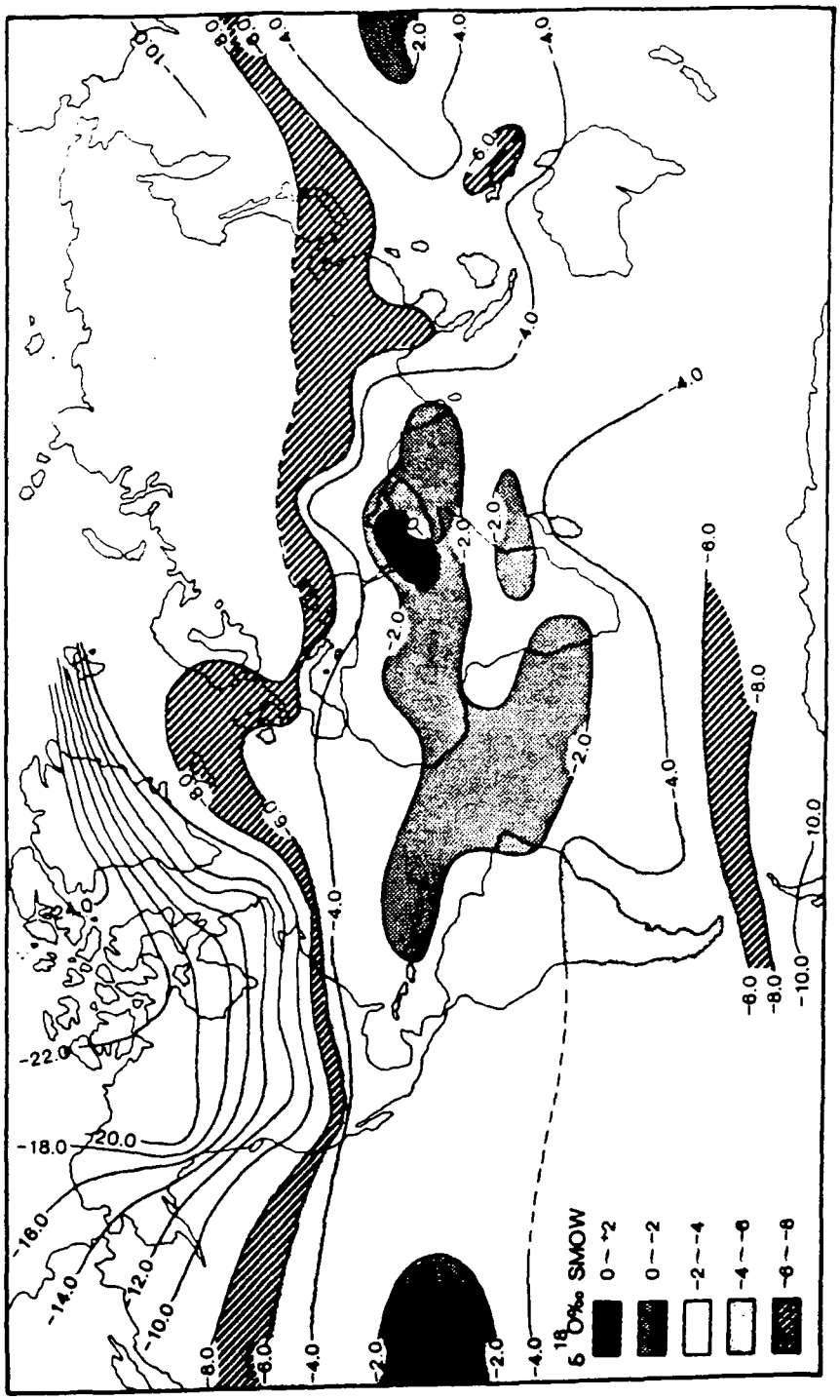

Fig. 8.17. Mean annual $\delta^{18}O$ values of precipitation from the IAEA network stations (from Yurtsever, 1975 in Anderson & Arthur, 1983).

and a decrease in $\delta^{18}O$ of between 2 and 4 permil from parental limestones/dolomites and their derived soils in western Europe. The dedolomitized horizons are locally related to Recent/subrecent karstic and calcrete horizons and the observed depletion of about 10 permil in $\delta^{13}C$ between the local carbonate and the dedolomite/calcite spar is inferred to be a result of near-surface soil-processes in the relatively warm Spanish climate.

The two less negative 'pure' dedolomite samples at -4 $\delta^{13}C$ mentioned in 8.5.4.2 may define part of a 'meteoric calcite line' of relatively invariant ^{18}O coupled with variable ^{13}C (Lohmann, 1988). This geochemical trend has been attributed to variation in the amount of dissolved soil-gas carbon dioxide and to the extent of rock-water interaction. The two 'pure' dedolomitic samples which have less negative carbon isotopic value have a rhombohedral calcite fabric (see Section 8.3.1) preserving the original dolomite mosaic suggesting that calcitization was in a relatively closed system of minor rock-water interaction in a meteoric diagenetic system.

8.5.2.4 Stable isotopic synthesis

Stable isotope results suggest that the pseudomorphic calcite spar after evaporites and dedolomitic calcite were precipitated from fluids of similar isotopic composition, and broadly compatible with modern meteoric water altered by local soil and near-surface dissolution processes.

Dedolomites which have preserved the original dolomitic texture appear to have partially inherited the carbon isotopic composition of the precursor dolomite as a result of the relatively minor rock-water interaction.

8.5.3 Carbonate cation analysis

Carbonate cation analysis was performed by Inductively Coupled Plasma - Atomic Emission Spectrometry (ICP-AES) on dedolomite and calcite spar samples (Appendix 3) from five localities. The dedolomite and calcite spar samples are compared with Lower Muschelkalk limestones in Fig.s 6.1, 6.2, 6.3 and 6.4.

8.5.3.1 Contamination by dolomite

The strontium, iron and manganese concentrations are not linearly related to the calculated dolomite percentage (see Appendix 3) in each sample (Fig.s 8.18, 8.19, 8.20). The eight 'pure' dedolomite samples (less than 10% calculated dolomite percentage) show a range of trace element concentrations with variable amounts of iron, manganese, and strontium, so that the effect of the remnant dolomite in the

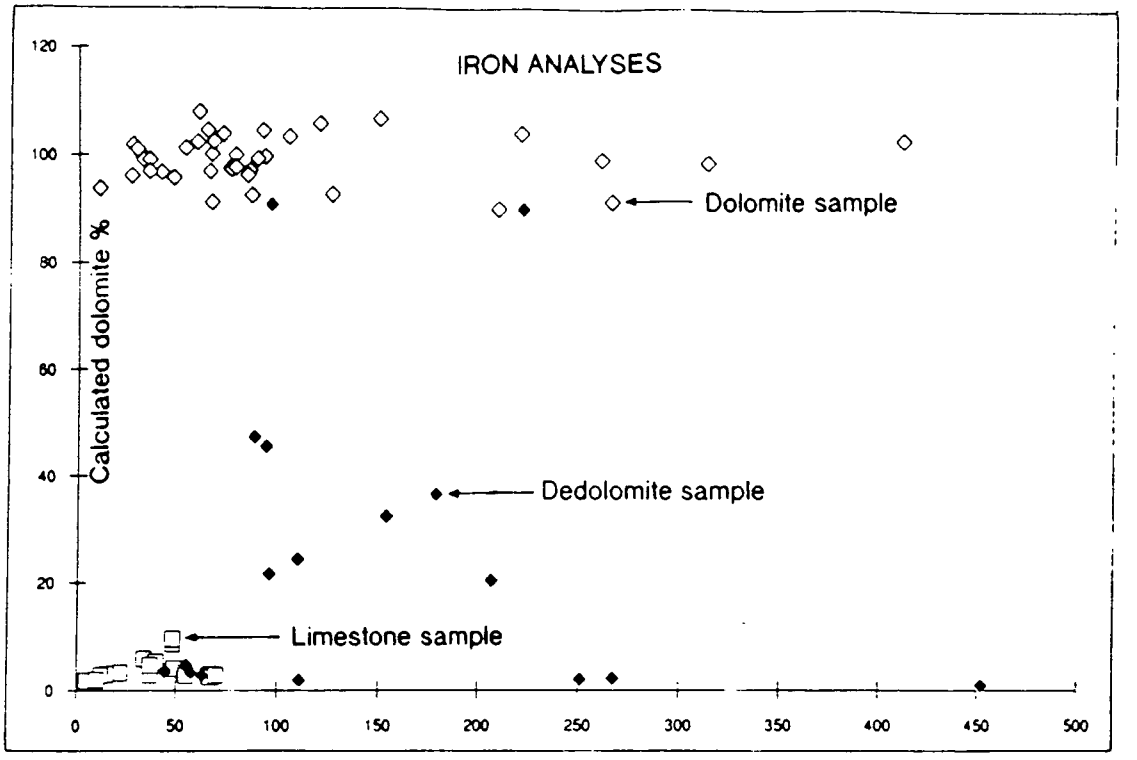

Fig. 8.18. Iron analyses plotted against calculated dolomite percentage for dolomite, limestone and dedolomitic calcite samples.

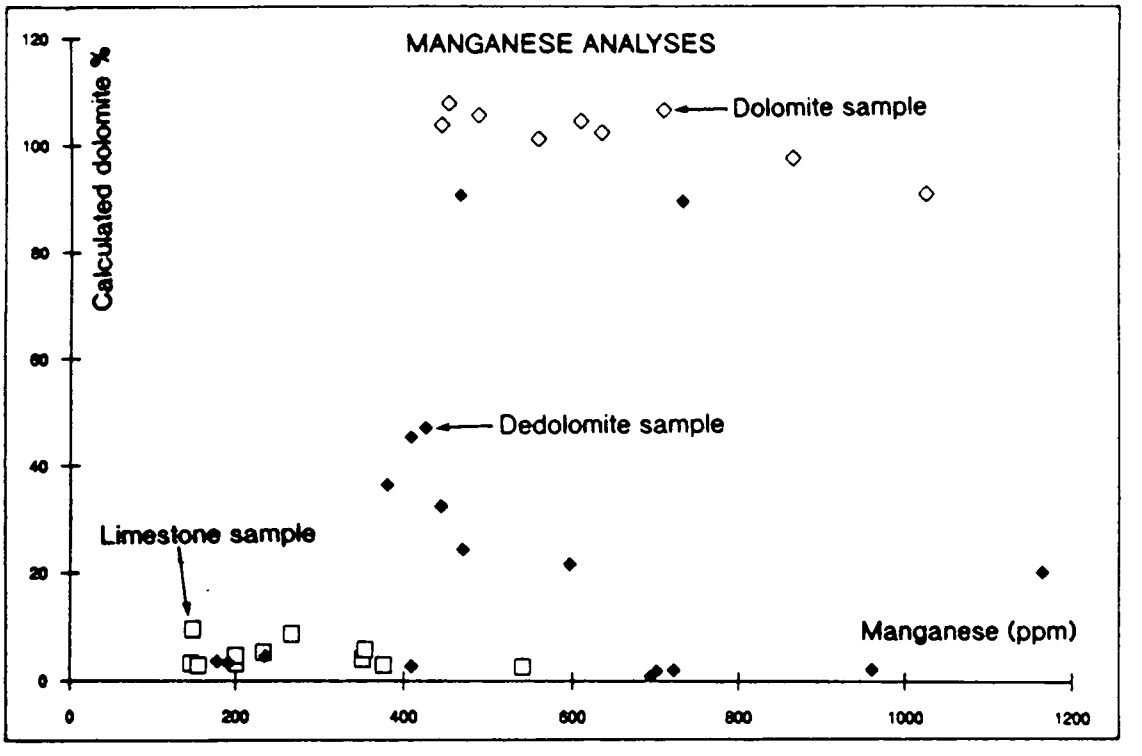

Fig. 8.19. Manganese analyses plotted against calculated dolomite percentage for dolomite, limestone and dedolomitic calcite samples.

contaminated samples cannot be simply quantified.

8.5.3.2 Comparison of dolomite and dedolomite data

The dedolomites generally contain more strontium (*ca.* 120ppm; Fig. 8.20) and more manganese (50-500ppm; Fig. 8.19) than the dolomite samples from the same localities, but a similar amount of iron (100-1000ppm; Fig. 8.18). The calcite spar samples are more depleted in strontium and manganese than most of the dedolomites. Iron concentrations were not available for the calcite spars.

8.5.3.3 Interpretation of carbonate cation analysis

At low activities (or concentrations) and constant temperature and pressure the partitioning of a trace element between liquid and solid phases is given by:

$$(m_t/m_c)_{solid} = D \,.\, (m_t/m_c)_{liquid}$$

(where m=moles, t=trace element, c=major element, D=distribution coefficient). See Land (1980) and Veizer (1983) for further information.

The distribution coefficients for calcite are:

D^{Sr}	= 0.14 at 25°C	(Kinsman, 1969)
	= 0.07 at ca. 40°C	(Katz *et al.*, 1972)
D^{Mn}	= 15 at near-surface	(Pingitore, 1978)
D^{Fe}	= 4	(Ichikuni, 1983)

The distribution coefficients may depend upon the crystal growth rate, any coupled substitution, the nature of the overall reaction (*e.g.* replacement versus cementation), temperature, pressure and pH (as discussed in Barnaby & Rimstidt, 1989). Clay diagenesis and scavenging of trace elements by organic matter may also affect the incorporation of trace elements into a cement phase from a fluid (Machel, 1985; Searl, 1988). Thus, the spread of trace element concentrations may not only reflect local variations in the chemistry of the pore fluid but also differences in the value of the distribution coefficient controlled by the above factors. However, in the following discussion the chemistry of the precipitating fluid is considered to be the main control (the value of the distribution coefficients can vary markedly without affecting the argument).

The Sr/Ca ratio of the liquid which precipitated the dedolomite and calcite spar can be estimated from the measured strontium concentration in the solid using the above equation and the values for D^{Sr}, as argued by Magaritz & Kafri (1981) and shown in Fig. 8.21. Simple dissolution of the limestones or dolomites in the area would produce

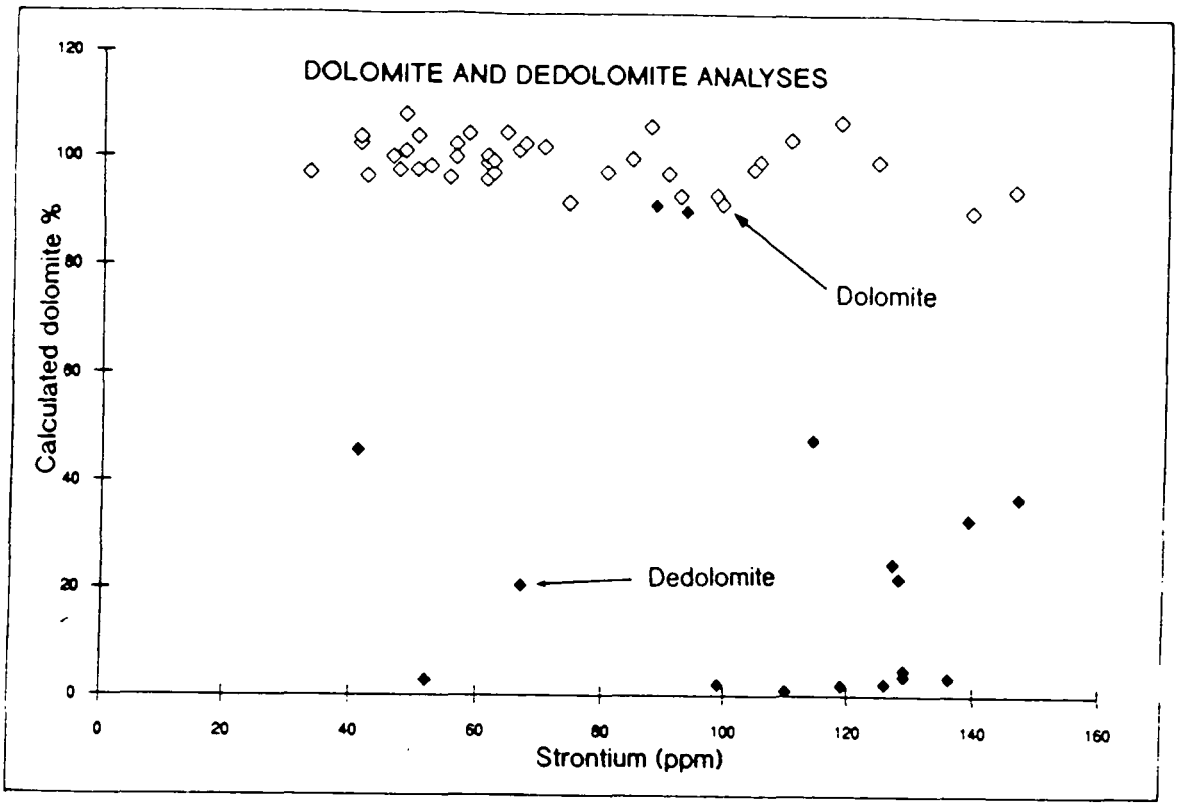

Fig. 8.20. Strontium analyses plotted against calculated dolomite percentage for dolomite, limestone and dedolomitic calcite samples.

	Strontium (ppm)	$(Sr/Ca)_{liquid}$ (calculated using D_{Sr}=0.14 and D_{Sr}=0.07)
Dedolomite	120	9.8×10^{-4} to 19.6×10^{-4}
Calcite spar	50 to 100	4.1×10^{-4} to 16.3×10^{-4}
	Strontium (ppm)	$(Sr/Ca)_{solid}$
Dolomite	40 to 80	0.71×10^{-4} to 1.4×10^{-4}
Limestone	100 to 3000	1.1×10^{-4} to 34.2×10^{-4}
Gypsum	800 to 2500	15.4×10^{-4} to 49×10^{-4}

Fig. 8.21. Table showing the calculation of Sr/Ca ratios for the dedolomite and calcite spar samples and the measured Sr compositions in the dolomites, limestones and gypsum.

a liquid of Sr/Ca ratio equal to that of the solid carbonate. Thus, the calculated Sr/Ca_{liquid} can be compared with the measured Sr/Ca ratio of the dolomites and limestones to assess their involvement in the calcitization (Fig. 8.22). ICPAES analyses of gypsum from outcrops of the Middle Muschelkalk were used to gain the trace element ratios that would be produced in groundwater by dissolution of gypsum (Appendix 3). The values for the Middle Muschelkalk are similar to other ancient evaporite sequences (Butler, 1973, Holser, 1979b; Fig. 8.21).

Similar calculations have been performed for Mn/Ca and Fe/Ca.

i) Consider the Sr/Ca ratios in Fig. 8.22.

Clearly dolomite dissolution is involved before and during the precipitation of the dedolomitic calcite. However, simple dolomite dissolution results in a liquid with too low a Sr/Ca ratio to precipitate the dedolomitic calcite. Therefore, a source of enriched Sr/Ca must also have been dissolved by the liquid. Hence the fluid which precipitated the dedolomitic calcite must also have dissolved the evaporites and/or the strontium-rich limestones prior to dissolution of the dolomite.

Similarly the liquid which precipitated the calcite spar (which did not necessarily involve dolomite dissolution) may have resulted simply from dissolution-reprecipitation of limestone from the Lower Muschelkalk or dissolution of dolomite/low-Sr limestone and sulphate dissolution.

ii) Consider the Mn/Ca and Fe/Ca in Fig. 8.22.

The manganese and iron contents of the Lower Muschelkalk limestones suggest that simple limestone dissolution could not have resulted in the fluid that precipitated the calcite spar and therefore was probably unimportant in the formation of the dedolomitic calcite. Thus, evaporite dissolution is the only process which could combine with dolomite dissolution to result in the observed trace element concentration in the dedolomite calcite.

To some extent the low iron and manganese concentrations in the dedolomitic calcite are probably due to precipitation of iron oxides and hydroxides which give the characteristic 'rusty' colour. The reddening indicates an oxidising fluid. The iron oxides may be the by-product of calcitization of ferroan dolomite (Franck, 1981). The reddening is generally pervasive and not just limited to weathered surfaces suggesting that this has been a phreatic process and probably related to the actual dedolomitization.

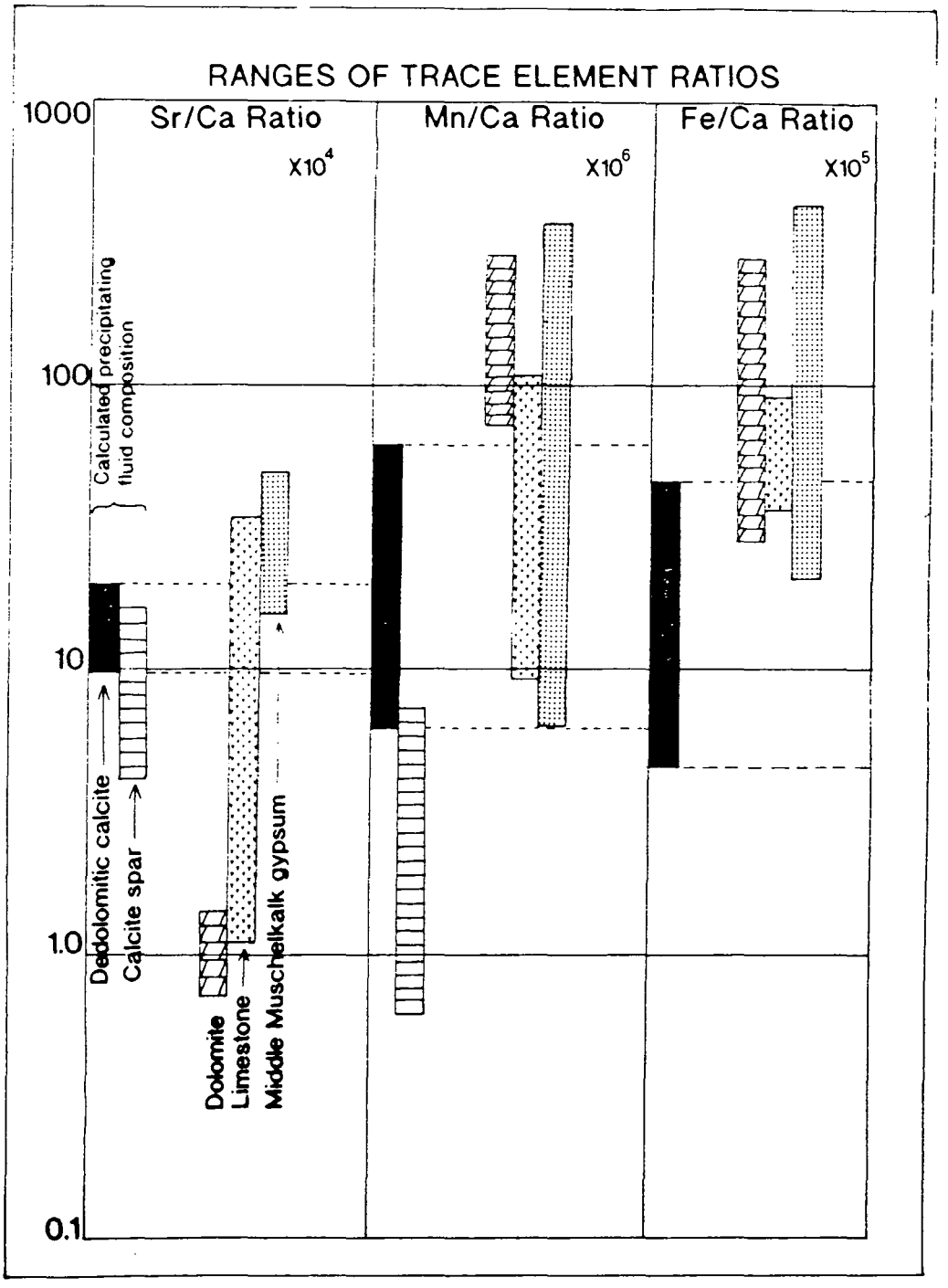

Fig. 8.22. Sr/Ca, Mn/Ca and Fe/Ca trace element ratios in fluids produced by dissolving Lower Muschelkalk dolomite, limestone and Middle Muschelkalk gypsum compared with calculated trace element ratios required to precipitate dedolomitic calcite and calcite spar with the observed compositions.

8.5.3.4 Mass balance calculation

A simple mass-balance calculation (see Appendix 2.3) indicates that one volume of dolomite, given complete reaction, may be calcitized by calcium resulting from the dissolution of 1.2 volumes of gypsum or 0.7 volumes of anhydrite. Thus, given the abundance of sulphates both within, and stratigraphically above and below the Lower Muschelkalk the provision of the necessary calcium ions for dedolomitization by sulphate dissolution is clearly a feasible process

8.5.3.5 Cation analysis synthesis

Cation analyses show that the dedolomitic calcite contains variable amounts of iron, manganese and strontium. The spread of trace element concentrations reflects variations in fluid chemistry and/or conditions during precipitation. The measured trace element concentrations of the dedolomitic calcite, pseudomorphic calcite spar, dolomite and limestones, and Middle Muschelkalk evaporites suggest that sulphate dissolution was an essential step in the formation of the calcitizing fluid.

Mass-balance calculations indicate that even minor evaporite dissolution would provide ample calcium ions for the dedolomitization reaction.

8.6 TIMING OF DEDOLOMITIZATION

The dedolomitization of the Lower Muschelkalk of the Catalan Coastal Ranges appears to have been related to uplift and associated meteoric-derived groundwaters. The exposed Triassic of the Catalan Coastal Ranges generally subsided during the Mesozoic and was then uplifted during the Tertiary (Fig. 2.11; Section 2.7). The principal phase of uplift was the early Paleogene and resulted in local exposure of the Triassic. Subsequently, thick Paleogene sediments were deposited unconformably on the Triassic in the Ebro Basin and in the northern Catalan Coastal Ranges. During the Neogene some areas continued to subside to produce grabens filled with Neogene sediments, however in the areas of Triassic outcrop in the Catalan Coastal Ranges there was renewed uplift and erosion. The presence of sulphates in the Lower Muschelkalk of the subsurface of the Ebro Basin suggests that sulphate dissolution did not occur during the early Paleogene uplift. Hence the evaporite dissolution of the Lower Muschelkalk of the Catalan Coastal Ranges has occurred during the Neogene uplift (*i.e.* since about 25Ma B.P.).

Both phreatic and vadose textures occur in the calcite pseudomorphs after evaporites, suggesting that dissolution and replacement was occurring above and below the water

table and probably in oxidising and reducing conditions.

The stable isotopic composition of the dedolomites, whilst compatible with modern meteoric water, does not tightly constrain the timing of the calcitization. The process may have been occurring for thousands to millions of years in the meteoric phreatic environment since the onset of Neogene uplift.

8.7 DEDOLOMITIZATION SYNTHESIS

i) Dedolomitization has affected different dolomite facies and resulted in a wide variety of textures and fabrics. Ferroan dolomite has been preferentially calcitized.

ii) Evaporite minerals (gypsum and anhydrite) were dissolved and replaced on uplift in the near-surface meteoric phreatic and vadose environments to give collapse breccias and calcite-quartz pseudomorphs.

iii) Stable isotope compositions indicate that the pseudomorphic calcite spar and dedolomitic calcite were precipitated from fluids of similar isotopic composition, compatible with modern meteoric water altered by locally-controlled soil and near-surface dissolution processes.

iv) Cation analysis confirms that dissolution of evaporites was an essential source of calcium and trace element ions for the dedolomitizing fluid and that simple dissolution of limestone/dolomite by meteoric water could not have produced a liquid capable of precipitating calcite with the observed trace element concentrations.

v) Dedolomitization has occurred after the onset of Neogene uplift of the Catalan Coastal Ranges.

8.7 DEDOLOMITIZATION DISCUSSION

The Catalan Basin dedolomites formed as a result of near-surface processes and dissolution of sulphates by meteoric-derived waters. The Triassic of the Catalan Coastal Ranges has been brought into the meteoric phreatic and vadose zones as a result of post-Paleogene uplift and erosion and this has resulted in dedolomitization. Sulphate dissolution is clearly a requirement for the formation of these dedolomites and thus by analogy the presence of dedolomites may be expected at unconformities through ancient dolomites particularly in peritidal-evaporite related dolomitic sequences where the unconformity was developed in a non-arid climate. The presence of dedolomites, together with karstic processes may enhance porosity-permeability at such unconformities in the subsurface.

CHAPTER 9: GENERAL CONCLUSIONS

1. The Triassic of Spain generally rests unconformably upon Paleozoic basement. The most easterly and marine-influenced of the principal Triassic facies belts of northeast Spain is the Mediterranean Triassic which occurs in the Catalan Coastal Ranges (Catalan Basin), the eastern Iberian Ranges (Valencia-Cuenca Basin) and in the subsurface of much of the Ebro Basin. (see Section 2.1)

2. The Mediterranean Triassic consists of packages of siliciclastics and evaporites (Buntsandstein, Middle Muschelkalk, Keuper) interposed with carbonates (Lower Muschelkalk, Upper Muschelkalk, Imon Formation). The siliciclastics and evaporites show considerable regional thickness and facies variations partly related to syntectonic faulting whereas the carbonates are more uniform in thickness and deposited during times of relative quiescence. (see Section 2.4)

3. The Lower Muschelkalk is the lowermost carbonate horizon of the Mediterranean Triassic of northeast Spain and rests upon red Buntsandstein siliciclastics. An evaporite-carbonate-lutite complex is locally developed at the top of the Buntsandstein below the Lower Muschelkalk. The Lower Muschelkalk is sharply overlain by Middle Muschelkalk evaporites and shales. (see Section 2.4.3)

4. The Lower Muschelkalk is Anisian in age and reaches a maximum thickness of about 100m in the Catalan Coastal Ranges and thins to the north and west until it becomes absent in the Iberian Triassic facies. (see Section 2.5)

5. The Lower Muschelkalk was buried under 2-3km of Jurassic and Cretaceous sediments during the Mesozoic and was uplifted and locally exposed during the early Paleogene. Subsidence of the Ebro Basin occurred during the rest of the Paleogene and locally during the Neogene and the Triassic was buried under thick Tertiary deposits. In the Catalan Coastal Ranges and eastern Iberian Ranges uplift occurred during the Neogene and the Lower Muschelkalk was exposed in hills separated by Neogene basins. (see Section 2.6)

6. The Lower Muschelkalk of the Catalan Coastal Ranges is considered to have been deposited on a homoclinal carbonate ramp and consists of four units: the El Brull Unit (peritidal dolomites and limestones); the Olesa Unit (locally dolomitized bioclastic limestones); the Vilella Baixa Unit (locally dolomitized, poorly oxygenated lagoonal to oolitic and bioclastic sand-belt deposits); and the Colldejou Unit (Lower Member: only locally developed subtidal to intertidal limestones and dolomites; Upper Member: intertidal to supratidal dolomicrites). The four units can be recognised in the Triassic of the subsurface of the Ebro Basin adjacent to the Catalan Basin and in the

southeast of the Valencia-Cuenca Basin. However, towards the northwest as the Lower Muschelkalk thins, the Olesa Unit and Vilella Baixa Unit pinch out and the succession becomes dominated by peritidal facies. Proximity to a locally clastic shoreline is indicated by the increase in siliciclastics. (see Sections 3.2, 3.3, 3.4, 4.4)

7. Lateral facies changes in the Olesa Unit and Vilella Baixa Unit of the Catalan Basin from lagoonal-dominated facies in the northeast to sandbelt deposits in the southwest indicate a downramp transition. Paleoslopes on the Lower Muschelkalk ramp were probably less marked than in the Upper Muschelkalk. (see Section 3.6)

8. The El Brull Unit, Olesa Unit and Vilella Baixa Unit represent a broadly transgressive facies pattern and are interpreted as a Transgressive Systems Tract (TST-1). The Colldejou Unit is interpreted as a Highstand Systems Tract (HST-1). The top of the Lower Muschelkalk is interpreted to be a sequence boundary and the Middle Muschelkalk evaporites and shales to be the Lowstand Systems Tract (LST-2) of the next depositional sequence. (see Section 3.7)

9. Paleokarstic surfaces are common in the Vilella Baixa Unit and the Lower Member of the Colldejou Unit. Underlying oolites of the Vilella Baixa Unit are commonly pisolitic with vadose compaction features and have undergone local dissolution and formation of oomoldic porosity later occluded by coarse ferroan calcite spar. The meteoric-stabilized horizons underneath paleokarstic surfaces appear to have resisted subsequent dolomitization. (see Sections 4.3, 4.6.1, 4.10)

10. Subsurface paleokarsts covered by a red silty marl and locally associated with Pb-Zn mineralization are present in the Lower Muschelkalk particularly in the northern Catalan Coastal Ranges. The paleokarsts are developed where the base-Paleogene unconformity truncates the Triassic and are best developed where the unconformity actually cuts the Muschelkalk. The base-Paleogene unconformity is considered to represent the ground surface to which the subsurface paleokarsts are related. The subsurface paleokarsts locally separate dolomite above from limestone below and are interpreted to be exploiting the solubility difference between limestone and dolomite. Dolomitization occurred prior to the formation of the subsurface paleokarsts. (see Section 4.6.2)

11. Sulphates (gypsum and anhydrite) are common in the Lower Muschelkalk of the subsurface of the Ebro Basin and their former presence can be inferred at surface outcrop from collapse breccias and pseudomorphs. Most of the sulphates occur in the peritidal facies and are considered to be penecontemporaneous with deposition. Other sulphates are unrelated to the depositional environment and are interpreted to have

been precipitated from a diagenetic dolomitizing hypersaline brine. (see Sections 4.8, 8.4)

12. Sulphate dissolution and replacement occurred during two distinct phases. The early phase is only of local importance and occurred during burial and resulted in pseudomorphs consisting of baroque dolomite, ferroan calcite. and locally quartz and fluorite and is related to hydrothermal mineralization. The more important late phase was during uplift into locally vadose conditions and resulted in geopetal crystal silt infills and coarse calcite spar cements which are zoned under cathodoluminescence.

13. Silicification resulting in chert nodules, veins and lenses and locally selective replacement of bioclasts is quite common in dolomitized and undolomitized parts of the Lower Muschelkalk and is interpreted as a late diagenetic process occurring post-dolomitization and probably related to uplift and near-surface meteoric-derived groundwaters. (see Section 4.9)

14. Three types of dolomite can be recognised petrographically and geochemically in the Lower Muschelkalk of the Catalan Basin and Valencia-Cuenca Basin and are inferred to be present in the subsurface of the Ebro Basin. The peritidal dolomite is fine-grained, preserves fine-scale sedimentary features and occurs in the Upper Member of the Colldejou Unit and in the peritidal facies of the El Brull Unit. The fabric-replacive dolomite is a replacement after near-normal marine limestones and occurs stratigraphically beneath the peritidal dolomite of the Colldejou Unit. The fabric-replacive dolomite is variable in extent and its lower boundary is a bedding-discordant dolomite front which separates limestone below from dolomite above indicating that the dolomitizing fluid had at least a component of downwards migration. The baroque dolomite is of only local importance and generally occurs as a cement lining fractures and within early-formed pseudomorphs after sulphates. Baroque dolomite mosaics are locally important especially in the Valencia-Cuenca Basin. (see Sections 5.2, 5.3, 5.4, 5.9)

15. The fabric-replacive dolomite exhibits a wide range of petrographic textures from fabric-preservative fine-grained dolomicrites to coarse-grained fabric-destructive xenotopic to idiotopic mosaics. The degree of fabric preservation appears to be at least in part related to variation in the original mineralogy with aragonitic precursors tending to be better preserved than calcitic. (Section 5.5)

16. The petrography and depositional setting of the peritidal dolomite suggest an original mineralogy of aragonite, high-Mg calcite and probably some penecontemporaneous dolomite. (see Section 5.6)

17. Petrography and field relations indicate that the fabric-replacive dolomitization occurred during shallow-burial prior to the onset of any considerable chemical compaction. (see Section 5.10)

18. The limestone geochemistry indicates depletion of strontium and ^{18}O and enrichment of iron and manganese during diagenesis attributable to stabilization in the near-surface during shallow-burial in a meteoric (and possibly brackish) phreatic, reducing environment. The least depleted values indicate an isotopic composition for marine precipitates during the Muschelkalk of around -3 to -4 $\delta^{18}O$. (see Section 6.2)

19. The fabric-replacive dolomite is consistently depleted in ^{18}O and strontium with respect to the overlying peritidal dolomite. The magnitude of the difference and the absolute values vary between different localities. Iron and manganese show different trends within the peritidal dolomite and fabric-replacive dolomite, commonly constant or decreasing downwards in the peritidal dolomite and then increasing downwards in the fabric-replacive dolomite. Burial recrystallization does not appear to have been a major influence on the fabric-replacive dolomite and peritidal dolomite geochemistry. (see Section 6.3)

20. The baroque dolomite clearly cross-cuts the fabric-replacive dolomite and peritidal dolomite and represents a distinct late dolomitization process. The baroque dolomite is generally depleted in ^{18}O and greatly enriched in iron and manganese with respect to the fabric-replacive dolomite and peritidal dolomite. (see Section 64., 6.5)

21. The peritidal dolomite is considered to be the result of dolomitization of unstable aragonite-rich, ^{18}O-rich sediments by downward-migrating hypersaline brines mainly derived from the Middle Muschelkalk evaporites. The fabric-replacive dolomite is considered to have resulted from the same downward-migrating brines reacting with a principally calcitic, meteoric-stabilized precursor. The petrographic and geochemical variations within the fabric-replacive dolomite are due to grain-size, mineralogy and permeability contrasts within the precursor. The consistent geochemical contrasts between the peritidal dolomite and fabric-replacive dolomite are due to differences in the original mineralogies of the precursor. (see Section 7.4)

22. The baroque dolomite was the consequence of only locally important dolomitization by late, highly-reducing iron and manganese-rich hydrothermal fluids which principally migrated through fractures within the limestones and dolomites and is associated with sulphate reduction and hydrothermal mineralization. The geochemical source for the baroque dolomite was local pressure dissolution of the surrounding carbonates. (see Section 7.4)

23. The fabric-replacive dolomite and peritidal dolomite can be usefully considered in terms of the sequence stratigraphic framework of the Lower Muschelkalk enabling easier comparison with other examples of reflux dolomitization. The main phase of dolomitization of the Lower Muschelkalk resulted from downwards brine migration from the lower part of the LST-2 through the underlying HST-1 to give the peritidal dolomite and into the meteoric-stabilized TST-1 to result in the fabric-replacive dolomite. Climate is an important control on the style of diagenesis associated with sequence boundaries. Dolomitization by brines will be common in a semi-arid climate whereas meteoric-weathering and karstification will be more prevalent in humid conditions.

24. Calcitization has locally affected both the fabric-replacive dolomite and peritidal dolomite and resulted in a wide variety of petrographic textures which principally depend upon the precursor dolomite fabric. Ferroan dolomite has locally been preferentially calcitized. (see Sections 8.2, 8.3).

25. The calcitized dolomites are geochemically distinct from limestones and dolomites and are considerably depleted in ^{13}C and slightly depleted in ^{18}O but unusually enriched in strontium with respect to the precursor dolomites. The comparable isotopic compositions of the calcitized dolomites and the late calcite spar of the pseudomorphs after evaporites formed during uplift suggests precipitation from similar groundwaters. Trace element concentrations infer evaporite dissolution was an essential step in the formation of the calcitizing fluid. (see Section 8.5)

26. Calcitization of the dolomites of the Lower Muschelkalk is considered to have occurred during Neogene uplift as a result of dissolution of evaporites in the phreatic and vadose environments by meteoric-derived waters affected by locally-controlled pedogenic and near-surface dissolution processes. Similar calcitization processes may be expected to have occurred below unconformities through ancient evaporite-related dolomite sequences where the unconformity was developed in a non-arid climate. (see Sections 8.6, 8.7).

APPENDIX 1: MAP REFERENCES FOR ALL LOCALITIES

A:1.1 CATALAN BASIN LOCALITIES

Grid references based on the IGME 1:50,000 *Segunda Serie* geological maps for the localities in the Catalan Coastal Ranges are given below.

Name	Grid Ref.	IGME Sheet	Number
Pontons	10360769	Vilafranca del Penedes	419, 35-16
Pratdip	09840727	Reus	472, 33-18
Colldejou	09840731	"	"
Torre de la Fontaubella	09810734	"	"
Falset	09800737	"	"
Argentera	09830735	"	"
Cabra del Campo	10150765	Montblanch	418, 34-16
Puig Gracios	10930805	La Garriga	364, 37-14
Centelles	10910815	"	"
El Brull	10950816	"	"
Vilaplana	09970748	Cornudella	445, 33-17
Arboli	09890746	"	"
Prades	09910753	"	"
Ciurana	09860749	"	"
Castelvell	10000741	"	"
Prades Cliff	09890755	"	"
Capcanes	09750732	Mora de Ebro	471, 32-18
Guiamets	09720731	"	"
Masroig	09720734	"	"
Olesa	10670788	Sabadell	392, 36-15
Vacarisses	10690789	"	"
Pauls	09440710	Horta de San Juan	496, 31-19
Palleja	10730772	Hospital de Llobregat	420, 36-16
Corbera	10660773	"	"

La Riba	10060757	Valls	446, 34-17
Vilella Baixa	09700745	Flix	444, 32-17
Begues	10710762	Prat de Llobregat	448, 36-17
Rojals	10020761	Espluga de Francoli	417, 33-16

A:1.2 VALENCIA-CUENCA BASIN LOCALITIES

The eastern Iberian Ranges localities are given in terms of latitude and longitude from a Michelin 1:400,000 sheet of *North East Spain: Catalunya, Aragon-Baleares* (sheet no 443).

Serra	0°25'E 39°42'N
Chelva	0°59'E 39°47'N
Malpaso	1°27'E 39°50'N
Barranco de la Hoya	1°38'E 40°02'N
Albarracin	1°27'E 40°24'N

A:1.3 EXPLANATION OF GRAPHIC LOG SYMBOLS

The symbols are taken from the 'Standard Legend' of Shell International Petroleum Exploration and Production Departments, 1976 edition.

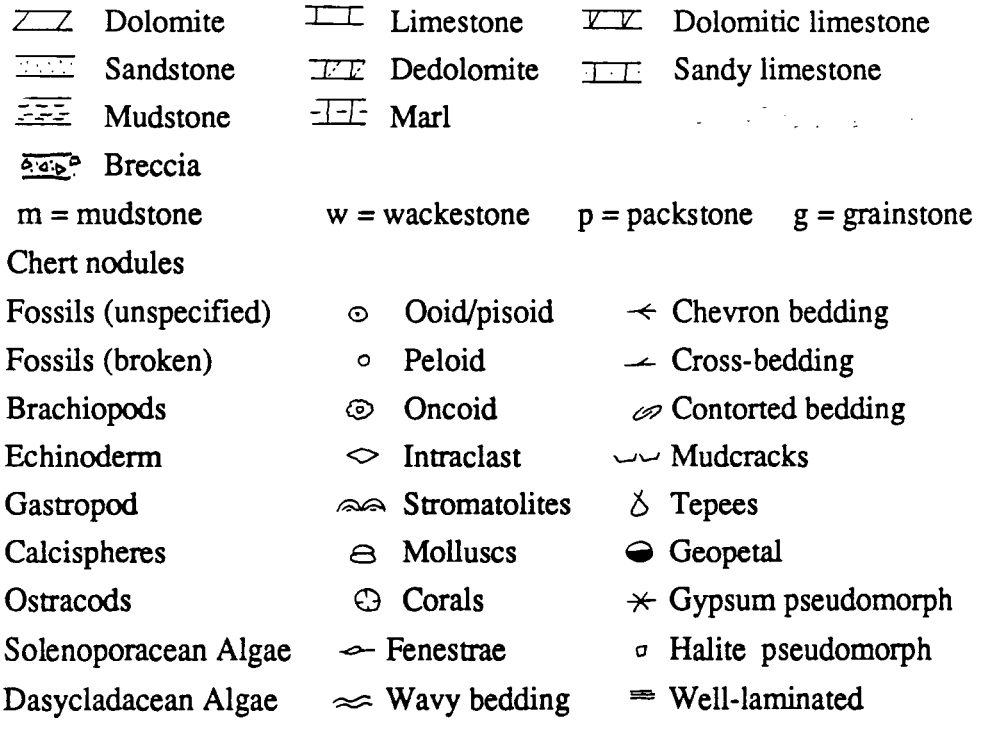

APPENDIX 2: MASS-BALANCE CALCULATIONS

A:2.1 RATIO OF CALCIUM SULPHATE TO REPLACIVE DOLOMITE

This calculation considers the amount of calcium sulphate (gypsum and anhydrite) that could be produced in a perfect closed system from a given volume of seawater relative to the amount of dolomite that could be produced by replacement of calcium carbonate by magnesium from the same volume of seawater. The calculation assumes i) all the calcium in seawater forms gypsum or anhydrite, ii) all magnesium forms stoichiometric dolomite, iii) a modern composition for seawater.

Modern seawater contains: Mg = 1290ppm, Ca = 411ppm (Veizer, 1983)

[Gypsum] = $[CaSO_4.2H_2O]$ = 172

[Anhydrite] = $[CaSO_4]$ = 136

[Dolomite] = $[CaMgCO_3]$ = 184

[Mg] = 24.3

[Ca] = 40.1

ρ(gypsum) = 2.34 (Deer *et al.*, 1966)

ρ(anhydrite) = 2.95 "

ρ(dolomite) = 2.90 "

(where [xxxx] denotes relative formula mass or relative atomic mass and ρ = density)

Therefore,

Volumes (Dolomite : gypsum) = 1290/24.3*184/2.90 : 411/40.1*172/2.34
= 4.5 : 1

Volumes (Dolomite : anhydrite) = 1290/24.3*184/2.90 : 411/40.1*136/2.95
= 7 : 1

A:2.2 RATIO OF CHLORITE TO DERIVED DOLOMITE

This calculation considers the volume of chlorite that would be required to provide the magnesium by loss of loosely bound ionic magnesium ions to produce one volume of dolomite. The calculation considers a range of chlorite compositions to give the end-members for the chlorite volume. The calculation assumes stoichiometric dolomite composition and a closed system.

Chlorite contains = 24 to 4% MgO (Deer *et al.*, 1966)

Chlorite relative density = 2.6 to 3.3 (Deer *et al.*, 1966)

Dolomite contains = $[MgO]/[CaMgCO_3]$ = 22% MgO

Dolomite relative density = 2.9 (Deer *et al.*, 1966)

Consider $1m^3$ of dolomite = 2900Kg
= 630Kg of MgO
= 2600Kg to 14,400Kg of chlorite
= $1m^3$ to $5m^3$ of chlorite

However, assuming a more realistic 20% loss of Mg from any chlorite then 1 volume of dolomite requires 5 to 25 volumes of chlorite (depending upon composition).

A:2.3 AMOUNT OF GYPSUM REQUIRED TO CALCITIZE DOLOMITE

This calculation considers the volume of gypsum or anhydrite required to provide the calcium in order to convert one volume of dolomite to calcite by the following reaction.

$$CaMg(CO_3)_2 + CaSO_4 = 2CaCO_3 + MgSO_4$$

Therefore, assuming perfect reaction in a closed system and using the values for relative formula mass and densities for dolomite, gypsum and anhydrite given in A:2.1.

Moles of Dolomite : gypsum : anhydrite	=	1	:	1	:	1
Mass of Dolomite ; gypsum ; anhydrite	=	184	:	172	:	136
Volume Dolomite : gypsum : anhydrite	=	184/2.90	:	172/2.34	:	136/2.95
	=	1.0	:	1.2	:	0.7

APPENDIX 3: CARBONATE CATION CHEMISTRY ANALYSIS

A:3.1 INTRODUCTION

Trace and major cation analysis was carried out for limestones and dolomites from the study-area. Two techniques were used: Inductively Coupled Plasma Atomic Emission Spectrometry (ICPAES) and Atomic Absorption Spectrophotometry (AAS; Tucker, 1988; Robinson, 1980; Angino & Billings, 1972).

ICPAES was used for the majority of the analyses owing to the rapidity and ease of the method together with small required sample size. AAS was much slower but did provide data for sodium and iron which were not always measurable on the ICPAES.

A:3.2 ICPAES ANALYSIS

A:3.2.1 Sample preparation

The sampling techniques were the same as those used as for isotopic analysis and are described in A:4.2.

A:3.2.2 Analytical method

An accurately determined (to 0.1mg) mass of about 40.0mg of oven-dried powder was reacted with 5mL of 10% HCl and placed in an oven at 60°C for two hours and then 5mL of deionised water was added to each sample. Blanks and standards (spec-pure calcium carbonate, calcite) were prepared in a similar way.

The solutions were run on an ICPAES instrument at RHBNC, Egham and the $CaCO_3$ and laboratory standards were run every ten unknowns to check for drift.

Comparison of analyses of samples of spec-pure calcite prepared as above and those prepared in exactly the same way but with rapid reaction under room conditions in a few minutes (instead of the two hours in the oven) were identical (within analytical error) and thus evaporation of solution during the oven-warming was negligible. Hence, the sample volume could be taken as 10mL.

A:3.2.3 Data Correction

The ICPAES measures wavelength intensity and these are processed on-line to give

concentrations (assuming 100mg of sample in 10mL of solution). The ICPAES output was of the form:

sample	CaO(wt%)	MgO(wt%)	Fe_2O_3(wt%)	Mn(ppm)	Sr(ppm)
x	CAO	MGO	FE2O3	MN	SR

and for each sample there is a mass of sample (dissolved in 10mL) in mg = MASS.

A SPSS-X statistics program was written to convert the above to :

CARBPCT = % carbonate fraction (assuming all Ca and Mg are from calcite and/or stoichiometric dolomite)

DOLPCT = % dolomite fraction (assuming that all the Mg is from stoichiometric dolomite and that there is no high-Mg calcite)

DOLVCCT = % dolomite in the carbonate fraction

FES, MNS, SRS = Fe, Mn, Sr expressed as ppm of the carbonate fraction

and these were calculated as follows:

CARBPCT = (CAO * [$CaCO_3$]/[CaO] + MGO * [$MgCO_3$]/[MgO]) * 100/MASS
= (CAO * 1.784 + MGO * 2.092) * 100/MASS

DOLPCT = (MGO * [$CaMg(CO_3)_2$] / [MgO]) * 100/MASS
=MGO * 4.575 * 100/MASS

DOLVCCT = DOLPCT/CARBPCT * 100

FES = FE2O3 * 100/MASS * 100/CARBPCT * [FE2O3]/[FeO] * 10000
= FE2O3 * 100/MASS * 100/CARBPCT * 3497

MNS = MN * 100/MASS * 100/CARBPCT

SRS = SR * 100/MASS * 100/CARBPCT

(where [$CaCO_3$] denotes the relative formula mass of calcite *etc*).

A: 3.2.4 Error Estimation

Drift was found to be negligible and reproduceability was excellent. The following values

are on-line calculations of concentrations for 15 KC11 standard determinations (one every 10 unknowns) during one analysis session:

KC11	CaO	= 6.76 +/- 0.06 %
	MgO	= 4.17 +/- 0.04 %
	Fe_2O_3	= 8.72 +/- 0.08 %
	Mn	= 1078 +/- 8 ppm
	Sr	= 372 +/- 4 ppm

Therefore error at this stage is *ca.* 1%. The estimated error in the CARBPCT is ca. 3% leading to an error in DOLVCCT of *ca.* 6%. The error in FES, MNS, and SRS is estimated to be *ca.* 5%.

A:3.2.5 ICPAES results

ICPAES analytical results are given in tables in Appendix 6.

A:3.3 AAS CATION ANALYSIS

A:3.3.1 Sample preparation

All the samples were prepared by powdering small, clean, whole-rock chips using a tungsten carbide ball-mill.

A:3.3.2 Analytical method

An accurately determined mass of about 0.2g of oven-dried powdered sample was digested in 25mL of 10% HCl in an oven at 60°C for 2 hours and then made up to 50mL with deionised water in a standard flask. Samples were then diluted to a range of concentrations and analysed by interpolation between deionised water and elemental standard solutions on a Perkin-Elmer AAS instrument at Durham University for Na, Sr, Fe, Mn, Ca. and Mg concentrations using standard operating conditions. Blanks were prepared in a similar way.

A:3.3.3 Data correction

The measured concentrations were normalised in a similar way to the ICPAES data.

A:3.3.4 Error estimation

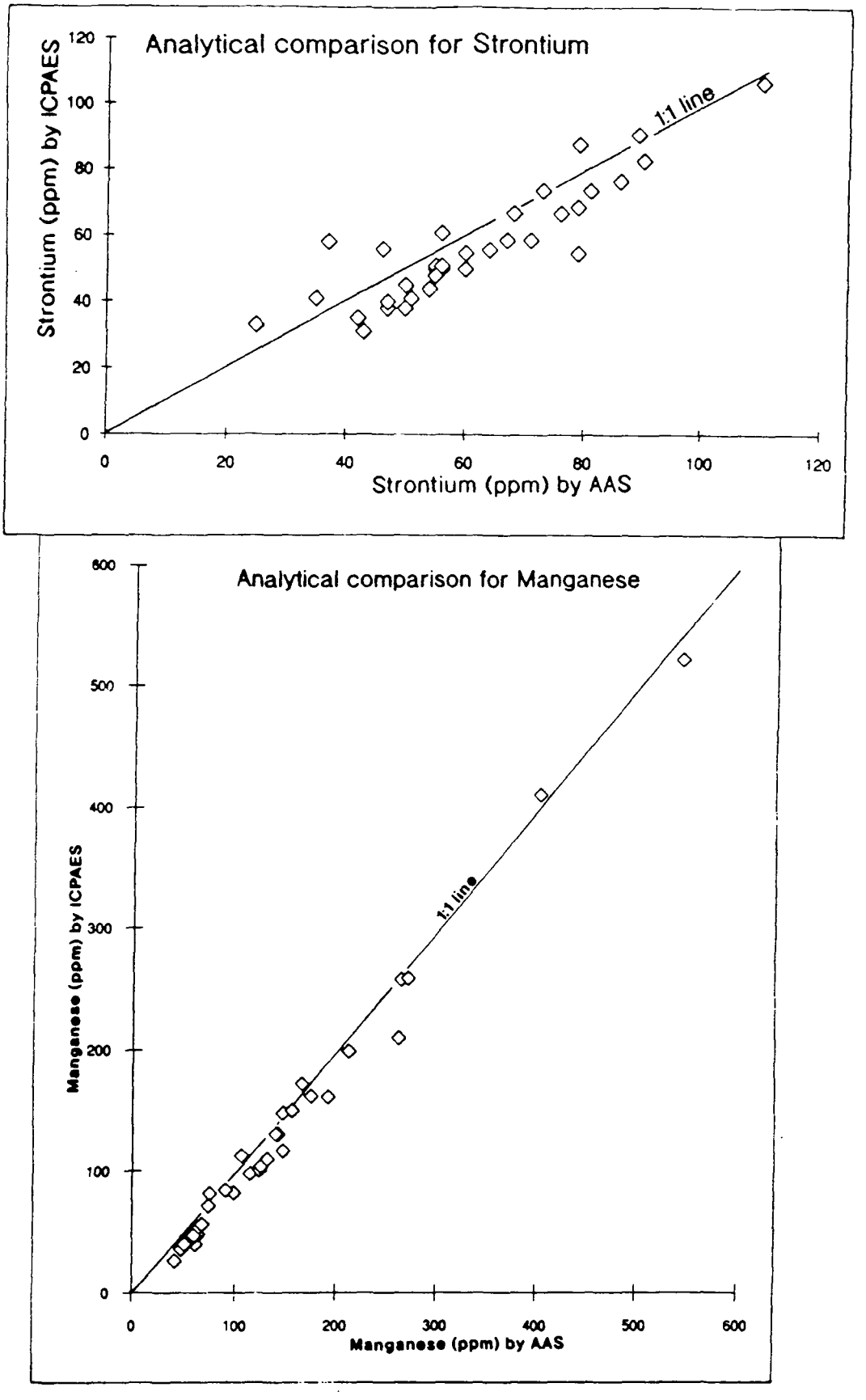

Fig. A:3.1. Comparison of AAS and ICPAES analyses for strontium and manganese in the same samples from Falset and Colldejou localities.

The repeatability of the AAS analyses, especially for Ca, Mg and Sr analyses was sometimes erratic owing to machine problems. A comparison of the same analyses by ICPAES and AAS for Sr and Mn determinations allow a visual estimation around the ideal 1:1 gradient line (Fig. A:3.1). The scattter is greater for the Sr than for the Mn and this is considered to be mostly due to fluctuations in the AAS measurements.

A:3.3.4 AAS results

The AAS results are shown in tables in Appendix 6.

A:3.4. MIDDLE MUSCHELKALK SULPHATE SAMPLES

Samples of the Middle Muschelkalk evaporites were collected at Colldejou locality and analysed by ICPAES for major and trace elements in a similar way to the carbonate samples described above. The results are given here after normalisation to 100% sulphate.

Sample	Lithology	Fe (ppm)	Sr (ppm)	Mn (ppm)
C38b	Speckled gypsum	2142	2376	1700
C38a	Clean white gypsum	595	914	128
C40	Clean white gypsum	70	2241	3
C41	Brown, speckled gypsum	2142	2376	1700
C39	Marly sulphate	2177	1167	152

APPENDIX 4: STABLE ISOTOPIC ANALYSIS

A:4.1 NOTATION

All carbon and oxygen isotopic compositions are reported relative to the PDB international standard in permil ($^{o}/_{oo}$) using the δ notation :

$$\delta\,(x) = \{\, R(x) - R(std) \,\}/\, R(std) \;\times\; 1000$$

where $R(x) = {}^{13}C/{}^{12}C$ or ${}^{18}O/{}^{16}O$ sample

and $R(std) = {}^{13}C/{}^{12}C$ or ${}^{18}O/{}^{16}O$ standard = PDB

Isotopic fractionation between two substances A and B during some physico-chemical process is expressed as a fractionation factor, $\alpha_{A\text{-}B}$

$$\alpha_{A\text{-}B} = R(A)/R(B) = \{1000 + \delta(A)\}/\{1000 + \delta(B)\}$$

A:4.2 SAMPLING METHOD

Isotopic analysis of carbonates was performed after petrographical study and generally after cation analysis. Various sampling methods were used:
i) Powdering of small, clean whole-rock chips using a tungsten carbide ball mill.
ii) Drilling with a hand-held dentist drill (0.5 - 1.0mm tungsten carbide burr) on sawn faces of hand specimens or on thick (250micron) sections.
iii) Scratching using a pin-chuck mounted needle from thick (250micron) sections.

Method i) for micritic limestones and dolomitic mudstones.
Method ii) for sampling particular areas of hand specimens and calcite veins.
Method iii) for sampling bioclasts and thin veins.

A:4.3 ANALYTICAL METHOD

About 10mg of carbonate powder were left for upto 24 hours to completely react under vacuum with 4mL of anhydrous 100% phophoric acid in a temperature bath at 25°C (calcites) or 55°C (dolomites).

The evolved carbon dioxide gas was collected and analysed on a V.G. micromass 903 triple collector mass spectrometer. The samples were generally run in batches of twelve

unknowns (plus two duplicates and two samples of the laboratory standard, TDS for dolomite or MCS for calcite). A carbon dioxide sample of a lab standard was run at the start and finish of each batch and used to correct for drift.

Additional correction factors were required to correct for the temperature dependant fractionation of ^{18}O during the acid reaction (see Tucker, 1988) and the factors used were:

$$\text{calcite } \alpha^{25} = 1.01025$$

$$\text{dolomite } \alpha^{55} = 1.01000$$

and were applied using:

$$\delta^{18}O_{\text{solid}} = (\delta^{18}O_{\text{gas, measured}} + 1000) / \alpha - 1000$$

A: 4.4 ESTIMATION OF ERRORS

The MCS and TDS standards that were ran in duplicate with each batch of calcite or dolomite unknowns gave,

	n	$\delta^{18}O$	S.D.	$\delta^{13}C$	S.D.
TDS	12	-10.84	+/-0.16	+1.80	+/-0.06
MCS	8	-9.36	+/-0.16	-0.84	+/-0.09

Sample duplicates were run in each batch and the average reproduceability (based on 30 samples) is

$$\delta^{18}O = +/- 0.06$$

$$\delta^{13}C = +/- 0.03$$

The error of the small needle-picked samples is probably greater than above (which were based on crushed/drilled whole-rock powders) owing to contamination by unwanted surrounding matrix.

A:4.5 ISOTOPIC ANALYSIS RESULTS

The results of isotopic analysis are given in the Tables in Appendix 6.

APPENDIX 5: XRD AND SEM TECHNIQUES

A:5.1 X-RAY DIFFRACTION METHODS

XRD analysis was carried out on powdered dolomite samples in order to measure the molar % $CaCO_3$ within the dolomite (stoichiometry) and the ordering of the cations in the crystal strucure (ordering).

Powdered dolomite samples were ground with cerium oxide powder (used as an internal standard) and analysed on a Phillips PW 1130 generator/diffractometer using Fe-filtered Co K_α radiation. The change in the angular separation of the d_{104} dolomite peak was used to estimate the stoichiometry of the dolomite (Goldsmith & Graf, 1958). The dolomite ordering was determined by measuring the ratio of the 015 and 110 peak areas (Goldsmith & Graf, 1958).

The XRD results are given in table 1 in Appendix 6.

A:5.2 SCANNING ELECTRON MICROSCOPE (SEM) STUDIES

SEM studies were carried out in the Servei de Microscopica Electronica, University of Barcelona, Spain and in the Dept of Engineering, University of Durham using standard operating procedures on gold-plated specimens on Cambridge Instruments machines. To examine fracture faces rock chips were mounted directly upon SEM stubs using silver colloid paste. Dolomicrite samples were found to be most usefully studied as etched, polished surfaces. Broken fragments of polished thin section were etched in 1.5% HCl and then mounted on stubs. Etching times of about 10-13minutes proved to be most satisfactory.

APPENDIX 6: DATA TABLES

A:6.1 INTRODUCTION

The tables are arranged by analytical method and sample type *e.g.* limestone, dolomite, dedolomite *etc.*Within each table the samples are generally arranged by locality and given in ascending order up the stratigraphy. Localities are identified by the initial letter part of the sample identifier.

A	Arboli	B	Begues	C	Colldejou
F	Falset	G	Guiamets	M	Masroig
M	Masroig	PA	Pauls	PT	Pontons
PG	Puig Gracios	CC	Cabra del Campo	VB	Vilella Baixa
OM	Olesa	PJ, Q	Palleja	CB	Corbera
LR	La Riba	BH	Barranco de la Hoya	CV	Chelva
Al	Albarracin	ST	Serra	MP	Malpaso
CF	Castelvells	PR, PP	Prades	VC	Vacarisses
PD	Pratdip	TF	Torre de la Fontaubella	CT, HC	Centelles

In the lithology column of the tables information is given regarding:

i) Stratigraphic position (except for Valencia-Cuenca Basin samples), E = El Brull Unit, O = Olesa Unit, V = Vilella Baixa Unit, C1 = Lower Member of the Colldejou Unit, C2 = Upper Member of the Colldejou Unit, C = Colldejou Unit, undifferentiated.

ii) Lithology/mineralogy, PD = Peritidal dolomite, FD = Fabric-replacive dolomite, L = Limestone, BD = Baroque dolomite, C = Calcite

iii) Fabric *etc.* m = mudstone, w = wackestone, p = packstone, g = grainstone, v = vein, mo = crystal mosaic.

A:6.2 DATA TABLES

Table 1: XRD stoichiometry and ordering data.

Table 2: ICPAES and isotope data for limestones, calcite spar, allochems *etc.*

Table 3: ICPAES and isotope data for dedolomitic samples.

Table 4: ICPAES and isotope data for samples from eastern Iberian Ranges.

Table 5: ICPAES and isotope data for dolomites of the Catalan Coastal Ranges.

Table 6: AAS data for Colldejou and Falset localities.

Table 1: XRD stoichiometry and ordering data.

sample	Lithology	stoichiometry	ordering		sample	Lithology	stoichiometry	ordering
F1a	O/FD	49.68	0.68		C26a	C2/PD	49.82	0.62
F3a	O/FD	49.92	0.81		C35a	C2/PD	49.87	0.57
F4a	O/FD	49.64	0.84		C35b	C2/PD	49.92	0.69
F6a	O/FD	49.66	0.74		C34a	C2/PD	49.87	0.56
C1a	V/FD	49.56	0.82		C32a	C2/PD	49.65	0.79
C3a	V/FD	49.76	0.75		C31a	C2/PD	49.66	0.91
C5a	V/FD	49.82	0.88					
C7a	V/FD	49.63	0.74					
C10a	V/FD	49.66	0.81					
C14a	V/FD	49.79	0.85					
C15a	V/FD	49.92	0.84					
C20a	V/FD	49.87	0.84					
C26b	V/FD	49.69	0.63					

Table 2: ICPAES and isotope data for limestones, calcite spar, allochems *etc.*

SAMPLE	CAO	MGO	CARBPCT	DOLPCT	DOLVCCT	FES	MNS	SRS	C13ISOT	O18ISOT	Lithology
OM-MX2									0.6	-6.8	O/L/m
PT12	21.1	0.7	97	8	9	267	48	953			O/L/w
PT13	21.4	0.3	97	4	4	351	49	1194			O/L/w
PT14MIC									1.8	-5.0	O/L/w
CB3	22.3	0.3	100	3	3	147	54	587	1.3	-6.2	O/L/m
PG26YEL	21.6	0.3	97	3	3	376	67	251			O/L/w
PG27YEL	20.3	1.7	99	19	19	554	63	455			O/L/w
PG27GRY	22.2	0.3	100	3	3	200	22	1592	2.5	-4.5	O/L/w
PG28YEL	19.4	0.5	89	5	6	354	34	545			O/L/w
PD13	21.1	0.2	95	3	3	541	66	189			O/L/m
CC23	22.1	0.5	100	5	5	233	40	358			O/L/m
CC25	22.3	0.3	101	3	3	156	37	300			O/L/m
Q1LST	22.1	0.4	100	5	5	200	37	1394			O/L/w
VB11	22.3	0.2	99	3	3		55	109			O/L/m
VB15	23.0	0.2	102	3	2		67	161			O/L/m
VB26	22.7	0.3	102	3	3		15	2128	2.2	-4.6	V/L/w
VB27	23.2	0.3	103	3	3		12	2833			V/L/w
M17	21.4	0.8	100	10	10	149	48	363	0.3	-7.5	E/L/m
G13CMIC									2.1	-6.4	V/L/w

Table 2 (cont.): ICPAES and isotope data for limestones, calcite spar, allochems *etc.*

SAMPLE	CAO	MGO	CARBPCT	DOLPCT	DOLVCCT	FES	MNS	SRS	C13ISOT	O18ISOT	Lithology
G3	23.5	0.2	102	2	2		9	345	1.2	-6.7	O/L/m
G17	22.6	0.2	101	2	2		5	485	1.7	-6.8	V/L/m
G18	23.3	0.2	101	2	2		10	315	1.1	-6.7	V/L/m
LR29	21.3	0.2	96	3	3		70	960	1.2	-4.8	V/L/w
VB5CSP	23.1	0.8	103	8	8		61	98	-5.5	-8.1	O/C/v
M9CSP	23.6	0.1	103	1	1		21	47	-8.8	-7.2	E/C/ps
M34CSP	24.8	1.1	106	12	11		6	43	-7.3	-7.4	V/C/v
G30CSP	19.8	2.7	107	32	30		5	46	-5.9	-7.5	V/C/v
VB62CSP1									-7.3	-7.7	E/C/v
VB62CSP2									-4.9	-8.5	E/C/v
G13CSP									-5.5	-6.8	V/C/v
G32COO1									0.0	-8.5	Ooid
G32COO2									-0.1	-8.5	Ooid
G32CWR									1.0	-7.9	Oolite
G10CE									-0.9	-8.6	Echin.frag
PT14BR									-7.1	-12.4	Brach.
OM-B2									-1.9	-8.6	Brach
OM-B3									0.2	-7.0	Brach.
OM-B4									-1.6	-8.2	Brach.

Table 3: ICPAES and isotope data for dedolomitic samples.

SAMPLE	CAO	MGO	CARBPCT	DOLPCT	DOLVCCT	FES	MNS	SRS	C13ISOT	O18ISOT	Lithology
VB78	22.7	0.3	102	4	4	178	44	129			C2/DD/w
VB77	22.3	0.3	101	3	3	191	57	136	-3.5	-6.8	C2/DD/w
VB1	20.0	2.1	99	24	24	470	110	127	-4.8	-7.2	C2/DD/p
VB45	22.1	0.4	100	5	5	234	55	129	-3.5	-7.0	C2/DD/w
VB62 MAS	18.1	4.2	103	48	47	425	88	114	-4.6	-5.8	E/DD
VB62LAM	20.5	0.2	91	2	2	701	111	119	-8.7	-6.8	E/DD
VB3	20.5	1.9	101	22	22	596	96	128	-7.1	-6.6	E/DD/m
G51	22.2	0.1	100	1	1	694	452	110	-8.4	-7.9	E/DD/m
G50	20.2	0.2	91	2	2	722	251	99	-8.5	-7.2	E/DD/m
G52	22.0	0.2	98	2	2	960	267	126	-8.2	-7.0	E/DD/m
M30	20.3	0.2	91	3	3	409	63	52	-8.3	-6.1	V/DD/m
M14	17.5	3.9	98	45	46	408	94	41	-4.9	-6.1	E/DD
LR34	12.8	7.6	96	86	90	732	222	93	-3.7	-5.1	O/DD
LR39	13.0	7.9	99	90	91	466	96	88	0.7	-3.7	O/DD
PA44	19.6	2.9	101	33	33	444	154	139	-4.5	-5.4	V/DD/p
PA63	19.3	3.3	102	37	37	380	179	147	-4.4	-5.5	V/DD/p
PA41	19.9	1.7	97	20	20	1164	207	67			V/DD
G13d2									-4.0	-7.0	O/DD/m

Table 4: ICPAES and isotope data for samples from eastern Iberian Ranges.

SAMPLE	CAO	MGO	CARBPCT	DOLPCT	DOLVCCT	FES	MNS	SRS	C13ISOT	O18ISOT	Lithology
BH1VEIN	22.9	0.2	102	3	3	42	34	94	-7.7	-7.2	C/v
BH1DOL	7.4	0.3	34	3	10	1925	2158	101	-7.2	-7.5	BD/v
BH3VEIN	22.5	0.3	102	3	3	69	150	110			C/v
BH2	11.3	8.6	94	97	103	1581	823	100	1.6	-2.8	PD/m
BH7	9.1	6.7	75	76	101	2715	687	112	1.8	-3.4	PD/m
BH8	16.8	3.4	92	39	42	2090	961	92			PD/m
CV2	4.5	14.3	94			9025	3203	95			Magnesite
CV1VEIN	11.8	8.0	92	89	97	16031	3424	101	-0.1	-11.2	BD/v
CV4	12.4	6.8	91	77	85	13981	3453	165			BD/mo
CV5	11.4	8.4	93	95	101	1738	941	74	1.2	-3.1	PD/m
CV14	11.8	8.6	97	98	101	2068	1262	67	1.7	-4.8	PD/m
AL8	10.7	8.1	89	92	103	2844	866	61	1.4	-3.2	FD/m
AL7	10.0	7.5	83	86	103	3041	786	68	1.3	-3.2	FD/m
AL12	11.7	9.1	99	103	104	1698	543	48	1.2	-3.3	FD/m
AL14	12.1	8.7	99	99	100	1588	492	65	1.4	-3.6	FD/m
AL16	11.4	8.7	96	99	103	1061	360	111	1.4	-2.2	PD/m
ST6	13.7	7.4	98	83	85	3087	993	50	0.1	-9.0	BD/mo
ST7DOL	12.6	8.4	99	95	96	4193	1627	40	0.9	-9.6	BD/mo
ST10	11.8	7.5	91	85	94	17299	3182	33	0.8	-7.7	BD/mo
ST9	11.1	7.2	85	81	95	14014	3526	40	0.5	-7.7	DD/m
ST8	11.7	8.5	96	97	101	1693	184	75	1.6	-3.6	PD/m
MP4	10.3	7.8	86	89	103	1705	303	66	1.7	-4.4	FD/m
MP1	11.2	8.7	95	99	104	1284	307	50	1.9	-4.1	FD/m
MP2	10.9	8.4	91	94	104	1569	481	57	1.3	-4.2	FD/m
MP7	11.8	9.2	99	104	104	1094	221	62	2.1	-4.6	PD/m
MP10	21.8	16.9	91	94	104	1385	292	89	2.4	-4.0	PD/m
MP14	18.4	0.3	83	3	4	2297	816	168			C/mo

Table 5: ICPAES and isotope data for dolomites of the Catalan Coastal Ranges.

SAMPLE	CAO	MGO	CARBPCT	DOLPCT	DOLVCCT	FES	MNS	SRS	C13ISOT	O18ISOT	Lithology
PT20	12.4	9.4	104	107	103	790	418	36			O/FD/w
PT21	12.5	9.4	105	108	103	758	391	33			O/FD/w
PT30	14.0	8.0	104	91	88	260	103	91			O/FD/w
PT31	13.4	8.2	102	93	91	188	102	88			O/FD/w
PT42	12.0	9.1	101	104	103	425	186	69			V/FD/m
PT43	11.9	9.1	101	104	104	391	104	74			V/FD/m
PT44	12.1	9.1	102	105	103	352	84	81			V/FD/m
PT45	12.1	9.2	102	105	103	404	81	88			V/FD/w
PT51	11.8	9.3	101	106	105	466	136	69			C2/PD/m
PT56	11.8	9.2	100	105	105	657	223	99			C2/PD/m
PT57	11.9	9.3	101	106	105	705	349	103			C2/PD/m
CB23	12.5	9.6	105	108	104	157	61	45			V/FD/m
CB27	12.3	9.0	101	103	101	404	74	96			V/FD/m
CB28DK	12.1	9.5	103	108	105	219	48	43			V/FD/m
CB28LT	11.3	8.7	95	98	104	492	63	52			V/FD/m
CB31	12.2	9.7	103	109	106	258	90	36			V/FD/w
CB44	12.0	9.5	103	108	105	263	49	66			C1/PD/m
CB55DOL	12.4	9.7	105	110	105	363	42	90			C2/PD/m
CB60	12.1	9.6	103	109	105	201	43	79			C2/PD/m
CB63	12.2	9.7	104	110	105	232	59	40			C2/PD/w
CB66	12.1	9.6	103	109	105	244	63	43			C2/PD/m
CF8	12.6	9.4	105	107	102	340	76	78			?/FD/w
CF1	12.6	8.7	101	99	98	241	101	93			C/PD/m
CF2	12.3	9.4	102	105	103	227	190	103			C/PD/m
CF3	12.6	9.2	103	104	101	143	175	62			C/PD/m

Table 5 (cont.): ICPAES and isotope data for dolomites of the Catalan Coastal Ranges.

SAMPLE	CAO	MGO	CARBPCT	DOLPCT	DOLVCCT	FES	MNS	SRS	C13ISOT	O18ISOT	Lithology
PG39	13.1	8.8	104	100	96	276	62	69			V/FD/mo
PG41	12.2	9.4	103	107	104	311	118	79			V/FD/mo
PG42	12.7	9.4	104	106	102	182	88	85	2.0	-3.8	V/FD/mo
PG48	12.0	9.3	101	105	104	360	51	86			C2/PD/m
PG53	11.7	9.3	99	105	105	375	50	80			C2/PD/m
PG58DOL	12.5	9.0	102	102	100	297	53	73	1.3	-4.7	C2/PD/m
PG63	12.1	9.4	101	105	104	314	85	95			C2/PD/m
PG66	16.5	4.5	96	51	53	1106	509	139			C2/PD/m
PD14	12.3	9.2	102	104	102	468	90	80			V/FD
PD17	11.9	9.0	99	102	103	437	82	112			C/PD
PD18	12.2	9.6	103	108	105	376	74	88			C/PD
OM25	12.4	9.7	105	110	105	272	118	57			V/FD/mo
OM27	12.4	9.8	106	111	105	222	129	47			V/FD/mo
OM28	12.2	9.7	105	110	106	274	119	50			V/FD/mo
OM33	12.3	9.6	104	109	105	299	62	78			C2/PD/m
OM43	12.3	9.6	104	109	105	416	74	67			C2/PD/m
OM47	12.4	8.6	99	97	98	453	100	92			C2/PD/m
VC19	12.4	9.1	102	103	101	282	51	88			V/FD/mo
VC20	12.7	9.4	103	104	101	223	43	102			V/FD/mo
VC21	12.4	9.6	105	108	104	232	40	109			V/FD/mo
VC32	12.0	9.4	101	105	104	503	117	115			C2/PD/m
VC35	12.3	9.4	101	105	104	489	104	67			C2/PD/m
VC36	11.7	8.2	94	93	99	1065	465	110			C2/PD/m
PP21	12.7	8.6	101	98	97	481	447	96			FD
PP22	12.4	9.7	105	110	105	190	50	45			FD

Table 5 (cont.): ICPAES and isotope data for dolomites of the Catalan Coastal Ranges.

SAMPLE	CAO	MGO	CARBPCT	DOLPCT	DOLVCCT	FES	MNS	SRS	C13ISOT	O18ISOT	Lithology
CC31	12.7	8.8	102	100	98	357	32	80			FD
CC32	11.9	9.2	99	103	104	208	30	60			FD
CC33	12.3	9.8	104	110	105	272	35	40			FD
CC39	12.1	9.7	102	107	106	344	38	84			PD
CC40	12.0	9.5	101	106	105	501	46	80			PD
Q1DOL	13.3	6.2	91	70	77	410	196	117			
Q3	12.9	8.8	102	99	98	321	97	53			
PJ22	12.2	9.5	102	107	104	319	101	46			FD
PJ24	12.6	9.8	104	108	104	269	154	56			FD
PJ26	12.1	9.6	103	109	106	252	75	31			?PD
PJ28	12.3	9.7	105	110	105	314	182	59			?PD
PJ30	12.2	9.6	104	109	105	475	148	76			?PD
PA43	13.7	8.0	102	91	89	1024	266	99	1.5	-4.1	
PA74	15.0	6.9	102	78	77	635	223	111			
PA58	12.3	9.4	102	106	104	488	120	87	2.0	-3.2	
PA61	12.1	9.5	102	107	105	709	150	118	2.3	-2.4	
CT40	12.5	5.7	86	66	77	3039	225	120			
CT46	12.7	9.7	105	108	103	343	79	91			
CT48	12.5	9.5	105	108	103	406	100	73			
HC2	11.6	8.8	97	100	103	508	120	82			
HC3	12.2	8.2	97	93	97	2118	298	69			
CT39	11.3	8.7	94	97	104	539	57	86			
B30	13.2	9.0	104	101	97	331	92	52			V/FD/
B1	12.4	9.4	101	104	103	235	91	67			V/FD/
B24	11.7	9.1	99	103	104	421	110	103			C2/PD/

Table 5 (cont.): ICPAES and isotope data for dolomites of the Catalan Coastal Ranges.

SAMPLE	CAO	MGO	CARBPCT	DOLPCT	DOLVCCT	FES	MNS	SRS	C13ISOT	O18ISOT	Lithology
PR33	12.5	9.9	106	112	105	456	107	51			FD/
PR35	12.4	9.8	106	112	105	418	98	54			FD/
PR38	12.4	9.7	104	108	104	636	139	69			FD/
PR43	12.0	9.5	102	108	106	585	85	102			PD/
PR44	11.7	9.2	99	104	105	564	77	99			PD/
PR45	12.5	9.4	103	106	103	826	112	91			PD/
C2	13.3	8.1	99	90	91		148	44	2.8	-6.7	V/FD/w
C7	12.2	8.6	95	94	99		81	38	2.7	-7.0	V/FD/m
C11	12.7	9.2	99	100	101		117	33	2.6	-6.5	V/FD/m
C15	12.3	9.3	99	102	103		113	31	2.5	-7.8	V/FD/m
C19	12.7	8.2	98	93	94		121	45			V/FD/m
C28	12.9	9.6	101	104	102		172	40	2.3	-5.7	C2/PD/m
C29	12.7	8.9	100	99	99		210	58	2.4	-5.4	C2/PD/w
C35	13.0	9.0	104	101	98		131	107	1.4	-4.1	C2/PD/m
C32	12.7	9.2	103	103	100		199	50	2.4	-5.0	C2/PD/m
C30	12.2	8.8	99	99	100		82	77	2.5	-3.9	C2/PD/m
F3	12.8	9.3	102	102	101		522	50	2.1	-5.1	O/FD/w
F35	12.8	9.5	102	104	102		411	56	2.3	-5.3	V/FD/w
F31	12.4	9.2	103	105	102		258	55	2.1	-5.0	V/FD/w
F29	12.6	9.4	102	104	102		259	55	1.6	-4.7	V/FD/w
F27	12.2	9.1	102	104	102		98	61	2.1	-4.6	V/FD/m
F19A	11.6	8.7	96	98	102		101	88	1.9	-4.1	C2/PD/m
F16	11.8	8.8	98	101	103		162	91	2.2	-4.3	C2/PD/m
F13	12.3	9.2	101	103	102		131	41	2.5	-4.7	C2/PD/m
F10	12.2	9.0	100	102	101		84	69	2.5	-4.5	C2/PD/m
F9	12.1	9.1	101	104	103		104	59	2.4	-4.4	C2/PD/m

Table 5 (cont.): ICPAES and isotope data for dolomites of the Catalan Coastal Ranges.

SAMPLE	CAO	MGO	CARBPCT	DOLPCT	DOLVCCT	FES	MNS	SRS	C13ISOT	O18ISOT	Lithology
A8	12.8	8.7	102	98	97		161	51	1.8	-4.1	V/FD/m
A10	12.5	9.2	103	104	101		150	51	1.8	-4.2	V/FD/w
A12	12.8	9.4	102	103	101		110	56	2.0	-4.1	V/FD/w
A14DWRW	11.8	8.3	95	94	99		112	57	2.3	-3.4	V/FD/w
A14DWRB	12.3	9.0	100	101	101		37	64	2.6	-3.4	V/FD/w
A18DWRW	12.2	8.9	100	101	101		62	52			V/FD/p
A18DWRB	12.6	9.3	102	104	101		48	52			V/FD/p
A22	12.1	9.1	99	101	103		40	35	2.8	-3.8	V/FD/p
A37	12.5	9.2	100	101	101		36	48	2.4	-3.0	C1/PD/m
A40	12.3	9.4	99	103	103		26	38	2.5	-3.7	C1/PD/w
A54	12.5	9.3	99	101	102		48	67			C2/PD/m
A55	12.1	9.0	100	102	102		50	74	2.2	-3.3	C2/PD/m
A56	12.4	9.2	101	103	102		44	41	2.2	-3.7	C2/PD/m
A58	12.3	8.9	100	100	101		44	67	2.4	-2.7	C2/PD/m
A59	12.1	8.9	98	99	102		47	50	2.6	-3.6	C2/PD/m
A60	11.9	8.8	97	98	101		40	83	2.9	-2.3	C2/PD/m
A61	12.4	8.9	100	101	100		56	59	2.5	-3.6	C2/PD/m
A63DWRB	12.9	8.5	101	97	95		71	74	1.7	-3.3	C2/PD/m
A63DWRW	12.2	8.8	100	101	100		72	67	1.7	-3.4	C2/PD/m
G28	13.6	8.7	102	96	94		47	61	1.9	-4.4	V/FD/m
G30DWR	13.2	9.2	104	102	98		59	56	2.2	-4.2	V/FD/m
G39	12.1	8.3	95	93	98		126	98	2.4	-2.7	C1/PD/m
TF7	12.9	8.9	101	99	98		48	53	2.8	-5.5	C1/PD/m
TF8	13.3	9.0	102	99	97		84	54	2.6	-5.8	C1/PD/m
TF9	13.8	8.8	101	95	94		235	56	1.7	-5.4	C1/PD/m
TF14	13.1	8.1	99	91	92		189	75	1.8	-4.5	C1/PD/m
TF17	12.9	8.4	100	95	95		96	74	2.2	-4.8	C1/PD/m
TF18	12.6	8.4	99	95	96		78	70	1.9	-4.6	C1/PD/m

Table 5 (cont.): ICPAES and isotope data for dolomites of the Catalan Coastal Ranges.

SAMPLE	CAO	MGO	CARBPCT	DOLPCT	DOLVCCT	FES	MNS	SRS	C13ISOT	O18ISOT	Lithology
VB67	12.3	9.0	99	100	101		93	84	1.5	-3.3	E/PD/m
VB68	12.5	8.1	98	92	94		86	92	1.2	-3.2	E/PD/m
VB5DWR	12.4	8.6	99	98	98		75	50	1.7	-3.3	E/PD/m
VB63	12.3	8.7	98	97	99		85	80	2.3	-3.3	O/FD/m
VB52	13.1	7.3	96	83	87		26	179	2.5	-3.7	V/FD/w
VB74	16.5	5.7	99	63	64		19	162			V/FD/g
VB37	13.2	8.4	100	94	94		10	146	-0.8	-3.1	V/FD/g
VB81	12.8	9.0	101	100	99		31	46	2.7	-3.0	C2/PD/m
VB87	12.6	8.9	103	102	99		27	70	2.0	-2.5	C2/PD/m
VB88	12.9	8.8	99	97	97		41	90	1.7	-2.6	C2/PD/m
VB93DWRD	12.4	8.7	100	99	99		32	124	2.0	-2.2	C2/PD/m
VB93DWRL	12.2	8.8	99	99	100		35	105			C2/PD/m
M4	12.3	9.1	102	103	102		105	110	1.0	-5.0	E/FD
M9DWR	11.4	8.4	95	96	101		84	42	2.0	-6.0	E/FD
M12	12.2	8.6	98	97	99		65	33	2.1	-7.8	E/FD/m
M18	12.7	8.8	102	100	98		78	56	2.1	-6.5	O/FD/w
M23	12.3	9.5	104	108	104	452	60	48			O/FD/w
M24	12.7	9.1	104	104	100	444	72	50			O/FD/w
M29	12.7	8.6	100	97	97		76	47	2.4	-6.5	V/FD/m
M33	13.0	8.9	104	101	98		29	48	2.1	-6.2	V/FD/m
M34DWR	13.6	8.5	103	96	93		26	55	2.2	-5.0	C1/?PD/m
M36	12.4	8.7	98	97	99		35	62	2.7	-4.8	C1/?PD/m
M20									1.5	-7.3	BD/mo
M22									2.3	-7.4	BD/mo
M23									2.8	-6.2	BD/mo
M24									1.9	-6.1	BD/mo
M28									0.7	-6.6	BD/

Table 5 (cont.): ICPAES and isotope data for dolomites of the Catalan Coastal Ranges.

SAMPLE	CAO	MGO	CARBPCT	DOLPCT	DOLVCCT	FES	MNS	SRS	C13ISOT	O18ISOT	Lithology
LR8	12.8	9.0	104	102	99		412	41	1.5	-5.0	E/FD/w
LR7	13.4	9.0	103	99	96		261	61	1.5	-5.5	E/FD/w
LR4	13.1	9.0	101	98	97		314	52	1.3	-5.3	E/FD/m
LR6	12.7	8.9	101	100	99		66	61	1.6	-3.4	O/FD/w
LR11	12.5	9.1	103	104	101		221	41	1.8	-4.1	O/FD/m
LR28DWRY	14.4	6.0	95	68	72		313	110			V/FD/w
LR28DWRD	12.8	8.0	97	90	92		210	139			V/FD/w
LR1	12.5	8.7	101	99	98		89	62	1.2	-3.9	V/FD/m
LR18	11.1	8.0	91	91	100		66	74	1.7	-3.0	V/FD/m
LR20DWRD	13.4	9.9	204	207	101		67	79	1.8	-3.3	V/FD/m
LR20DWRY	12.5	9.2	103	104	101		92	58	1.7	-3.5	V/FD/m
LR52	11.7	8.9	98	101	103	559	53	66	1.8	-3.1	C2/PD/m
LR51	12.1	9.2	102	105	103	609	64	64	1.8	-3.8	C2/PD/m
LR49	12.0	9.0	100	102	103	634	67	67	2.0	-3.4	C2/PD/m
LR48	11.4	8.7	95	98	103	864	78	104	1.8	-2.9	C2/PD/m

SAMPLE	CARBPCT	DOLVCCT	NAS	SRS	MNS	FES	Lithology
C1	103	87	148	53	111	476	V/FD/w
C2	100	85	207	54	147	601	V/FD/w
C3	102	98	131	45	147	722	V/FD/w
C4	100	94	137	46	141	685	V/FD/w
C5A	101	97	256	36	105	441	V/FD/p
C6A	103	88	197	40	92	592	V/FD/p
C7A	100	94	225	47	75	512	V/F/m
C8A	97	87	289	54	145	673	V/F/m
C9A	95	62	115	56	135	600	V/F/w
C10	99	89	110	49	89	387	V/F/w
C11A	103	91	114	25	147	616	V/F/m
C12A	105	72	83	56	202	602	V/F/w
C13A	101	80	150	53	92	432	V/F/m
C14A	101	76	133	48	136	525	V/FD/w
C15A	102	95	188	43	106	792	V/FD/m
C17A	70	39	43	136	233	1013	V/FD/m
C18A	65	45	88	23	169	1613	V/FD/p
C19	105	89	123	50	248	649	V/FD/g
C20	106	32	57	96	172	584	V/FD/g
C21A	86	94	124	20	234	867	V/FD/m
C16A	103	45	73	84	560	1510	V/FD/p
C23	104	19	41	81	1827	1100	V/FD/g
C24A	92	103	146	84	350	995	V/FD/g
C25A	101	93	146	26	219	1110	V/FD/g
C22B	100	99	132	39	249	1146	V/FD/g
C26B	90	100	173	61	303	1740	V/FD/g
C22A	96	99	166	44	197	1153	C2/PD/m
C26A	90	99	193	28	226	1552	C2/PD/m
C27	95	97	157	46	174	1178	C2/PD/m
C28	100	96	146	47	166	1186	C2/PD/m
C29A	94	98	201	37	262	922	C2/PD/w
C35	92	94	361	110	142	762	C2/PD/m
C34	96	96	410	67	213	1004	C2/PD/w
C33A	102	82	210	86	203	1256	C2/PD/m
C32A	91	101	209	55	212	1183	C2/PD/m
C31	102	95	329	80	93	450	C2/PD/m
C30	92	95	584	86	99	1062	C2/PD/m
C36	77	14	128	115	162	3293	C2/PD/m
A1	88	89	238	72	556	3374	E/FD/w
A2	91	92	184	54	257	3588	E/FD/w
A3	95	85	279	65	496	2244	E/FD/w
A4	93	96	290	34	133	833	E/FD/p
A5	87	101	229	35	143	943	E/FD/p
A6	91	96	327	95	133	530	O/FD/w
A7	98	86	241	74	190	495	O/FD/w
A8	89	94	224	55	192	844	O/FD/m
A9	92	97	254	69	158	642	O/FD/p
A10	100	95	303	56	156	625	V/FD/w
A11	98	91	308	81	169	807	V/FD/w
A12	95	96	308	64	131	674	V/FD/w
A13	98	89	247	86	142	779	V/FD/w
A14	88	92	388	70	87	440	V/FD/w
A15	104	87	134	58	60	248	V/FD/g

Table 6: AAS data

SAMPLE	CARBPCT	DOLVCCT	NAS	SRS	MNS	FES	Lithology
A19	99	98	160	27	96	574	V/FD/m
A17	93	97	318	65	80	273	V/FD/p
A18	99	95	286	58	73	529	V/FD/p
A20	101	98	312	49	78	388	V/FD/w
A21	112	96	167	35	74	626	V/FD/w
A22	87	98	217	42	61	510	V/FD/p
A23	113	95	184	31	57	426	V/FD/p
A24	96	97	196	35	55	392	V/FD/p
A25	101	92	412	71	56	483	V/FD/m
A29	91	96	129	38	64	531	V/FD/m
A28	98	94	198	55	47	387	V/FD/w
A26	96	95	370	65	54	481	V/FD/p
A27	100	87	245	72	43	361	V/FD/g
A30	101	96	167	34	48	379	V/FD/m
A32	101	97	189	36	54	358	V/FD/w
A31	104	96	168	33	49	460	V/FD/m
A33	100	98	275	36	51	440	V/FD/m
A34	99	96	208	37	56	444	V/FD/p
A35	100	96	206	32	47	375	V/FD/g
A36	98	101	268	52	48	447	V/FD/g
A37	101	96	481	55	48	485	C1/ / m
A38	97	98	309	66	45	452	C1/ / p
A39	103	100	122	34	41	404	C1/ / m
A40	98	99	150	50	42	412	C1/ / w
A41	102	97	155	54	41	411	C1/ / w
A42	97	77	102	121	44	332	C1/ / g
A44	97	98	156	55	54	421	C1/ / m
A45	96	95	130	65	47	398	C1/ / m
A43	99	95	169	64	56	597	C1/ / m
A46	34	100	285	59	41	643	C1/ / w
A47	103	94	140	68	52	641	C1/ / w
A48	98	100	145	45	52	671	C1/ / w
A49	99	101	160	48	60	785	C1/ / g
A50	101	96	170	62	44	504	C1/ / m
A52	100	99	154	59	61	706	C1/ / g
A51	96	98	243	65	46	777	C1/ / g
A53	97	101	157	45	64	997	C1/ / g
A54	93	101	293	76	64	1033	C2/PD/m
A55	96	100	201	81	61	997	C2/PD/m
A57	96	100	309	86	62	1011	C2/PD/m
A56	97	100	200	51	57	1100	C2/PD/m
A58	101	99	257	68	55	1124	C2/PD/m
A59	100	96	168	60	60	1236	C2/PD/m
A60	96	96	302	90	51	831	C2/PD/w
A61	100	99	187	67	68	1256	C2/PD/m
A62	98	96	191	69	79	1558	C2/PD/m
A63	109	93	197	73	74	1497	C2/PD/m
A64	89	93	453	94	158	3019	C2/PD/m
A66	88	4	61	167	260	970	C2/PD/m
A65	109	15	47	178	97	1345	C2/PD/m

Table 6 (cont): AAS data

Adams, J.E. & Rhodes, M.L. (1960) Dolomitization by seepage refluxion. *Bull. Am. Assoc. petrol. Geol.* 44, 1912-1920.

Adams, A.E., McKenzie, W.S. & Guilford, C. (1984) *Atlas of sedimentary rocks under the microscope.* pp. 104. Longman, Harlow.

Ahr, W.M. (1973) The carbonate ramp: an alternative to the shelf model. *Trans. Gulf-Cst. Ass. geol. Socs* **23**, 221-225.

Aigner, T. (1984) Dynamic stratigraphy of epicontinental carbonates, Upper Muschelkalk (M. Triassic), South German Basin. *Neues. Jb. Geol. Palaont. Abh.* **169**, 127-159.

Aigner, T. (1985) *Storm depositional systems.* Lecture notes in Earth Sciences. Vol. 3, p. 174, Springer-Verlag, Berlin.

Aissaoui, D.M. (1988) Magnesian calcite cements and their diagenesis: Mururoa Atoll. *Sedimentology* **35**, 821-841.

Al-Hashimi, W.S. & Hemingway, J.E. (1973) Recent dedolomitisation and the origin of the rusty crusts of Northumberland. *J. sedim. Petrol.* **43**, 82-91.

Allan, J.R. & Matthews, R.K. (1982) Isotope signatures associated with early meteoric diagenesis. *Sedimentology* **29**, 797-817.

Anadon, P., Cabrera, L., Guimera, J. & Santanach, P. (1985) Paleogene strike-slip deformation and sedimentation along the south eastern margin of the Ebro Basin. In: *Strike-slip Deformation, Basin Formation, and Sedimentation* (Ed. by K.T.Biddle & N.Christie-Blick) Spec. Publ. Soc. econ. Paleont. Miner. 37, 303-318.

Anadon, P., Colombo, F., Esteban, M., Marzo, M., Robles, S., Santanach, P. & Sole Sugranes, Ll. (1979) Evolucion tectonoestratigrafica de los Catalanides. *Homenetage a Ll.Sole Sabarts Acta Geologica Hispanica* **14**, 242-270.

Anderson, T.F. & Arthur, M.A. (1983) Stable isotopes of oxygen and carbon and their application to sedimentologic and paleoenvironmental problems. In: *Stable isotopes in sedimentary geology* (Ed. by M.A.Arthur & T.F.Anderson) Soc. econ. Paleont. Miner. Short Course No. 10, 1.1-1.151.

Andreu, A., Calvet, F., Font, X., & Viladevall, M. (1987) Las mineralizaciones de Pb-Zn-Ba en el Muschelkalk inferior de los Catalanides. *Cuad. Geol. Iberica*, **11**, 779-795.

Angino, E.E. & Billings, G.K. (1972) *Atomic Absorption Spectrometry in Geology.* Elsevier, Amsterdam.

Asquith, G.B. (1979) *Subsurface Carbonate Depositional Models*, p. 121. Penwell Books, Tulsa.

Assereto, R.L. & Kendall, C.G.St.C (1977) Nature, origin and classification of peritidal tepee structures and related breccias. *Sedimentology* **24**, 153-210.

Back, W., Hanshaw, B.B., Plummer, L.N., Rahn, P.H., Rightmire, C.T. & Rubin, M. (1983) Process and Rate of dedolomitization: Mass Transfer and ^{14}C dating in a regional carbonate aquifer. *Bull. geol. Soc. Am.* **94**, 1415-1429.

Bally, A.W. (1987) *Atlas of Seismic Stratigraphy*, vol. 1, Am. Assoc. petrol. Geol. Studies in Geology, No. 27.

Barnaby, R.J. & Rimstidt, J.D. (1989) Redox conditions of calcite cementation interpreted from Mn and Fe contents of authigenic calcites. *Bull. geol. Soc. Am.* **101**, 795-804.

Bathurst, R.G.C. (1975) *Carbonate sediments and their diagenesis*, pp.658. Elsevier, Amsterdam.

Beales, F.W. & Hardy, J.W. (1980) Criteria for the recognition of diverse dolomite types with an emphasis on studies of host rocks for Mississippi Valley-type ore deposits. In: *Concepts and Models of Dolomitization* (Ed. by D.H.Zenger, J.B.Dunham & R.L.Ethington) Spec. Publ. Soc. econ. Paleont. Miner. 28, 197-214.

Bein, A. & Land, L.S. (1983) Carbonate sedimentation and diagenesis associated with Mg-Ca-chloride brines: The Permian San Andres Formation in the Texas Panhandle. *J. sedim. Petrol.* 53, 243-260.

Blake, D.F., Peacor, D.R. & Wilkinson, B.H. (1982) The sequence and mechanism of low-temperature dolomite formation: calcian dolomite in a Pennsylvanian echinoderm. *J. sedim. Petrol.* **52**, 59-70.

Bosence, D.W.J., Rowlands, R.J. & Quine, M.L. (1985) Sedimentology and budget of a Recent carbonate mound, Florida Keys. *Sedimentology* **32**, 317-343.

Braun, M. & Friedman, G.M. (1970) Dedolomitization fabric in peels: A possible clue to unconformity surfaces. *J. sedim. Petrol.* **40**, 417-419.

Budai, J.M., Lohmann, K.C. & Owen, R.M. (1984) Burial dedolomite in the Mississippian Madison Limestone, Wyoming and Utah Thrust Belt. *J. sedim. Petrol.* **54**, 276-288.

Budd, D.A. & Land, L.S. (1990) Geochemical imprint of meteoric diagenesis in Holocene ooid sands, Schooner Cays, Bahamas: Correlation of calcite cement geochemistry with extant groundwaters. *J. sedim. Petrol.* **60**, 361-378.

Bullen, S.B. & Sibley, D.F. (1984) Dolomite selectivity and mimic replacement. *Geology*, **12**, 655-658.

Butler, G.P. (1973) Strontium geochemistry of modern and ancient calcium sulphate minerals. In: *The Persian Gulf* (Ed. by B.H.Purser) pp.423-452. Springer-Verlag, Berlin.

Cabaneros, M.C. & Masriera, A. (1977) Contribucion al conocimiento sedimentologico del Muschelkalk Medio de los Catalanides. *Cuad. Geol. Iberica* **4**, 149-156.

Calvet, F. & Julia, R. (1983) Pisoids in the caliche profiles of Tarragona (northeast Spain). In: *Coated Grains* (Ed. by T.M.Peryt) p. 456-473. Springer-Verlag, Berlin.

Calvet, F. & Ramon, X. (1987) Estratigrafia, sedimentologia y diagenesis del Muschelkalk inferior de los Catalanides. *Cuad. Geol. Iberica* **11,** 141-169.

Calvet, F. & Tucker, M.E. (1988) Outer Ramp cycles in the Upper Muschelkalk of the Catalan Basin, northeast Spain. *Sedim. Geol.* **57**, 185-198.

Calvet, F., Tucker, M.E. & Henton, J.M. (1990) Middle Triassic carbonate ramp systems in the Catalan Basin, north-east Spain: facies, systems tracts, sequences and controls. In: *Carbonate Platforms, Facies, Sequences and Evolution.* (Ed. by M.E.Tucker, J.L.Wilson, P.D.Crevello, J.R.Sarg, & J.F.Read) p. 79-108. Spec. Publ. No. 9 of the International Association of Sedimentologists.

Calzada, S. & Gaetani, M. (1977) Nota paleocologica sobre *M. mentzeli* (Brachiopoda, Anisiense, Catalanides). *Cuad. Geol. Iberica* **4,** 157-169.

Carballo, J.D., Land, L.S. & Miser, D.E. (1987) Holocene dolomitization of supratidal sediments by active tidal pumping, Sugarloaf Key, Florida. *J. sedim. Petrol.* **57**, 153-165.

Choquette, P.W. & James, N.P. (1987) Diagenesis in limestones - 3, the deep burial environment. *Geoscience Canada* **14**, 3-35.

Choquette, P.W. & James, N.P. (1988) Introduction. In: *Paleokarst* (Ed. by N.P.James & P.W.Choquette) pp. 1-21. Springer-Verlag, New York.

Choquette, P.W. & Steinen, R.P. (1980) Mississippian non-supratidal dolomite, Ste. Genevieve Limestone, Illinois Basin: evidence for mixed-water dolomitization. In: *Concepts and models of dolomitization.* (Ed. by D.H.Zenger, J.B.Dunham and R.L.Ethington) Spec. Publ. Soc. econ. Paleont. Miner. 28, 168-196.

Clarkson, E.N.K. (1979) *Invertebrate Paleontology and evolution.* George Allen & Unwin Ltd., London. pp 323.

Conley, C.D. (1977) Origin of distorted ooliths and pisoliths. *J. sedim. Petrol.* **47**, 554-564.

Crevello, P.D., Wilson, J.L., Sarg, J.F., & Read, J.F. (Ed.s) (1989) *Controls on carbonate platform and basin development.* Spec. Publ. Soc. econ. Paleont. Miner. **44**, p. 405.

Dawans, J.M. & Swart, P.K. (1988) Textural and geochemical alternations in Late Cenozoic Bahamian dolomites. *Sedimentology* 35, 385-403.

De Groot, K.D. (1967) Experimental dedolomitization. *J. sedim. Petrol.* **37**, 1216-1220.

Deer, W.A., Howie, R.A., Zussman, J. (1966) *An introduction to the rock-forming minerals.* p. 528. Longman Group Ltd., Harlow, England.

Deffeyes, K.S., Lucia, F.J. & Weyl, P.K. (1965) Dolomitization of Recent and Plio-Pleistocene sediments by marine evaporite waters on Bonaire, Netherlands Antilles. In: *Dolomitization and Limestone Diagenesis - a Symposium* (Ed. by L.C.Pray and R.C.Murray) Spec. Publ. Soc. econ. Paleont. Miner. 13, 71-88.

Dickson, J.A.D. (1980) Artificial colouration of fluorite by electron bombardment. *Mineral. Mag.* **43**, 820-822.

Dickson, J.A.D. & Coleman, M.L. (1980) Changes in carbon and oxygen isotope composition during limestone diagenesis. *Sedimentology* **27**, 107-118.

Dickson, J.A.D. & Coleman, M.L. (1989) Preservation potential of Carboniferous brachiopods (Abs.). 28th AGM of the BSRG Leeds 1989 Abstract Volume.

Dodd, J.R. (1966) Processes of conversion of aragonite to calcite with an example from the Cretaceous of Texas. *J. sedim. Petrol.* **36**, 733-741.

Dolan, J.F. (1989) Eustatic and tectonic controls on deposition of hybrid siliciclastic/carbonate basinal cycles: discussion with examples. *Bull. Am. Assoc. petrol. Geol.*, **73**, 1233-1246.

Dravis, J. & Yurewicz, D.A. (1985) Enhanced carbonate petrography using fluorescence microscopy. *J. sedim Petrol.* **55**, 795-804.

Esteban, M. & Klappa, C.F. (1983) Subaerial exposure environment. In: *Carbonate depositional environments* (Ed. by P.A.Scholle, D.G.Bebout and C.M.Moore) Mem. Am. Assoc. petrol. Geol. 33, 1-54.

Esteban, M., Pomar Goma, L., Marzo Cardio, M. & Anadon Monzon, P. (1977) Natureleza del Contacto entre el Muschelkalk inferior y el Muschelkalk Medio de la zona de Aiguafreda. *Cuad. Geol. Iberica* **4**, 201-210.

Esteban, M & Pray, L.C. (1983) Pisoids and pisolite facies (Permian), Guadelupe Mountains, New Mexico and West Texas. In: *Coated Grains* (Ed. by T.M.Peryt) p. 503-537. Springer-Verlag, Berlin.

Evamy, B.D. (1967) Dedolomitization and the development of rhombohedral pores in limestones. *J. sedim. Petrol.* **37**, 1204-1215.

Flugel, E. (1982) *Microfacies analysis of limestones.* pp. 633. Springer-Verlag, Berlin.

Folk, R.L. & Land, L.S. (1975) Mg/Ca ratio and salinity: two controls over crystallization of dolomite. *Bull. Am. Assoc. petrol. Geol.* 59, 60-68.

Frank, J.R. (1981) Dedolomitization in the Taum Sauk Limestone (Upper Cambrian), southeast Missouri. *J. sedim. Petrol.* **51**, 7-18.

Fraser, D.G., Feltham, D. & Whiteman, M. (1989) High-resolution scanning proton microprobe studies of micron-scale trace element zoning in a secondary dolomite: implications for studies of redox behaviour in dolomite. *Sedim. Geol.* **65**, 223-232.

Freeman, T. (1972) Sedimentology and Dolomitization of Muschelkalk Carbonates (Triassic), Iberian Range, Spain. *Bull. Am. Ass. Petrol. Geol.* **56**, 434-453.

Frisia-Bruni, S., Jadoul, F. & Weissert, H. (1989) Evinosponge in the Triassic Esino limestone (Southern Alps): documentation of early lithification and late diagenetic overprint. *Sedimentology* **36**, 685-699.

Gagan, M.K., Johnson, D.P. & Carter, R.M. (1988) The cyclone Winifred storm bed, central Great Barrier Reef Shelf, Australia. *J. sedim. Petrol.* **58**, 845-856.

Gandin, A., Tongiorgi, M. & Virgili, C. (1982) Some examples of the Middle Triassic Marine Transgression in south-western Mediterranean Europe. *Geol. Runds.* **71**, 881-894.

Garrido-Megias, A. & Villena, J. (1977) El Trias Germanico en Espana: Paleogeografia y estudio secuencial. *Cuad. Geol. Iberica* **4**, 37-56.

Gebelein, C.D. (1977) Mixing zone dolomitization of Holocene tidal flat sediemnts, south-west Andros Island, Bahamas (Abs.). *Bull. Am. Assoc. petrol. Geol.* **61**, 787-788.

Goldberg, M. (1967) Supratidal dolomitization and dedolomitization in Jurassic rocks of Hamakhtesh Haqatan, Israel. *J. sedim. Petrol.* **37**, 760-773.

Goldsmith, I.R. (1987) *Cementation in modern and ancient reefs*. Unpubl. Ph.D. thesis. Durham University.

Goldsmith, J.R. & Graf, D.L. (1958) Relations between lattice constraints and composition of the Ca- Mg carbonates. *Am. Miner.* **43**, 84-101.

Gregg, J.M. & Shelton, K.L. (1989) Minor and trace-element distributions in the Bonneterre Dolomite (Cambrian), southeast Missouri: evidence for possible multiple basin fluid sources and pathways during lead-zinc mineralization. *Bull. geol. Soc. Am.* **101**, 221-230.

Gregg, J.M. & Sibley, D.F. (1984) Epigenetic dolomitization and the origin of the xenotopic dolomite texture. *J. sedim. Petrol.* **54**, 908-931.

Guimera, J. (1984) Paleogene evolution of deformation in the northeastern Iberian Peninsula. *Geol. Mag.* **121**, 413-420.

Hallam, A. (1985) A review of Mesozoic climates. *J. geol. Soc.***142**, 433-445.

Handford, C.R. (1988) Review of carbonate sand-belt deposition of ooid grainstone and application to Mississippian Reservoir, Damme Field, southwestern Kansas. *Bull. Am. Ass. Petrol. Geol.* **72**, 1184-1199.

Haq, B.L., Hardenbol, J. & Vail, P.R. (1987) Chronology of fluctuating sea levels since the Triassic. *Science* **235**, 1156-1167.

Hardie, L.A. (1987) Dolomitization: a critical view of some of the current views. *J. sedim Petrol.* **57**, 166-183.

Harris, P.M., Kendall, C.G.St.C. & Lerche, I. (1985) Carbonate cementation - a brief review. In: *Carbonate cements* (Ed. by N.Schneidermann and P.M.Harris) Spec. Publ. Soc. econ. Paleont. Miner. 36, pp. 79-96.

Harwood, G.M. (1988) Microscopical techniques: II Principles of sedimentary petrography. In: *Techniques in Sedimentology* (Ed. by M.E.Tucker) pp. 108-173, Blackwells, Oxford.

Heinrich, R. & Zankl, H. (1986) Diagenesis of Upper Triassic Wetterstein Reefs of the Bavarian Alps. In: *Reef Diagenesis* (Ed. by J.H. Schroeder and B.H.Purser) pp. 245-268, Springer-Verlag, Berlin.

Hemming, N.G, Meyers, W.J. & Grains, J.C. (1989) Cathodoluminescence in diagenetic calcites: the roles of Fe and Mn as deduced from electron probe and spectrophotometric measurements. J. sedim. Petrol. 59, 404-411.

Hine, A.C. (1977) Lily Bank, Bahamas: history of an active oolite sand shoal. *J. sedim. Petrol.* **47**, 1554-1581.

Hird, K. (1986) *Petrography and geochemistry of some Carboniferous and Precambrian dolomites* Unpubl. PhD. Thesis, University of Durham.

Hird, K. & Tucker, M.E. (1988) Contrasting diagenesis of two Carboniferous oolites from South Wales: a tale of climatic influence. *Sedimentology* **35**, 587-602.

Holser, W.T. (1979a) Mineralogy of Evaporites. In: *Marine Minerals* (Ed. by R.G.Burns) pp. 211-294, Reviews in Mineralogy Vol. 6, Mineralogical Society of America.

Holser, W.T. (1979b) Trace elements and isotopes in evaporites. In: *Marine Minerals* (Ed. by R.G.Burns) pp. 295-346, Reviews in Mineralogy Vol. 6, Mineralogical Society of America.

Hsu, K.J. & Siegenthaler, C. (1969) Preliminary experiments on hydrodynamic movement induced by evaporation and their bearing on the dolomite problem. *Sedimentology* **12**, 11-25.

Hubbard, R.J. (1988) Age and significance of sequence boundaries on Jurassic and early Cretaceous rifted continental margins. *Bull. Am. Assoc. petrol. Geol.* **72**, 49-72.

Hudson, J.D. (1977) Stable isotopes and limestone lithification. *J. geol. Soc. Lond.* **133**, 637-660.

Ichikuni, M. (1983) Anionic substitution in calcium carbonate. In: *The significance of trace elements in solving petrogenetic problems and controversies* (Ed. by S.S.Augustithis) p. 83-94. Athens, Greece, Theophrastus Publications.

Inden, R.F. & Moore, C.H. (1983) Beach. In: *Carbonate depositional environments* (Ed. by P.A.Scholle, D.G.Bebout and C.M.Moore) Mem. Am. Assoc. petrol. Geol. 33, pp. 211-265.

James, N.P. & Choquette, P.W. (1984) Diagenesis 9. Limestones - the meteoric diagenetic environment environment. *Geoscience Canada*, **11**, 161-194.

James, N.P. & Choquette, P.W. (1988) *Paleokarst*. pp. 416. Springer-Verlag, New York.

Jurado, M. (1988) *El Triasico del subsuelo de la Cuenca del Ebro*. Unpubl. Ph.D. Thesis, Departament de Geologia Dinamica Geofisica i paleontologia, University of Barcelona.

Kaldi, J. and Gidman, J. (1982) Early diagenetic dolomite cements: examples from the Permian Lower Magnesian Limestone of England and the Pleistocene carbonates of the Bahamas. *J. sedim. Petrol.* **52**, 1073-1085.

Katz, A. & Matthews, A. (1977) The dolomitization of $CaCO_3$: an experimental study at 252-295°C. *Geochim. Cosmochim. Acta* **37**, 1563-1586.

Katz, A., Sass, E., Starinsky, A. & Holland, H.D. (1972) Strontium behaviour in the aragonite-calcite transformation: an experimental study at 40-98°C. *Geochim. Cosmochim. Acta* **36**, 481-496.

Kendall, A.C. (1989) Brine mixing in the Middle Devonian of western Canada and its possible significance to regional dolomitization. *Sedim. Geol.* **64**, 271-285.

Kendall, A.C. & Harwood, G.M. (1989) Shallow-water gypsum in the Castile Formation - significance and implications. In: *Subsurface and outcrop examination of the Capitan shelf margin, northern Delaware Basin* (Ed. by P.M.Harris and G.A.Grover). SEPM Core Workshop No. 13, San Antonio, April 23, 1989, pp 451-458.

Kendall, C.G.St.C. & Lerche, I. (1988) The rise and fall of eustasy. In: *Sea-level Changes: an integrated approach.* (Ed. by Wilgus, C.K., Hastings, B.S., Kendall C.G.St.C., Posamentier, H.W., Ross, C.A. & Van Wagoner, J.C.) Spec. Publ. Soc. econ. Paleont. Miner. 42., pp. 3-18.

Kendall, C.G.St.C. & Skipwith, P.A.d'E. (1969) Holocene shallow-water carbonate and evaporite sediments of Khor al Bazam, Abu Dhabi, southwest Persian Gulf. *Bull. Am. Assoc. petrol. Geol.* **53**, 841-869.

Kendall, C.G.St.C. & Warren, J. (1987) A review of the origin and setting of tepees and their associated fabrics. *Sedimentology* **34**, 1007-1027.

Kinsman, D.J.J. (1969) Interpretation of Sr^{2+} concentrations in carbonate minerals and rocks. *J. sedim. Petrol.* **39**, 486-508.

Knauth, L.P. (1979) A model for the origin of chert in limestone. *Geology* **7**, 274-277.

Knauth, L.P. & Epstein, S. (1976) Hydrogen and oxygen isotope ratios in nodular and bedded cherts. *Geochim. Cosmochim. Acta* **40**, 1095-1108.

Kretz, R. (1982) A model for the distribution of trace elements between between calcite and dolomite. *Geochim. Cosmochim. Acta* **46**, 1979-1981.

Kukal, Z. & Saadallah, A. (1973) Aeolian admixtures in the sediments of the northern Persian Gulf.In: *The Persian Gulf* (Ed. by B.H.Purser) pp.115-122. Springer-Verlag, Berlin.

Kuslansky, G.H. & Friedman, G.M. (1981) Chertification of crinoids may yield a product resembling "dedolomite". *J. sedim. Petrol.* **51**, 795-798.

Land, L.S. (1973) Holocene meteoric dolomitization of Pleistocene limestones, north Jamaica. *Sedimentology* **70**, 411-424.

Land, L.S. (1980) The isotopic and trace element geochemistry of dolomite: the state of the art. In: *Concepts and Models of Dolomitization* (Ed. by D.H.Zenger, J.B.Dunham & R.L.Ethington) Spec. Publ. Soc. econ. Paleont. Miner. 28, 87-110.

Land, L.S. (1983) The application of stable isotopes to studies of the origin of dolomite and to problems of diagenesis of clastic sediments. In: *Stable isotopes in sedimentary geology* (Ed. by M.A.Arthur and T.F.Anderson) Soc. econ. Paleont. Miner. Short Course No. 10, 4.1-4.22.

Land, L.S. (1985) The origin of massive dolomite. *J. geol. Educ.* **33**, 112-125.

Land, L.S., Salem, M.R.I. & Morrow, D.W. (1975) Paleohydrology of ancient dolomites: geochemical evidence. *Bull. Am. Assoc. petrol. Geol.* **59**, 1602-1625.

Lasemi, Z. & Sandberg, P.A. (1984) Transformation of aragonite-dominated lime muds to microcrystalline limestones. *Geology* **12**, 420-423.

Lasemi Z., Boardman, M.R. & Sandberg, P.A. (1989) Cement origin of supratidal dolomite, Andros Island, Bahamas. *J. sedim. Petrol.* **59**, 249-257.

Lee, M.R. & Harwood, G.M. (1989) Dolomite calcitization and cement zonation related to uplift of the Raisby Formation (Zechstein carbonate) northeast England. *Sedim. Geol.* **65**, 285-305.

Llompart, C., Rosell, J., Marquez-Aliaga, A. & Goy, A. (1987) El Muschelkalk de la Isla de Menorca. *Cuad. Geol. Iberica* **11**, 323-335.

Lohmann, K.C. (1988) Geochemical patterns of meteoric diagenetic systems and their applications to studies of paleokarst. In: *Paleokarst* (Ed. by N.P.James & P.W.Choquette) pp. 58-80. Springer-Verlag, New York.

Longman, M.W. (1980) Carbonate diagenetic textures from near-surface diagenetic environments. *Bull. Am. Assoc. petrol. Geol.* **64**, 461-487.

Longman, M.W. (1982) *Carbonate diagenesis as a control on stratigraphic traps* Education Course Note Series #21. Am. Assoc. petrol. Geol., Tulsa, Oklahoma. p 159.

Longman, M.W. & Mench, P.A. (1978) Diagenesis of Cretaceous limestones in the Edwards aquifer system of south-central Texas: A scanning electron microscope study. *Sedim. Geol.***21**, 241-276.

Lopez Gomez, J. (1987) Aspectos sedimentologicos y estratigraficos de las facies Bunsandstein y Muschelkalk entre Cueva del Hierra y Chelva (provincias de Cuenca y Valencia), Serrania de Cuenca, Espana. *Cuad. Geol. Iberica*, **11**, 647-664.

Lumsden, D.N. & Chimahusky, J.S. (1980) Relationship between dolomite nonstoichiometryand carbonate facies parameters. In: *Concepts and Models of Dolomitization* (Ed. by D.H.Zenger, J.B.Dunham & R.L.Ethington) Spec. Publ. Soc. econ. Paleont. Miner. 28, 123-137.

Machel, H.G. (1985) Cathodoluminescence in calcite and dolomite and its chemical interpretation. *Geoscience Canada* **12**, 139-147.

Machel, H.G. (1987) Saddle dolomite as a by-product of chemical compaction and thermochemical sulphate reduction. *Geology* **15**, 936-940.

Machel, H.G. (1988) Fluid flow direction during dolomite formation as deduced from trace-element trends. In: *Sedimentology and Geochemistry of dolostones* (Ed. by V.J.Shukla and P.A.Baker) Spec. Publ. Soc. econ. Paleont. Miner. 43, pp. 115-127.

Machel, H.G. & Mountjoy, E.W. (1986) Chemistry and environments of dolomitization - a reappraisal. *Earth Sci. Rev.* **23**, 175-222.

Magaritz, M. (1975) Sparitization of a pelleted limestone: A case study of carbon and oxygen isotopic composition. *J. sedim. Petrol.* **45**, 599-603.

Magaritz, M. & Kafri, U. (1981) Stable isotope and Sr^{2+}/Ca^{2+} evidence of diagenetic dedolomitization in a schizohaline environment: Cenomanian of northern Israel. *Sedim. Geol.* **28**, 29-41.

Maliva, R.G. (1987) Quartz geodes: Early diagenetic silicified anhydrite nodules related to dolomitization. *J. sedim. Petrol.* **57**, 1054-1059.

Manspeizer, W. (1988) Triassic-Jurassic rifting and opening of the Atlantic: An overview. In: *Triassic-Jurassic Rifting. Continental Break-up and the origin of the Atlantic Ocean and Passive Margins* (Ed. by W.Manspeizer) pp. 41-79 Elsevier, Amsterdam.

Markello, J.R. & Read, J.F. (1981) Carbonate ramp-to-deeper shale shelf transitions of an Upper Cambrian intrashelf basin, Nolichucky Formation, southwest Virginia, Appalachians. *Sedimentology* **28**, 573-597.

Marzo, M. (1980) El Buntsandstein de los Catalanides: Estratigrafia y procesos de sedimentacion. Unpubl. Ph.D. Thesis, University of Barcelona, p. 317.

Marzo, M. & Calvet, F. (1985) *Guia de la excursion al Triasico de los Catalanides.* II Coloquio de Estratigrafia y Paleogeografia del Permico y Triasico de Espana. La Seu d'Urgell, p. 175.

Mazzulo, S.J., Reid, A.M. & Gregg, J.M. (1987) Dolomitization of Holocene Mg-calcite supratidal deposits, Ambergris Cay, Belize. *Bull. geol. Soc. Am.* **98**, 224-231.

McKenzie, J.A. (1981) Holocene dolomitization of calcium carbonate sediments from the coastal sabkhas of Abu Dhabi, UAE: a stable isotope study. *J. geol.* **89**, 185-198.

Melim, L.A. & Scholle, P.A. (1989) Dolomitization model for the forereef facies of the Permian Capitan Formation, Guadalupe Mountains, Texas-New Mexico. In: *Subsurface and outcrop examination of the Capitan shelf margin, northern Delaware Basin* (Ed. by P.M.Harris and G.A.Grover). SEPM Core Workshop No. 13, San Antonio, April 23, 1989, pp 407-414.

Meyers, W.J. & Hill, B. (1983) Quantitative studies of compaction in Mississippian limestones, New Mexico. *J. sedim. Petrol.* **53**, 231-243.

Milliken, K.L. (1981) The silicified evaporite syndrome- two aspects of the silicification history of former evaporite nodules from southern Kentucky and northern Tennessee. *J. sedim. Petrol.* **49**, 245-256.

Moore, C.H., Smitherman, J.M. & Allen, S.H. (1972) Pore system evolution in a Cretaceous carbonate beach sequence. International Geological Congress, 24th, Montreal, section 6, p. 64-91.

Morrow, D.W. (1982a) Diagenesis I. Dolomite - part I. The chemistry of dolomitization and dolomite precipitation. *Geoscience Canada* **9**, 5-13.

Morrow, D.W. (1982b) Diagenesis II. Dolomite - part II. Dolomitization models and ancient dolostones. *Geoscience Canada* **9**, 95-107.

Morrow, D.M. & Mayers, I.R. (1978) Simulation of limestone diagenesis - a model based on strontium depletion. *Can. J. Earth Sci.* **15**, 376-396.

Murray, R.C. (1969) Hydrology of south Bonaire, Netherlands Antilles - a rock selective dolomitization model. *J. sedim. Petrol.* 15, 987-1035.

Nicholls, K.M. (1974) Coextensive supratidal dolomite and underlying secondary dolomite in the Triassic of north-central Nevada. *J. sedim. Petrol.* **44**, 783-789.

Nicholls, K.M. & Silberling, N.J. (1980) Eogenetic dolomitization in the pre-Tertiary of the Great Basin. In: *Concepts and models of dolomitization.* (Ed. by D.H.Zenger, J.B.Dunham and R.L.Ethington) Spec. Publ. Soc. econ. Paleont. Miner. 28, 237-246.

Orti Cabo, F. (1982) Sur les conditions de depot, la diagenese et la structure des evaporites dans l'est d'Espagne. *Sciences de la Terre* **XXV**, 179-199, Nancy.

Orti Cabo, F. (1987) Aspectos sedimentologicos de las evaporitas del Triasico y del Liasico inferior en el E de la Peninsula Iberica. *Cuad. Geol. Iberica* **11**, 215-236.

Patterson, R.J. & Kinsman, D.J.J. (1982) Formation of diagenetic dolomitein coastal sabkhas along the Arabian (Persian) Gulf. *Bull. Am. Assoc. petrol. Geol.* **65**, 1457-1475.

Payton, C.E. (1977) *Seismic stratigraphy- Applications to hydrocarbon exploration.* Mem. Am. Assoc. petrol. Geol. 26.

Perez Arlucea, M. (1987) Distribucion paleogeografica de las unidades del Permico y del Triasico en el sector Molina de Aragon-Albarracin. *Cuad. Geol. Iberica* **11**, 607-622.

Peryt, T.M. & Magaritz, M. (1990) Genesis of evaporite-associated platform dolomites: case study of the Main Dolomite (Zechstein, Upper Permian), Leba elevation, northern Poland. *Sedimentology* **37**, 745-761.

Pingitore, N.E Jr. (1978) The behaviour of Zn^{2+} and Mn^{2+} during carbonate diagenesis: Theory and applications. *J. sedim. Petrol.* **48**, 799-814.

Plummer, L.N. & Back, W. (1980) The mass balance approach: Application to interpreting the chemical evolution of hydrologic systems. *American Journal of Science* **280**, 130-142.

Popp, B.N., Anderson, T.F. & Sandberg, P.A. (1986) Brachiopods as indicators of original isotopic composition in some Paleozoic limestones. *Bull geol. Soc. Am.* **97**, 1262-1269.

Posamentier, H.W. & Vail, P.R. (1988) Eustatic controls on clastic deposition II - sequence and systems tracts models. In: *Sea-level Changes: an integrated approach.* (Ed. by Wilgus, C.K., Hastings, B.S., Kendall C.G.St.C., Posamentier, H.W., Ross, C.A. & Van Wagoner, J.C.) Spec. Publ. Soc. econ. Paleont. Miner. 42., pp. 125-154.

Posamentier, H.W., Jervey, M.T. & Vail, P.R. (1988) Eustatic controls on clastic deposition I - conceptual framework. In: *Sea-level Changes: an integrated approach.* (Ed. by Wilgus, C.K., Hastings, B.S., Kendall C.G.St.C., Posamentier, H.W., Ross, C.A. & Van Wagoner, J.C.) Spec. Publ. Soc. econ. Paleont. Miner. 42., pp. 109-124.

Purser, B.H. & Evans, G. (1973) Regional sedimentation along the Trucial coast, SE Persian Gulf. In: *The Persian Gulf* (Ed. by B.H.Purser) pp.211-232. Springer-Verlag, Berlin.

Purser, B.H. & Loreau, J.P. (1973) Aragonitic, supratidal encrustations on the Trucial Coast, Persian Gulf. In: *The Persian Gulf* (Ed. by B.H.Purser) pp.343-376. Springer-Verlag, Berlin.

Radke, B.H. & Mathis, R.L. (1980) On the formation and occurrence of saddle dolomite. *J. sedim. Petrol.* **50**, 1149-1168.

Ramon, X. (1985) *Estratigrafia y sedimentologia del Muschelkalk Inferior del Dominio Montseny-Llobregat* Unpubl. MSc. thesis, University of Barcelona, p. 100.

Ramon, X. & Calvet, F. (1987) Estratigrafia y sedimentologia del Muschelkalk Inferior del Dominio Montseny-Llobregat (Catalanides). *Estudios Geologicos*, **43**, 471-487.

Rast, N. (1988) Variscan-Alleghanian orogen. In: *Triassic-Jurassic Rifting. Continental Break-up and the origin of the Atlantic Ocean and Passive Margins* (Ed. by W.Manspeizer) pp. 1-27 Elsevier, Amsterdam.

Read, J.F. (1985) Carbonate platform facies models. *Bull. Am. Assoc. petrol. Geol.* **69**, 1-21.

Robinson, P. (1980) Determination of calcium, magnesium, manganese, strontium, sodium and iron in the carbonate fraction of limestones and dolomites. *Chem. Geol.* **28**, 135-146.

Sacrista, R., Viladevall, M., Font, X., Peris A. & Palacios, J. (1980) Apercu sur les mineralizations plombo-zinciferes du Trias carbonate de Barcelona (Espagne). In: *Cristillisation-Deformation-Dissolution des carbonates*. 17-18 Nov. 1980, Bordeaux, pp. 413-420.

Salomons, S.W. (1975) Chemical and isotopic composition of carbonates in Recent sediments and soils from western Europe. *J. sedim. Petrol.* **45**, 440-449.

Salvany, J.M. & Orti Cabo, F. (1987) El Keuper de los Catalanides. *Cuad. Geol. Iberica* **11**, 215-236.

Sandberg, P.A. (1983) An oscillating trend in Phanerozoic non-skeletal carbonate mineralogy. *Nature* **305**, 19-22.

Sangster, D.F. (1988) Breccia-hosted lead-zonc deposits in carbonate rocks. In: *Paleokarst* (Ed. by N.P.James & P.W.Choquette) pp. 102-116.

Sarg, J.F. (1988) Carbonate sequence stratigraphy. In: *Sea-level Changes: an integrated approach.* (Ed. by Wilgus, C.K., Hastings, B.S., Kendall, C.G.St.C., Posamentier, H.W., Ross, C.A. & Van Wagoner, J.C.) Spec. Publ. Soc. econ. Paleont. Miner. 42., pp. 155-181.

Schmidt, M. (1932) Uber die ceratiten von Olesa bei Barcelona. *Bull. Inst. Cat. Hist. Nat.* **XXXII**, 195-222.

Schmoker, J.W., Krystinik, K.B. & Halley, R.B. (1985) Selected characteristics of limestone and dolomite reservoirs in the United States. *Bull. Am. Assoc. petrol. Geol.* **69**, 733-741.

Scholle, P.A. (1978) *A color illustrated guide to carbonate rock constituents, textures, cements and porosities*. Mem. Am. Assoc. petrol. Geol. **27**, p. 241.

Scholle, P.A. & Kinsman, D.J.J. (1974) Aragonaite and high magnesian calcite caliche from the Persian Gulf, a modern analogy for the Permian of Texas and New Mexico. *J. sedim. Geol.* **44**, 904-916.

Scoffin, T.P. (1987) *An introduction to carbonate sediments and rocks*.p. 274. Blackie, Glasgow.

Searl, A. (1988) The limitations of 'cement stratigraphy' as revealed in some Lower Carboniferous oolites from South Wales. *Sedim. Geol.* **57**, 171-183.

Sears, S.O. & Lucia, F.J. (1980) Dolomitization of northern Michigan Niagara reefs by brine refluxion and freshwater/seawater mixing. In: *Concepts and Models of Dolomitization* (Ed. by D.H.Zenger, J.B.Dunham & R.L.Ethington) Spec. Publ. Soc. econ. Paleont. Miner. 28, 215-236.

Shinn, E.A. (1983) Tidal flat environment. In: *Carbonate Depositional Environments* (Ed. by P.A. Scholle, D.G. Bebout and C.H. Moore) Mem. Am. Assoc. petrol. Geol. 33, 173-210.

Shukla, V. & Baker, P.A. (1988) *Sedimentology and geochemistry of dolostones*. pp. 266. Spec. Publ. Soc. econ. Paleont. Miner. 43.

Sibley, D.F. (1980) Climatic control of dolomitization, Seroe Domi Formation (Pliocene), Bonaire, N.A. In: *Concepts and models of dolomitization*. (Ed. by D.H.Zenger, J.B.Dunham and R.L.Ethington) Spec. Publ. Soc. econ. Paleont. Miner. 28, 247-258.

Sibley, D.F. (1982) The origin of common dolomite fabrics: clues from the Pliocene. *J. sedim. Petrol.* **52**, 1087-1100.

Sibley D.F. & Gregg, J.M. (1987) Classification of dolomite rock texture. *J. sedim. Petrol.* **57**, 967-975.

Simms, M. (1984) Dolomitization by groundwater-flow systems in carbonate platforms. *Trans. Gulf-Cst, Ass. geol. Socs* 34, 411-420.

Smith, D.B. (1981) Bryozoan-algal patch reefs in the Upper Permian Magnesian limestones of Yorkshire, Northeast England. In: *European Fossil Reef Models* (Ed. by D.F.Toomey) Spec. Publ. Soc. econ. Paleont. Miner. 30, 187-202.

Sole de Porta, N., Calvet, F. & Torrento, L. (1987) Analisis palinologico del Triasico de los Catalanides (NE Espana). *Cuad. Geol. Iberica* **11**, 237-254.

Sopena, A., Lopez, J., Arche, A., Perez Arlucea, M., Ramos, A., Virgili, C., & Hernando, S. (1988) Permian and Triassic rift basins of the Iberian Peninsula. In: *Triassic-Jurassic Rifting. Continental Break-up and the origin of the Atlantic Ocean and Passive Margins* (Ed. by W.Manspeizer) pp. 757-786. Elsevier, Amsterdam.

Sopena, A., Virgili, C., Arche, A., Ramos, A. & Hernando, S. (1983) El Triasico. In: *La Etapa Permo-Triasica* Programa Internacional de Correlacion Geologica (P.I.C.G.) **106**, 47-64.

Stoessel, R.K., Ward, W.C., Ford, B.H. & Schuffert, J.D. (1987) Water chemistry and $CaCO_3$ dissolution in the saline part of an open-flow mixing zone, coastal Yucatan peninsula, Mexico. *Bull. geol. Soc. Am.* **101**, 159-169.

Theriault, F. & Hutcheon, I. (1987) Dolomitization and calcitization of the Devonian Grosmont Formation, northern Alberta. *J. sedim. Petrol.* **57**, 955-966.

Torok, A. (1990) Multiphase dolomitization and calcite cementation as revealed by CL, BSEM, EXDRA, Triassic, South Hungary. (Abs.) Abstracts of Posters Volume, 13th International Sedimentological Congress 26th-31st August, 1990, Nottingham, England.

Tucker, M.E. (1976) Quartz replaced anhydrite nodules (Bristol diamonds) from the Triassic of the Bristol District. *Geol. Mag.* **113**, 569-574.

Tucker , M.E. (1988) *Techniques in sedimentology*, pp. 394. Blackwells, Oxford.

Tucker, M.E. & Benton, M.J. (1983) Triassic environments, climates, and reptile evolution. *Palaeogeogr. Palaeoclimatol. Palaeoecol.* **40**, 361-380.

Tucker, M.E. & Wright, V.P. (1990) *Carbonate Sedimentology.* Blackwell Scientific Publications, Oxford, UK.

Vacher, H.L., Bengtsson, T.D., Plummer, L.N. (1990) Hydrology of meteoric diagenesis: residence time of meteoric ground water in island freshwater lenses with application to aragonite-calcite stabilization rate in Bermuda. *Bull. geol. Soc. Am.* **102**, 223-232.

Vahrenkamp, V.C. & Swart, P.K. (1990) New distribution coefficient of strontium into dolomite and its implications for the formation of ancient dolomites. *Geology* **18**, 387-391.

Vail, P.R., Colin, J.P., Jan du Chene, R., Kuchly, J., Mediavilla, F. & Triflief, V. (1987) La stratigraphie sequentielle et son application aux correlations chronostratigraphiques dans la Jurassique du bassin de Paris. *Bull. Soc. Geol. France* (8), III, 1301-1321.

Vail, P.R., Mitchum, R.M. & Thompson, S. (1977) Seismic stratigraphy and global changes in sea-level, part 4: global cycles of relative changes of sea-level. In: *Seismic stratigraphy- Applications to hydrocarbon exploration.* (Ed. by C.E.Payton) pp. 83-97. Mem. Am. Assoc. petrol. Geol. 26.

Van Wagoner, J.C., Posamentier, H.W., Mitchum, R.M.Jr., Vail, P.R., Sarg, J.F., Loutit, T.S. & Hardenbol, J. (1988) An overview of the fundamentals of sequence stratigraphy and key definitions. In: *Sea-level Changes: an integrated approach.* (Ed. by Wilgus, C.K., Hastings, B.S., Kendall C.G.St.C., Posamentier, H.W., Ross, C.A. & Van Wagoner, J.C.) Spec. Publ. Soc. econ. Paleont. Miner. 42., pp. 39-46.

Vegas, R. & Banda, E. (1982) Tectonic framework and alpine evolution of the Iberian Peninsula. *Earth Evol. Sci.* **4**, 320-343.

Veizer, J. (1983) Chemical diagenesis of carbonates: theory and application of trace element techniques. In: *Stable isotopes in sedimentary geology* (Ed. by M.A.Arthur & T.F.Anderson) Soc. econ. Paleont. Miner. Short Course No. 10, 3.1-3.100.

Veizer, J. & Demovic, R. (1974) Strontium as a tool in facies analysis. *J. sedim. Petrol.* **44**, 93-115.

Veizer, J., Holser, W.T., & Wilgus, C.K. (1980) Correlation of $^{13}C/^{12}C$ and $^{34}S/^{32}S$ secular variations. *Geochim .Cosmochim. Acta* **44**, 579-587.

Veizer, J., Lemieux, J., Jones, B. Gibling, M.R. & Savelle, J. (1977) Sodium: paleosalinity indicator in ancient carbonate rocks. *Geology* **5**, 177-179.

Veizer, J., Lemieux, J., Jones, B., Gibling, M.R. & Savelle, J. (1978) Paleosalinity and dolomitization of a Lower Paleozoic carbonate sequence, Somerset and Prince of Wales Islands, Arctic Canada. *Can. J. earth. Sci.* **15**, 1448-1461.

Virgili, C. (1958) El Triasico de los Catalanides. *Bol. Inst. Geol. Min. Esp.* **69**, 1-856.

Virgili, C., Sopena, A., Ramos, A., & Hernando, S. (1977) Problemas de la cronoestratigrafia del Trias en Espana. *Cuad. Geol. Iberica* **4**, 57-88.

Wanless, H.R. (1979) Limestone response to stress: pressure solution and dolomitization. *J. sedim. Petrol.* **49**, 437-462.

West, I.M. (1975) Evaporites and associated sediments of the basal Purbeck Formation (upper Jurassic) of Dorset. *Proc. Geol. Ass.* **86**, 205-226.

Wilgus, C.K., Hastings, B.S., Kendall C.G.St.C., Posamentier, H.W., Ross, C.A. & Van Wagoner, J.C. (1988) *Sea-level changes: an integrated approach.* Spec. Publ. Soc. econ. Paleont. Miner. 42.

Wilkinson,B.H., Owen, R.M. & Carroll, A.R. (1984) Submarine hydrothermal weathering, global eustasy, and carbonate polymorphism in Phanerozoic marine oolites. *J. sedim. Petrol.* **55**, 171-183.

Wilson, J.L. (1975) *Carbonate facies in geologic history.* pp. 471. Springer-Verlag, Berlin.

Wood, G.V. & Armstrong, A.K. (1975) Diagenesis and stratigraphy of the Lisbeurne Group limestones of the Sadlerochit Mountains and adjacent areas, northeastern Alaska. U.S. Geol. Surv. Prof. Paper 857, p. 47.

Wright, V.P. (1982) The recognition and interpretation of paleokarsts: two examples from the Lower Carboniferous of South Wales. *J. sedim. Petrol.* **52**, 83-94.

Wright, V.P. (1984) Peritidal carbonate facies models: a review. *Geol. J.* **19**, 309-325.

Wright, V.P. (1989) Terrestrial stromatolites and laminar calcretes: a review. *Sedim. Geol.* **65**, 1-13.

Zenger, D.H., Dunham, J.B. & Ethington, R.L. (1980) *Concepts and models of dolomitization.* pp. 320. Spec. Publ. Soc. econ. Paleont. Miner. 28.

Zenger, D.H. (1973) Syntaxial calcite borders on dolomite crystals, Little Falls Formation (Upper Cambrian), New York. *J. sedim. Petrol.* **43**, 118-124.

Zhao, X. & Fairchild, I.J. (1987) Mixing-zone dolomitization of Devonian carbonates, Guangxi, South China. In: *Diagenesis of Sedimentary Sequences* (Ed. by J.D. Marshall) Spec Publ. Geol. Soc. Lond. 36, 157-170.

Ziegler, P.A., (1982) Triassic rifts and facies patterns in western and central Europe. *Geol. Runds.* **71**, 747-772.